CHEMICAL EVOLUTION AND MINERALIZATION OF THE SULPHUR SPRINGS CSDP SITE, VALLES CALDERA, NEW MEXICO

by

John A. Musgrave

Submitted in Partial Fulfillment of
the Requirements for the Degree of
Doctor of Philosophy

NEW MEXICO INSTITUTE OF MINING AND TECHNOLOGY

Socorro, New Mexico

May 1992

ABSTRACT

The Valles caldera hosts an active hydrothermal system with deep fluids at temperatures as high as 300°C. The thermal and chemical evolution of the Sulphur Springs subsystem of the Valles hydrothermal system was studied by fluid inclusion microthermometry and microanalysis of material from core holes VC-2A and VC-2B, which were drilled as part of the Continental Scientific Drilling Program at Sulphur Springs.

Temperature and composition of the past fluids in the Sulphur Springs hydrothermal system were different from those at present. Fluid inclusion data indicate a complex hydrothermal history in which fluids of ≈ 5 equiv. wt.% NaCl entered fractures in compositionally discrete pulses at shallow depths (<700 m) of the hydrothermal system. However, the inclusion data indicate the predominant fluid at shallow depths was 0.5-1 equiv. wt. NaCl., whereas the fluid at depth (>700 m) was 3-5 equiv. wt.% NaCl. At shallow depths, temperatures are about 100°C lower and at depth, fluid temperatures have decreased about 10 to 30°C. Important hydrologic aspects of the evolution of the Sulphur Springs hydrothermal system include the existence of a deep seated saline fluid, possibly derived from the crystallizing Bandelier magma, which was periodically injected into shallow levels or mixed with the shallow fluid through a stratigraphically stratified hydrothermal system; and the water table, which controls hydrodynamic boiling conditions, descended as much as 400 m when compared to the present level of the water table. The process which led to the lowering of the water table was collapse of the southwestern caldera wall and draining of intracaldera lakes, and this may have lead to greater incursion of the shallow fluid into deeper portions of the system thereby diluting the deep hydrothermal fluid to its present composition (1.1 equiv. wt.% NaCl) or the saline fluid has retreated to a deeper level. Presently there is no evidence of the high salinity fluid.

Inclusion gases were extracted *in vacuo* and analyzed by mass spectrometry. The principal volatile is H_2O; the principal gases are CO_2, H_2S, N_2, and C_nH_n which account for 2.4 to 22.7 mole % of inclusion volatiles. Highest H_2S concentrations were from samples of early quartz associated with molybdenite and base metal deposition. Organic compounds are C_1-C_6 species,

and they are most concentrated in late stage mineralization. Gas data permit calculation of fO_2 and fS_2. Furthermore, the inclusion gas data yielded information on possible origins of gaseous components in the hydrothermal fluid, and when combined with noble gas data from fluid inclusions and present day fluids indicate the input of ^3He, and therefore the input (heat and some volatiles) from a cooling magma has been constant for, at least, the past 1.0 Ma.

Integration of fluid inclusion temperature and gas data, with phase petrology and stable isotopic results provides a coherent picture of elemental transport and deposition in this sytem. Sulfide minerals appear to have been deposited by mixing of the two endmember fluids and to a lesser extent boiling. Molybdenite deposition was apparently the result of paleo-groundwaters leaching Mo from surrounding country rocks and mixing of these Mo-laden fluids with the sulfur-rich hydrothermal fluids, rather than a deep Climax-type source. Modeling Sulphur Springs meteoric water under convecting conditions at different water:rock mass ratios and temperatures indicate the isotopic composition of the meteoric water responsible for hydrothermally altering rocks and vein minerals was about 10 per mil lighter in δD than current meteoric water. Temperature controlled fractionation influenced the isotopic composition of near-surface rock. Marine carbonate rocks underwent extensive isotopic exchange with the hydrothermal fluid, with some samples indicating the $\delta^{18}O$ of the limestone approaches that of the fluid. However, carbon isotopic composition of vein calcites was controlled by the carbon isotopic composition of the marine limestones.

ACKNOWLEDGMENTS

I am indebted to a number of people for their support and expertise in the completion of this thesis. Many of these people are in the Earth and Environmental Sciences Division (EES) and the Isotope and Nuclear Chemistry Division (INC) at Los Alamos National Laboratory (LANL). I would like to give special thanks to the following individuals:

EES-1: Fraser Goff for his "day-one" support of this project, technical advisement and my start at LANL, Jamie Gardner for technical and moral support, Peggy Snow for assistance with the electron microprobe, Sue Goff for just "chewing the fat," and Wayne Morris for my start at LANL.

INC-7: Bob Charles for his interest and support in this endeavor, David Curtis for allowing me to remain at LANL to complete my research, the entire office staff for all their assistance, Jane Poths for her interest in the measurement of noble gases in fluid inclusions, Paul Dixon for the technical discussions and moral support, Drew Tait for his interest in my research and wanting to continue with certain aspects of this research, and David Janecky for the stimulating discussions, assistance with the various modeling codes, and as the LANL committee member for the thesis defense.

I am equally indebted to everyone at the New Mexico Institute of Mining and Technology including my advisor David Norman for his continued interest and enthusiasm in this project, and my other committee members Andrew Campbell, William Chavez, and Fred Phillips; and fellow graduate students Kurt Panter, Ingar Walder, Issac Boadi, Laurie Benton, and David Mitcheltree for their comradery and a good laugh.

Thanks also go to Jeff Hulen of the Earth Sciences Laboratory, University of Utah Research Institute for being a good "springboard" to bounce ideas around and Cathy Janik of the U.S. Geological Survey for providing the original data for VC-2A and Redondo Creek discharge gases.

Finally, I would like to thank my wife, Barbara, for putting up with another degree and my children, Laura and Karen, for making the whole ordeal tolerable. I could not have made it without their support.

This thesis was supported by the Office of Basic Energy Sciences/U.S. Department of Energy,

Los Alamos National Laboratory, New Mexico Geological Society Grants-in-aide, and the Geological Society of America.

TABLE CONTENTS

TABLE OF CONTENTS (continued)

APPENDIX A
GEOCHEMISTRY OF HYDROTHERMAL ALTERATION AND MINERALIZATION

LIST OF FIGURES

LIST OF TABLES

PART I

PURPOSE

The formation of geochemical anomalies known as ore deposits involves complex geologic and geochemical processes, and the understanding of these processes is benefitted from the detailed physical, chemical and isotopic data now available from the exploration and exploitation of active geothermal systems. Study of the active Sulphur Springs hydrothermal system in the Valles caldera, New Mexico provides an opportunity to investigate the processes that lead to hydrothermal alteration and epithermal mineralization. Major questions to be addressed from this study are:

1) Have the P-T-X conditions of the Sulphur Springs hydrothermal system changed with time?
2) Did the presently active hydrothermal system deposit the ore minerals observed at Sulphur Springs?
3) Is the alteration and mineralization (past and present) produced by the same hydrothermal system?

STATEMENT OF PROBLEM

Active geothermal systems and thermal regimes of the crust are the foci of increased interest for potential resource exploitation and deep drilling for scientific purposes. The Rio Grande rift is the major thermal regime of the southwestern U. S., and the Jemez Mountains containing the Valles caldera represent the largest geothermal prospect in the region. The Valles caldera in the Jemez Mountains of north-central New Mexico (Fig. 1.1) is one site of the Thermal Regimes segment of the emerging Continental Scientific Drilling Program (CSDP) because it offers opportunities for the studies of magma genesis, ore deposition, and hydrothermal processes (Goff and Nielson, 1986). Intrusion of magma to shallow depths, as has recently occurred under the Jemez Mountains, results in tens to hundreds of km^3 of H_2O fluxing through the areas near the

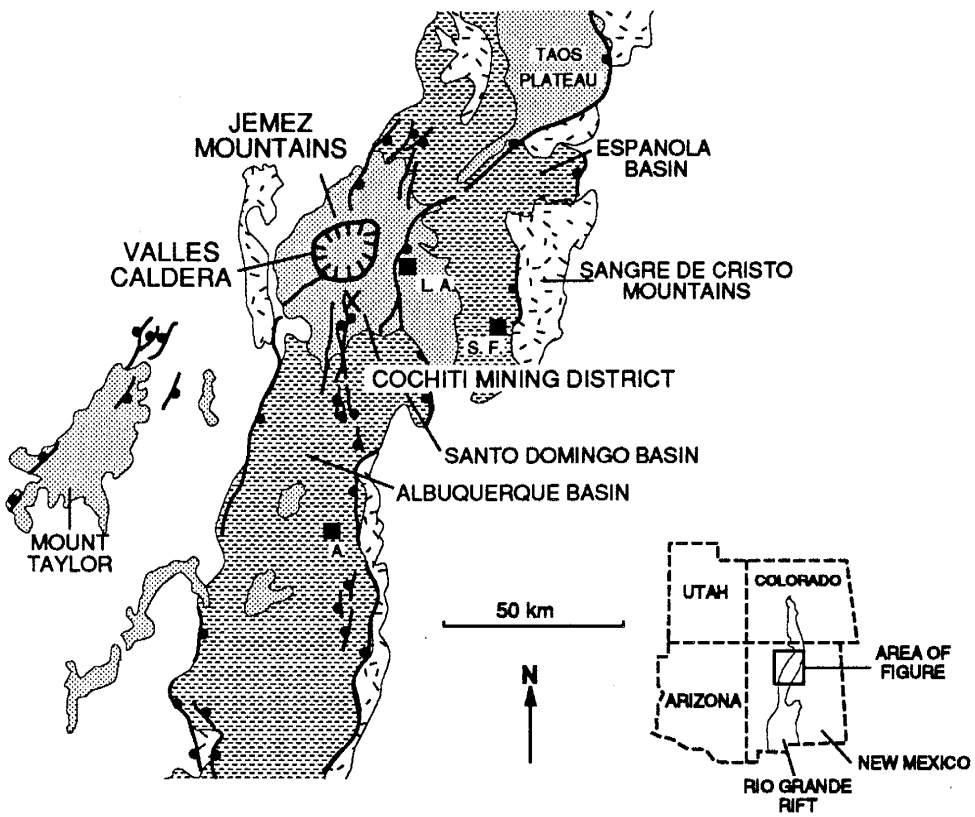

Figure 1.1 Location map of the Jemez Mountains and volcanic field, Valles caldera (closed depression), and the Rio Grande rift. Regular stipple = Tertiary-Quaternary basin fill sediments; close-spaced stipple = Tertiary-Quaternary volcanic rocks; jackstraw = Precambrian rocks.

intrusion. These fluids redistribute heat, change the mineralogy of the rocks, redistribute elements, and in some cases form major mineral deposits. Many of the stated research objectives have been realized in the first two CSDP core holes, VC-1 and VC-2A (Goff et al, 1986; 1987). Unexpected shows of subore grade molybdenum mineralization have sparked much additional interest and research (Hulen et al, 1987). The active geothermal systems of the Valles caldera are the modern analogues to fossil ore-depositing systems (Hulen and Nielson, 1986), and the present Valles hydrothermal system and precursor systems of the Jemez Mountains are similar to those that deposited the precious metal/base metal ores of the San Juan Mountains, southwestern Colorado (Hulen and Nielson, 1986). These similarities include host lithology, tectonic setting, alteration mineralogy, temperature range and fluid composition (Barton et al., 1977; Casadevall and Ohmoto, 1977; Slack, 1980; Hulen and Nielson, 1986). Hulen and Nielson (1986) note the similarity of the Valles system to that of the Questa molybdenum deposit in tectonic setting, with Valles situated on the western margin of the Rio Grande rift and the Questa caldera on the eastern margin of the rift, and in spatial location of molybdenum mineralization in the ring fracture zones of both calderas.

Core hole VC-2A, Sulphur Springs area, intersected subore grade molybdenum mineralization with attending pyrite, fluorite, rhodochrosite, and sphalerite (Hulen et al., 1987) (Fig. 1.2). VC-2B, a companion core hole to VC-2A, 400 m to the northeast, was completed in October of 1988. Preliminary results from VC-2B show zones of hydrothermal alteration, brecciation and mineralization, which includes pyrargarite, sphalerite, stibnite and/or jamesonite, fluorite, rhodochrosite and sphalerite. Sampling of fluids and acquisition of physical parameters from a hydrothermal system actively depositing such ores would be an extremely important contribution to ore genesis and to the geochemistry of hydrothermal ore deposits.

APPROACH

The approach chosen in this investigation of the chemical evolution and mineralization of an active hydrothermal system is the use of fluid inclusion, hydrothermal alteration chemical, stable isotopic, and chemical data on the present fluids and the modeling of metal solubilities.

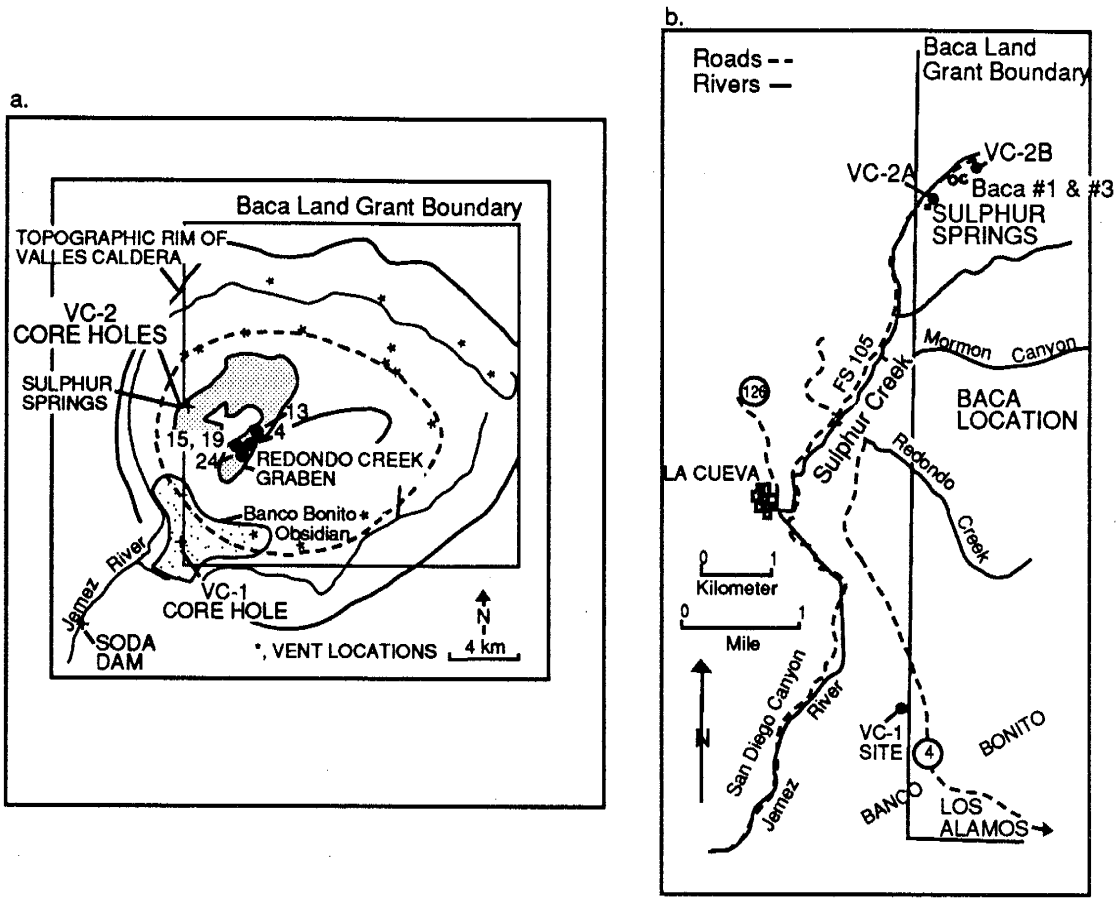

Figure 1.2
a. Location map of CSDP core holes VC-1 and VC-2 in the Valles caldera. The shaded area of the figure is the region of intense surface hydrothermal alteration. Baca wells 4, 13, 15, 19, and 24 drilled by UNOCAL are located in the Redondo Creek area. b. Detailed location map of CSDP core holes VC-1 and VC-2A and VC-2B.

Geochemical calculations based on the above data provided information on the pH, fO_2, fS_2, fCO_2 and metal carrying capacity of the present and past fluids. The results presented here allow significant conclusions to be made about the physicochemical evolution of a hydrothermal system that has been active for approximately one million years.

ORGANIZATION

This work is organized into four main parts, with an introduction and conclusion section to each part. The first section contains the introductory material. The second part deals with the fluid inclusion data - microthermometry and the interpretation of these data. The third section pertains to the analysis of inclusions gases by mass spectrometry, calculation of gas fugacities from the gas data and comparison with fugacities from alteration mineral analyses, origin of the gases and finally comparison of the Sulphur Springs gas data with data from other systems. The fourth part deals with the geochemistry of the hydrothermal alteration minerals, the present day fluids, and the processes responsible for the mineralization. Finally, a concluding remark follows part four.

PART II

FLUID INCLUSION MICROTHERMOMETRY

INTRODUCTION

Fluid inclusion data from an active geothermal system, when compared with present conditions, allows the thermal and compositional evolution to be deduced. Such results also provide insight into the interpretation of fluid inclusion data from some hydrothermal ore deposits. Deep scientific drilling into the Valles caldera hydrothermal system by nearly 40 deep wells makes it the best explored Quaternary caldera complex in the United States (Goff et al,. 1989). Therefore, an extensive database exists on the chemistry of present day fluids, much is known about the configuration of the present system, and the chronology of various geologic events is well constrained (Hulen and Nielson, 1986; Goff and Shevenell, 1987; Goff et al., 1988; Goff et al., 1989; WoldeGabriel and Goff, 1989). Furthermore, the system has not been altered by commercial exploitation. Sulphur Springs hydrothermal system (a subsystem of the Valles hydrothermal system) provides an opportunity to study the evolution of a geothermal system because it has been explored to a depth of 1762 m by 2 continuously cored, scientific drillholes, and the reservoir fluid has been characterized by downhole sampling and discharge tests (Goff et al., 1989 and 1990). The continuous core allows detailed study of vein mineralogy and paragenesis, and hence detailed fluid inclusion analysis. Microthermometry was performed on inclusions in 5 minerals in drill core from depths of 29 to 1725 m. In general, the results compare well with the present day system in temperature and composition, but the results do show the system has evolved over time.

Valles caldera located in the Jemez Mountains volcanic field of north-central New Mexico has been the target of geothermal exploration for the last 20 years because of its abundant hot springs and Quaternary volcanic features (Figs. 1.1 and 1.2). The caldera complex possesses a diverse suite of thermal waters that are typical of those existing at many geothermal areas around the world (Henley and Ellis, 1983; Goff and Grigsby, 1982). Each type of water of the volcanic field possesses distinct geologic and structural control and unique chemical and isotopic characteristic (Goff and Grisby, 1982). Thermal meteoric waters are dilute groundwaters heated by the relatively

high subsurface temperatures at shallow depths and occur at isolated spots throughout the western ring-fracture zone (Goff and Grisby, 1982). Acid-sulfate waters with associated mud pots and fumaroles occur in the Redondo Creek and Sulphur Springs areas (Fig. 1.2) (Goff et al., 1985). These waters are the result of oxidation of H_2S and condensation of steam to produce H_2SO_4 that mixes with groundwater. Deep reservoir fluids encountered by wells in the Redondo Creek and Sulphur Springs were areas beneath the acid-sulfate/vapor zone capping the liquid-dominated reservoir portion of the hydrothermal system (Goff et al., 1989), and these waters range in TDS (total dissolved solids) from 4500 to 11,000 mg/kg (ppm). Deep fluids are neutral-chloride waters, typical of those found in other volcanic geothermal systems such as Yellowstone and Broadlands, with anomalous concentrations of As, B, Br, Cs, Li, and Rb (Goff et al., 1989). Chemically, the fluids produced from the scientific core holes at Sulphur Springs are similar but have higher TDS (total dissolved solids) and they are isotopically heavier in δD and $\delta^{18}O$ than other reservoir fluids in Valles caldera (Goff et al., 1989). Derivative waters are mixtures of reservoir water and groundwater, and these fluids are encountered along the Jemez fault zone (San Diego Canyon, Fig. 1.2) and in wells drilled in the surrounding plateaus (Goff et al., 1989).

Stable isotope and tritium data on thermal and nonthermal waters in the Valles caldera and the surrounding areas indicate recharge to the hydrothermal system comes from meteoric precipitation and the slow infiltration of cold groundwaters from the resurgent dome, and particularly the basins of the northern and eastern caldera moat (Goff et al., 1985; Vuataz and Goff, 1986). The recharge fluids equilibrate at depths of 2-3 km and temperatures of about 300°C in caldera-fill tuffs and precaldera volcanic rocks (Goff et al., 1989). Thermal waters rise convectively to depths of roughly 500-600 m, then flow laterally crossing the southwestern caldera wall and continue along the Jemez fault above the Precambrian basement rocks (Goff et al., 1989). A vapor zone, which extends from the western flanks of the resurgent dome to the western ring-fracture zone, has developed above a boiling horizon at about 200°C. This boiling horizon defines the upper surface of the liquid-dominated system (Goff et al., 1989)

Chronology of Hydrothermal Events

Hydrothermally altered rocks occur in precaldera volcanic rocks throughout the central and western portions of the Valles caldera and the southeastern flanks of the caldera (Cochiti mining district, Fig. 1.1). Surface mapping, crosscutting relationships of veins and intrusive rocks and K-Ar dates on volcanic units indicate that gold-bearing quartz veins and hydrothermally altered rocks of the Cochiti mining district are about 6 Ma (Wronkiewcz et al., 1984; Gardner et al., 1986). K-Ar ages on hydrothermal illites have constrained this event at 6.5 to 5.6 Ma (WoldeGabriel and Goff, 1989). Mafic and intermediate rocks of the Keres Group in the southern Jemez volcanic field were hydrothermally altered between 10-7 Ma (Gardner et al.,1986).

Chronology of hydrothermal events since formation of the Valles caldera is better constrained than earlier hydrothermal events. Uranium-thorium disequilibrium and U-U dating of past and present travertine deposits at Soda Dam hot springs indicate the presently active hydrothermal system was initiated at about 1 Ma (Goff and Shevenell, 1987), and there are no indications that this hydrothermal activity has ever completely stopped and resumed again in its present configuration (Goff and Shevenell, 1987; Trainer, 1984). Hydrothermal illites from throughout VC-2A core indicate K-Ar dates of 0.83 to 0.66 Ma (WoldeGabriel and Goff, 1989). K-Ar dates from hydrothermal illites of Precambrian to Tertiary rocks from VC-2B core range from 8.1 to 1.0 Ma (WoldeGabriel and Goff, 1991), including a few at about 6.5 Ma suggesting these illites formed as a result of earlier hydrothermal events in the Jemez volcanic field, possibly related to hydrothermal activity associated with mineralization at Cochiti.

Less is known about timing of the vapor horizon development. However, cessation of travertine deposition of the oldest and largest travertine deposits at Soda Dam occurred at about 0.5 Ma (Goff and Shevenell, 1987), and this also coincides with the age of breaching of the southwest caldera wall, draining of intracaldera lakes and deep erosion of the southwestern caldera moat zone (Doell et al., 1968; Hulen and Nielson, 1984). Thus from these inferences, the vapor zone began forming about 0.5 Ma.

GEOLOGIC SETTING

The Jemez Mountains volcanic field contains a suite of basaltic through rhyolitic rocks that were erupted beginning at least 16 Ma, (Smith and Bailey, 1968; Bailey et al., 1969; Smith et al., 1970; Gardner et al., 1986). This volcanic field is localized by the intersection of western boundary faults of the Rio Grande Rift with the Jemez lineament, a northeast-trending regional feature defined by alignment of Cenozoic volcanic centers and major structures such as the Jemez fault zone (Aldrich and Laughlin, 1984) (Fig. 1.1). Calderas of the Valles complex commenced development as early as 1.78 Ma (Spell et al., 1989) when felsic ash-flow tuffs of limited extent began erupting from what is now the western margin of the Valles caldera, and may have formed a small caldera, which is now buried by the present-day caldera complex (Goff et al., 1989). At 1.50 Ma (Spell et al., 1989), a major felsic pyroclastic eruption of at least 300 km^3 resulted in the formation of the Toledo caldera and the deposition of the Otowi Member of the Bandelier Tuff. A second major eruption of felsic ignimbrite at 1.13 Ma (Spell et al., 1989) of similar volume produced the Tshirege Member of the Bandelier Tuff and formed the present Valles caldera. Shortly following collapse, the Valles caldera underwent resurgent doming and emplacement, along the ring fracture system, of a series of 8 rhyolite domes (Fig. 1.2). These domes range in age from the time of caldera formation to about 0.45 Ma (Spell and Kyle, 1989).

Sulphur Springs Hydrothermal System and Core Holes VC-2A and VC-2B

The Sulphur Springs hydrothermal system consists of an acid-sulfate condensation zone (<5 m deep), a vapor zone extending to roughly 240 m depth, a "transitional" layer or cap rock of fractured but tightly sealed rock (240 to 490 m depth), and a liquid-dominated zone (>490 m deep) (Goff et al., 1989)(Fig. 2.1). Acid-sulfate type waters comprise the spring fluids (Goff et al., 1985; Charles et al., 1986) - no deep fluids discharge. Outside the main hot spring area, the surface waters are cold (average 5°C), and there is a lack of siliceous sinter in the Sulphur Springs area. Deep reservoir fluids were encountered by drilling at Sulphur Springs beneath the acid

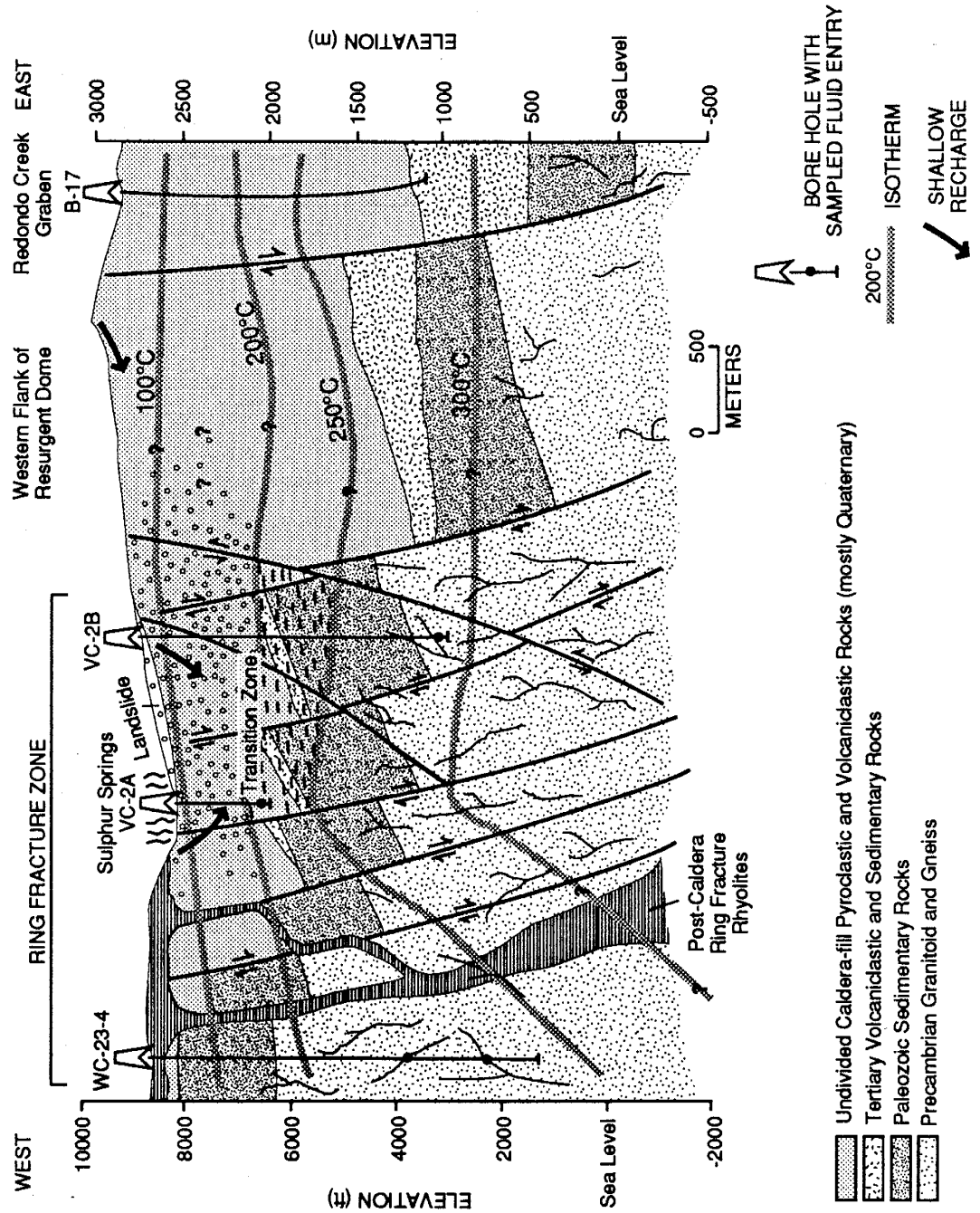

Fig. 2.1 Idealized cross section of the Sulphur Springs hydrothermal area showing configuration of the system based on drill hole data and temperature logs (From Gardner et al., 1989).

sulfate/vapor-dominated zone. In this study, the hydrothermal system is divided into shallow (depths <700 m) and deep systems (depths >700 m). This division is based on the last occurrence of major veins in the volcanic rocks of Sulphur Springs and the paucity of veins in the siliciclastic units. Vein density does not increase again until the Pennsylvanian Madera Limestone.

Core holes VC-2A and VC-2B, which were drilled at Sulphur Springs in 1986 and 1988 (Goff et al., 1987; Gardner et al., 1989), respectively, and are located in the western ring fracture zone of the caldera (Fig. 1.2). VC-2A was completed to a depth of 528 m and has bottom hole temperature of 212°C, while VC-2B was drilled to 1762 m and has a bottom hole temperature of 295°C. Dissolved constituents are dominantly NaCl solutions, with total concentrations about 7000 and 9000 ppm, respectively. Water levels in VC-2A and VC-2B are at 152 m and 204 m, respectively, below the present land surafce. Fluid analyzed from the Baca wells in the Redondo Creek area have concentrations that range from 3000 to 5000 ppm and bottom hole temperatures of 220 to 340°C (Goff et al., 1985; Vuataz and Goff, 1988).

The stratigraphy of the Sulphur Springs area based on core retreived from VC-2A and VC-2B, consists of Quaternary caldera-fill ignimbrite and volcaniclastic units, Tertiary Santa Fe Group sandstones, Permian Yeso Formation (sandstones), Permian Abo Formation (mudstones and sandstones), Pennsylvanian Madera Limestone, Pennsylvanian Sandia Formation (sandstones), and biotite quartz monzonite of Precambrian age (See Hulen and Gardner, 1989 or Hulen et al., 1989 for details on stratigraphy). The entire stratigraphic sequence penetrated by the core holes has undergone varying degrees of fracturing of both tectonic and hydrothermal origin, with intensity of fracturing strongly dependent on rock type and depth in the Sulphur Springs system (Hulen et al., 1989); however, fracturing is strongest in the upper 600 m, and it is above this depth that hydrothermal breccias are most concentrated. The fluid production zone in VC-2B at 1755 m is a hydrothermal breccia. An 80 m (402.5 to 481.4 m) zone in VC-2B is extensively but moderately broken by hydraulic fracture networks (crackle breccia) and hydrothermal breccias (Hulen and Gardner, 1989).

VEIN MINERALIZATION

Vein mineralization is typically scant throughout both core holes, and vein fillings range from complete, to partial fillings with abundant open spaces, to fractured rock with sparse secondary mineralization. A representative fracture is one which is coated with one mineral phase making it difficult to construct a detailed paragenesis for Sulphur Springs; however, several veins containing multiple vein-filling events are present, and a detailed paragenesis can be worked out for that particular vein. Comparing detailed paragenetic studies with textural relations from veins with one or two vein-filling minerals allowed construction of a generalized paragenetic diagram for VC-2A and VC-2B. Furthermore, as will be shown later, the fluid inclusion data help constrain the paragenesis. Veins of Sulphur Springs are characteristically narrow, ranging in width from 0.5 to 20 mm, but one vein in VC-2B at 586.6 m is 0.25 m wide.

Twenty-four gangue and ore minerals have been identified in the vein fillings of Sulphur Springs (Fig. 2.2). In order of approximate decreasing volumetric abundance within a particular vein, these minerals are quartz (5-100%), calcite (2-100%), fluorite (1-100%), illite/illite-smectite (<1-80%), (1-30%), molybdenite, (1-25%), anhydrite (<1-20%), hematite (<1-10%), sphalerite (<1-10%), pyrite (<1-5%), rhodochrosite (<1-5%), and trace amounts of chalcopyrite, galena, pyrargyrite, stibnite, chalcocite, adularia, albite, kaolinite, wairakite, Fe-dolomite, barite, and a bismuth telluride (tellurobismuth?) (Musgrave and Hulen, 1989). Most vein minerals form fine- to coarse-grained intergrowths of subhedral to euhedral grains. Calcite exhibits massive and bladed or "snowflake" textures, and the bladed habit of calcite is noted to a depth of 1679.3 m. Bladed calcite at this depth is after quartz. Small (0.5 to 1 mm) epitaxial cappings of euhedral sulfides are present on the terminations of quartz and calcite.

Early mineralization in VC-2A is characterized by euhedral quartz, molybdenite, illite, pyrite, sphalerite, and fluorite. Chlorite and early rhodochrosite of this stage are found deeper in the corehole, below the molybdenite zone. Molybdenite ranges from a well crystallized form to a poorly crystalline form. Later mineralization is characterized by euhedral to subhedral quartz and calcite, sphalerite, pyrite, galena, chalcopyrite, and late fluorite and rhodochrosite. Sphalerite color (in thin

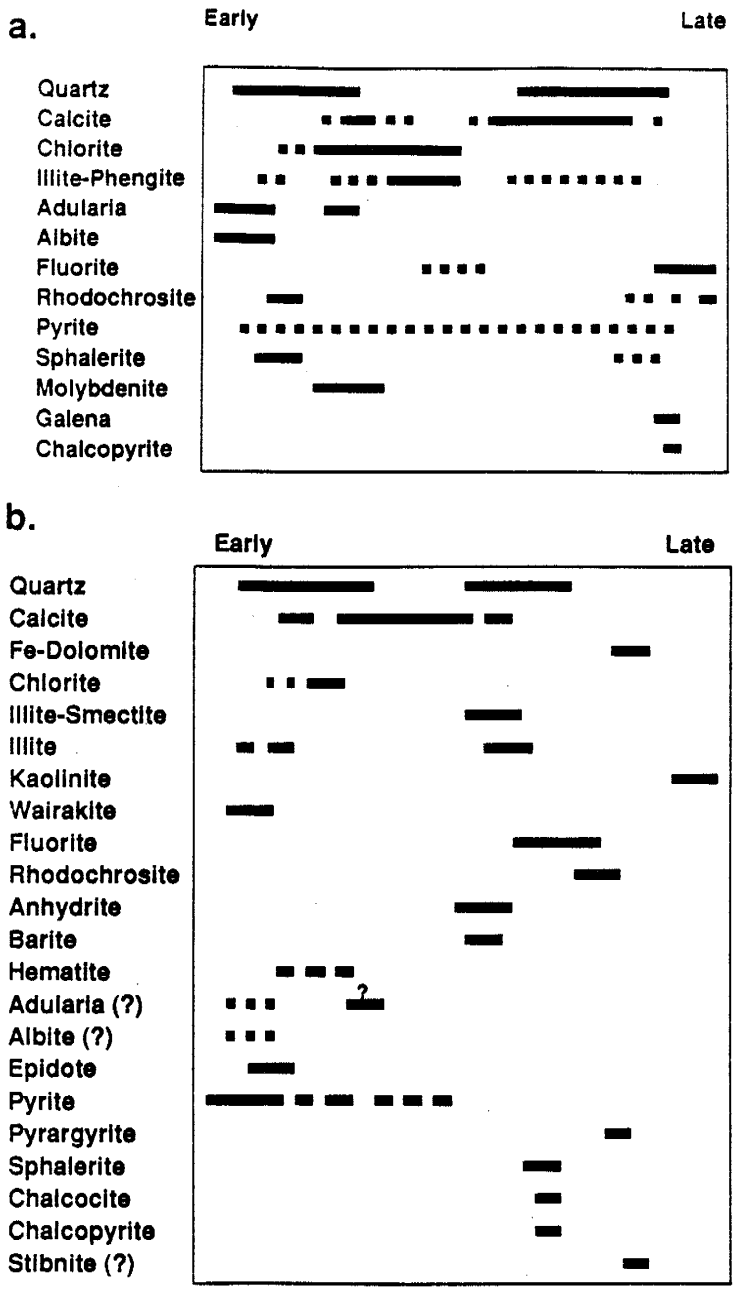

Figure 2.2 a. Generalized paragenetic diagram, VC-2A. b. Generalized paragenetic diagram, VC-2B. (From Musgrave and Hulen, 1989).

section) ranges from colorless to honey yellow, without color zonation. Potassium-argon dates on hydrothermal illites from the molybdenite zone indicate a minimum age of formation of about 0.66 Ma for the molybdenite mineralization (WoldeGabriel and Goff, 1989).

Although drilled only 600 m from VC-2A, VC-2B penetrated none of the unusual molybdenite mineralization found in the shallower corehole. The paragenesis of the gangue minerals is similar to VC-2A, but the ore minerals appear to be a late stage event (Fig. 2.2). There are at least 2 examples of bladed calcite chlorite (1-30%), epidote deposition followed by fluorite at depths of 403.1 and 665.6 m. Some of this calcite is intergrown with the fluorite. In VC-2B, however, the ore minerals (although in trace amounts) show a distinct vertical zonation; stibnite and pyrargyrite occur at higher elevations with base metal sulfides confined to deeper levels.

OTHER FLUID INCLUSION STUDIES

Previous fluid inclusion studies in the Valles caldera and vicinity include the work of Gonzales (1988), Hulen and Nielson (1988), Hulen et al. (1987, 1989), Musgrave and Norman (1988, 1989, 1990a and 1990b), Sasada (1987, 1988 and 1989), Sasada and Goff (1989), and Wronkiewicz et al. (1984). Wronkiewicz et al. (1984) demonstrated in their fluid inclusion investigation of the Cochiti mining district (Fig. 1.1) that the veins formed at temperatures of 195-375°C and salinities of 0-4 equiv. wt.% NaCl. Sasada (1989) has indicated that there has been a recent increase in temperature at the Fenton Hill hot dry rock geothermal test site just west of the caldera margin (Fig. 1.2) The investigations by Gonzales (1988), Hulen et al. (1987), and Sasada (1987) and Sasada and Goff (1989) suggest that mineralization at Sulphur Springs took place as a result of deposition from dilute fluids at temperatures around 200°C. Sasada's (1988) data from VC-1 inclusions indicate a deep paleofluid had salinities of up to 5 equiv wt.% NaCl., a maximum temperature of 275°C, a possible $CaCl_2$ component, and at least 0.35 wt.% CO_2, while a younger, shallow fluid (above 723 m) had a maximum temperature of 220°C and maximum salinity of 2 equiv. wt.% NaCl. In their investigation of hydrothermal breccias in VC-1, Hulen and Nielson (1988) also suggested a two-fluid model, noting salinities as high as 23.1 equiv. wt. % NaCl.

FLUID INCLUSIONS

Approximately 90 samples as thick sections plus numerous cleavage chips were prepared for fluid inclusion observation and analysis. Samples were collected from veins which range in width from 1 mm to as wide as 0.25 m, although the veins are typically narrow, averaging 2-4 mm. Microthermometric analyses were made on an SGE-adapted USGS gas flow heating-freezing stage that was calibrated by Los Alamos National Laboratory's standards and calibration group; melting points of a series of organic and inorganic standards were also used, and accuracy for the temperature range -10°C to 400°C is ±0.2°C. Measurements were made on nearly 900 inclusions in quartz, calcite, sphalerite, fluorite, and epidote, with all freezing runs conducted prior to heating runs (Table 2.1). Sizes of inclusions measured range from 3 to 70 μm, with most between 8 and 15 μm. Much of the quartz is clear prismatic crystals thus making it ideal for inclusion study. Inclusion density in quartz ranges from almost zero to about 10 volume percent. Calcite is usually transparent enough to permit inclusion petrography, however, some calcite is too turbid to enable study of the inclusions. Inclusion density in calcite and fluorite ranges from a few to 10 volume percent and higher in fluorite (≈20%). Sphalerite is devoid of or contained ≤1 volume percent fluid inclusions. Epidote is typically devoid of inclusions.

Criteria for distinguishing primary, pseudosecondary and secondary inclusions follow those outlined by Roedder (1984). Fluid inclusions in calcite and fluorite are predominantly of secondary origin. Many of the inclusions in quartz and calcite had "tails" suggesting necking-down had occurred, and these inclusions were not measured.

Fluid inclusions in the Sulphur Springs samples can be grouped into three types based on the degree of filling (F) by liquid at room temperature. Type 1 inclusions are liquid-rich (F >70%) and include all primary inclusions in sphalerite, most primary and secondary inclusions in fluorite and most primary inclusions in quartz and calcite. Type 2 inclusions are vapor-rich; most have F <10% but a lesser number have F=10 to 30%. These commonly occur with liquid-rich inclusions in the same growth zone; however, the high volume of vapor precluded measurement of Th. Type

Table 2.1 Summary of all inclusion measurements, Sulphur Springs hydrothermal system. P=Primary, PS=Pseudosecondary, S=Secondary, QTZ=Quartz, CC=Calcite, EPI=Epidote, FLR=Fluorite, SL=Sphalerite. Values in parentheses denote number of measurements.

Sample	Depth (m)	Mineral	Type	Th, degrees C	Tm_{ICE}, degrees C	Salinity, equiv. wt.% NaCl
VC2A 96	29.27	FLR	P	154.9-196.8(39)	-0.15- -2.40	0.26-4.08(32)
VC2A 96	29.27	FLR	S	133.5-143.7(3)		
VC2A 107	32.62	QTZ	P	198.4-291.6(37)	-1.30- -3.40	2.30-5.50(9)
VC2A 173	52.74	QTZ	P	197.1-286.4(28)	-0.90- -2.20	1.50-3.70(17)
VC2A 192	58.54	QTZ	P	201.2-258.9(32)	-1.30- -2.20	2.20-3.70(24)
VC2A 277	84.45	QTZ	P	183.9-277.0(26)	-0.02- -0.10	0.08-0.35(11)
VC2A 277	84.45	QTZ	S	175.1-165.4(2)	-0.10- -0.15	0.17-0.26(2)
VC2A 313	95.12	QTZ	P	198.4-294.6(20)	0.00- -0.20	0.00-0.40(6)
VC2A 425	129.57	SL	P	217.6		
VC2A 425	129.57	QTZ	P	192.7-276.5(38)	-0.15- -2.35	0.26-3.90(21)
VC2A 555	169.21	FLR	P	155.9-202.3(12)	0.00- -0.05	0.00-0.08(2)
VC2A 555	169.21	FLR	S	157.1-182.4(21)	0.00- -1.08	0.00-1.80(6)
VC2A 645	196.65	FLR	P	194.4-197.5(6)	-0.50- -0.55	0.87-0.98(6)
VC2A 645	196.65	FLR	S	161.3-180.2(5)	-0.20- -0.50	0.35-0.87(15)
VC2A 1108	337.80	FLR	P	180.5-210.6(27)	0.00- -0.45	0.00-0.78(23)
VC2A 1108	337.80	FLR	S	150.6-182.9(19)	0.00	0.00(1)
VC2A 1137	346.65	CC	P	213.9-314.8(16)	0.00- -0.60	0.00-1.05(9)
VC2A 1485	452.74	CC	P	199.2-228.3(17)	-0.30- -0.45	0.52-0.78(6)
VC2A 1485	452.74	SL	P	224.6-319.4(14)	-0.20- -0.90	0.35-1.56(10)
VC2A 1485	452.74	QTZ	P	209.0-294.7(23)	-0.20- -1.00	0.35-1.73(21)
VC2B 656	200.00	CC	P	213.9-218.7(18)	-0.10- -0.20	0.17-0.35(14)
VC2B 757	230.79	QTZ	P	198.0-269.6(38)	0.00- -0.25	0.00-0.44(16)
VC2B 932	284.15	QTZ	P, S	209.9-262.8(33)	0.00- -0.05	0.00-0.04(19)
VC2B 1246	379.88	FLR	P	188.2-212.0(11)	-0.20- -0.40	0.35-0.7(8)
VC2B 1246	379.88	FLR	S	148.6-181.4(59)	-0.10- -0.20	0.17-0.35(11)
VC2B 1322	403.05	FLR	P	219.0		
VC2B 1322	403.05	FLR	S	155.9-187.1(21)	-0.10- -0.20	0.17-0.35(9)
VC2B 2183	665.55	CC	P	215.5-236.2(21)	-0.20- -0.30	0.35-0.53(9)
VC2B 2183	665.55	FLR	P	184.4-193.8(14)	-0.40	0.70(1)
VC2B 2183	665.55	FLR	S	174.2-179.9(14)	-0.40- -0.50	0.70-0.87(6)
VC2B 3017	919.82	CC	P	216.8-226.4(31)	0.00- -0.25	0.00-0.44(13)
VC2B 4565	1391.77	CC	P	258.6-313.0(36)	-1.70 -3.10	2.88-5.10(12)
VC2B 4755	1449.70	QTZ	P	266.7-329.6(37)	-1.00- -2.00	1.89-3.37(18)
VC2B 5237	1596.65	EPI	P	292.4		
VC2B 5237	1596.65	QTZ	P, PS	269.5-334.4(31)	-1.00- -2.50	1.89-4.07(23)
VC2B 5533	1686.89	QTZ	P	238.1-302.0(41)	-0.35- -1.50	0.58-2.5(17)
VC2B 5661	1725.91	FLR	P, PS	232.4-319.0(23)	-0.55- -1.03	0.91-1.70(7)
VC2B 5661	1725.91	CC	P	287.1-308.4(5)		

2 inclusions occur in quartz, calcite, and fluorite, but are most common in quartz and calcite, which have been observed to a depth of 1450 m. The third type has F=100%. Only 2 Type 3 inclusions were identified in fluorite from a depth of 169 m, and no vapor bubble nucleated upon supercooling. A fourth type was identified, which is similar to type 1 with a small, apparently isotropic mineral, which appears to be an accidental crystal of fluorite. Type 3 and 4 inclusions were observed only in fluorite. Liquid CO_2 or clathrate melting was not observed in this study nor have these properties been observed in the pervious fluid inclusion studies (e.g. Hulen and Nielson, 1988; Sasada, 1987, 1988; Sasada and Goff, 1989).

Microthermometry

Primary fluid inclusions show an increase of homogenization temperature (T_h) with depth (Fig 2.3). T_h measured in early quartz, calcite, and sphalerite from depths <700 m of the Sulphur Springs system cluster between 180°C and 250°C, whereas T_h values for inclusions from depths greater than 700 m are mostly between 245°C and 334°C (Fig. 2.3 and Table 2.1). Primary inclusions in late fluorite from depths <700 m range from 175 to 219°C, whereas primary inclusions in fluorite from below 1558 m in VC-2B have T_h values of 305°C ±15°C (Fig 2.4). Base metal deposition at 452 m in VC-2A occurred at temperatures that range from 230-240°C, based on primary inclusions in sphalerite and molybdenite deposited at 220-230°C from T_h data for quartz intergrown with molybdenite. One T_h determination in the mostly inclusion-free sphalerite at 129.6 m in VC-2A is 218°C. Only a few secondary fluid inclusions in quartz were measured in this study. However, Sasada and Goff (1989) measured mostly secondary inclusions in quartz, which indicate the average T_h for these secondary inclusions is 195°C. This average T_h also is the average T_h for primary inclusions in fluorite. Secondary inclusions in fluorite range from 134-183°C.

Equivalent salinities calculated from Tm_{ICE} (Brown and Lamb, 1989) range from 0 to 5.5 equiv. wt% NaCl with more saline values generally associated with inclusions from greater depths. Inclusions in all phases studied from depths <700 m have salinities mainly <0.7 equiv. wt.% NaCl, while data from >700 m range in salinity from 0 to 5.1 equiv. wt% NaCl (Fig 2.4). One group of

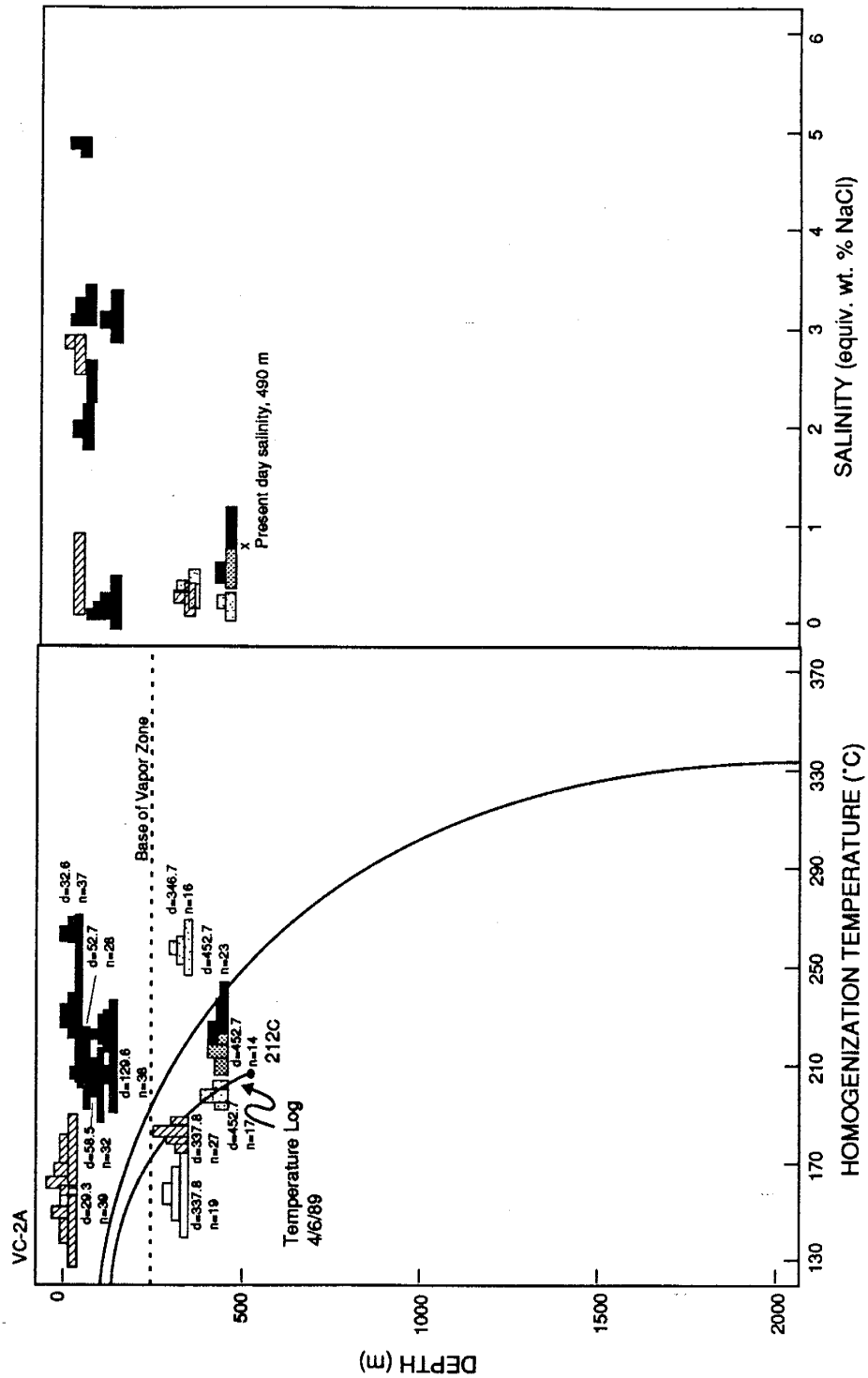

Figure 2.3 a. Temperature-salinity versus depth for VC-2A. Open histograms are secondary inclusions in fluorite, diagonal lines are primary inclusions in fluorite, stippled pattern is primary inclusions in calcite, and filled is primary inclusions in quartz. Plotted on figure is temperature log with current bottom hole temperature, reference hydrostatic boiling-point curves (pure water) set to the present land surface, and the present fluid salinity.

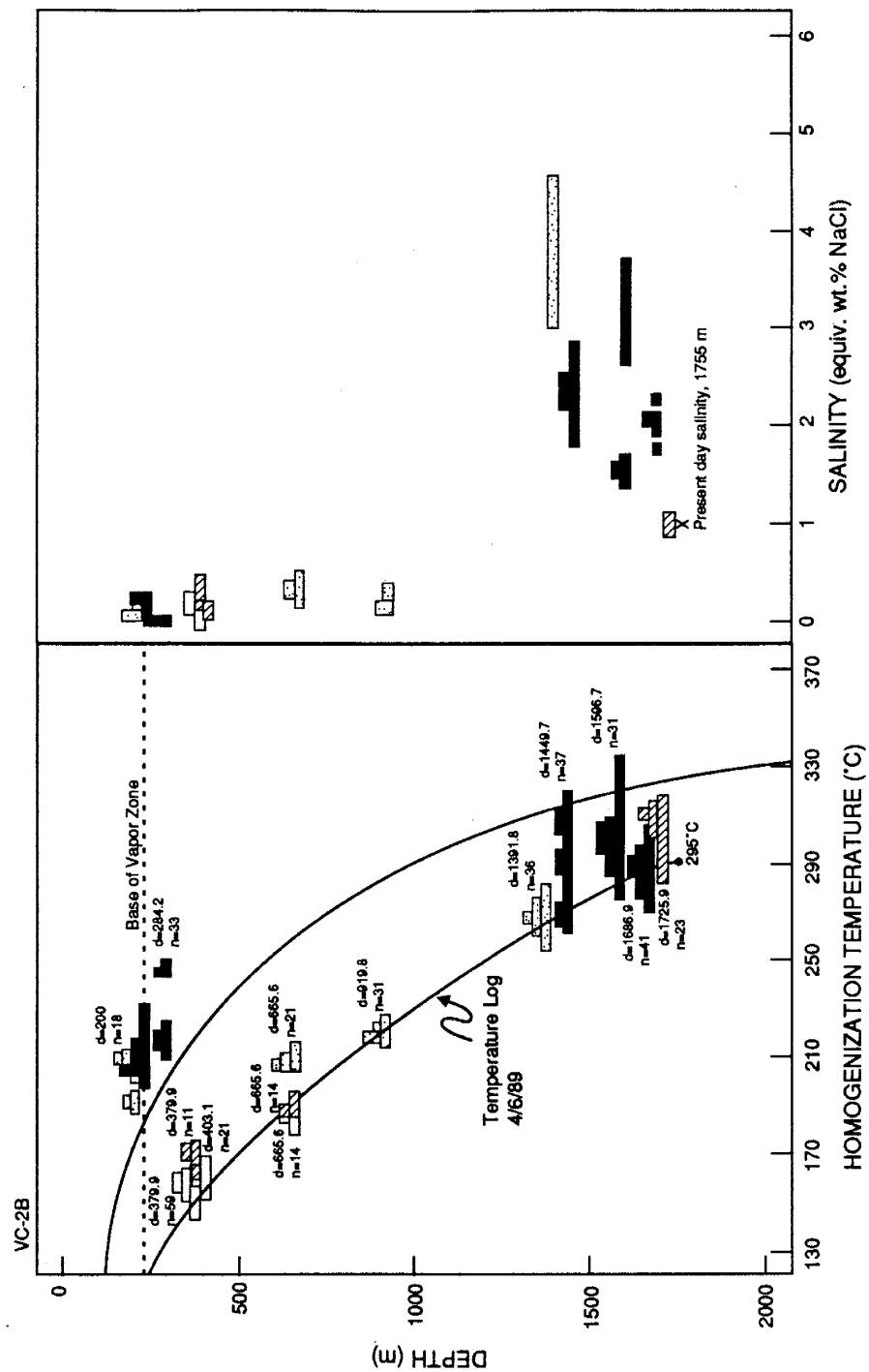

Figure 2.3 b. Temperature-salinity versus depth for VC-2B. Open histograms are secondary inclusions in fluorite, diagonal lines are primary inclusions in fluorite, stippled pattern is primary inclusions in calcite, and filled is primary inclusions in quartz. Plotted on figure is temperature log with current bottom hole temperature, reference hydrostatic boiling-point curves (pure water) set to the present land surface, and the present fluid salinity.

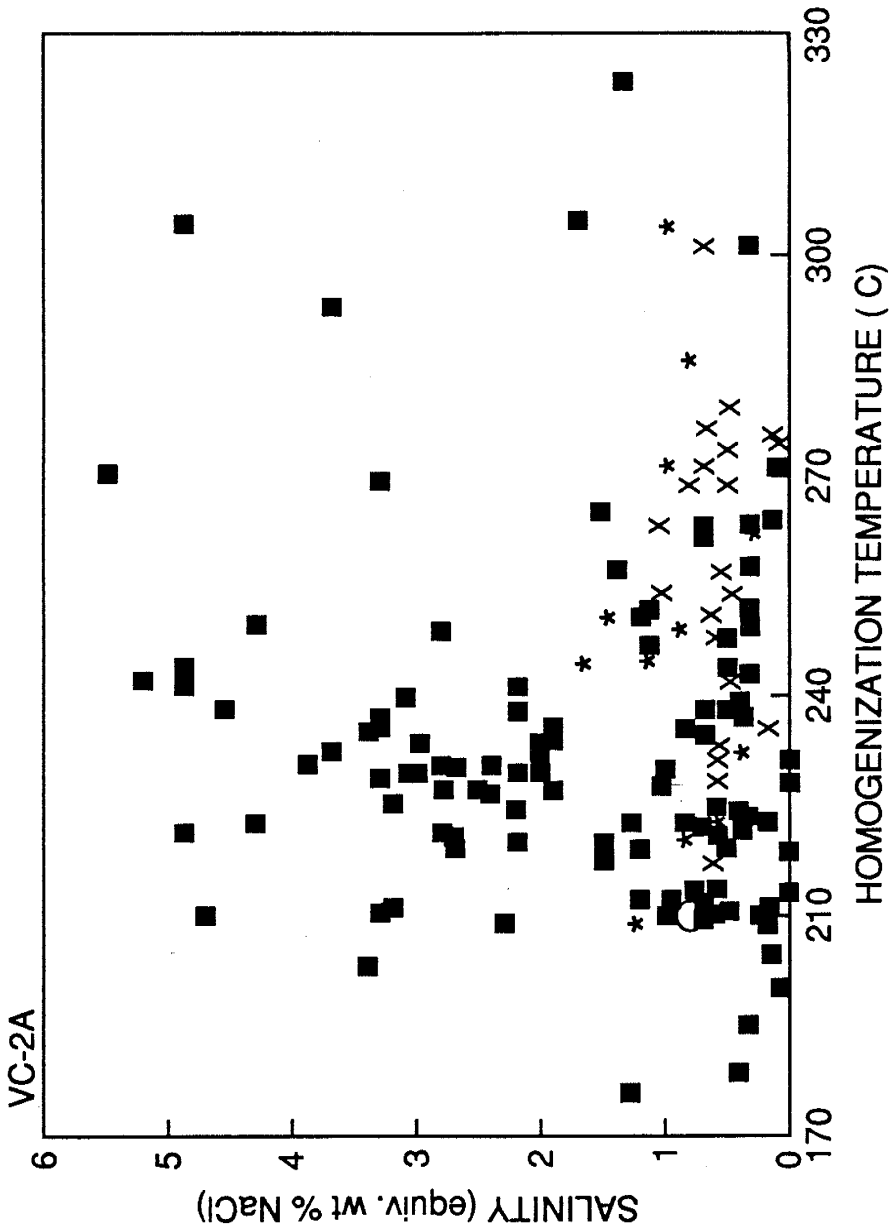

Figure 2.4 a. Homogenization temperature versus salinity for primary fluid inclusions from VC-2A. Squares = quartz, asterisks = sphalerite, Xs = calcite, open circle = present day fluid.

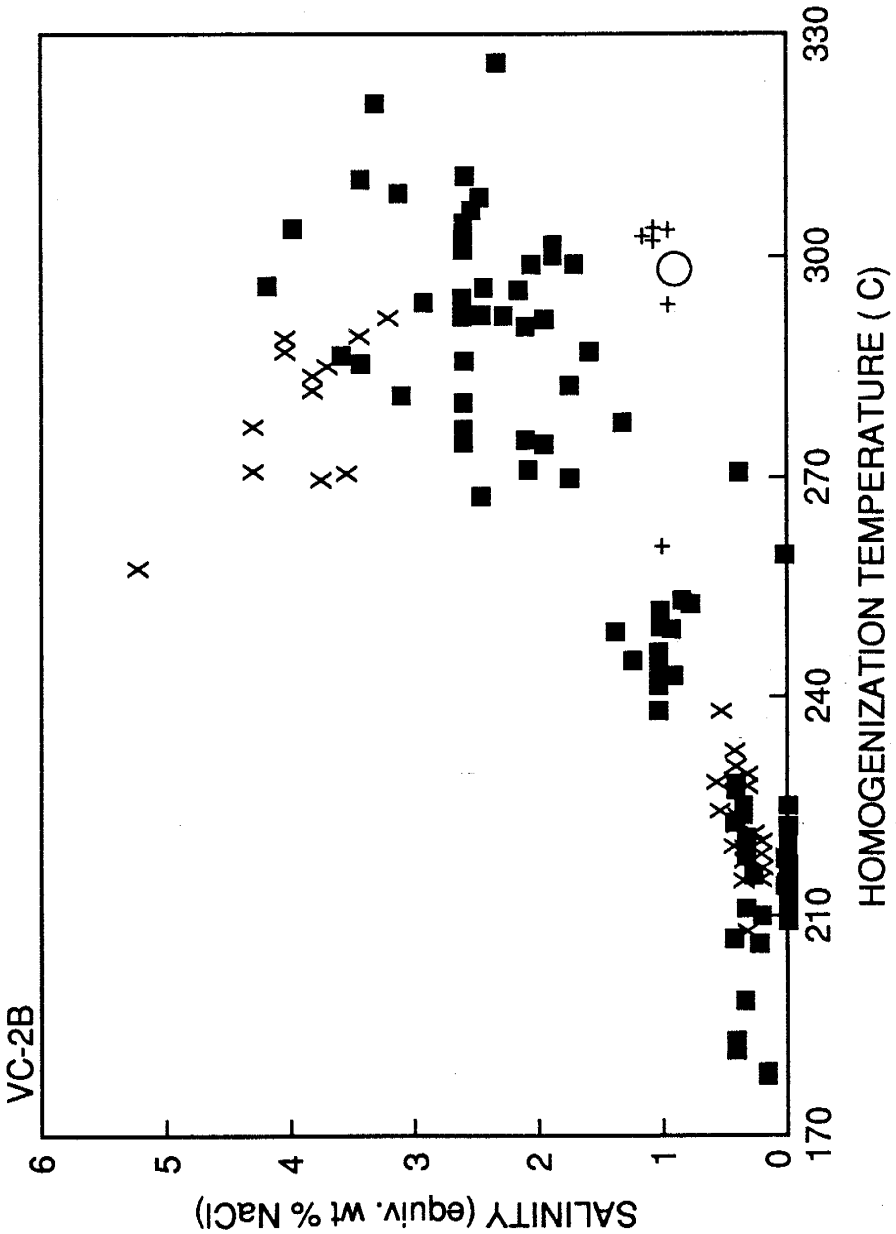

Figure 2.4 b. Homogenization temperature versus salinity for primary fluid inclusions from VC-2B. Squares = quartz, asterisks = sphalerite, Xs = calcite, crosses = late fluorite, open circle = present day fluid.

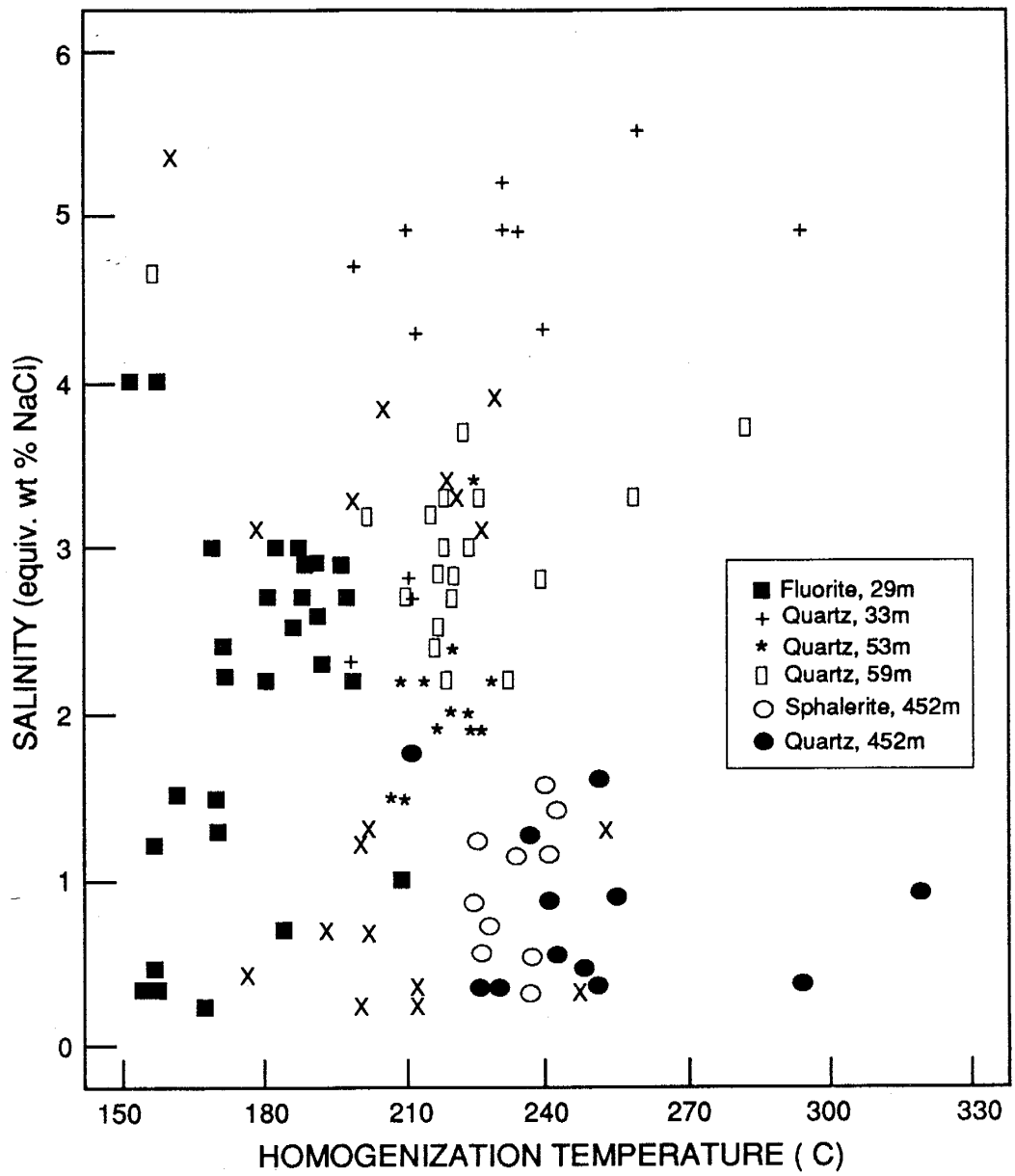

Figure 2.5 Homogenization temperature versus salinity for early mineralization for primary fluid inclusions in fluorite, sphalerite and quartz, VC-2A. There is a clustering together of data from each sample location, e.g samples from 29 m, 59 m, and 129 m. There are no clear boiling or mixing trends; therefore, the data are more suggestive of pulses or injection of fluids into fractures; see text for further discussion. Note scale change for Th.

inclusions in quartz and fluorite from VC-2A has salinities between 0 and 1.4 equiv. wt.% NaCl while the other group ranges between 1.5 and 5.5 equiv. wt.% NaCl (Fig 2.5). Salinity data for primary inclusions in fluorite have two groupings similar to the quartz data (Fig. 2.5), whereas data for secondary inclusions fall into one group.

Inclusions in late stage minerals, some quartz, calcite and fluorite, have T_h and salinity values similar to present fluids in temperature and composition. In contrast, early-formed minerals (quartz, calcite, sphalerite, epidote, fluorite) have higher T_h values than present fluids and salinities that range from concentration levels similar to present geothermal waters to values nearly a magnitude higher. For example, primary inclusions in early quartz and sphalerite from VC-2A and early quartz and calcite from VC-2B for depths <700 m have T_h on average 30-40°C higher than primary inclusions in late stage fluorite. Fluid inclusions in early quartz, calcite and epidote in VC-2B for depths between 1449 and 1686 m have T_h 5-15°C higher than late stage fluorite at this depth. Salinities from the early minerals of the shallow system average 0.3 equiv. wt.% NaCl higher than the late stage fluorite. The salinity data of the early minerals in the deep system average 1.3 equiv. wt.% NaCl higher than the late stage fluorite and the present day fluid.

When early VC-2A mineralization is plotted for T_h versus salinity each sample, for the most part, plots as an individual grouping with little or no trend from high salinity and high T_h to lower salinity and lower T_h (Fig. 2.5). Whereas early VC-2B mineralization displays a progression from high salinity and high T_h values to lower values (Fig. 2.4b), and it is also related to depth (Fig. 2.3).

Two samples at depths of 29.3 (VC2A 96) and 129.6 (VC-2A 425) m in VC-2A are of interest because they reveal changes in fluid temperature and/or composition over the period in which the crystal grew (Fig. 2.6a). Heating-freezing results for fluorite from VC-2A 96 indicate the presence of two chemically distinct fluids which, for crystal centers, range in salinity from 2.2 to 4.1 equiv wt.% NaCl and have T_h ranging from 151 to 190°C. Inclusions along rims of the crystals have salinites which range between 0.26 to 1.3 equiv. wt.% NaCl and T_h values of 155 to 183°C. There is deposition of quartz which preceeded fluorite in this sample, but the crystals are small and apparently inclusion free. Heating-freezing results for one quartz crystal from VC-2A 425 show

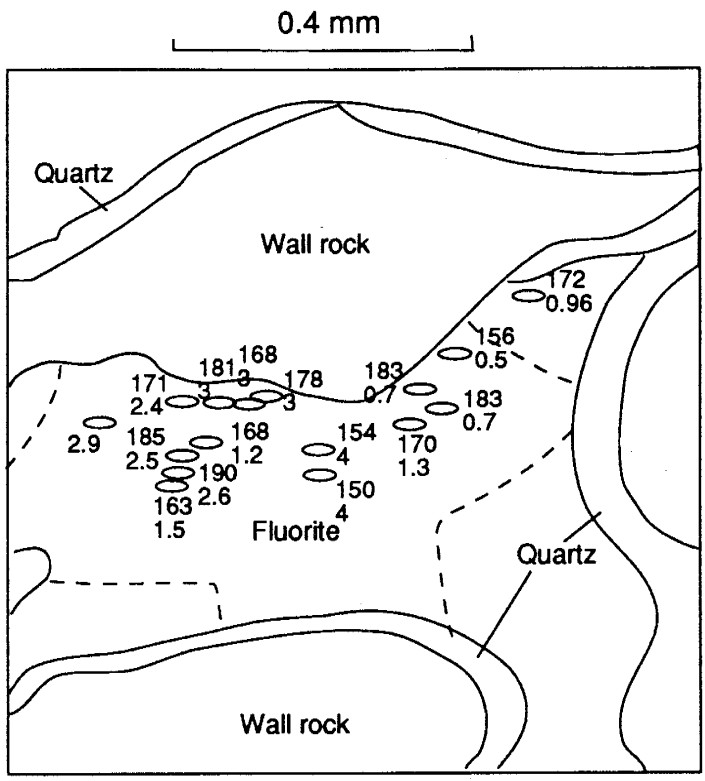

Figure 2.6 a. Sketch of fluorite crystals VC-2A 96 showing the distribution of Th and salinity measurements on primary inclusions.

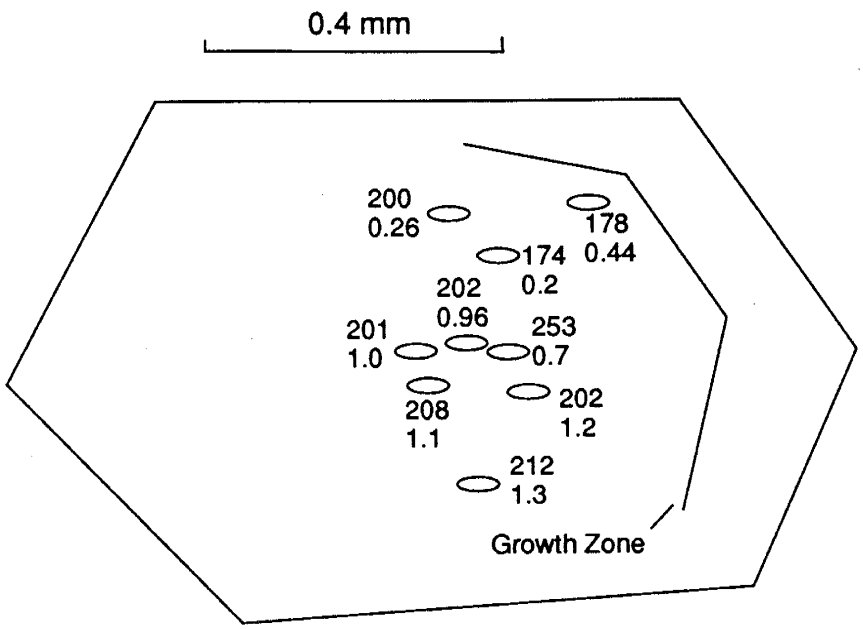

Figure 2.6 b. Sketch of a quartz crystal from VC-2A 425 showing the distribution of Th and salinity measurements on primary inclusions.

changes in temperature and composition from core to rim (Fig. 2.6b). Salinity for inclusions at the crystal center range between 0.96 to 1.3 equiv. wt.% NaCl and have T_h values from 176 to 253°C, whereas inclusions from the rim have salinity values between 0.26 to 0.44 equiv. wt.% NaCl and T_h from 173 to 200°C. It is interesting to note that these salinity and tempertaure ranges are similar to those for inclusions in the rims of fluorite from 29.3 m. Other quartz crytals at 129.6 m show similar trends from core to rim in temperature and salinity, but salinities even higher are noted, up to 4 equiv. wt.% NaCl. However, other crystals in this sample have a more random distribution of salinity values.

A single vein sample from a depth of 452 m in VC-2A allows evaluation of temperature and compositional changes through the paragenetic sequence (Fig. 2.7). Fluid inclusions in quartz and sphalerite have T_h values ranging from 209-294°C and 225-319°C, respectively. T_h greater than about 270°C for these minerals is considered spurious and due to trapping of two-phase inclusions during boiling or in the case of sphalerite stretching. Salinity values for the quartz and sphalerite range between 0.35-1.73 and 0.35-1.53, respectively. T_h from inclusions in calcite cluster around 210°C and salinities are about 0.7 equiv. wt.% NaCl. The calcite data are similar to present day conditions at this depth.

DISCUSSION OF MICROTHERMOMETRIC DATA

Constraints on Paragenesis

One of the problems pointed out in the section on vein mineralogy was that of creating a detailed paragenesis from mineralization that is mostly scanty. The fluid inclusion data presented place additional constraints on relative timimg of mineralization when only one mineral phase is present in a fracture because samples which have minerals that have Th and salinity values the same as the present day fluid temperatures and composition represent mineralization that is currently taking place or is from the recent past (Fig. 2.3). This would constitute late mineralization and includes quartz, calcite, and fluorite. Mineralization that departs in temperature and composition

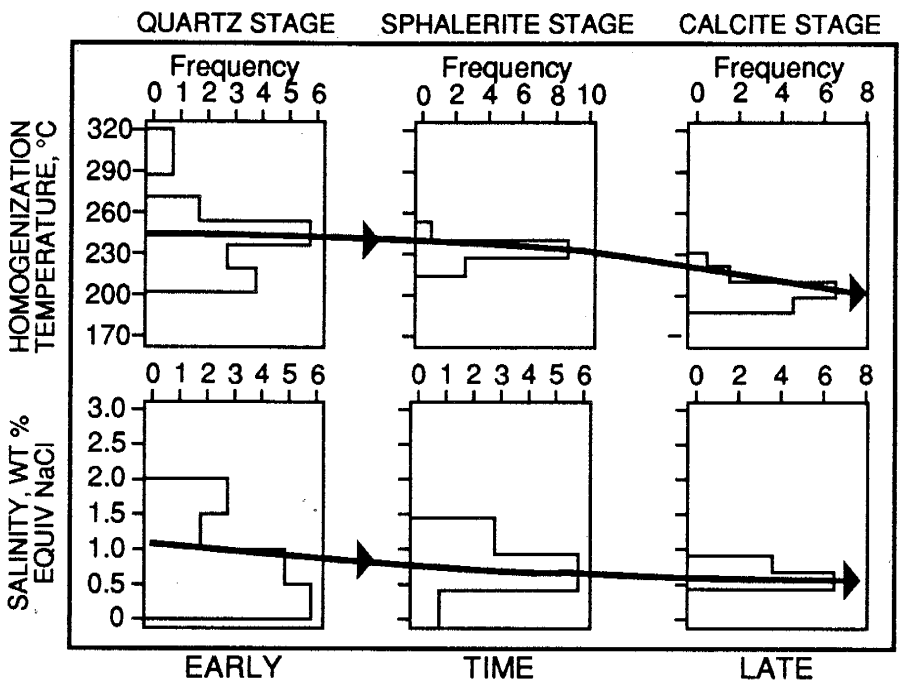

Figure 2.7 Temporal variation in temperature and salinity of an individual sample from 452 m, VC-2A. Quartz was deposited first, followed by sphalerite and finally, by calcite. Calcite data are similar to present day conditions at this depth. Line through data is to simply illustrate trend in data with time.

(e.g. higher temperature and/or salinity) from current conditions would be part of early mineralization. This would include quartz, calcite, fluorite, sphalerite and epidote.

Fluid Interaction

Clustering of particular samples of early mineralization from VC-2A suggests that fluids flowed as discrete pulses with little mixing as might be expected of fluids having different compositions (and density) (Fig. 2.5). However, some crystals in samples VC-2A 96 and VC-2A 425 do exhibit changes in composition and temperature during the growth of the crystal (Fig. 2.6). On the other hand, there are crystals in these samples which display random distribution in salinity and temperature values. This indicates that some deposition was the result of mixing of fluids, while other crystals were the result of another depositional mechanism, decompression? Quartz (VC-2A 1485QTZ) and sphalerite (VC-2A 1485SL) from 452 m in VC-2A show no evidence of mixing. Early quartz from VC-2B is suggestive of mixing (Fig. 2.4b) of relatively cooler, dilute fluids with hotter, more saline fluids from depth. A caveat to this discussion is that it is assumed in establishing whether mixing has or has not taken place is that the fluids were trapped in minerals that are approximately coveal. When only one mineral phase generally occupies a fracture and the same mineral occupies another fracture 100 m elsewhere in the system, it is assumed (and possibly erroneously) based on texture that thay are of the same period of fluid flow. As explained above, the microthermometric data may have helped clarify this dilemma.

Evidence for Boiling

Vapor- and liquid-rich inclusions coexisting in a crystal within the same growth plane, and which have similar T_h values (Bodnar et al., 1985) is good evidence for boiling. Although T_h could not be measured in Valles vapor-filled inclusions, several lines of evidence, in addition to the coexistence of vapor-rich and liquid-dominant inclusions, indicate that boiling of deep reservoir fluids has taken place at Sulphur Springs in the past. Subsurface boiling zones in active hydrothermal systems have also been identified on the basis of mineral assemblages (adularia) and textures

(bladed calcite) (Browne and Ellis, 1970; Keith et al., 1978; Tulloch, 1982). Hydrothermal breccias themselves are not evidence for boiling, but the hydraulic fracturing attending breccia development results in fluid decompression which in turn may lead to boiling (Sillitoe, 1985). The large variation in sulfur isotopes reported by McKibben and Eldridge (1990) in sulfides from VC-2A may be explained by boiling. Changes in fluid pH, fO_2, and ionic strength can bring about sulfur isotopic variation (Ohmoto, 1972), and boiling is an effective means to cause changes in fluid composition (Drummond and Ohmoto, 1985; Spycher and Reed, 1989).

The presence of coexisting liquid- and vapor-rich inclusions indicates that boiling occurred as deep as 1450 m relative to the present ground surface. However, bladed calcite at depths around 1680 m in VC-2B is suggestive of boiling conditions, and there are occasional hydrothermal breccias. Boiling of the fluid could have occurred at this depth during decompression of the fluid in response to formation of these breccias. Furthermore, speciation calculations based on the fluid inclusion gas data (see Part III, Fluid Inclusion Gas Chemistry), mineral stabilities, and synthetic fluid inclusions grown in the bottom of VC-2B indicate that the CO_2 content in the paleo-fluid and the present reservoir fluid is at least 0.5 mole percent (Musgrave et al., 1990; Charles et al., 1990; Bethke et al., 1990). A 300°C, 1.0 wt.% NaCl aqueous fluid containing 0.5 mole % CO_2 would boil at about 1350 m. Clearly, boiling could have occurred to depths 1680 m based on these observations, and this is not unreasonably deep, considering that drilling to over 2500 m depth at Broadlands has not extended beneath the boiling zone (Henley et al., 1984). Data on the existence of vapor-rich inclusions in a variety of minerals (both early and late), deposition of paragentically later bladed calcite, and the intergrown nature of some bladed calcite with fluorite suggests boiling has continued throughout the life of the system.

Estimation of Pressure

Evidence of boiling conditions throughout much of the history of the Sulphur Springs hydrothermal system permits the estimation of fluid pressure. The T_h represents the temperature of inclusion formation (trapping temperature), obviating the need for pressure corrections to the fluid

inclusion data. Pressure for recent mineralization can be estimated from using representative values of 200°C and 0.7 equiv. wt.% NaCl (an average value for recent mineralization) for depths <700 m and 300°C and 1.2 equiv. wt.% NaCl for depths >700 m. Assuming the fluids are only H_2O-NaCl, pressure determinations are 16 bars for depths <700 m and 85 bars for depths >700 m, respectively. Representative values for early mineralization at depths <700 m are 220°C, 3.0 equiv. wt.% NaCl and depths >700 m 300°C, 5.0 equiv. wt.% NaCl), and the pressure determinations are 23 and 83 bars, respectively. Therefore, these values bracket the pressure determinations (gas free basis) for other primary fluid inclusions generations with evidence of boiling.

Temperature Gradients

Hydrothermal fluids in the upper most portions of the earth's crust (<2 km) are generally under hydrostatic pressure conditions (Hedenquist and Henley, 1985; Hedenquist, 1991) or more acurately hydrodynamic pressure conditions (Hedenquist and Henley, 1985). As a result boiling is a common phenomena in the upflow portions of hydrothermal systems, and boiling often continues all the way to the surface, where the fluid discharges as boiling springs (Hedenquist, 1991).

The spatially distributed fluid inclusion data, temporally constrained by mineral paragenesis, together with present day measured downhole temperatures from VC-2A and VC-2B give an indication of the temperature gradients at Sulphur Springs over the life of the hydrothermal system. The thermal gradient during the deposition of early formed mineralization was different from today and the recent past in that the fluid temperatures were higher for depths <700 m (Fig. 2.8). A nearly isothermal gradient is indicated for depths <700 m, which suggests the Sulphur Springs was a region of upflow and boiling, and it continues to be a region of upwelling because of the presence of boiling springs (Goff et al., 1985). The thermal gradient apparently changes to more of a conductive gradient with a stratigraphic change from volcanic rocks to siliclastic rocks at 800 to 900 with the inclusion data approaching boiling conditions at 1597 m.

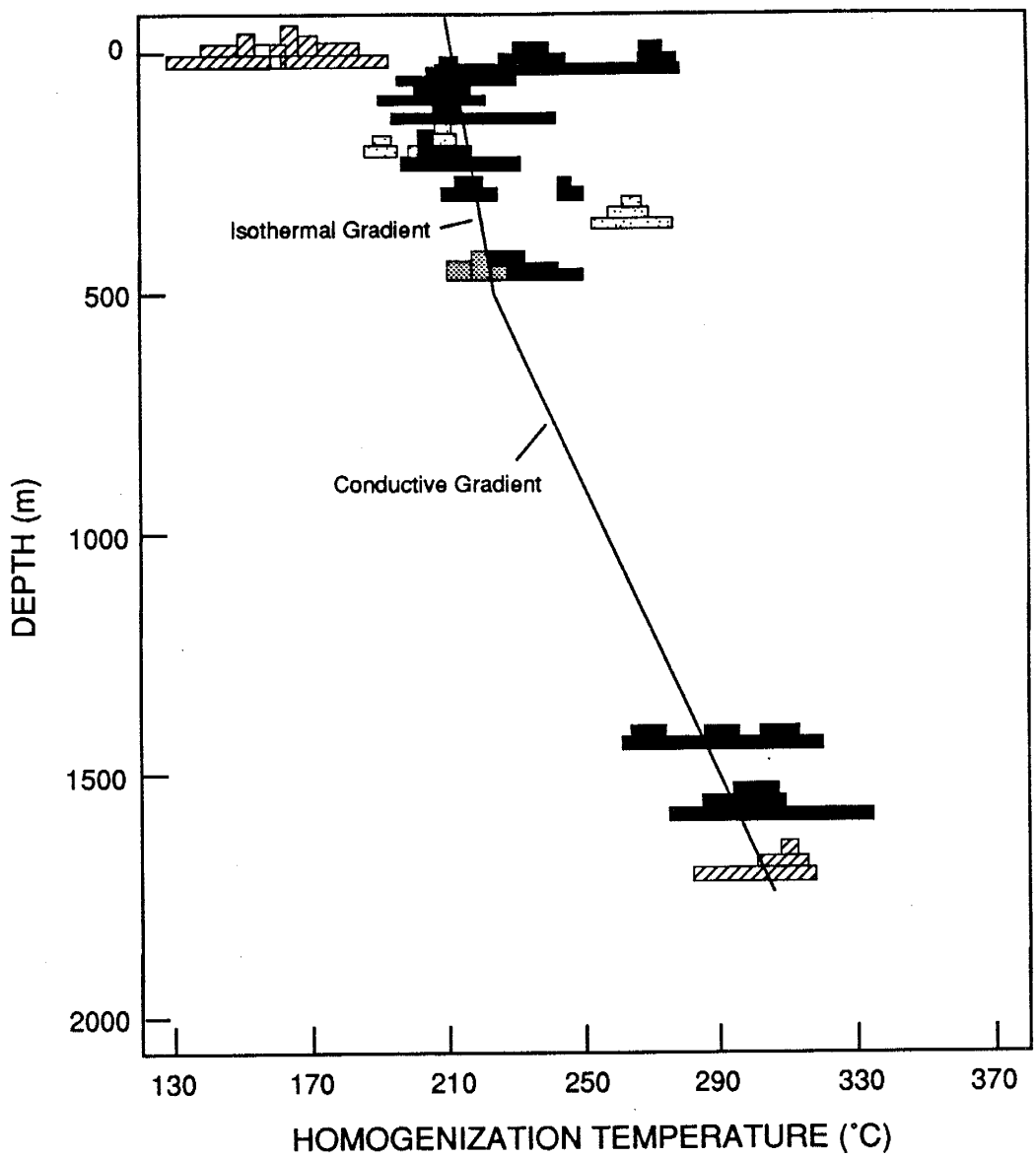

Figure 2.8 a. Fluid inclusion homogenization temperature data for early mineralization plotted versus depth showing thermal gradient. Data are combined VC-2A and VC-2B from Figure 2.3 and the symbols are the same.

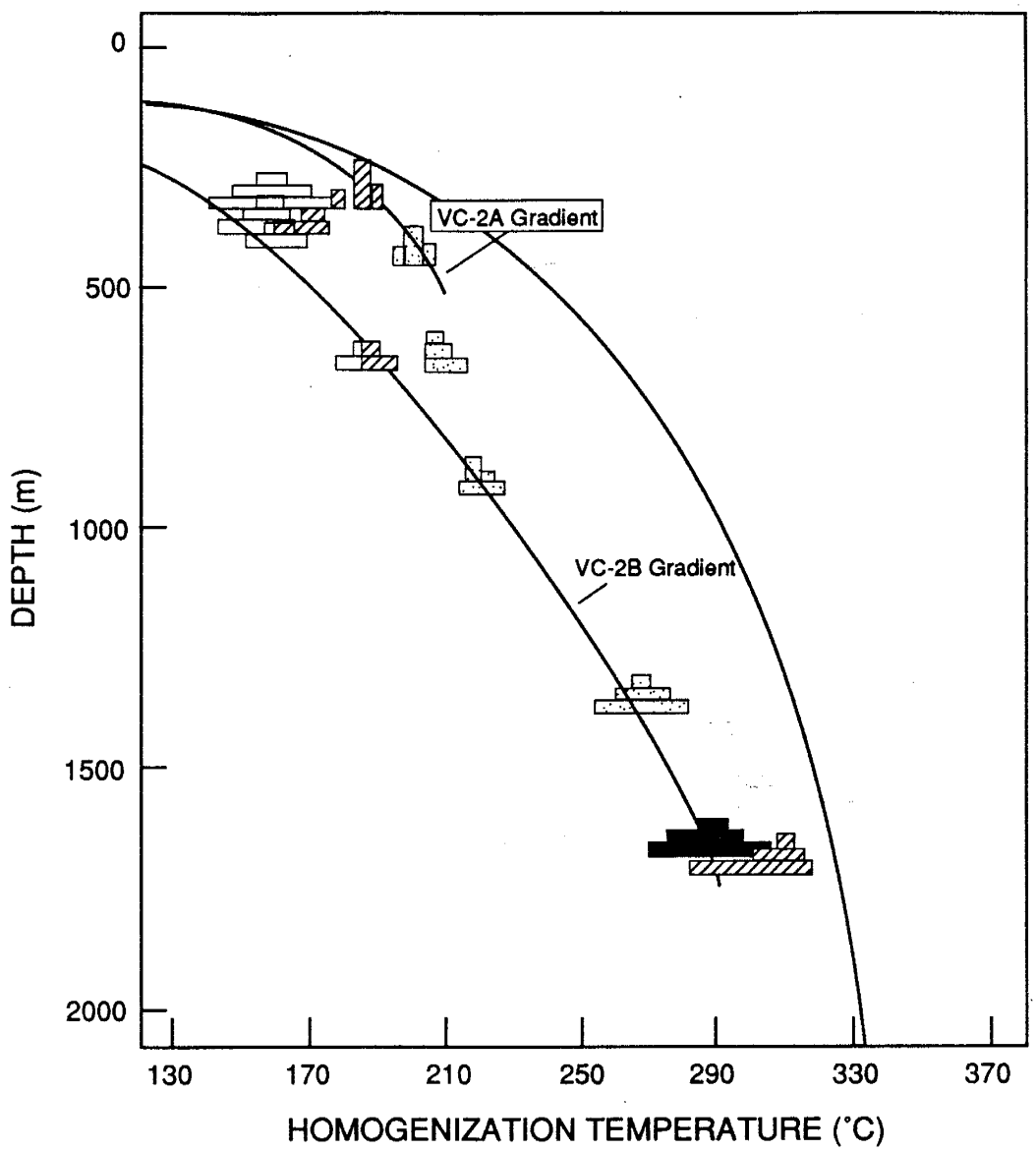

Figure 2.8 b. Fluid inclusion homogenization temperature data for recent mineralization and current temperature profile of VC-2A and VC-2B showing thermal gradient. Reference boiling-point curve set to present land surface. Data are combined VC-2A and VC-2B from Figure 2.3 and the symbols are the same.

Present day temperatures and those fluid inclusion samples that lie on or close to the current temperature profile indicate the vertical thermal gradient today and in the recent past for upper portions of the system (≤200 m) are close to hydrostatic boiling conditions (Fig. 2.8). Above about 100 m, the system is at boiling conditions as evidenced by boiling hot springs in the area. Below about 300 m, the temperature logs and fluid inclusion samples from the recent past depart from near boiling conditions to temperatures substanially lower than boiling, and follow a linear trend (conductive gradient). However, VC-2B temperature profile (below about 700 m) and fluid inclusion samples from depths >700 m are once again close to boiling conditions (Fig. 2.8b).

High Near-Surface Temperatures

Average T_h data for primary inclusions in quartz (from VC-2A) within 33 m of the present ground surface are 220°C; therefore, the minimum depth at trapping, assuming hydrostatic pressure conditions and an overlying column of pure, hot water, is 250 m (Fig. 2.3a). Several interpretations are possible for these high, near-surface, fluid inclusion T_h values 1) extensive erosion, 2) a caldera lake, 3) fluid overpressuring, and 4) trapping of two-phase fluids during boiling. Erosion may have been accelerated in the Sulphur Springs area due to the breaching of the caldera wall and uplift associated with the formation of the resurgent dome. Canyons cut in outflow sheets of the 1.1 Ma Tshirege Member of the Bandelier Tuff are in excess of 200 meters deep (J.B. Hulen, written communication, 1991). Therefore, 200 m and possibly more of rock may have been removed by erosion, considering the material probably would have been relatively soft non-welded tuff, debris flows and tuffaceous sediments.

The above estimated depth based on fluid inclusion data from quartz also gives an estimate of the position of the paleowater table at Sulphur Springs that being about 250 m higher than the present land surface and 400 to 450 m higher the present water levels in the two coreholes. There is evidence that numerous intracaldera lakes were present in the Valles caldera, and mapping in the Sulphur Springs area revealed that one of these caldera lakes was present (Goff and Gardner, 1980). Although a change in the effective water table of about 400 m seems large, it is plausible

through either topographic or tectonic effects. Breaching of the southwestern caldera wall at about 0.5 Ma (Goff and Shevenell, 1987) resulted in draining of intracaldera lakes, and a decrease in the hydraulic head of the hydrothermal system. This caused the maximum elevation of the hydrothermal fluids in the geothermal reservoir to drop (Trainer, 1984; Goff et al., 1989). Hence, it is concluded that draining of the lake resulted in a loss of about 400 m of hydrostatic head when compared to current fluid levels. Scenarios analogous to this with similar magnitude changes in water table levels have been suggested for several other active systems, e.g. Long Valley (Bailey et al., 1976), the Philippines (Reyes, 1990) and Yellowstone (Bargar and Fournier, 1988), and the fossil hydrothermal system at Fresnillo (Simmons, 1991).

Fluid inclusions in fluorite at 29 m of the present land surface of VC-2A allow modeling of the decent of the water table (Fig. 2.9). Fluorite is paragenetically later than quartz in the sample and quartz from nearby veins, and average the T_h for fluorite is 176°C which gives an estimated depth of about 88 m for pure water. This suggests the water table descended nearly 160 m from the time of quartz deposition to fluorite formation. The water table continued to descend and the present vapor zone at Sulphur Springs developed. Goff and Shevenell (1987) believe the vapor zone is a condition of the hydrothermal system that is <0.5 m.y. old.

Draining of these intracaldera lakes may have been catastrophic (Goff and Shevenell, 1987) and the sudden decrease in the water table with resulting decompression of the system lead to hydrothermal explosive activity and formation of hydrothermal breccias. It may have been during this period that the majority of hydrothermal brecciation occurred. Hydrothermal breccias occur throughout the hydrothermal system, but are most concentrated in the upper 600 m. Muffler et al. (1971) postulated that sudden decreases in the water table by draining of ice-dammed lakes during periods of glacial cover resulted in major hydrothermal explosive activity in Yellowstone. Alternatively, the hydrothermal breccias represent periods of self-sealing whereby the pressures and temperatures, especially in the near surface, increased. While it is unlikely fluids pressures were at 100% lithostatic during these periods of self-sealing, they could have easily been 50% of lithostatic pressure. Hulen and Nielson (1988a) show that hydrothermal brecciation in VC-1 occurred at

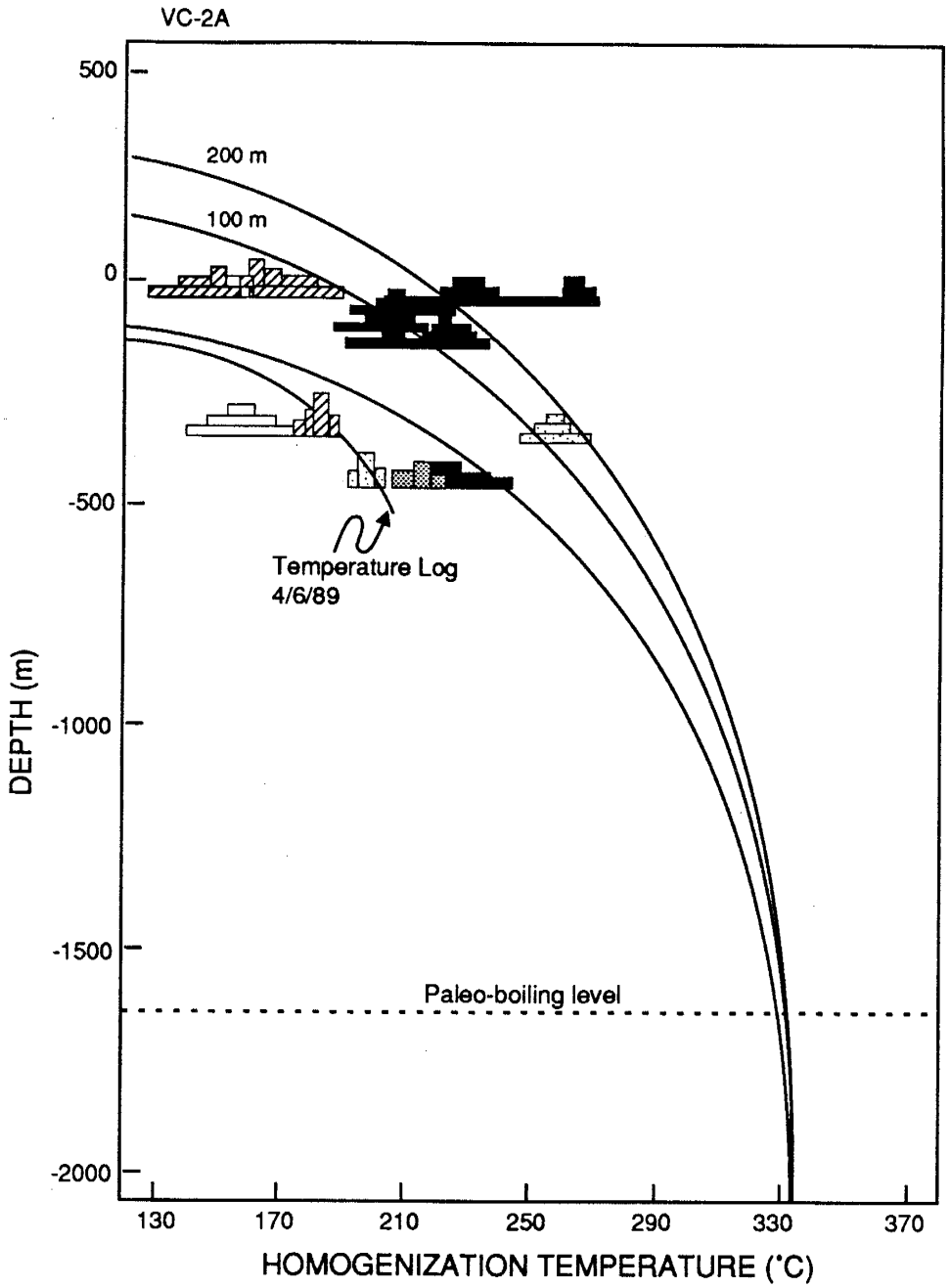

Figure 2.9 a. Temperature versus depth for VC-2A fluid inclusions with the interpreted position of the reference hydrostatic boiling-point curve (pure water) prior to extensive erosion or draining of intracaldera lakes at about 0.5 Ma. +200 denotes position of curve (and that of the water table) is 200 m above present land surface (approximately the position it would have been at the time of early quartz deposition) and +100 denotes position of curve at the time of early fluorite deposition (100 m above present land surface). This suggests the water table dropped at least 100 and possibly as much as 160 m between the time of quartz deposition and fluorite formation. Paleo-boilng horizon is based on last occurrence of bladed calcite. Symbols are the same Fig. 2.3.

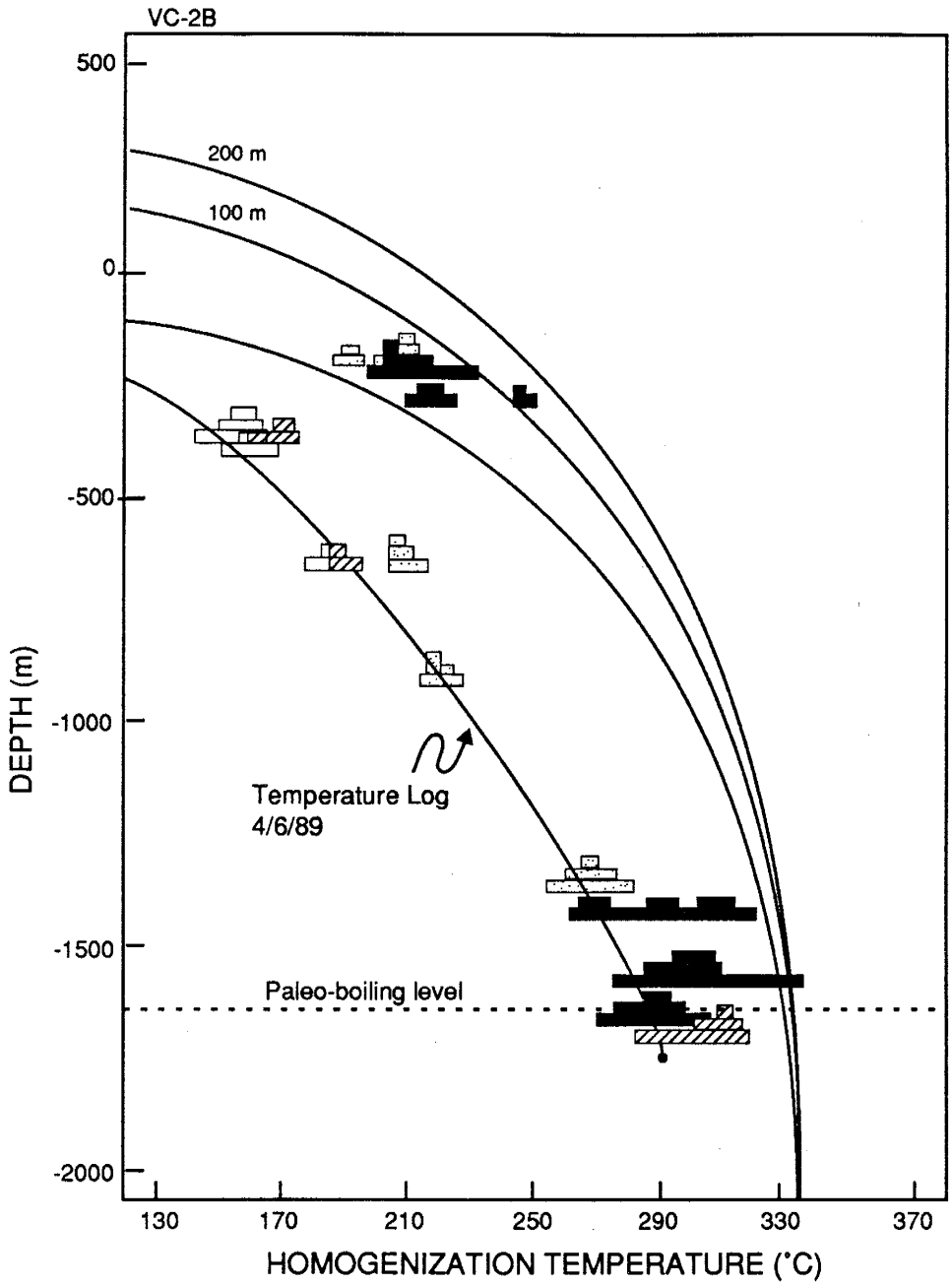

Figure 2.9 b. Temperature versus depth for VC-2B fluid inclusions with the interpreted position of the reference hydrostatic boiling-point curve (pure water) prior to extensive erosion or draining of intracaldera lakes at about 0.5 Ma. +200 denotes position of curve (and that of the water table) is 200 m above present land surface (approximately the position it would have been at the time of early quartz deposition) and +100 denotes position of curve at the time of early fluorite deposition (100 m above present land surface). This suggests the water table dropped at least 100 and possibly as much as 160 m between the time of quartz deposition and fluorite formation. Paleo-boilng horizon is based on last occurrence of bladed calcite. Symbols are the same Fig. 2.3.

pressures approximately 50% of lithostatic. Once the boiling point was exceeded, flashing fluids in fractures and intergranular pores comminuted enclosing rocks (Hulen and Nielson, 1988a). These pressure transients were short-lived and were dissipated by hydrothermal eruptions. During trapping of these boiling fluids, the fluid inclusions would display the characteristic liquid- and vapor-rich inclusions, which when analyzed microthermometrically would add to scatter in the data, especially toward high temperatures.

Other Data in Support of Fluid Inclusion Data

Clay mineralogy and zoning in VC-2A and VC-2B support fluid inclusion data suggesting that a high-temperature, liquid-dominated reservoir once extended up to, and probably above the level of the present land surface (Hulen and Nielson, 1988b), even though the system is now vapor-dominated to a depth of about 240 m. Other wells in the Valles caldera show a similar cooling of 50 to 100°C relative to past activity, which also is attributed to draining of intracaldera lakes (Hulen and Nielson, 1998b). Temperatures based on the appearance of illitic sericite (<5% expandable layers) are in excess of 200°C, and Hulen and Nielson (1988b) found sericites from the sericitized zone of VC-2A to contain between 5-14% smectite interlayers. Chlorite appearance usually coincides with temperatures of >220°C in active hydrothermal systems (Browne, 1978), which is consistent with the observation that chlorite is first noted at depths below about 160 m in VC-2A. Fluid inclusion temperatures from early quartz for this depth are around 230°C. Epidote appearance in VC-2B is about 1470 m, which has a current and past temperature of 270 to 280°C. Epidote is typically present in active systems above temperatures of about 250°C (Browne, 1978). From these mineralogic oberservations, there is good agreeement between the fluid inclusion temperatures, geothermometry based on sericite and temperatures noted for first appearance of other alteration phases in active hydrothermal systems.

Salinity Data

The fluid inclusion evidence presented indicates that saline inclusion fluids of about 5.0

equiv. wt.% NaCl existed in the Sulphur Springs hydrothermal system. Fluid inclusion data for VC-2A indicated that injection of this saline fluid occurred at depths <700 m early in the history of the system since these data are from early mineralization and may have been closely associated with sulfide deposition. Injection of saline fluids is believed to be short-lived; by contrast, the majority of the inclusion data from depths <700 m indicate that the prevailing fluids were dilute (0.5-1 equiv. wt.% NaCl). Dilute inclusion fluids suggest that these fluids dominated the upper 700 m of the Sulphur Springs system while saline fluids occupied the system at depths >700 m. The Permian shales would act as an aquitard, prevent large sacle mixing in support of this hypothesis. It should be noted that there is no evidence of this saline fluid in the present day waters.

Evidence for a brine reservoir is known for the active hydrothermal system at Salton Sea (McKibben et al., 1987). There the interface between deep hypersaline brines and shallow dilute fluids is represented by a sharp gradation in salinity. Mineralogic and fluid inclusion evidence suggests the deep hypersaline fluid once occupied shallower levels (McKibben et al., 1988). A brine reservoir has also been proposed by Simmons (1991) for the Fresnillo hydrothermal system where fluid inclusion evidence indicates that saline fluids of 10 equiv. wt.% NaCl were intermittently injected into the hydrothermal system. These pulses of the saline fluid were short-lived since fluid inclusions in quartz and calcite indicate that prevailing fluid compositions were dilute (≈2 equiv. wt.% NaCl). It is interesting to note that at both Sulphur Springs and Fresnillo the saline fluid and the prevailing dilute fluid differ by a factor of 5.

Two mechanisms may have lead to the injection of these brines into the upper portion of the Sulphur Springs hydrothermal system. Tectonic adjustments along the Sulphur Creek fault and its subsidiaries allowed release of saline fluids from depth to shallow levels. During periods when the system was under pressures greater than hydrostatic (periods of self-sealing), fluid circulation would have been reduced. Rupturing of these self-sealed zones result in short duration pulses of increased fluid flow when these deep fluids could migrate along newly formed fractures. Periodic intrusion of small, shallow magma bodies associated with post-caldera, dome-forming rhyolites may have evolved a saline fluid.

Origin of the saline fluid is uncertain, though isotopic measurements of helium and sulfur in vein material and the present day fluids are suggestive of a magmatic source of these components (McKibben and Eldridge, 1990; Musgrave et al., 1991; F. Goff, personal communication; B.M. Kennedy, personal communication). Dissolution of small evaporitic horizons of the Permian-Pennsylvannian section is another possible origin for the saline fluids. Unaltered tuffs equivalent to those filling the caldera depression contain as much as 2800 ppm Cl (Gardner et al., 1986), therefore it is not necessary to call upon magmatic Cl as a source for Cl in the dilute inclusion or present day reservoir fluids.

HYDROTHERMAL SYSTEM EVOLUTION

The evolution of the Sulphur Springs hydrothermal system can be interpreted in light of the models put forth for the present day Valles caldera hydrothermal system (Goff et al., 1985; Goff and Shevenell, 1987; Goff et al., 1988; Goff et al., 1989) and volcanic-hosted hydrothermal systems world-wide (Henley and Ellis, 1983). Inception of the Sulphur Springs hydrothermal system was shortly after formation of the Valles caldera (Goff and Shevenell, 1987), and is driven by heat derived from crystallization of the Bandelier magma with additional heat from post-caldera volcanic activity which continued until about 0.13 Ma (Fig. 2.10a). A saline fluid (3-5 equiv. wt.% NaCl) formed above the crystallizing magma, from which Cl^-, sulfur, helium, and other volatiles (N_2 and CO_2) were derived. Above the saline fluid, which was restricted to depth by the overlying impermeable Permian rocks, a convection cell of dilute (0.5-1 equiv. wt.% NaCl), neutral pH, chloride water was established in faults and fractures. Deposition of sulfide minerals took place between 0.66 to 0.83 Ma based on illite from wall-rock alteration and illite intergrown with vein quartz and sulfides (WoldeGabriel and Goff, 1989). Temperatures of deposition ranged between 220 to 240°C and salinities were 0.5 to 5.0 equiv. wt.% NaCl. Upflow was centered and continues to be centered at what is now the main hot spring area, in close proximity to the Sulphur Creek fault. Ascending fluids were under state steady conditions at or near hydrodynamic temperature and pressures, except for short periods of transient overpressuring. Intermittent injection of deep, saline fluids into

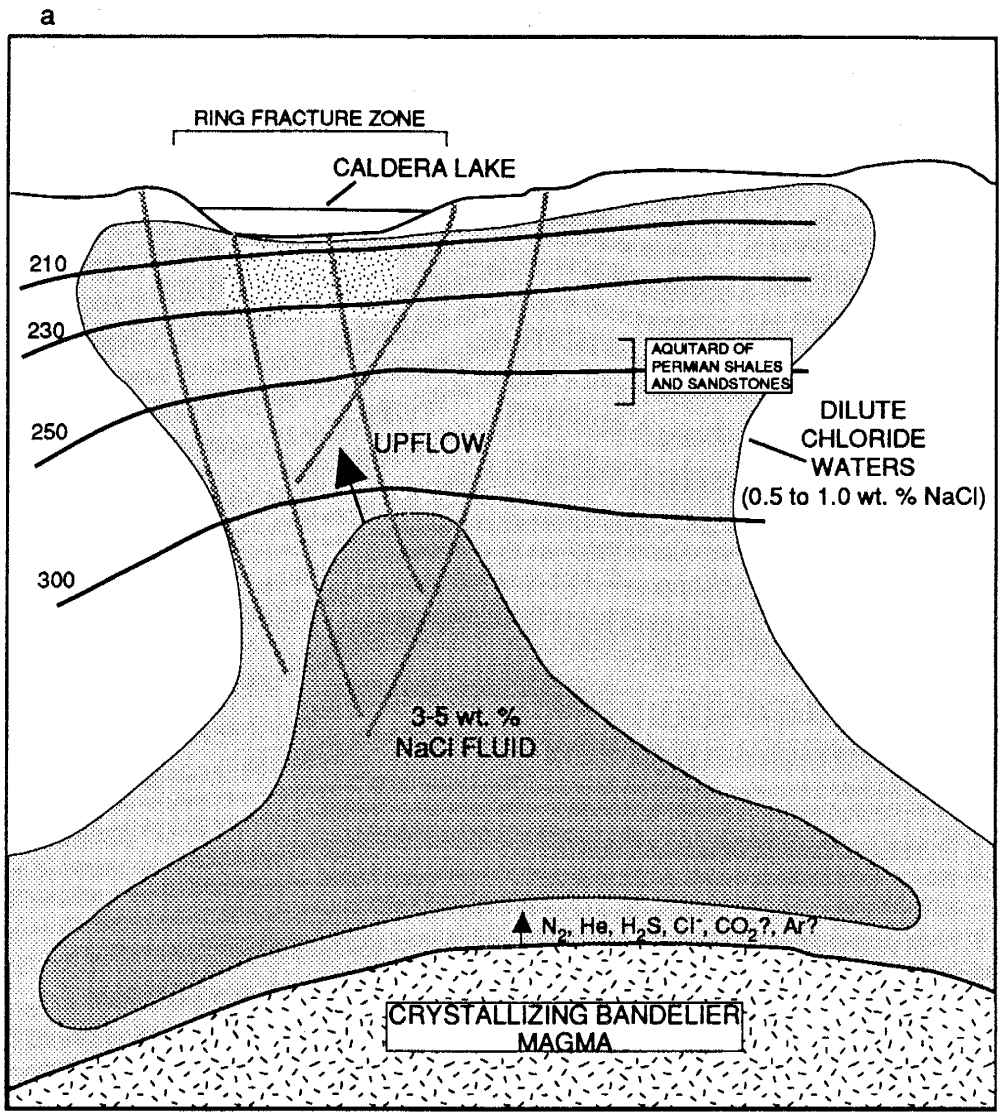

Figure 2.10 Schematic illustration of the evolution of the Sulphur Springs hydrothermal system. a. Configuration of the system at about 1 Ma showing the elevated thermal gradient, dilute chloride fluids in the shallow and peripheral? portions, aquitard composed of shales, saline fluid at depth, and caldera lake. Saline fluid was intermittently injected into the shallow portions of system or mixed with shallow fluids. Position of isotherms based on fluid inclusion data. Deposition of molybdenite and base metals was between 0.66 and 0.83 Ma (WoldeGabriel and Goff, 1989).

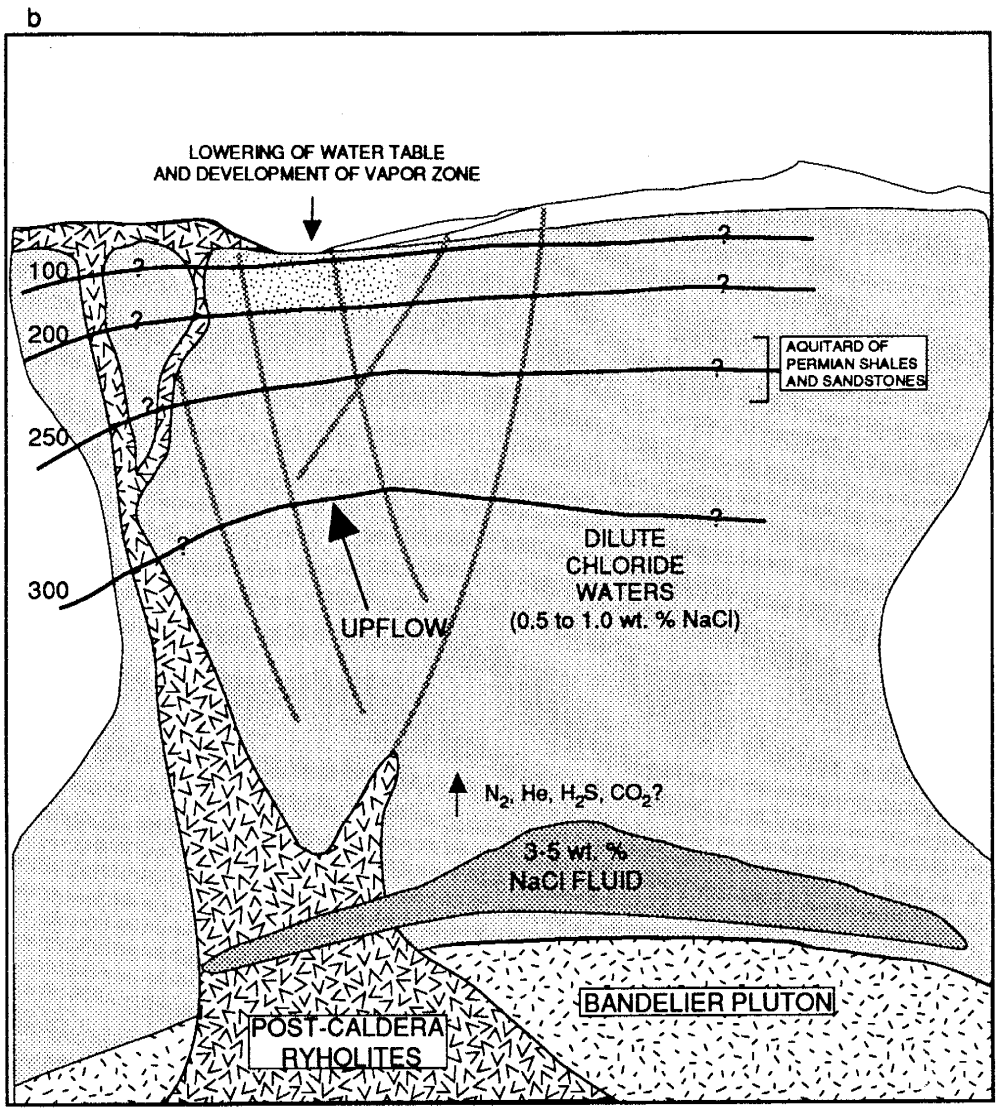

Figure 2.10 b. System at about 0.5 Ma following breaching of southwestern caldera wall and draining of intracaldera lakes with concomittent drop in water table. Intrusion of post-caldera rhyolites in the vicinity of Sulphur Springs occurred between 0.45 to 0.55 Ma (Doell et al., 1968; Spell and Kyle, 1989). Position of isotherms in shallow portion is conjectural for this time period since the age of fluid inclusion samples is not well constrained.

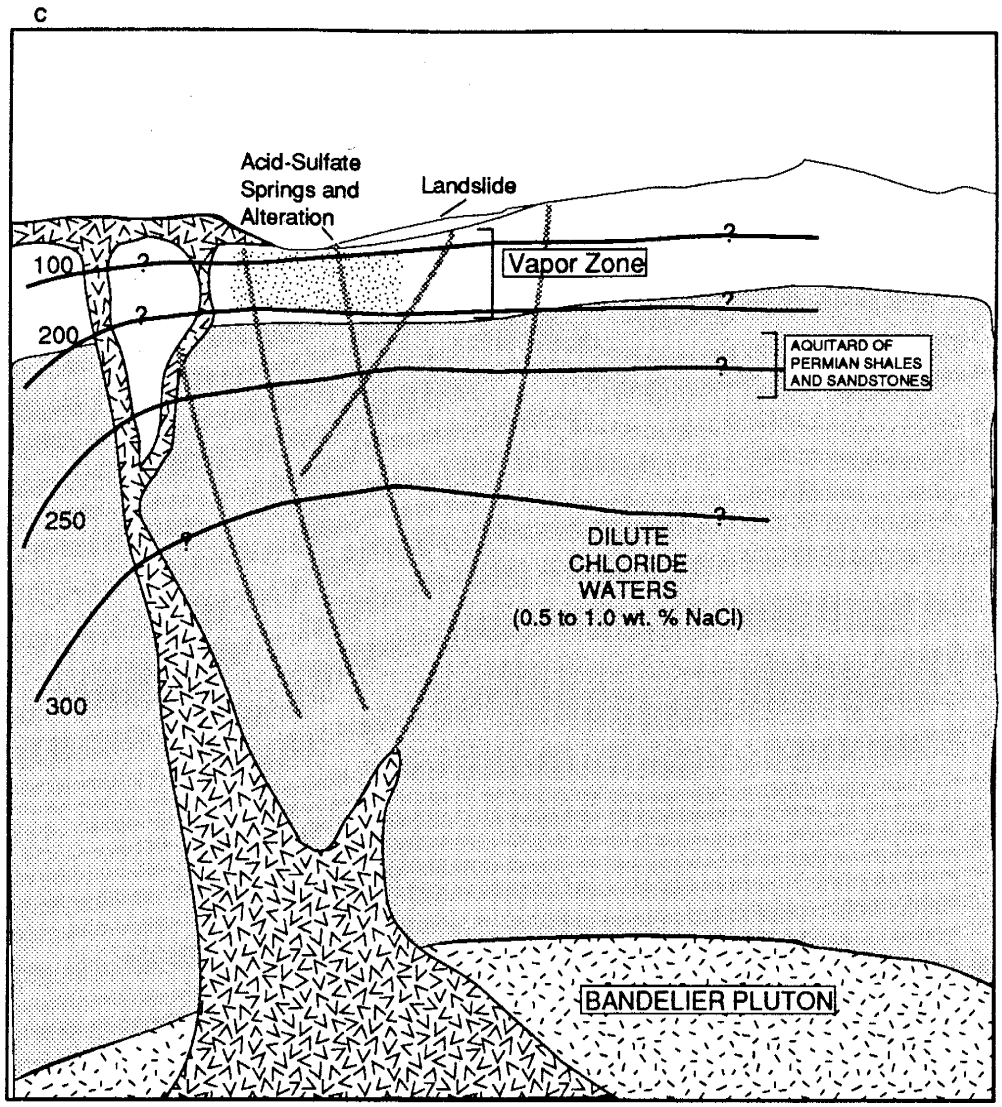

Figure 2.10 c. Current configuration of hydrothermal system showing present day position of vapor zone, liquid-dominated zone, position of isotherms based on drill hole data, and acid-sulfate alteration (essentially a surface veneer). Saline fluid no longer exists or it has retreated to deeper levels of the system. Stippled pattern in upper portion of all figures is zone of molybdenite and major base metal deposition.

the shallow portions of the system occurred in the upflow region. Injection of saline fluids in the upflow zone accompanied periods of overpressuring. That portion of the system represented by VC-2B may have been peripheral to the main upflow zone which was less dynamic where the deep, saline fluids and shallow, dilute fluids had more time to interact and hence mix more thoroughly (Fig. 2.4). At 0.45 to 0.6 Ma intrusion of rhyolitic magma and emplacement of rhyolite domes in the vicinity of Sulphur Springs took place. This igneous activity supplied additional heat and possibly Cl^- to the hydrothermal system. Intrusion of this magma may have been another source of transient overpressures.

A major truning point in the evolution of the Sulphur Springs hydrothermal system (and the Valles hydrothermal system as a whole) occurred about 0.5 Ma. Between 0.5 and 0.43 Ma, a large breach developed in the southwestern wall of the caldera near its intersection with the Jemez fault zone (Doell et al., 1968). As a result of this sudden geomorphical incision, intracaldera lakes drained, and recharge to the hydrothermal system changed, lowering the water table as upper San Diego Canyon was cut (Fig. 2.10b) (Goff and Shevenell, 1987). Lowering of the water table by approximately 400 m (when compared to its current level in the system), depressed boiling hydrodynamic temperature-pressure gradients. Accompanying this drop in fluid level in the hydrothermal system was the development of the present vapor-dominated zone above the system (Fig. 2.10c). The drop in the water table may have caused the saline fluid to retreat to deeper levels, or permitted the incursion of dilute fluids into deep portions of the system. Alternatively, since the Bandelier pluton is cystallized, save for a few isolated pockets of residual melt (Olsen et al., 1986), a source of higher Cl^- is no longer available. Boiling in the current hydrothermal system and release of H_2S through this process along with subsequent oxidation of H_2S produces surface acid-sulfate alteration and acid-sulfate waters in the main hot spring area (Goff et al., 1985; Charles et al., 1986).

CONCLUSIONS

Temperature and composition of the past fluids in the Sulphur Springs hydrothermal system

were different from those at present. Fluid inclusion data indicate a complex hydrothermal history in which fluids of ≈ 5 equiv. wt.% NaCl entered fractures in compositionally discrete pulses at shallow depths (<700 m) of the hydrothermal system. However, the inclusion data indicate the predominant fluid at shallow depths was 0.5-1 equiv. wt. NaCl., whereas the fluid at depth (>700 m) was 3-5 equiv. wt.% NaCl. At shallow depths, temperatures are about 100°C lower and at depth, fluid temperatures have decreased about 10 to 30°C. Important hydrologic aspects of the evolution of the Sulphur Springs hydrothermal system include the existence of a deep seated saline fluid, possibly derived from the crystallizing Bandelier magma, which was periodically injected into shallow levels or mixed with the shallow fluid through a stratigraphically stratified hydrothermal system; and the water table, which controls hydrodynamic boiling conditions, descended as much as 400 m when compared to the present level of the water table. The process which led to the lowering of the water table was collapse of the southwestern caldera wall and draining of intracaldera lakes, and this may have lead to greater incursion of the shallow fluid into deeper portions of the system thereby diluting the deep hydrothermal fluid to its present composition (1.1 equiv. wt.% NaCl) or the saline fluid has retreated to a deeper level. Presently there is no evidence of the high salinity fluid.

PART II

FLUID INCLUSION GAS CHEMISTRY

INTRODUCTION

Since there is so little knowledge concerning inclusion volatiles, data on the gaseous species and their average composition in an assemblage of inclusions is of great value (Norman and Sawkins, 1987). Gases exist in hydrothermal fluids as solutes and as a separate gas phase. They occur in ore and gangue minerals both in substitution in crystal structures and trapped in fluid inclusions (Landis and Rye, 1989). Gaseous species in fluid inclusions at concentrations of a few to tens of mole per cent can best be measured by a direct method. Although sufficient volatiles for analysis can be obtained from an individual inclusion, a more accurate analysis can be obtained by bulk analysis of individual inclusions. Fluid inclusion gas analyses yield qualitative and quantitative information about the gases dissolved at the time of trapping, and from these data the fugacities of the principal gases can be calculated. Changes in oxygen and sulfur fugacities of the mineralizing solution may indicate the processes that led to ore deposition.

The geochemical evolution of an active hydrothermal system can be elucidated by comparison of present day gas chemistry to the gas chemistry of past fluids extracted from fluid inclusions. Gas abundance data help indicate sources, prevailing rock/fluid processes, and physical-chemical conditions of the system (Norman and Sawkins, 1987). The gas data provide complimentary information to that obtained from fluid inclusion temperature and salinity measurements and from the interpretation of mineral stabilities.

This section will focus on the analysis of inclusion gases from Sulphur Springs. Data from the Redondo Creek area are included for comparison. It will be shown that the data can clarify sources and processes, and when combined with well documented fluid inclusion data provide a very useful tool to study processes in any hydrothermal system. The data will be compared to inclusion gas data from hydrothermal systems hosted in volcanic and sedimentary rocks such as Cochiti, Creede, Jerrit Canyon, and Salton Sea.

ANALYTICAL METHODS

The analytical system consists of a vacuum extraction line and a quadrupole mass spectrometer (QMS). The extraction line is constructed of Pyrex glass tubing and glass-body bellow-seal-type valves and can be evacuated to mid-10^{-8} Torr. There is little metal in the extraction line to minimized reaction with sulfur species gases.

The QMS is a Balzers QM 420. The QMS is preferred over the magnetic sector mass spectrometer for the analysis of gases because it is capable of scans as fast as 1 milliseconds/atomic mass unit (amu) and is extremely sensitive in the lower limit of detection for routine analyses of individual gases in the 0.1 ppm range and detection limits as low as $5x10^{-13}$ mbar. Quoted instrument stability is ± 1% per day.

Figure 3.1 illustrates the essential components of the gas analysis system. The QMS and the extraction line are pumped by turbomolecular pumps. A capacitance manometer is used to measure the amount of gas. Gaseous species are identified and their ratios measured by the quadrupole. Precise control on sample introduction into the mass spectrometer is accomplished by a leak valve. Two 3 mm capillary tubes allow collection of H_2O and CO_2 for later isotopic analysis.

All volumes of the extraction line have been measured and the "effective volume" of the trap has been determined at liquid nitrogen (LN_2) and dry-ice temperatures. The QMS is calibrated with reference gases to previously establish the ion fragmentation patterns of the gases of interest and the ionization efficiencies relative to N_2.

Mineralization at Sulphur Springs is typically scant; therefore, samples sizes are small; 0.1 to 0.6 g of useable material after hand picking. The hand-picked sample was crushed to approximately 0.5 mm and cleaned in warm 3.0 M NaOH (followed by 10% HCl for quartz and fluorite) and washed in hot distilled-deionized water for 12 to 24 hours. The cleaned sample was loaded into the quartz tube, lowered into the furnace, and the quartz tube is pumped on at 100°C for several hours, which results in a pressure of mid-10^{-7} Torr or better. The extraction line is then isolated from the vacuum system, the background gases measured, LN_2 is put on the trap and the

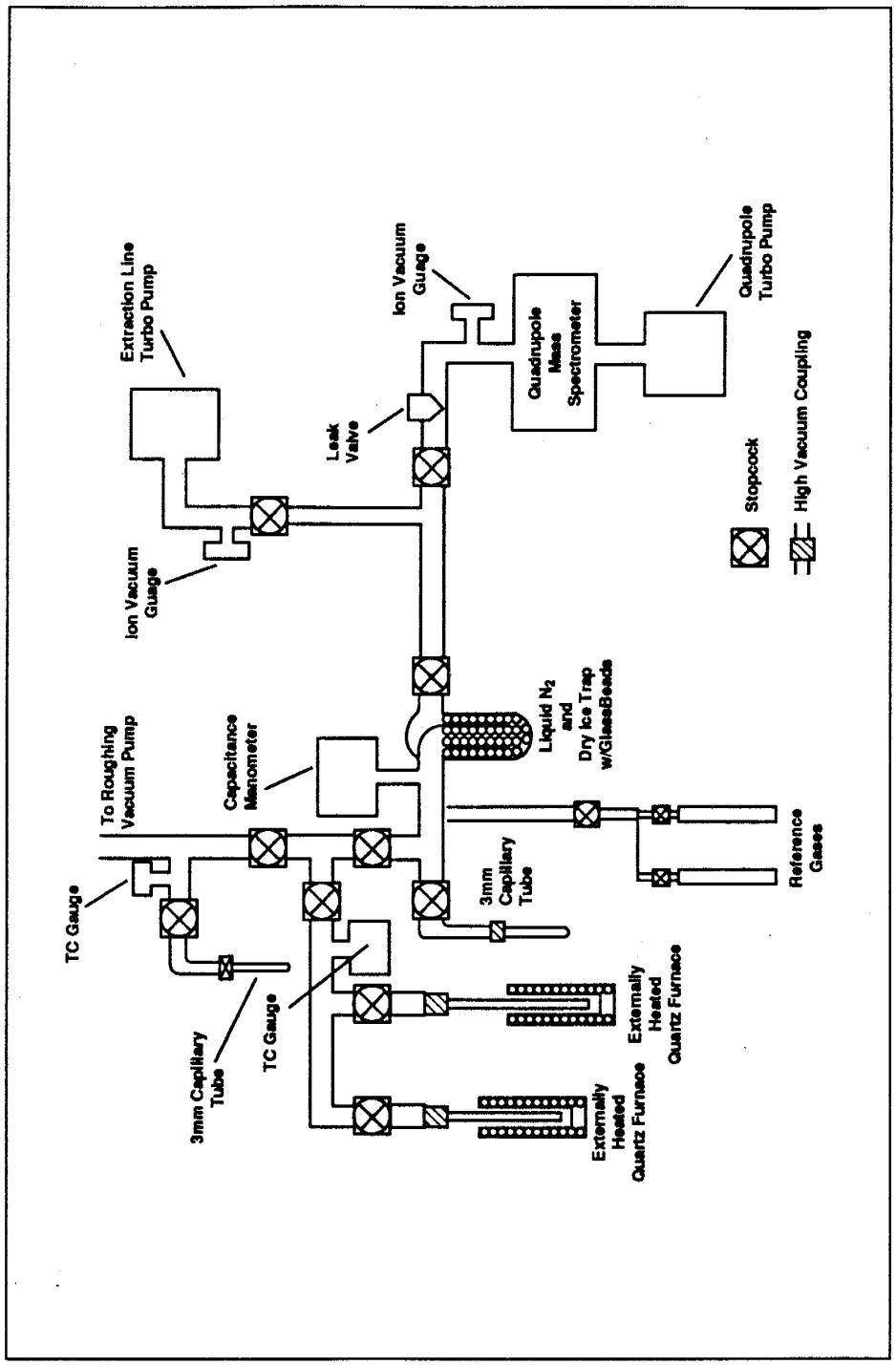

Figure 3.1. Schematic diagram of the gas extraction line.

furnace heated to 400-500°C for 10-15 min. The LN_2 noncondensable gases are measured first, the LN_2 is replaced by an isopropanol-dry-ice slurry and the LN_2 condensable gases are measured. The dry-ice-alcohol mixture is removed and the water is measured.

Water is measured by freezing it into a capillary and weighing and by pressure measurement. These methods were calibrated for amounts of H_20 between 0.01 to 2.0 mg by introduction of known amounts of H_2O into the extraction line. These techniques yield an accurate gas/water ratio; estimated errors based on analyses of gases dissolved in water are ±5% for major species and ±10% for minor species. However, there is no way to know how accurately volatiles in inclusionliquids are measured because there are no accurate standards. Recently, workers using synthetic fluid inclusions have tried preparing standards for major species such as CO_2, CH_4, and N_2 (Frantz et al., 1989).

The principal area of uncertainty in the analyses is whether or not the volatiles measured represent those actually present in the inclusions. Verification of the analytical results agree with the data from the physical and chemical characteristics of the present hydrothermal fluid determined by other means.

RESULTS

The analyses indicate that the inclusion volatiles consist of water containing 2.4 to 22.7 mole % gases except for one sample from 1679 m, in which 60.3 mole % gases was measured (Table 3.1). The principal gaseous species are CO_2, N_2, CH_4, and multi-carbon organic compounds. A few generalizations can be made regarding gas content versus depth in the Sulphur Springs hydrothermal system (Figs. 3.2 and 3.3). Gas species are in higher concentration in the shallow levels of the system (<700 m), with the exception of Ne and Ar that reach highest concentration at the deepest levels. He is at highest concentrations at depths <700 m (Fig. 3.3).

Correlation coefficients calculated for the gas species indicate that several species correlate positively with one another (Table 3.2). Those pairs of species which are strongly correlated (>0.85) are He-Ar, N_2-Ar, O_2-Ar, He-N_2 O_2-N_2, and CS_2-C_nH_n and those that are strongly to moderately

Table 3.1. Fluid Inclusion Gases, Present Day Gases, and Calculated Fugacities

Analysis	Sample No. VC2A 129	VC2A 160	VC2A 339	VC2A 541	VC2A 1137	VC2A 1485QTZ	VC2A 1485CC	VC2A 1712	VC2B 760
Gas species (mole %)									
CO_2	3.66	5.98	1.07	9.63	2.92	6.44	14.52	4.65	1.503
CH_4	0.24	0.629	0.1	0.031	0.3903	0.048	0.0868	0.197	0.938
CO	0.2	5.434	0.1	0.037	4.582	4.201	6.759	0.062	6.065
CS_2	n.d.	0.0017	0.0006	n.d.	0.219	0.076	0.124	n.d.	n.d.
Ar	0.0014	0.0066	0.002	0.0002	0.00013	0.0016	0.0012	0.002	0.0134
Ne	n.a.	0.0027	n.a.	n.a.	n.d.	0.0046	0.0199	n.a.	n.d.
He	0.00012	0.00059	0.00001	n.d.	0.00001	0.00005	0.0001	0.00001	0.0022
H_2S	1.16	0.335	0.93	0.22	0.00054	0.0088	0.0008	0.002	0.0029
SO_2	n.d.	0.0003	0.034	0.35	0.00027	0.0058	0.0007	n.d.	0.0042
N_2	0.141	0.601	0.01	0.008	0.527	0.394	0.482	0.026	0.5398
H_2	1.17	0.4904	0.17	0.17	0.137	0.004	0.552	0.196	0.753
O_2	n.a.	0.019	n.a.	n.a.	0.0002	0.0013	0.0015	n.a.	0.012
CnHn	0.0165	0.171	0.103	0.74	2.154	0.685	0.708	n.d.	0.0384
H_2O	93.4	86.32	97.5	88.8	89.07	88.13	76.75	94.9	90.13
Mineral Phase	Quartz	Quartz	Quartz	Fluorite	Calcite	Quartz	Calcite	Calcite	Quartz
Corrected Analysis									
CO_2	3.37	5.86	1.03	9.58	2.91		14.38	4.61	1.34
CH_4	0.532	0.751	0.14	0.074	0.407		0.225	0.22	1.096
CO	0.2	5.43	0.1	0.037	4.58		6.76	0.062	6.065
CS_2	n.d.	0.0017	0.0006	n.d.	0.219		0.124	n.d.	n.d.
Ar	0.0014	0.0066	0.002	0.0002	0.00013		0.0012	0.002	0.0134
Ne	n.a.	0.0027	n.a.	n.a.	n.d.		0.0199	n.a.	n.d.
He	0.00012	0.00059	0.00001	n.d.	0.00001		0.0001	0.00001	0.0022
H_2S	1.18	0.335	0.93	0.22	0.00054		0.0008	0.002	0.0029
SO_2	n.d.	0.0003	0.034	0.35	0.00027		0.0007	n.d.	0.0042
N_2	0.14	0.601	0.01	0.008	0.527		0.482	0.026	0.5398
H_2	0.00007	0.0001	0.00011	0.00002	0.064		0.00003	0.061	0.119
O_2	n.a.	0.019	n.a.	n.a.	0.0002		0.0015	n.a.	0.012
CnHn	0.017	0.171	0.103	0.74	2.154		0.708	n.d.	0.0384
H_2O	94.56	86.82	97.65	88.99	89.14		77.30	95.02	90.77
log f(CO_2)	2.31	2.54	1.79	2.77	2.21	2.55	2.93	2.44	1.89
log f(H_2S)	1.14	0.58	1.03	0.43	-2.24		-2.02	-1.63	-3.15
log f(N2)	1.94	2.57	0.79	0.7	2.35	2.23	2.46	1.14	2.47
log fO_2	-41.9	-40.9	-40.9	-42.3	-38.9	-34.9	-41.4	-41.7	-41
log fS_2	-8.2	-9.2	-8.3	-9.1	-13.9	-7.4	-14	-13.5	-12.9

* Average of unpublished analyses of VC2A gases collected on 8/27 and 8/28/87 by C. Janik.
^ From modified Goff et al. 1990
# From Truesdell and Janik, 1986

Table 3.1. Fluid Inclusion Gases, Present Day Gases, and Calculated Fugacities (Cont.).

	Sample No.								
Analysis	VC2B 882	VC2B 895	VC2B 933	VC2B 1254	VC2B 1322FLR	VC2B 3017	VC2B 4565	VC2B 4755	VC2B 5507
Gas species (mole%)									
CO_2	3.26	4.14	4.93	1.54	9.46	5.8	4.13	4.18	5.94
CH_4	0.062	0.874	1.303	0.042	0.159	0.288	0.249	0.168	0.223
CO	4.679	1.257	2.656	2.442	3.123	3.972	0.49	5.52	1.19
CS_2	n.d.	0.00078	0.308	n.d.	0.0008	n.d.	0.0028	n.d.	0.0072
Ar	0.0051	0.0086	0.003	0.0004	0.0023	0.00002	0.0006	0.0008	0.11
Ne	n.d.	n.d.	n.d.	0.0055	n.d.	n.d.	n.d.	0.0083	0.008
He	0.00004	0.00067	0.00044	0.00003	0.0008	n.d.	0.00039	0.00004	0.0033
H_2S	0.0052	0.015	0.105	0.0017	0.0405	0.00007	0.0102	0.0002	0.0062
SO_2	0.0001	0.00008	0.0016	0.0005	0.022	0.00003	0.002	0.00009	0.0003.
N_2	0.166	0.327	1.766	0.112	5.89	0.233	0.788	0.323	45.63
H_2	0.052	0.157	0.574	0.0013	0.458	0.0502	0.344	0.098	0.161
O_2	0.00008	0.004	0.09	0.0001	0.335	n.d.	0.019	0.0004	6.988
CnHn	0.0911	0.103	1.436	0.1055	0.437	0.0421	0.161	0.108	0.077
H_2O	91.68	93.11	86.83	95.74	80.08	89.62	93.8	89.6	39.66
Mineral Phase	Quartz	Quartz	Quartz	Fluorite	Fluorite	Calcite	Calcite	Quartz	Quartz
Corrected Analysis									
CO_2	3.244	4.104	4.809		9.366	5.78	4.061	4.15	5.921
CH_4	0.0745	0.913	1.423		0.253	0.300	0.316	0.193	0.245
CO	4.679	1.257	2.656		3.123	3.97	0.49	5.52	1.19
CS_2	n.d.	0.00078	0.308		0.0008	n.d.	0.0028	n.d.	0.0072
Ar	0.0051	0.0086	0.003		0.0023	0.00002	0.0006	0.0008	0.11
Ne	n.d.	n.d.	n.d.		n.d.	n.d.	n.d.	0.0083	0.0084
He	0.00004	0.00067	0.00044		0.0008	n.d.	0.00039	0.00004	0.0033
H_2S	0.0052	0.015	0.105		0.0405	0.00007	0.0102	0.0002	0.0062
SO_2	0.0001	0.00008	0.0016		0.022	0.00003	0.0021	0.00009	0.0003
N_2	0.166	0.327	1.766		5.89	0.233	0.788	0.323	45.63
H_2	0.0001	0.0002	0.094		0.041	0.0003	0.077	0.0017	0.071
O_2	0.00008	0.004	0.09		0.335	n.d.	0.019	0.0004	6.988
CnHn	0.0911	0.103	1.436		0.437	0.0421	0.161	0.108	0.077
H_2O	91.73	93.27	87.31		80.49	89.67	94.07	89.69	39.74
log $f(CO_2)$	2.27	2.37	2.44	1.97	2.75	2.49	2.33	2.29	1.86
log $f(H_2S)$	-1.24	-0.77	-0.39	0	-0.91	-3.15	-0.38	-2.73	-1.12
log $f(N_2)$	1.95	2.26	2.94	1.83	3.56	1.92	2.26	1.8	3.38
log fO_2	-40.2	-39.8	-39.9	-39	-42.3	-37.8	-35.9	-35	-34.3
log fS_2	-11.6	-11.1	-9.5	-8.5	-10	-15.4	-9	-14.3	-11.2

* Average of unpublished analyses of VC2A gases collected on 8/27 and 8/28/87 by C. Janik.
^ From modified Goff et al. 1990
# From Truesdell and Janik, 1986

Table 3.1. Fluid Inclusion Gases, Present Day Gases, and Calculated Fugacities (Cont.).

Analysis	Sample No. VC2B 5533	VC2A*	VC2B90^	BACA 4#	BACA 13#	BACA 15#	BACA 19#	BACA 24#
Gas Species (mole%)								
CO_2	1.42	0.256	0.284	0.783	1.42	0.335	0.501	0.55
CH_4	0.258	0.0036	0.0001	0.0003	0.0003	0.00009	0.0003	0.00007
CO	1.24	n.a.	6.3E-06	n.a.	n.a.	n.a.	n.a.	n.a.
CS_2	0.057	n.a.	n.a.	n.a.	n.a.	n.a.	n.a.	n.a.
Ar	0.018	0.00019	1.6E-06	0.00007	0.00008	0.0001	0.00008	0.0003
Ne	0.197	n.a.	n.a.		n.a.	n.a.	n.a.	n.a.
He	0.001	4.0E-06	1.9E-06	0.00005	0.00007	7.6E-06	0.00003	9.4E-06
H_2S	0.001	0.00056	0.002	0.008	0.0073	0.006	0.0041	0.004
SO_2	0.0002	n.a.	n.a.	n.a.	n.a.	n.a.	n.a.	n.a.
N_2	2.21	0.011	0.0001	0.0028	0.0023	0.0026	0.0029	0.0039
H_2	0.105	0.0056	0.001	0.0005	0.0006	0.0039	0.0005	0.00025
O_2	0.038	0.00004	0.00003	n.d.	n.d.	n.d.	n.d.	n.d.
CnHn	0.321	n.d.	0.00004	n.d.	n.d.	n.d.	n.d.	n.d.
H_2O	94.13	99.74	99.71	99.2	98.57	99.65	99.49	99.44
Mineral Phase	Quartz							
Corrected Analysis								
CO_2	1.39							
CH_4	0.283							
CO	1.244							
CS_2	0.057							
Ar	0.018							
Ne	0.197							
He	0.001							
H_2S	0.001							
SO_2	0.0002							
N_2	2.21							
H_2	0.001							
O_2	0.038							
CnHn	0.321							
H_2O	94.24							
log f(CO_2)	1.83	1.67	1.05	1.49	1.78	1.25	1.42	1.47
log f(H_2S)	-2.06	-2.18	-1.48	-0.88	-0.9	-0.94	-1.1	-1.1
log f(N_2)	2.68	0.85	-1.7	-0.27	-0.22	-0.12	-0.07	0.11
log fO_2	-34.3	-40.3	-33	-33.9	-33.7	-34.9	-35.3	-36
log fS_2	-13.1	-14.2	-11.8	-10.6	-10.6	-10.6	-11.4	-11.3

* Average of unpublished analyses of VC2A gases collected on 8/27 and 8/28/87 by C. Janik.
^ From modified Goff et al. 1990
# From Truesdell and Janik, 1986

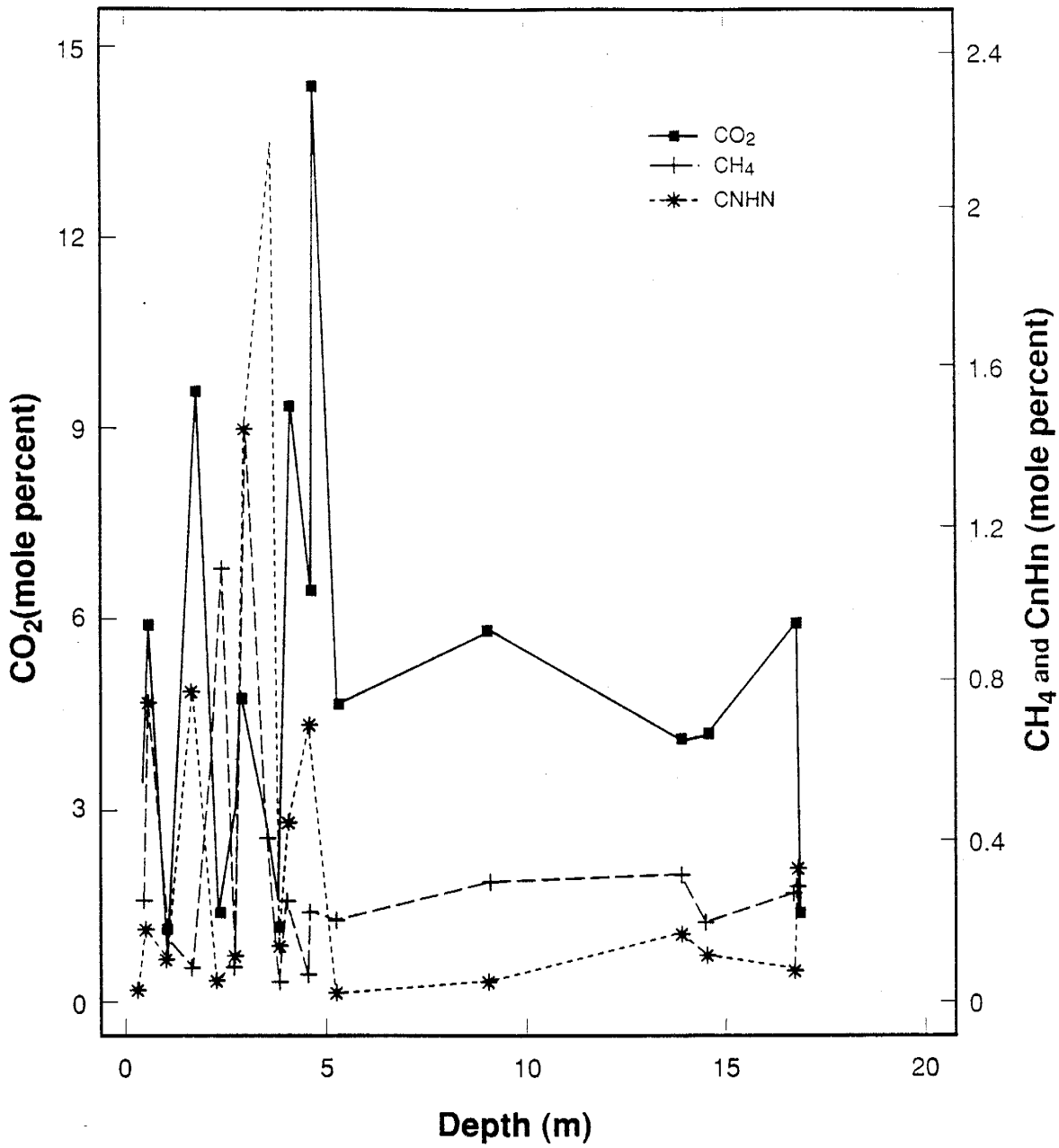

Figure 3.2. Depth versus concentration of carbon species gases (mole %) for Sulphur Springs. CH_4 and CnHn are plotted on the right-hand side of the figure.

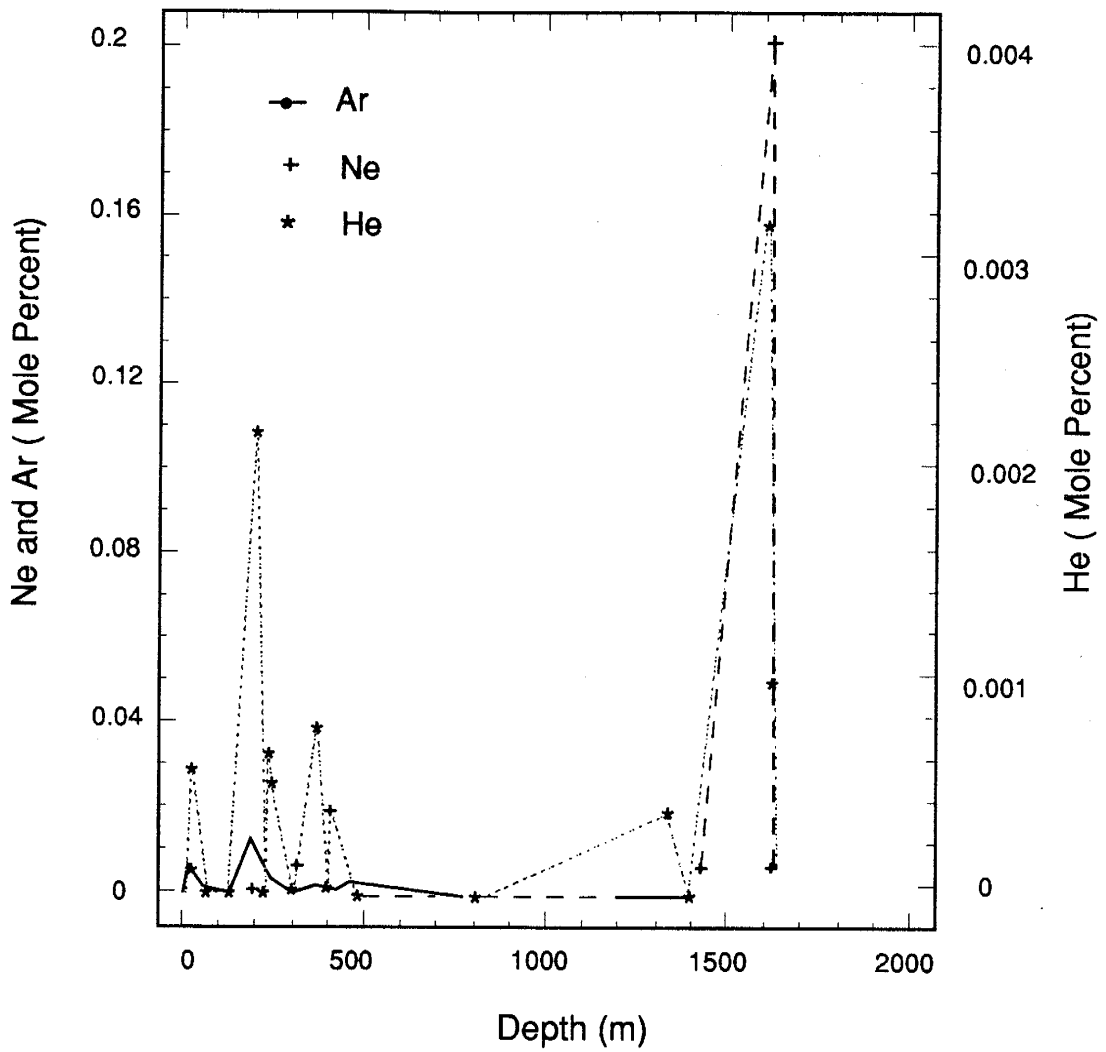

Figure 3.3. Depth versus concentration of noble gases (mole %) for Sulphur Springs. Helium is plotted on the right-hand side of the figure.

Table 3.2. Sample Correlation Coefficient, sample size, and significance level.

	CO_2	CH_4	CO	CS_2	Ar	Ne	He	H_2S	SO_2	N_2	H_2	O_2	C_nH_n	Total Sulfur	Depth
CO_2	1.0000 (21) 0.0000														
CH_4	-0.0479 (21) 0.8365	1.0000 (21) 0.0000													
CO	0.3408 (21) 0.1306	0.2836 (21) 0.2128	1.0000 (21) 0.0000												
CS_2	0.1571 (21) 0.4965	0.4832 (21) 0.0265	0.2660 (21) 0.2439	1.0000 (21) 0.0000											
Ar	0.0343 (21) 0.8826	0.0299 (21) 0.8975	-0.1042 (21) 0.6532	-0.0937 (21) 0.6861	1.0000 (21) 0.0000										
Ne	-0.1540 (21) 0.5052	-0.0566 (21) 0.8074	-0.0762 (21) 0.7428	0.0672 (21) 0.7724	0.1205 (21) 0.6030	1.0000 (21) 0.0000									
He	-0.0260 (21) 0.9110	0.3442 (21) 0.1265	0.0657 (21) 0.7772	-0.0985 (21) 0.6710	0.8603 (21) 0.0000	0.1592 (21) 0.4907	1.0000 (21) 0.0000								
H_2S	-0.1459 (21) 0.5280	-0.0506 (21) 0.8276	-0.3175 (21) 0.1608	-0.1411 (21) 0.5417	-0.1136 (21) 0.6239	-0.1194 (21) 0.6062	-0.1648 (21) 0.4754	1.0000 (21) 0.0000							
SO_2	0.3407 (21) 0.1307	-0.1714 (21) 0.4575	-0.2631 (21) 0.2491	-0.1192 (21) 0.6067	-0.0907 (21) 0.6958	-0.0753 (21) 0.7456	-0.1317 (21) 0.0000	0.1104 (21) 0.6337	1.0000 (21) 0.0000						
N_2	0.1263 (21) 0.5854	-0.0370 (21) 0.8735	-0.1226 (21) 0.5964	-0.0657 (21) 0.7772	0.9769 (21) 0.0000	0.0152 (21) 0.9477	0.8014 (21) 0.0000	-0.1131 (21) 0.6254	-0.0705 (21) 0.7614	1.0000 (21) 0.0000					
H_2	-0.1423 (21) 0.5383	0.5631 (21) 0.0079	0.0637 (21) 0.7839	0.3723 (21) 0.0965	0.2949 (21) 0.1944	-0.1827 (21) 0.4280	0.5585 (21) 0.0085	-0.1223 (21) 0.5975	-0.1211 (21) 0.6012	0.3021 (21) 0.1832	1.0000 (21) 0.0000				
O_2	0.1048 (21) 0.6513	-0.0527 (21) 0.8205	-0.1341 (21) 0.5623	-0.0812 (21) 0.7264	0.9792 (21) 0.0000	-0.0168 (21) 0.9424	0.7851 (21) 0.0000	-0.0985 (21) 0.6711	-0.0615 (21) 0.7912	0.9962 (21) 0.0000	0.2854 (21) 0.2099	1.0000 (21) 0.0000			
C_nH_n	0.2397 (21) 0.2953	0.2843 (21) 0.2117	0.2678 (21) 0.2405	0.8738 (21) 0.0000	-0.1468 (21) 0.5255	-0.0106 (21) 0.9638	-0.1648 (21) 0.4753	-0.1455 (21) 0.5291	0.1554 (21) 0.5013	-0.0932 (21) 0.688	0.3039 (21) 0.1804	-0.1112 (21) 0.6312	1.0000 (21) 0.0000		
Total Sulfur	-0.0218 (21) 0.9253	0.0333 (21) 0.8862	-0.298 (21) 0.1896	0.0882 (21) 0.704	-0.1532 (21) 0.5074	-0.1148 (21) 0.6202	-0.2128 (21) 0.3544	0.9476 (21) 0.0000	0.3062 (21) 0.177	-0.141 (21) 0.542	-0.0516 (21) 0.8242	-0.1288 (21) 0.5778	0.1156 (21) 0.6178	1.0000 (21) 0.0000	
Depth	0.1235 (21) 0.5938	0.2654 (21) 0.2449	0.1739 (21) 0.4509	0.1411 (21) 0.5418	-0.4386 (21) 0.0467	-0.45 (21) 0.0407	-0.3184 (21) 0.1595	0.4178 (21) 0.0595	0.2172 (21) 0.3442	-0.4315 (21) 0.0508	-0.1076 (21) 0.6424	-0.4237 (21) 0.0556	0.2259 (21) 0.3249	0.4855 (21) 0.0257	1.0000 (21) 0.0000

correlated (0.45-0.85) are CH_4-H_2, He-H_2, and CS_2-CH_4. Depth was included as a variable in order to determine if any gas correlated with depth, only H_2S had any significant correlation (0.42). Moderate negative correlation (-0.42) is noted for the principal atmospheric gases (N_2, O_2, and Ar) versus depth.

The results of the fluid inclusion gas analyses exhibit several systematic trends apparently related to depth and paragenesis. In Figure 3.4 early quartz associated with molybdenite and base metal deposition from the shallow portions of the system (<700 m) are distinguished from all other samples on the basis of total sulfur relative to CO_2. If H_2S is plotted instead of total sulfur, then the early quartz is the only phase that plots off the CO_2-H_2O/100 side of the diagram. In general, samples representing different paragenetic positions show a trend in total mutli-carbon organics relative to CO_2 and H_2O with those late in the paragenesis tending to be the richest in total multi-carbon organics (Fig. 3.5).

Further distinction between organic and sulfur contents can be made regarding gas chemistries of early versus late minerals and shallow versus deep portions of the Sulphur Springs hydrothermal system (Fig. 3.6). Samples from depths <700 m of late calcite and fluorite have greater total multi-carbon organic content compared to early quartz, and those samples from depth >700 m generally higher CH_4 and lower sulfur contents than samples from depths <700 m. However, fluids produced at 1755 m in VC-2B are similar to early quartz from depths <700 m in that they are lower in CH_4 and have higher sulfur than fluids analyzed from inclusions over the same depth interval.

There is generally little variation in CO_2-total sulfur-multi-carbon organic composition of the Sulphur Springs fluids; most of the samples cluster at the CO_2 apex. Early quartz associated with molybdenite-base metal mineralization plots away from the CO_2 apex. Calcite and fluorite mineralization tends to have high total organics relative to total sulfur (Fig. 3.7).

C_nH_n volatiles are C_2 to C_6 organic compounds. Because of the multiple organic species present, positive identification of individual compounds is not possible from the mass spectra. However, analysis of present day gases by gas chromatography indicates the presence of C_2H_6,

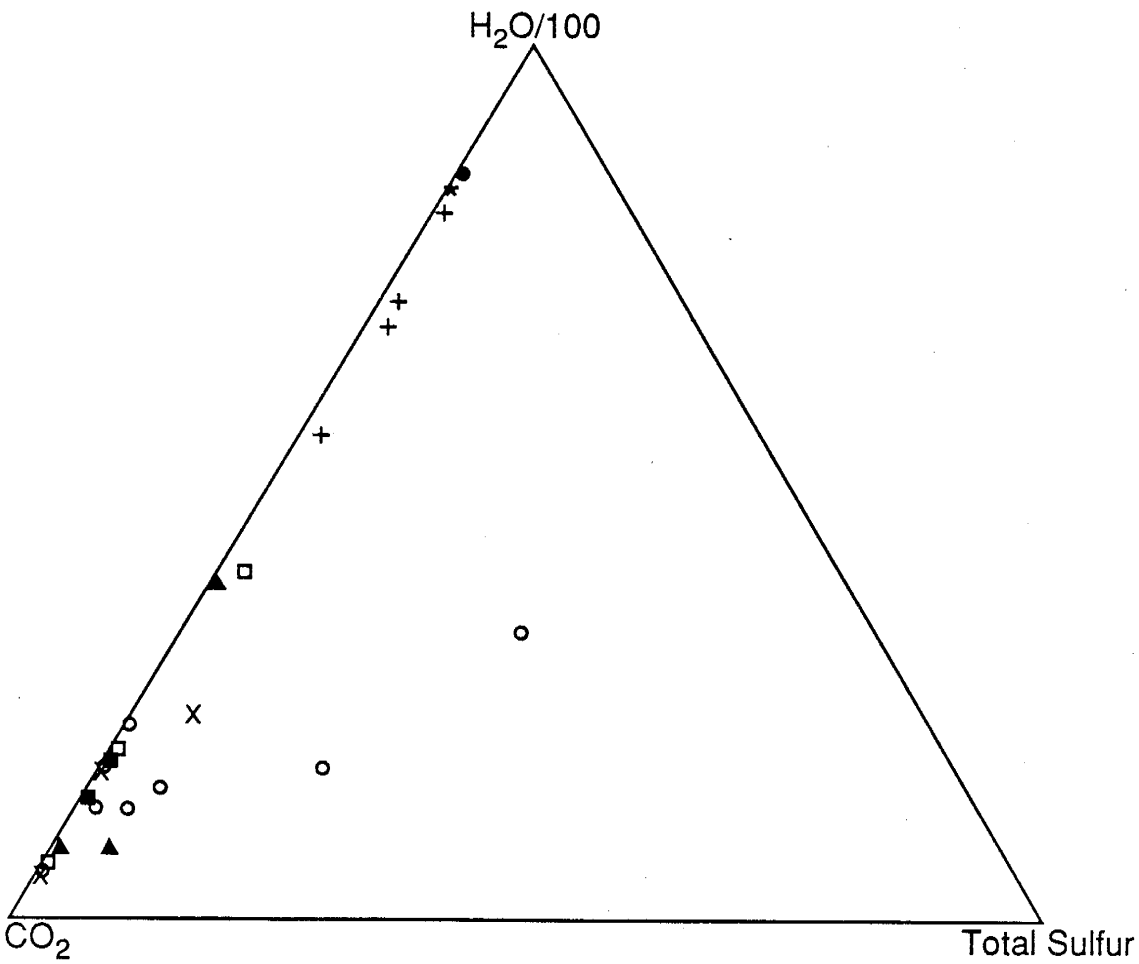

Figure 3.4. Ternary plot of H_2O-CO_2-Total Sulfur. Open circles are early quartz from depths <700 m, triangles are late fluorite from depths <700 m, Xs are intermediate to late stage calcite from depths <700 m, * is present day VC-2B gas composition, closed circle is present day VC-2A gas composition, crosses are present day Redondo Creek gas compositions, open squares are early quartz from depths >700 m, filled squares are from intermediate to late stage calcite from >700 m depths.

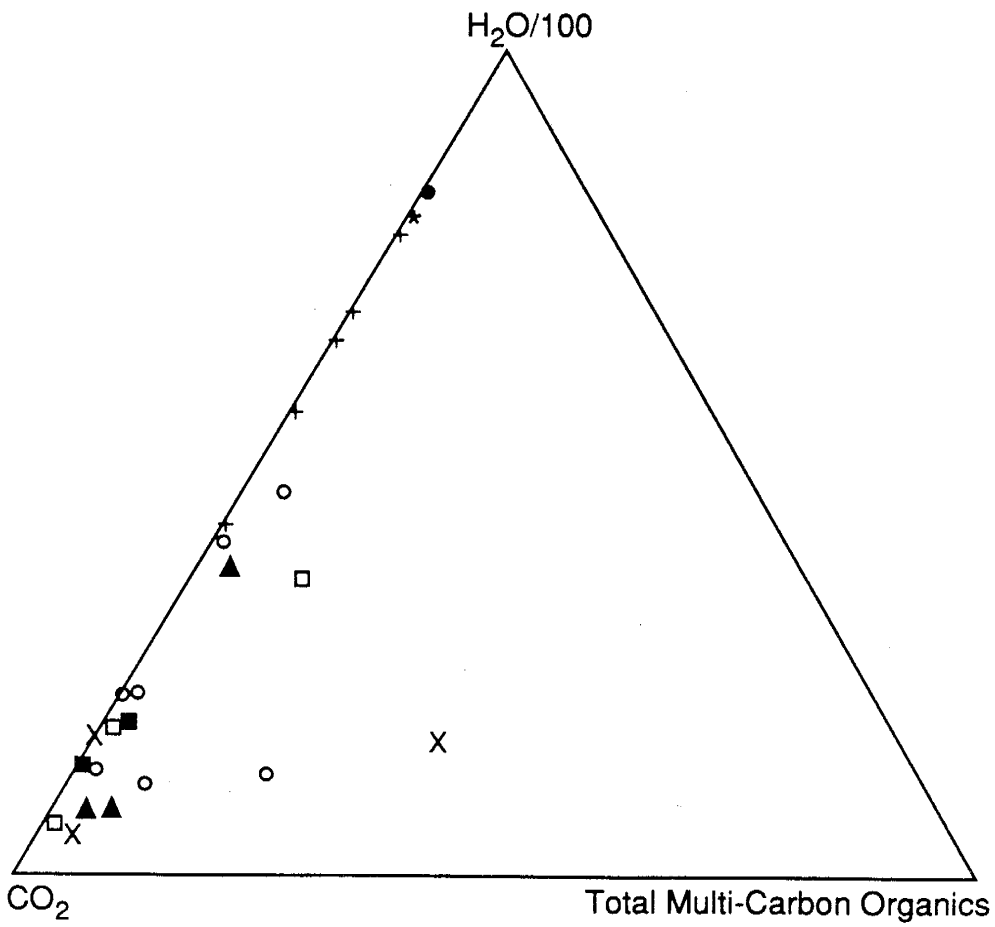

Figure 3.5. Ternary plot H_2O-CO_2-Total Multi-Carbon Organics. Same symbols as Figure 3.4.

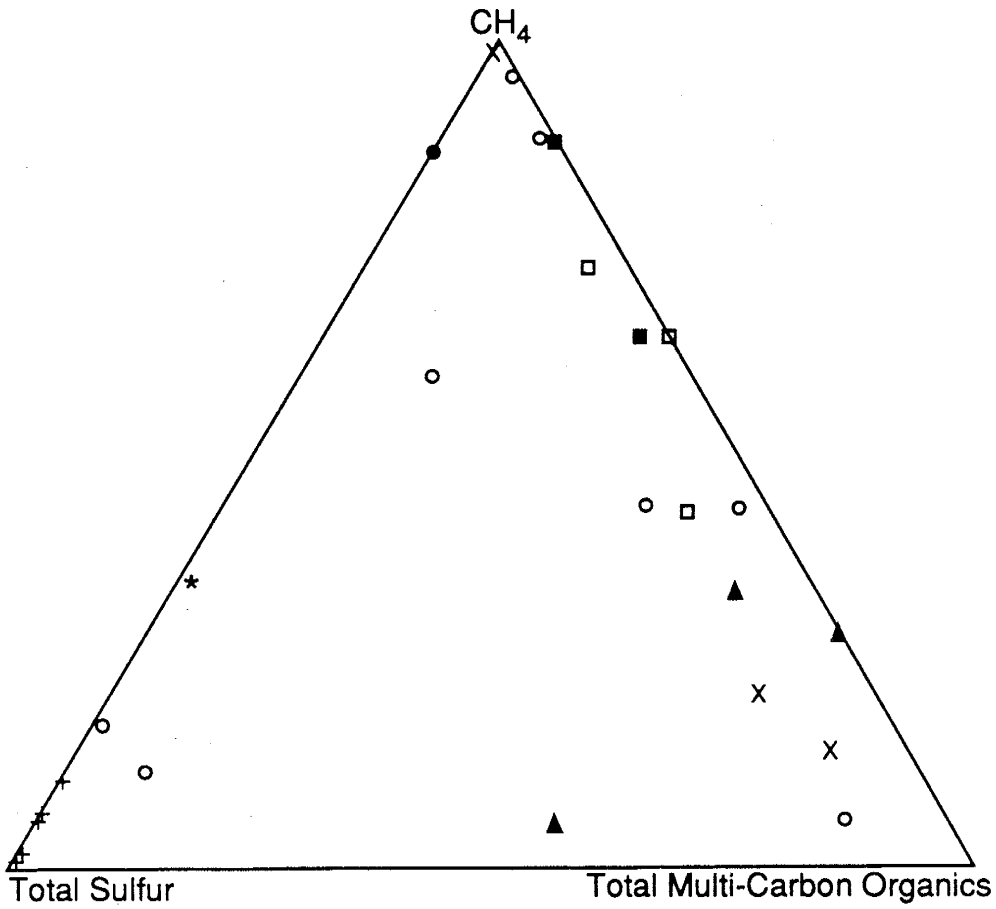

Figure 3.6. Ternary plot of CH_4-Total Sulfur-Total Multi-Carbon Organics. Same symbols as Figure 3.4. Redondo Creek gases were not analyzed for mutli-carbon organic species.

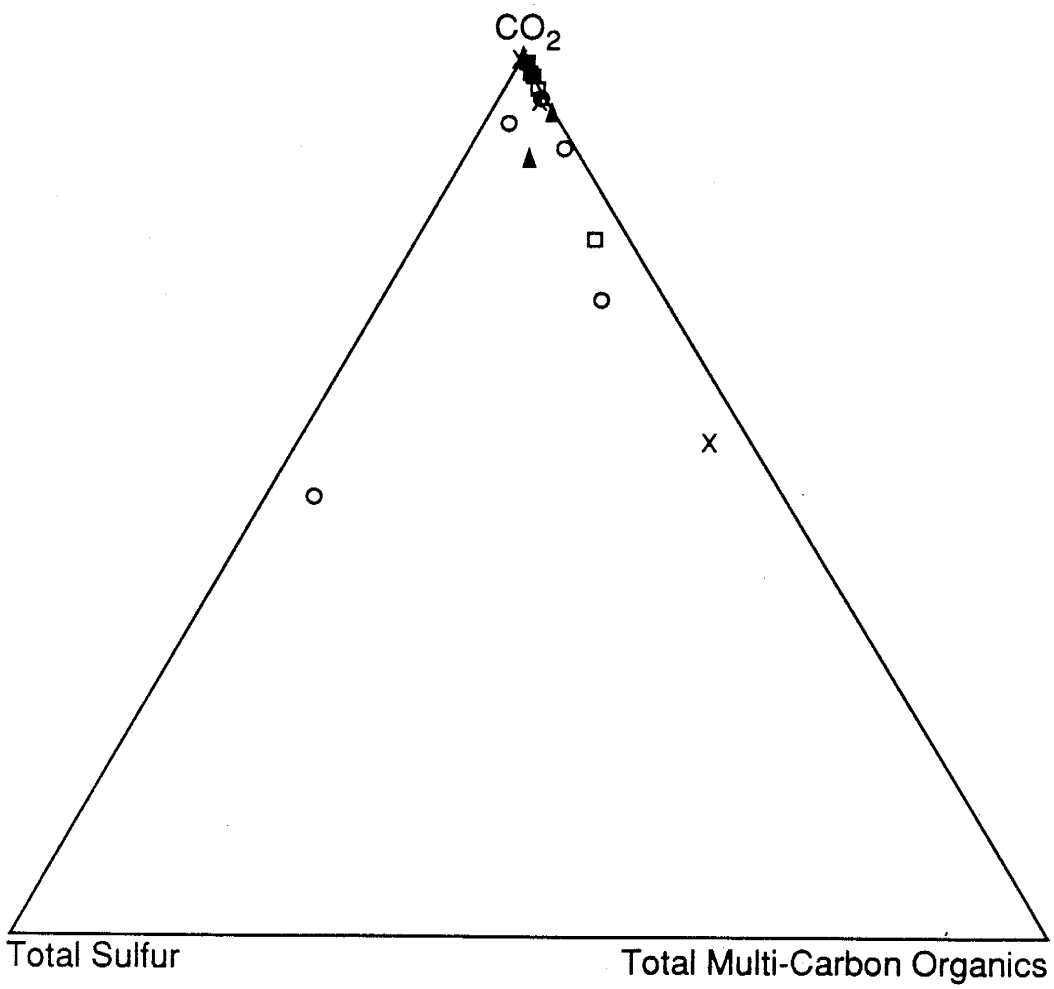

Figure 3.7. Ternary plot of CO_2-Total Sulfur-Total Multi-Carbon Organics. Same symbols as Figure 3.4.

C_3H_6, C_3H_8, C_4H_8 and C_4H_{10} (Goff et al., 1990).

One sample from 1697 m has approximately 60 mole % gas is present in the fluid. The amount of CO_2, H_2S, CH_4, SO_2, and the noble gases in this sample are within the ranges measured for other samples from depths >700 m. The major gases in this particular sample are N_2 (45.6 mole %) and O_2 (7 mole %). Examination of the noncondensible gas spectra indicates that it is typical of air measured in the QMS. Although this sample will be disregarded for the concentration of N_2, O_2, and Ar because of the air contamination, the concentrations of CO_2 and H_2S are little effected.

Variable amounts of H_2 were detected in the samples. H_2 can readily be produced during thermal decrepitation by reactions involving H_2O, CO_2, and C_nH_n, as well as through thermal decrepitation of organic compounds. Therefore, the amounts of H_2 can be anomalously high. The amount of H_2 can be corrected for (Norman et al., 1991b) and these corrected data are presented in Table 3.1. Like H_2, CO is similarly produced, and it is strongly suspected that some CO was produced during the thermal decrepitation process. However, many samples have significant quantities of CO (up to 6.8 mole %), and CO correlates weakly with other carbon-bearing species.

Hydrogen sulfide ranges from 0.00007 mole % to 1.2 mole %. The amount of H_2S found in the inclusion fluids is related to depth and to a lesser extent paragenesis. Minerals that were deposited later in the paragenesis generally have lower H_2S contents. H_2S is not the product of sulfide decomposition (Norman, 1977; Smith 1983).

Carbon disulfide was detected in more than half of the samples analyzed. Concentrations of CS_2 range from 0.00078 to 0.31 mole %. CS_2 has been reported in inclusion fluids from porphyry copper systems (Palin, 1983), and CS_2 may be an important emanation from some volcanic environments (Miller and Janecky, 1990). CS_2 may also be produced in the extraction line. There appears to be no correlation between the amounts of H_2S and CS_2. The highest H_2S values have no detectable CS_2. On the other hand, the 2 samples that have the highest C_nH_n contents have the highest CS_2 values.

Calculation of fO_2 and fS_2

Log fO_2 is calculated by means of the reactions:

$$CH_4 + O_2 = CO_2 + 2H_2 \quad (3.1)$$

$$H_2 + O_2 = H_2O \quad (3.2)$$

$$CH_4 + 2O_2 = CO_2 + 2H_2O \quad (3.3)$$

$$CH_4 + O_2 = C + 2H_2O \quad (3.4)$$

Equations 3.1-3.3 generally closely agree with one another for the calculated log fO_2 from the corrected gas analysis (Table 3.1); however, log fO_2 calculated from Equation 3.1 was used in all calculations requiring fO_2 and is the value reported in Table 3.1. Only for samples from depths >700 m where carbon is present did Equation 3.4 gave values similar to Equations 3.1-3.3.

Sulfur fugacities calculated form the inclusion analyses were obtained from the equation

$$2H_2O + S_2 = O_2 + 2H_2S \quad (3.5)$$

using fO_2 calculated from Eq. 3.1 and H_2S concentration obtained from the gas analyses.

Estimate of Pressure

Inclusion gases can be used to estimate the trapping pressure at the time of mineralization, if the following assumptions are met: (1) volatiles in the hydrothermal fluids are at the same concentrations as measured, (2) pressure at the time of trapping was equal to or greater than the sum of the vapor pressures of the individual species, and (3) the fluid was homogeneous. However, pressure calculations based on inclusion gas data from boiling systems generally lead to unreasonably high calculated pressures because excess gas (Norman and Sawkins, 1987). Most of the gas in boiling systems must reside in vapor-filled inclusions because the vapor-filled inclusions may be trapped in greater proportion than the liquid-filled inclusions and the high vapor to liquid partition coefficients of the principal gas species would result in a greater percentage of each gas

species to be in the gas phase (Giggenbach, 1980). Samples VC-2B 1254, 4565 and 5533 were chosen for the calculation of pressure because these samples show the least evidence of boiling (Table 3.3). For those samples deposited under nonboiling conditions, total pressure is then equal to the sum of partial pressures of principal gases:

$$P_T > P_{H2O} + P_{CO2} + P_{N2} \qquad (3.6)$$

where P_T is the total pressure and P_{H2O}, P_{CO2}, and P_{N2} are the partial pressures of H_2O, CO_2 and N_2, respectively.

Calculated partial pressures of H_2O range from 19 to 85 bars. Partial pressures of CO_2 and N_2 range from 93 to 215 bars and 69 to 182 bars, respectively; therefore, calculated P_T is between 176 and 447 bars. Pressure estimates from microthermometric data alone set a minimum pressure of 85 bars for purely hydrostatic conditions at 300°C and pure water.

Gases not used in the pressure calculation were H_2, CH_4, CO, SO_2, H_2S, and the multi-carbon organic species for the following reasons. Hydrogen, CH_4, and CO may have been partly or entirely produced during the extraction procedures. Besides, the amounts of these gases are such that not including them into the pressure estimate would not significantly affect the results. Organic species were not include in the calculation because (1) the Henry's Law coefficients of most organic species are not known at elevated temperatures (2) some of the organic compounds may have occurred as immiscible liquids in the hydrothermal fluid and (3) most importantly, the Henry's Law coefficients of organic species inferred in ore solutions are quite low. Hydrogen sulfide and SO_2 have such low Henry's Law coefficients that their contribution to total pressure can be neglected, and the noble gases are in such low concentration that their partial pressures are negligible.

Table 3.3 Calculated Minimum Pressure of Mineralization and Partial Pressures of CO_2, N_2, and H_2O

Sample (°C)	Mean Th	Mean Salinity Eq. Wt.% NaCl	$P(CO_2)$ bars	$P(N_2)$ bars	$P(H_2O)$ bars	Pt bars
VC2B-1254	210	1	93	69	14	176
VC2B-4565	275	3	215	182	51	447
VC2B-5533	300	2.5	65	117	85	266

ORIGIN OF GASES

Present day fluids produced at Sulphur Springs have relatively low gas contents typical of volcanic-hosted geothermal systems (Giggenbach, 1980), whereas data from fluid inclusion analyses indicate high concentrations of gases (up to 22 mole % gas). Gases produced in hydrothermal systems may be divided according to origin into atmospheric, metamorphic-magmatic, and equilibrium (those resulting from reactions in the reservoir) (Truesdell and Janik, 1986). Principal gases in hydrothermal systems are CO_2 and H_2S, but include also minor amounts of CH_4, N_2, H_2, and trace amounts of noble gases. Gases in the system C-O-H-N occur in equilibrium proportions in geothermal systems, while H_2S concentrations are related to H_2 concentrations and are controlled by the buffer system pyrite and Fe-bearing chlorite (Giggenbach, 1980; 1981).

Atmospheric Gases

In many geothermal systems N_2, Ne, Ar, Kr, and Xe are of atmospheric origin (Henley and Ellis, 1983; Truesdell and Janik, 1986). Geologic and isotopic evidence show that essentially all water in the Valles hydrothermal system is of meteoric origin (Vuataz and Goff, 1986; Goff et al., 1989), and geothermal fluids from systems without significant boiling have noble gas concentrations indicating air-saturated water (ASW) (Mazor, 1976).

Ar is usually of atmospheric origin (Mazor, 1976), and although N_2 behaves in part as a reactive gas, its origin is generally atmospheric (in the absence of abundant organic matter in the host rocks) (Truesdell and Janik, 1986). In Table 3.4, the concentrations of N_2, Ar, and He in ASW at 5°C. Also shown in Table 3.4 are the concentrations of these gases at several possible recharge elevations compared with the concentrations of these gases in the fluid inclusions and the present day fluids. Truesdell andJanik (1986) report N_2/Ar(atm) as high as 500 based on total Ar reported by Smith and Kennedy (1985) in Redondo Creek reservoir (Baca) fluids. In this study, N_2/Ar ratios are as high as 11600, much higher than air or ASW.

Concentrations of Ar and N_2 in Sulphur Springs fluid inclusions and present day fluids are up to $6x10^3$ times more concentrated in N_2 and up to $7.5x10^2$ times more concentrated in Ar versus

Table 3.4. Concentrations of Conservative Gases from Data in Table 3.1 Compared with Concentration in Air and Air Saturated Water

Sample	Ar	He	N_2	N_2/Ar^*
VC2A-129	1.4	0.12	140	100
VC2A-160	6.6	0.59	601	91
VC2A-339	2	0.01	10	5
VC2A-541	0.2	0	8	40
VC2A-1137	0.13	0.01	527	4054
VC2A-1485QTZ	1.6	0.05	394	246
VC2A-1485CC	1.2	0.1	482	402
VC2A-1712	2	0.01	26	13
VC2B-760	13.4	2.2	540	40
VC2B-882	5.1	0.04	166	33
VC2B-895	8.6	0.67	327	38
VC2B-933	3	0.44	1766	589
VC2B-1254	0.4	0.03	112	280
VC2B-1322FLR	2.3	0.8	5890	2561
VC2B-3017	0.02	0	233	11650
VC2B-4565	0.6	0.39	788	1313
VC2B-4755	0.8	0.04	323	404
VC2B-5533	18	1	2210	123
VC2A	0.19	0.004	11	58
VC2B90	0.04	0.04	4	100
ASW (2900 m)+	0.0238	2.7E-06	0.882	37.0
ASW (1700 m)+	0.0275	3.1E-06	1.02	37.0
ASW (20°C)	0.0277	1.04	37.5	
literature				
Air, literature	0.934 %		78.08 %	83.6

Units are mole % x1000

* Mole ratios

\+ ASW water saturated with air at 5oC and 0.70 or 0.81 bars abs (From Truesdell and Janik, 1986)

2900 m ASW. He is up to $8x10^5$ times the expected meteoric recharge composition. Several mechanisms are possible for the elevated concentrations of these gases (1) boiling and the analysis of vapor-rich inclusions, (2) addition of excess air, (3) chemical and/or metamorphic reactions, and (4) magma. Boiling is well documented in the Sulphur Springs hydrothermal system (Goff et al., 1985). Therefore, samples used for inclusion gas analysis contained both vapor- and liquid-rich inclusions. In these samples most of the gas analyzed resided in vapor-filled inclusions because the fugacities of the gases for near-surface samples would be unrealistically high if the liquid-rich inclusions contained more than a few tens of a percent total gas. N_2 and Ar in 2900 m ASW could have been concentrated into the volatile phase by boiling, but it is doubtful boiling could account for the very high values of N_2 and Ar.

Analysis of gases in groundwaters has shown that concentrations of N_2 and Ar can be elevated over what is expected for water in equilibrium with the atmosphere (Heaton and Vogel, 1981). It has been proposed that the addition of air occurs during recharge and seepage through the unsaturated zone. Air bubbles become trapped in the capillary-sized pore spaces of the vadose zone at the capillary fringe and carried down to below the water table (Heaton and Vogel, 1981). Total solution of the bubbles will occur at a depth where the hydrostatic pressure is sufficiently great.

Other potential sources for N_2 include NH_3, NH_4^+, and organic residues in the Pennsylvanian Madera Formation. NH_3 was not observed in the inclusion gases possibly because it was masked by mass peak overlap with CO_2 and H_2O, but NH_3 has been reported by Truesdell and Janik (1986) for the Redondo Creek area and by Goff et al. (1990) for Sulphur Springs. Low concentrations (or absence) of NH_3 in the mass spectra is consistent with theoretical calculations of Ferry and Baumgartner (1986) which show that N_2 predominates over NH_3 in most crustal environments. Above temperatures of 150°C, the free energy for the reaction

$$N_2 + 3H_2 = 2NH_3 \qquad (3.7)$$

is positive and, therefore, NH_3 is not the favored gas in high temperature environments. NH_4^+ can substitute into the structure of many sheet silicates (Srodon and Eberl, 1984). NH_4^+-bearing illites in black shales hosting a stratiform base metal deposit in Alaska have >50% NH_4^+ (Sterne et al., 1982). Also, up to 7% of the K sites are occupied by NH_4^+ in interlayered illite/smectites formed during burial diagenesis in the Texas Gulf Coast (Cooper and Adebin, 1981). N_2 could then be released from this source during prograde regional and/or contact metamorphism. Organic residues are potential sources for CO_2, CH_4, and N_2. During metamorphism, organic matter decomposes to CH_4, $\pm H_2S$, $\pm CO_2$ and pyrobitumen (Kinghorn, 1983; Evans et al., 1971; Evans and Staplin, 1971). The nitrogen content of bitumen is commonly on the order of 0.4 to 4.3 wt.% (Wen et al., 1978). The deepest well drilled in the Valles caldera contains rocks at a depth >2440 m which resemble those developed during isochemical thermal metamorphism (Hulen and Nielson, 1986). These data, therefore suggest that the nitrogen concentration observed at Sulphur Springs may be due to the combined processes of boiling and liberation of "fixed" nitrogen during metamorphism.

Ar and He concentrations are elevated over those for 2900 m ASW (Table 3.4). These concentrations could be the result of boiling and the analysis of vapor-filled inclusions. Argon concentrations can be modified by the addition of radiogenic Ar ($^{40}Ar^*$) derived from decay of ^{40}K and can be of crustal or magmatic origin. This excess $^{40}Ar^*$ may account for elevated amounts of Ar. Analysis of fluid inclusion noble gases indicate as much as 40% excess $^{40}Ar^*$ (Musgrave et al., 1991). Compared to typical crustal radiogenic He (R/R_a is 0.02 to 0.10, where R is the $^3He/^4He$ ratio in the sample and R_a is the ratio in air), the large excesses of total He is due to anomalous amounts of ^3He; data from fluid inclusions indicate high $^3He/^4He$ values (up to 6 times air)(Musgrave et al., 1991). Samples from Redondo Creek have similar values (up to 4.8 times air) (Smith and Kennedy, 1985). These ^3He excesses indicate that the hydrothermal fluids of Sulphur Springs and Redondo Creek contain a significant contribution of mantle-derived He.

The gas compositions indicate a magmatic dominance and an atmospheric domination for Sulphur Springs gases and a crustal dominance for Redondo Creek gases (Fig. 3.8). Samples from

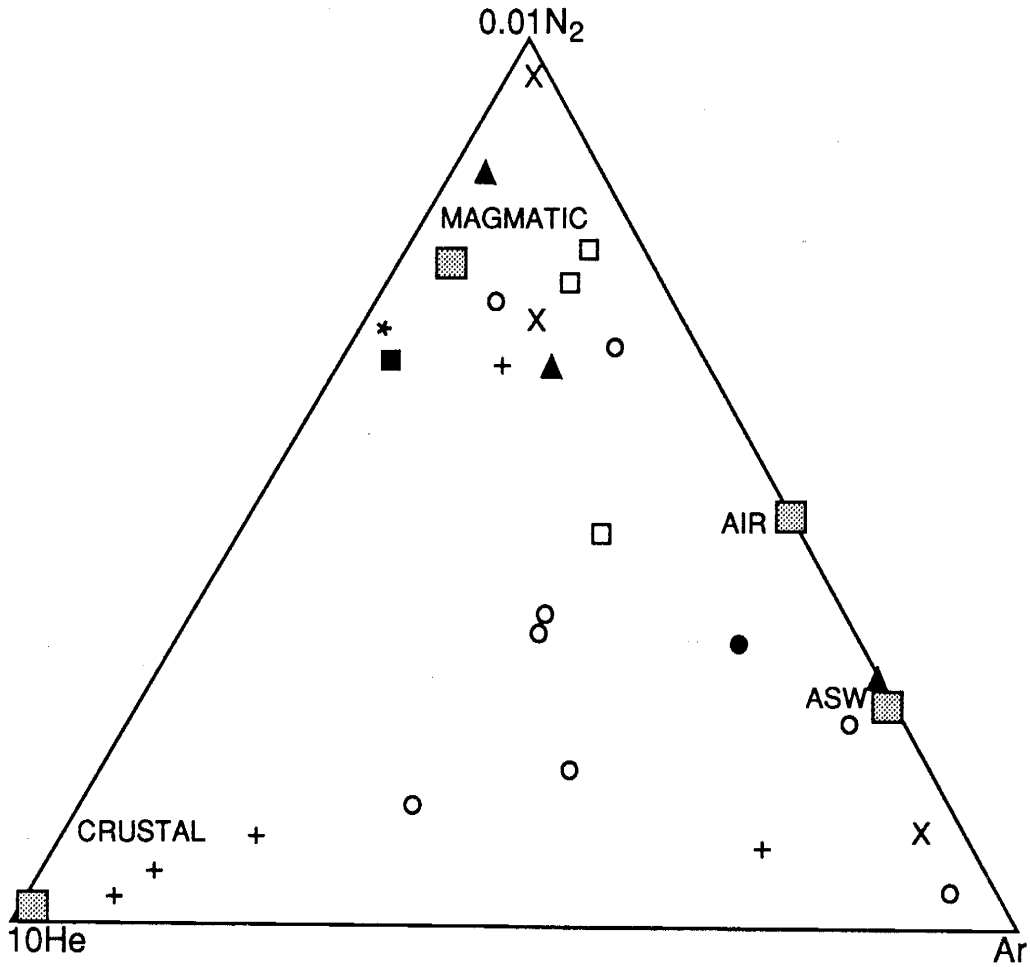

Figure 3.8. N_2-Ar-He plot for Sulphur Springs inclusion gases. Same symbols as Figure 3.4. Magmatic, air ASW and crustal fields from Giggenbach (1986).

depths <700 m cluster around the air and ASW fields, and those samples from depths >700 m cluster around the magmatic field. A few of the early quartz from <700 m also show a trend toward having a crustal component as do samples from Redondo Creek.

Metamorphic-Magmatic Gases

Although magmatic gases have been characterized from volcanic eruptions, their presence in most geothermal systems has not been conclusively demonstrated. The $\delta^{13}C$ values of marine limestones and volcanic CO_2 are = -5 to 2 per mil and -10 to -5 per mil, respectively (Hoefs, 1987). Values of $\delta^{13}C$ for CO_2 in the Redondo Creek fluids range between -4.8 to -4.5 per mil, (Truesdell and Janik, 1986), those for Sulphur Springs fumarolic CO_2 range from -5.0 to -2.5 per mil (Goff et al., 1985), and for fluids produced from VC-2A are between -4.8 to -4.6 per mil (C. Janik, unpublished data). Samples of unaltered Madera Formation from the southwestern portion of the Jemez volcanic field are in the range of -5.6 to -3.1 (average -4.4) per mil (Goff et al., 1985), and whole rock samples of the Madera Formation from VC-2B range between -7.2 to 0.4 per mil. The values of $\delta^{13}C$ in the produced fluids from Redondo Creek and Sulphur Springs are consistent with derivation of CO_2 from the marine limestones of the Madera Formation (Goff et al., 1985) and from cooling magma. Thermal metamorphism of the Madera Formation through reactions such as

3Actinolite + 6Calcite + K-feldspar = Phologopite + 12Diopside-Hedenbergite + $6CO_2$ + $2H_2O$ (3.8)

or

Epidote + 6Calcite + 2Quartz = Actinolite + Anorthite + $3CO_2$ + $3H_2O$ (3.9)

could account for the CO_2 observed at Sulphur Springs.

Hydrogen sulfide could be derived from a magmatic source, reduction of SO_4 in the

hydrothermal fluid, or leaching of sulfur from the country rocks. Sulfur dioxide was detected among the gases in all but two samples. SO_2 can be produced by thermal decomposition of some sulfates, but the fact that sulfate minerals constitute a very small portion of the vein material suggests that the chance of any sulfate minerals producing SO_2 is considered negligible. Samples VC-2B 3017 and VC-2B 4755 have associated anhydrite yet these samples yielded among the lowest SO_2 concentrations (Table 3.1). Another possibility for the production of SO_2 is an analytical decomposition product of some other sulfur species such as thiosulfate during heating and decrepitation of the sample in the vacuum system (Landis and Rye, 1989). It has been suggested that the SO_2 observed in the Creede hydrothermal fluids was produced by decomposition of intermediate and metastable sulfur species that were ultimately formed by oxidation of H_2S during mixing of the hydrothermal fluids with overlying low pH groundwater (Landis and Rye, 1989). SO_2 does appear to be related to the amount of H_2S. The highest amounts of SO_2 correlate with higher amounts of H_2S, though typically an order of magnitude or more less in concentration. It is curious to note the one sample with the highest H_2S (1.2 mole %) had no detectable SO_2.

Relationship of the mineralization at Sulphur Springs to a buried Climax-type Mo deposit by Hulen et al. (1987) allows further speculation on the possible source of the sulfur gases. SO_2 derived from a magmatic source disproportionates at $T<400°C$ according to the reaction:

$$4SO_2 + 4H_2O = 3H_2SO_4 + H_2S \quad (3.10)$$

The above reaction may be the most important mechanism by which H_2SO_4 is formed in the development of hypogene advanced argillic alteration deep within hydrothermal systems, and is exemplified by Matsukawa, Japan (Nakamura et al., 1970, an active system) and Summitville, Colorado (Stoffregen, 1987; Hayba et al., 1985, a fossil system). No hypogene advanced argillic alteration has been identified at Valles caldera. Calculations by Stoffregen (1987) for Summitville show a solution in equilibrium with a vapor phase consisting of subequal amounts of SO_2 and H_2S. Main stage ore formation at Butte, Montana took place with SO_2:H_2S ranging from 6:1 to 1:5

(Brimhall and Ghiorso, 1985). Brimhall and Ghiorso (1983) have assigned average sulfur valances to these ratios at Butte of +2 to -1. Since H_2S, in general, dominates over SO_2 at Sulphur Springs, the average sulphur valance of Brimhall and Ghiorso (1983) for Sulphur Springs fluids is between -1 and -2 or in terms of proportion of the gases $1/6SO_2 + 5/6H_2S$ and H_2S, respectively. In other words, the dominant sulfur species at Sulphur Springs is H_2S.

Sulfur isotopic data suggest a magmatic source for sulfur at Sulphur Springs. Aqueous H_2S in fluids produced from 490 m in VC-2A yielded $\delta^{34}S$ of 0.8 per mil and from 1755 m in VC-2B yielded a value of 2.5 per mil (McKibben and Eldridge, 1990), and sulfur isotopic data from fumarolic sulfur are 0 per mil, ±2 per mil (F. Goff, unpublished data). Ion microprobe studies of pyrite crystals in the upper 130 m of VC-2A indicate a $\delta^{34}S$ of 0 per mil, ±5 per mil, indistinguishable from the H_2S in the hydrothermal fluid (McKibben and Eldridge, 1990).

Equilibrium gases

Minor and trace gases known to be reactive may be produced from reactions involving more abundant forms of the same elements in the hydrothermal fluid and/or wall rocks. These gases include H_2, H_2S, and CH_4; the origins of H_2 and H_2S have been discussed previously.

Methane associated with high temperature geothermal areas has $\delta^{13}C$ values that are much lighter than the $\delta^{13}C$ of associated CO_2, reflecting partial origin from organic carbon (Henley and Ellis, 1983). Methane observed in the present day hydrothermal fluids is up to three orders of magnitude lower than the concentrations measured in the inclusion fluids. As previously stated, the CH_4 in the inclusions may have been produced totally by the extraction process or it may be derived by the thermal decomposition of organic residues in the Madera Limestone.

The concentrations of CO_2, N_2, and CH_4 are elevated over those observed in the present day fluids (Table 3.1). A possible explanation for this is that the CO_2, N_2 and CH_4 are products of thermal metamorphism, and at the onset of metamorphism large amounts of these gases were released to the fluid. Since the hydrothermal system has been active for the past 1 million years (Goff and Shevenell, 1987; Goff et al., 1989), the organic residues have now been mostly

devolatilized, and these gases are not being released in as high concentrations as in the past. Alternatively, excess gas because of the analysis of mixtures of liquid-rich and vapor-rich inclusions is another explanation of the observed high concentration of these gases.

Oxygen is observed in the present day fluids and the paleo-fluids (Table 3.1). Present day concentrations are due to the mixing of oxygenated groundwaters with the hydrothermal fluid. However, it would be expected that O_2 trapped in the fluid would have had time to react with various species in the fluid, such as Fe and H_2S and not be measured. It could be that there is an excess of O_2, following the model for excess Ar proposed by Heaton and Vogel (1981) and all of it is not consumed. Because these are bulk analyses the contribution of O_2 from relatively recent secondary inclusions containing more meteoric ASW than hydrothermal fluids also may explain the presence of O_2 in the inclusion analyses. Equations 3.3, 3.4 and 3.6, representing reactions among gases and minerals, also are potential sources of O_2 in the hydrothermal fluid. The negative correlation of O_2 (along with other atmospheric gases) with depth strongly suggest it is derived from oxygenated groundwater.

Carbon monoxide at the concentrations observed in the inclusion analysis is another interesting problem (Table 3.1). Piperov and Penchev (1973) discussed the problem of high amounts of H_2 and CO in their study of gases in fluid inclusions in allanite. They found large amounts of CO and H_2 were produced at decrepitation temperatures above 450°C, and proposed the CO and H_2 might be produced through reactions such as:

$$H_2 + CO_2 = H_2O + CO \quad (3.11)$$

and

$$CH_4 + H_2O = CO + 3H_2 \quad (3.12)$$

However, calculation of the free energies for these reactions from the data of Robie et al. (1979) indicates that the reactions will not proceed to the right below temperatures of about 700°C. Hence, it seems difficult to generate large amounts of CO for decrepitation temperatures of 450-500°C.

Alternatively, the CO is actually in the Sulphur Springs fluid and is produced from the reaction

$$2C + O_2 = 2CO \quad (3.13)$$

The Madera Limestone contains coaly horizons (Hulen and Gardner, 1989) which would supply the carbon necessary for the reaction to proceed.

DISCUSSION

Organic compounds

The detection of organic compounds in inclusion fluids agrees with the observed organic compounds in present day fluids (Goff et al., 1990). Organic compounds detected are all light hydrocarbons with less than seven carbon atoms. In part this may be due to the measurement and extraction methods used; electron bombardment in the ion source of the QMS would tend to fragment heavier hydrocarbons, hydrocarbons with more than seven carbon atoms would tend to condense with water in the dry ice-alcohol trap and not be detected, and thermal decrepitation of the sample would tend to crack the heavier hydrocarbons. However, the data suggest that the organic compounds were predominantly of the lighter types. The proportion of C_5 to C_7 compounds is less than that of C_2 to C_4 compounds based on mass peak-heights in the mass spectra. The detection of predominantly C_2 to C_4 hydrocarbons in the present day fluids also lends credibility to the inclusion data since the present day gases were detected by gas chromatography.

Oxidation State of the Fluids

Water is the major reservoir for elemental hydrogen in hydrothermal systems, which reacts with rock to produced buffered fugacities of O_2 and H_2. The oxidation state of the paleo-fluids versus depth and paragenesis and of present day fluids can be assessed by plotting the calculated

fO_2 versus the T_h of the inclusions for that particular sample, the measured temperature (VC-2A and VC-2B) and the NaKCa geothermometer or total enthalpy temperatures (Redondo Creek samples) along with various gas and mineral buffer species (Fig. 3.9). Early quartz shows a general trend of increasing fO_2 with depth (and temperature), and samples from depths <700 m lie above the FeS-FeS_2 line, whereas those from depths >700 m lie below the line suggesting pyrrhotite should be the stable phase for depths >700 m. However, for Sulphur Springs, the stable phase at low fS_2 is chlorite. All samples at temperatures >2.0 (Scale = 10^3/K) have no associated chlorite and plot in the FeS_2 field, whereas chlorite is present in all samples with temperatures <2.0 (Scale = 10^3/K). Calculations show that chlorite, pyrite and hematite are the stable Fe phases in the Sulphur Springs hydrothermal system (See Appendix A) and elemental carbon is present in the deep portions of the system (Hulen and Gardner, 1989). It would be, therefore, expected that the samples would lie between the C-CO_2 and the Magnetite-Hematite buffers, and indeed they do. Geothermal fluids are reduced, and these samples tend to cluster near a reduced buffer such as Ni-NiO. For inclusion samples from depths >700 m, these plot at or below the Ni-NiO buffer line and present day fluids plot above this line. Shallowest samples and late paragenetic phases (some calcite and all fluorite) plot well above the Ni-NiO buffer, including present day VC-2A and VC-2B fluids. This suggests the shallowest and the latest paleo-fluids are more oxidized than deep or earlier paleo-fluids and that the present day fluids are more oxidized. This may be due to greater mixing of oxygenated groundwater with the hydrothermal fluid as function of depth and time.

Calculated fO_2 using Eq. 3.1 for Redondo Creek fluids agree with those calculated by Truesdell and Janik (1986, Table 7). Truesdell and Janik also compare their calculated fugacities with those calculated for various mineral assemblages proposed by D'Amore and Gianelli (1984)(magnetite-hematite-pyrite and Assemblage 5 composed of clinozoisite, epidote, chlorite, K-spar, albite, anorthite, tremolite, quartz and pyrite; D'Amore and Gianelli, 1984). They got good agreement with the fO_2 calculated from the mineral assemblages and from their calculated fugacities using the H_2 concentration and the data of Henley et al. (1984). The calculated fO_2 in this study for Redondo Creek fluids also agree with those calculated from the D'Amore and Gianelli mineral

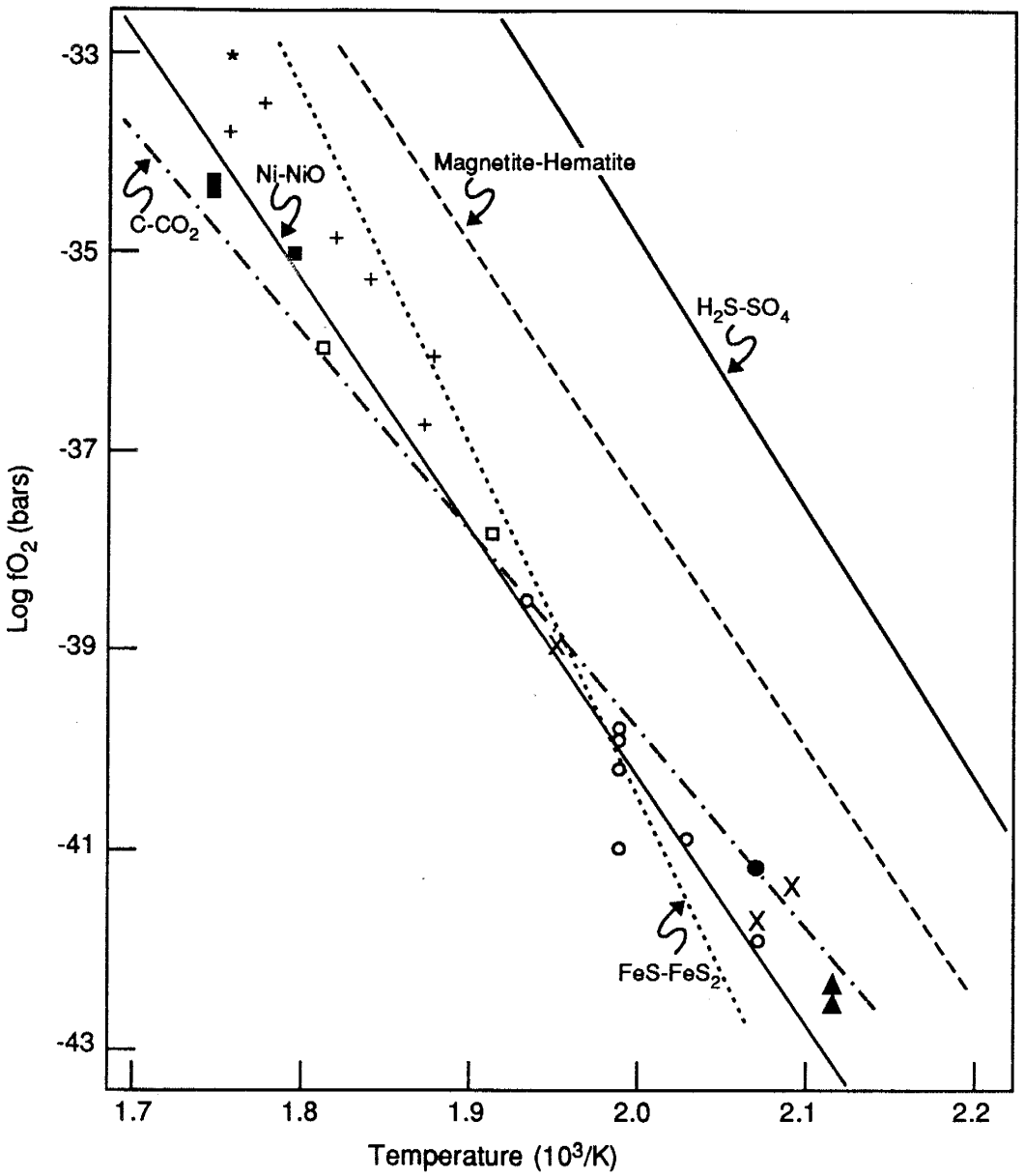

Figure 3.9 Plot of fO_2 calculated from the gas analyses versus temperature with reference buffers. Concentration of H_2S used in the construction of this diagram was 0.003 molal, CO_2 was 0.28 molal, and the activities of the solid phases were assumed to be unity. Same symbols as Figure 3.4.

assemblages. In fact, they agree a little more closely using Eq. 3.1. than by the method of Truesdell and Janik (1986).

The sulfur fugacities calculated in this study using Eq. 3.5 (Table 3.1) agree more closely with the fS_2 calculated by Truesdell and Janik using the D'Amore and Gianelli mineral assemblages than with the fS_2 Truesdell and Janik calculated using the concentrations of H_2 and H_2S from the well gases. Furthermore, the fS_2 calculated from chlorite-pyrite equilibria (Appendix A) for Sulphur Springs are in good agreement with those from Eq. 3.5, and the values calculated for Redondo Creek are similar to those for Sulphur Springs. Truesdell and Janik (1986) calculated fS_2 by yet another method based on H_2 concentration and the assemblage magnetite-pyrite. They got good agreement using this method with the fS_2 they calculated from H_2 and H_2S concentrations. They argue the good agreement between their two methods is because of the abundant pyrite and trace magnetite in Redondo Creek core, and that this mineral pair is the fS_2 buffer. However, pyrite and chlorite are the most abundant Fe-bearing phases alteration phases in Sulphur Springs and Redondo Creek (Hulen and Nielson, 1986; Hulen et al., 1989) samples. The agreement between the fS_2 calculated by Eq. 3.5 for Sulphur Springs and Redondo Creek, with the mineral assemblages of D'Amore and Gianelli (1984), and the Sulphur Springs chlorite-pyrite equilibria suggest that the fS_2 buffer is Fe-silicates and pyrite and not magnetite-pyrite as suggested by Truesdell and Janik (1986). This is consistent with the observation by Giggenbach (1980) that pyrite and an Fe-Al silicate control H_2-H_2S concentrations in geothermal systems.

Comparison of Sulphur Springs Inclusion Gas Analyses with Other Systems

Sulphur Spring fluid inclusion gas analyses indicate these fluids have highly variable gas contents (2.4 to 22.4 mole %, averaging 10 mole % gas), they are low in total sulfur (0.003 molal), and high in total organics (up to 2.4 mole %). Fluid inclusion gas analyses from the Cochiti mining district, Jemez Mountains, (Fig. 1.1) exhibit less variability in gas content (0.09 to 5.3 mole %), have high total sulfur (0.02 molal), and low total organics (Apodaca, 1989). Creede fluid inclusion gas analyses show more variability in gas contents (up to 87 mole % gas), similar to Sulphur Springs.

In general, Creede fluids contain less than 4 mole % gas, and they are also high in total sulfur (0.02 molal, Barton et al., 1977) and variable amounts of total organics (up to 6.1 mole %, excluding one sample that contained 32 mole % organics)(Landis and Rye, 1989). However, Creede and Sulphur Springs fluids typically contain less than 1 mole % total organics (Landis and Rye, 1989). In contrast, all samples analyzed from Cochiti contained <1 mole % total organics (Apodaca, 1989). The fluid which deposited the phases later in the paragenesis at Sulphur Springs are like Creede in that they are lower in total sulfur and CH_4, higher in total organics than the earlier deposited phases (Fig. 3.7). In contrast to these volcanic-hosted hydrothermal systems, the Carlin-type gold deposits are typically hosted in carbonaceous, calcareous siltstones to silty limestones. Analysis of inclusion gases from the Jerrit Canyon, Nevada gold deposit indicate the early fluids were dominated by hydrocarbons with high amounts of CH_4, C_2H_6, H_2, N_2, and CO_2, and less than 1 mole % short chain hydrocarbons and H_2S (Hofstra et al., 1987). Later fluids became less hydrocarbon rich, with CO_2 as the dominant gas (about 4 mole %), and the latest fluids were typically low total gas (<1.5 mole %) (Hofstra et al., 1987).

Analysis of inclusion gases from the sediment-hosted Salton Sea geothermal system indicates the same suite of gases measured at Sulphur Springs, Creede, and Cochiti; however, unlike Sulphur Springs and Creede, the lowest CO_2:H_2O ratios were measured in calcite-dominated veins (Sloan et al., 1991). No hydrocarbons were reported in the inclusion analysis from the Salton Sea system, but O_2 was reported (Sloan et al., 1991).

For epithermal systems such as Creede and Cochiti where quartz is the dominant gangue mineral by volume, the content of CO_2 rarely exceeds several mole %. Calcite is the dominant vein filling phase by volume at Sulphur Springs, and the amount of CO_2 in the fluid inclusions is typically 4-5 mole % with a few samples having values greater than 4-5 mole %. Quartz samples from Sulphur Springs also have high CO_2 contents. Fluids that deposited the carbonate minerals at Creede are more like those at Sulphur Springs with an average of 4-5 mole % CO_2 and greater contents of CO_2 are not uncommon. Therefore, not surprisingly, fluids that deposit predominantly carbonate gangue minerals are richer in CO_2 than those responsible for the deposition of quartz.

Composition of the gases from the analysis of fluid inclusion volatiles indicate Sulphur Springs fluids are typical of those other hydrothermal systems, both active and fossil. Typically CO_2 is the dominant gas in all systems with the other gases in varying amounts, which can in some cases equal or exceed the amount of CO_2. The concentration of CO_2 represented by the gas analyses would suggest liquid CO_2 should be present in the fluid inclusions at room temperature and clathrate also should be observed during inclusion freezing, but inclusion petrography and microthermometry do not indicate these high amounts of CO_2. Since boiling can elevate the amounts of gas trapped in vapor-rich fluid inclusions, the gases most concentrated by this process into vapor-rich inclusions are (in order of increasing solubility in the liquid) N_2, H_2, CH_4, and CO_2, and Norman and Sawkins (1987) have pointed out that gas analyses from boiling hydrothermal systems tends to produce anomalously high gas concentrations. Because CO_2 is the dominant gas it is not surprising that its concentration is high in Table 3.1. Other gases which may be high are N_2, H_2, and CH_4 because they are the least soluble of the principal gases (Henley et al., 1984). Fluid-mineral equilibria indicate the CO_2 concentration in the fluid at 300°C is about 0.5 mole % (Charles et al., 1990), an order of magnitude less than the gas analyses suggest. According to these same equilibria calculations, the concentration of H_2S is 0.005 mole %, which is about the average H_2S value from the gas data. This suggests that the principal gases with solubilities less than or equal to CO_2 (e.g. N_2) may be up to an order of magnitude too high in concentration (Table 3.1), while gases more soluble (e.g H_2S) than CO_2 are in appropriate concentrations.

During thermal maturation of hydrocarbons, aromatic hydrocarbons (AHC) break down through a series of light chain hydrocarbons (LCHC) to CH_4. This could be the origin of the high amounts of CH_4 in some samples of early quartz (from depths <700 m) (Fig. 3.10). In general, the intermediate stage calcite and late stage fluorite from depths >700 m have the greatest amounts of LCHC and AHC. This gas chemistry is a function of temperature since these phase were deposited from fluids that had temperatures ranging from 190-230°C, whereas the early quartz (<700 m deep) and intermediate calcite (>700 m deep) were deposited in the temperature range 230-280°C. It is interesting to note of the early quartz from depths >700 m one sample from a vein

in the organic-rich Madera Formation had the greatest amount of AHC (Fig. 3.10). Present day fluids from VC-2A and Redondo Creek were not analyzed for any hydrocarbons other than CH_4 and VC-2B fluids from 1750 m contained only very minor amounts of LCHC. Figure 3.7 also shows the distinction between the phases deposited late in the paragenesis and at cooler temperatures, clustering nearer the total multi-carbon organics apex, from those deposited earlier and/or at greater depth (higher temperature) trending toward the CH_4 apex. The early quartz samples with the highest total sulfur are those that are associated with the molybdenite and base metal deposition indicating the sulfur content of the fluid was higher during metal deposition (Figure 3.7) and lower in total multi-carbon organics and CH_4.

Unlike the fluids that deposited the ores at Creede, the Sulphur Springs fluids have little variation in CO_2-total sulfur-total multi-carbon organics (Fig. 3.7). The Sulphur Springs fluids are like those which deposited the carbonate minerals at Creede with most samples clustering at the CO_2 apex. Only those samples of early quartz associated with sulfide deposition have appreciable sulfur.

There is very little variation in CO_2-H_2S-SO_2 at Sulphur Springs with nearly all samples plotting in the CO_2 apex (Fig. 3.11). Again, the quartz samples associated with the ore minerals indicate H_2S was the dominant sulfur specie. The lack of gas compositions trending toward the SO_2 apex, especially for late fluorite suggest these fluids were not mixed with low pH, gas charged groundwaters as proposed by Landis and Rye (1989). This proposed mixing mechanism may produce metastable thiosulfate leading to the formation of SO_2 in near-surface hydrothermal fluids (Landis and Rye, 1989). Mixing of this type may not have occurred at Sulphur Springs because the upper 160-200 m of the hydrothermal system was abruptly changed when the hydraulic level of the system dropped suddenly in response to breaching of the southwestern wall of the caldera (Trainer, 1984; Goff and Shevenell, 1987; Goff et al., 1988). The near surface portion of the hydrothermal system did not undergo the gradual cooling and encroachment of groundwaters that probably took place at Creede.

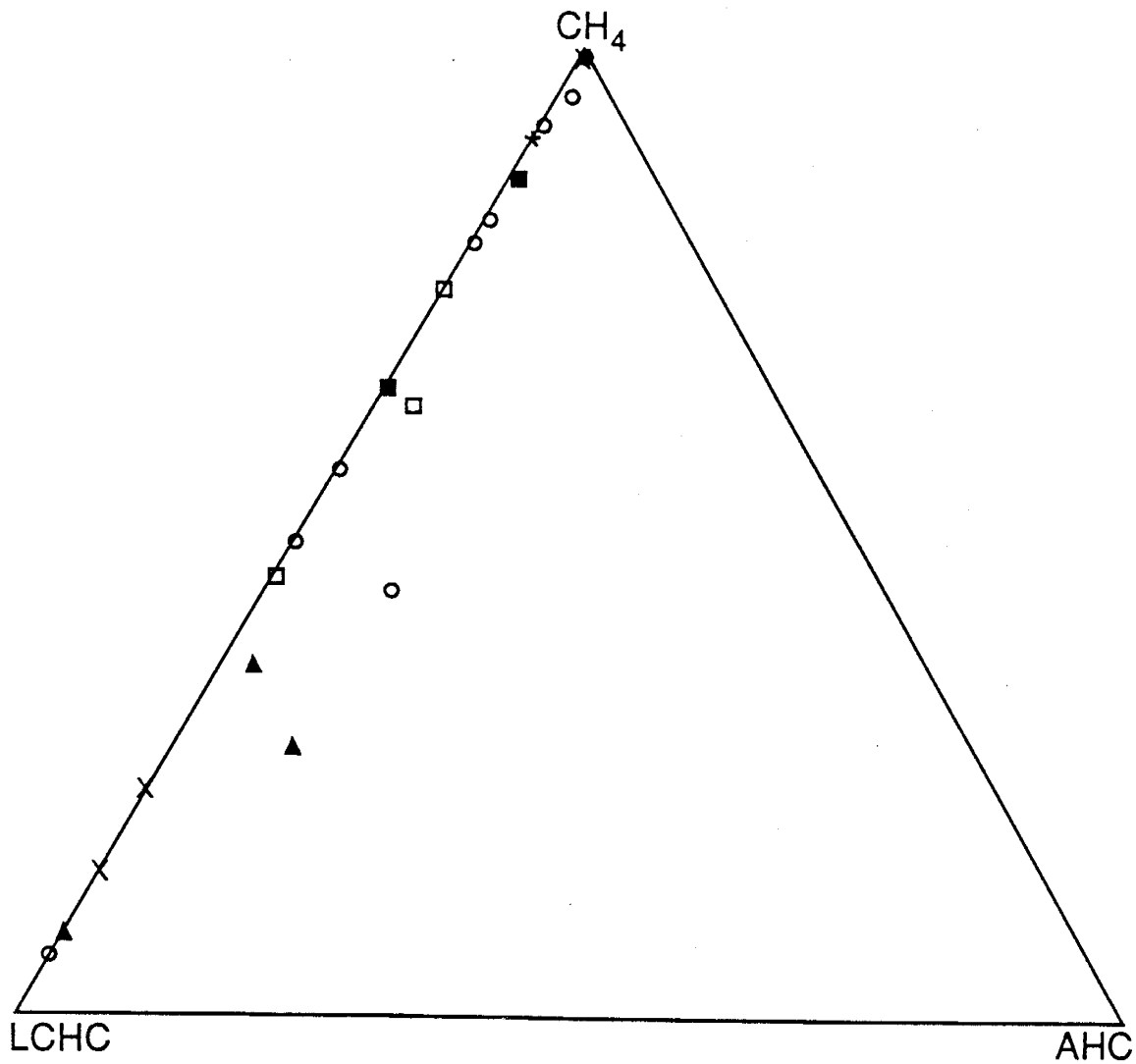

Figure 3.10. Ternary plot of CH_4-Light Chain Hydrocarbon-Aromatic Hydrocarbons. Same symbols as Figure 3.4.

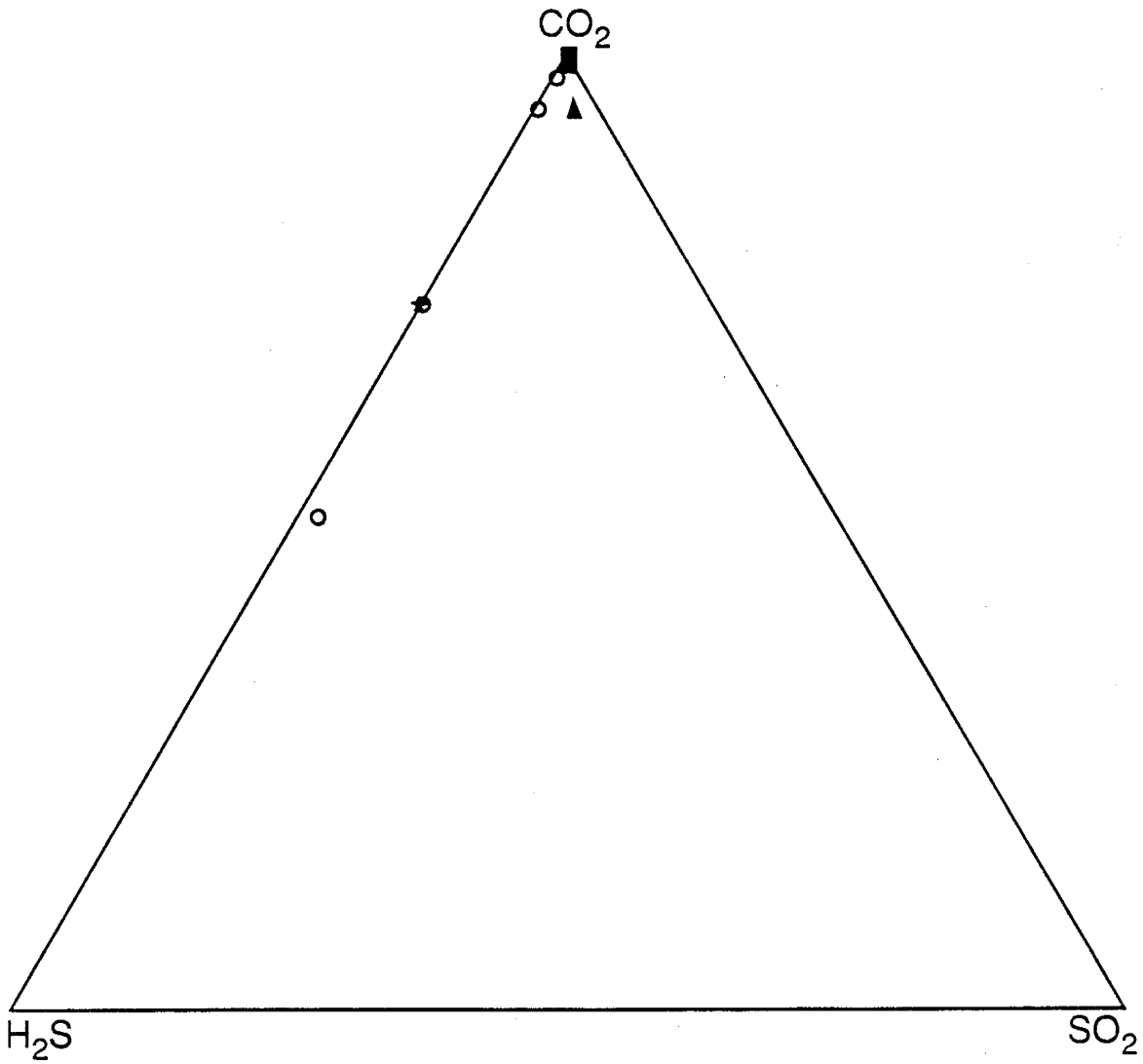

Figure 3.11. Ternary plot of CO_2-H_2S-SO_2. Same symbols as Figure 3.4.

CONCLUSIONS

The following conclusions have been reached based on the analysis of volatile components of fluid inclusions from the Sulphur Springs hydrothermal system:

1) Paleo-hydrothermal fluids were generally higher in total gas contents than present day fluids. However, this should be regarded as a qualitative assesment because the fluids were boiling during much of the mineral deposition; therefore, measured gas contents may be high.

2) Early fluids responsible for molybdenum and base metal sulfide deposition from the shallow portion (<700 m) of the system contained 0.006 m molal H_2S, and for depths >700 m these fluids

contained 0.003 molal H_2S.

3) Fugacities of oxygen and sulfur calculated from the inclusion analyses are in good agreement with those calculated obtained from mineral equilibria.

4) Gaseous components were derived from the atmosphere, thermal metamorphism of limestone and organic residues, magma, and reaction between fluid and reservoir rocks.

5) Separation of a vapor phase (boiling and possibly unmixing) was responsible for concentrating volatile species into vapor-filled inclusions and contributed to the high gas/water ratios.

CONCLUDING STATEMENT

Models of the anatomy and evolution of the Sulphur Springs hydrothermal system were deduced from presented and published data of the Valles hydrothermal system and comparison with other active hydrothemal systems. Data from fluid inclusion microthermometry and microanalysis of inclusion gases, the present day fluid compositions, electron microprobe analyses of hydrothermal sericite, chlorite, epidote, and carbonates together with thermodynamic data has allowed formulation of models regarding the chemical evolution and mineralization of the Sulphur Springs hydrothermal system.

Temperature and composition of the past fluids in the Sulphur Springs hydrothermal system were different from those at present. Fluid inclusion data indicate a complex hydrothermal history in which fluids of ≈ 5 equiv. wt.% NaCl entered fractures in compositionally discrete pulses at shallow depths (<700 m) of the hydrothermal system. However, the inclusion data indicate the predominant fluid at shallow depths was 0.5-1 equiv. wt. NaCl., whereas the fluid at depth (>700 m) was 3-5 equiv. wt.% NaCl. At shallow depths, temperatures are about 100°C lower and at depth, fluid temperatures have decreased about 10 to 30°C. Important hydrologic aspects of the evolution of the Sulphur Springs hydrothermal system include the existence of a deep seated saline fluid, possibly derived from the crystallizing Bandelier magma, which was periodically injected into shallow levels or mixed with the shallow fluid through a stratigraphically stratified hydrothermal system; and the water table, which controls hydrodynamic boiling conditions, descended as much as 400 m when compared to the present level of the water table. The process which led to the lowering of the water table was collapse of the southwestern caldera wall and draining of intracaldera lakes, and this may have lead to greater incursion of the shallow fluid into deeper portions of the system thereby diluting the deep hydrothermal fluid to its present composition (1.1 equiv. wt.% NaCl) or the saline fluid has retreated to a deeper level. Presently there is no evidence of the high salinity fluid.

The processes (fluid mixing, boiling, fluid overpressuring) that have been responsible for the evolution of the Sulphur Springs hydrothermal system and the Valles caldera hydrothermal as a whole are not unique to it. These processes have been identified in a variety of systems (e.g.

Hedenquist and Henley 1985b; Hedenquist and Browne, 1989; Taguchi and Hayashi, 1983; Muffler et al., 1971; Bargar and Fournier, 1988, Simmons, 1991).

Fluid inclusion gas data permit calculation of fO_2 and fS_2, and these fugacity data are in agreement with those determined from mineral equilibria. Furthermore, they are in agreement with fugacities calculated from other hydrothermal systems, active and fossil (e.g. Casadevall and Ohmoto, 1977; Truesdell and Janik, 1986; Norman et al., 1991a and b). The inclusion gas data yielded information on possible origins of the gaseous components in the hydrothermal fluid, which are consistent with observations by Giggenbach (1986) for origins of gases in the New Zealand geothermal systems. Bulk gas composition together with the noble gas data from fluid inclusions (Musgrave et al., 1991) and the noble gas data from the present day fluids (Smith and Kennedy, 1985; B.M. Kennedy, personal communication, 1990) indicate the input of ^3He, and therefore, the input (heat and some volatiles) from a cooling magma has been constant for at least the past 1.0 Ma.

Previous stable isotopic data have shown that the hydrothermal fluid in Valles caldera is derived from water of meteoric origin (Goff and Grisby, 1982; Goff et al., 1985; Goff et al., 1989). Modeling Sulphur Springs meteoric water under convecting conditions at different water:rocks mass ratios and temperatures indicate the isotopic composition of the meteoric water responsible for hydrothermally altering the rocks and depositing vein minerals was about 10 per mil lighter in δD than current meteoric water. Temperature controlled fractionation influenced the isotopic composition of near surface rock. Marine carbonate rocks underwent extensive isotopic exchange with the hydrothermal fluid, with some samples indicating the $\delta^{18}O$ of the limestone approaches that of the fluid. However, the carbon isotopic composition of vein calcites was controlled by the carbon isotopic composition of the marine limestones.

APPENDIX A

GEOCHEMISTRY OF HYDROTHERMAL ALTERATION AND MINERALIZATION

INTRODUCTION

Active geothermal systems provide a unique laboratory in which to study the chemical and physical processes that take place during hydrothermal alteration and epithermal mineralization because they offer insight into how variations in temperature, pressure, and chemical composition of the fluid influence the formation of the alteration and ore minerals. Until recently, detailed studies of the relationship between fluid chemistry, alteration mineralogy, and ore deposition were lacking, but work by Capuano and Cole (1982); Parry et al. (1984) on the Roosevelt Hot Springs; Bird and Norton (1981), McKibben and Elders (1985), McKibben and Williams (1989) on the Salton Sea; Hedenquist and Browne (1989) on the Waiotapu; and Lonker et al. (1990) on Ohaaki-Broadlands hydrothermal systems have provided important information on these relations.

The analogy of active geothermal systems to epithermal ore deposits was first proposed by White (1955) and has been further advocated by Henley and Ellis (1983) and Henley (1985) and others. It has become clear that the majority of volcanic-hosted ore deposits were formed within geothermal systems of similar size, chemistry and behavior to those we see today (Henley and Ellis, 1983). Hulen and Nielson (1986) have found numerous parallels between the Valles caldera geothermal system and fossil systems, namely the Adularia-Sericite type epithermal silver/base metal vein deposit (Hayba et al., 1985). Hulen and Nielson (1986) point out similarities between Valles and Creede calderas in tectonic setting, host rock type, alteration mineralogy and zoning, and water origin. Furthermore, trace element geochemistry in Valles core samples show vertical zoning similar to that described from active hydrothermal systems (Steamboat Springs and Broadlands) and fossil epithermal systems such as Bodie and Paramount (Musgrave and Norman, 1990b; Rogers et al., 1990; Silberman and Berger, 1985; Berger and Silberman, 1985).

In this section the geochemical conditions which led to the alteration and mineralization at

Sulphur Springs are examined. Fluids produced from two horizons in the hydrothermal system are used to calculate the distribution of species and stability relationships at temperatures ranging from 210 to 300°C. Electron microprobe analyses of vein-filling and wall rock minerals are used to calculate activities of the minerals, and these data are used to calculate pH, fO_2 and fS_2. Stable isotopic data on vein minerals and whole rocks provide insight into the origins of fluid components. The above data together with fluid inclusion data allow modelling of the metal carrying capacity of the past and present fluids and mechanisms for deposition of the ore minerals.

HYDROTHERMAL ALTERATION AND MINERALIZATION

Fluid flow in the Sulphur Springs hydrothermal system is primarily fracture controlled and hydrothermal alteration and mineralization are thus closely related to faults and fractures. Unlike the pervasively altered host rocks in the phyllic zones of porphyry Cu and Mo deposits (Beane and Titley, 1981), alteration intensity at Sulphur Springs is primarily controlled by density of fracturing and faulting. Only in portions of the systems where fracture density is high is the host rock intensely altered. Secondary controls on the distribution of alteration include primary permeability in clastic rocks and the degree of welding of the ignimbrite units.

The uppermost part of the Sulphur Springs hydrothermal system is characterized by surficial advanced argillic alteration composed of kaolinite, alunite, clays, native sulfur, quartz, and hydrated sulfates containing Fe, Al, Ca (Charles et al., 1986). This alteration is confined to the main hot spring and fumarole areas and near surface portions of faults and fractures. The advanced argillic assemblage is superimposed on a quartz-sericite-pyrite (QSP) alteration assemblage (Fig. A.1). The sericitic component of this assemblage (in near surface regions) is characterized by illite-rich mixed-layer illite/smectite (Hulen et al., 1989). QSP alteration in the vicinity of VC-2B is overprinted by near-surface kaolinization (Hulen et al., 1989). QSP alteration extends to a depth of at least 300 m. Sericite-chlorite alteration (SER-CHL) is dominant in the remainder of the ignimbrite section. Deep in the Sulphur Springs system the alteration is predominantly propylitic (chlorite-calcite-epidote-

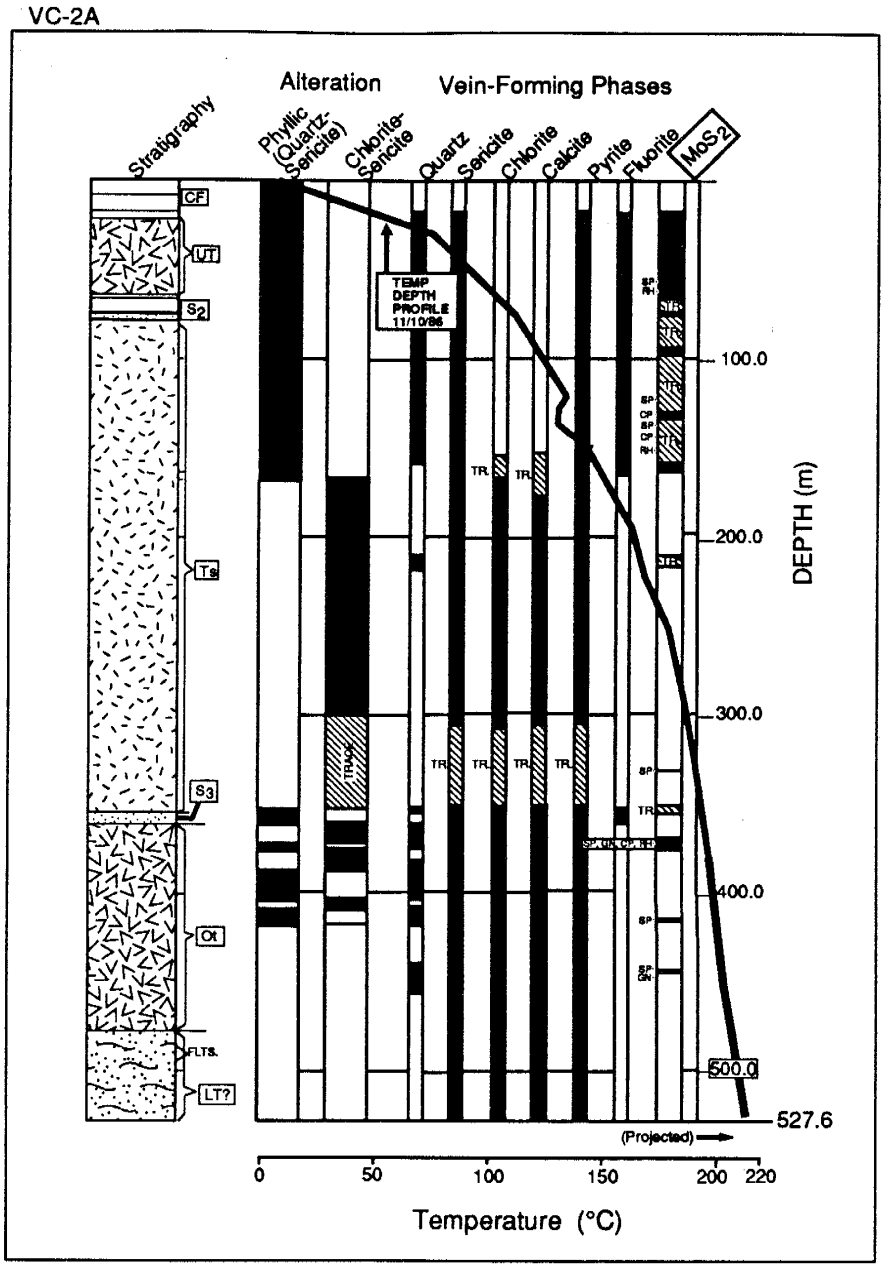

Figure A.1. a. Lithology-alteration-mineralization log for VC-2A. CF, Quaternary caldera fill; UT, Quaternary Upper Tuffs; S_2, Quaternary S_2 sandstone; Ts, Tshirege Member of Quaternary Bandelier Tuff; S_3, Quaternary S_3 sandstone; Ot, Otowi Member of Quaternary Bandelier Tuff; LT, Quaternary Lower Tuffs, sp, sphalerite; cp, chalcopyrite; gn, galena (Modified from Hulen et al., 1987).

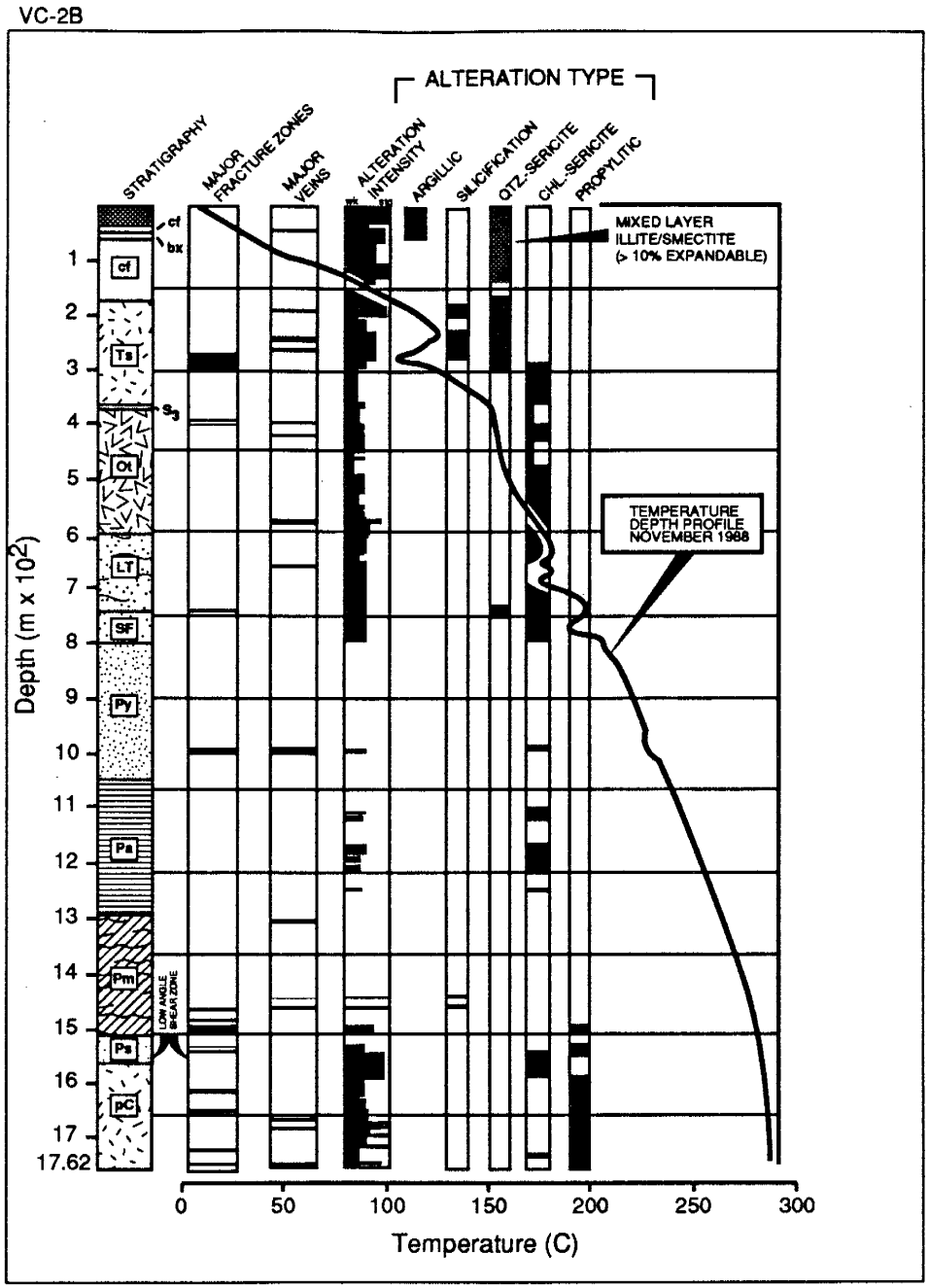

Figure A.1 b. Lithology-alteration-mineralization log for VC-2B. CF; Quaternary caldera fill; Ts, Tshirege Member of Quaternary Bandelier Tuff; S_3, Quaternary S_3 sandstone; Ot, Otowi Member of Quaternary Bandelier Tuff; LT, Quaternary Lower Tuffs; SF, Tertiary Santa Fe Group; Py, Permian Yeso Formation; Pa, Permian Abo Formation; Pm, Pennsylvanian Madera Limestone; Pennsylvanian Sandia Formation; pC, Precambrian Quartz Monzonite (Modified from Hulen et al., 1989).

sericite-pyrite) (PROP), but in intensely fractured regions of the Precambrian, the quartz monzonite displays moderate to strong chlorite-sericite alteration (Hulen et al., 1989). The propylitic alteration of the Pennsylvanian section contains varying amounts of illite, chlorite, epidote, wairakite, kaolinite, pyrite, calcite, and rectorite.

Clay mineralogy of the Pennsylvanian section presents a contradiction to the current T-X regime. The clay-sized fraction contains about 40% interlayer smectite in an R1 ordered, mixed-layer illite/smectite (Hulen et al., 1989). Additional XRD studies of selected samples from 1470 m in Pennsylvanian Madera Formation reveal that the smectite component is rectorite (Na-montmorillonite). The rectorite represents a metastable phase which should have transformed to illite at the current T (270°C) conditions and K^+ concentrations. The illite/smectite is probably diagenetic and has been isolated from the hot, K-bearing fluids necessary for the transformation (Hulen et al., 1989).

HYDROTHERMAL MINERAL COMPOSITIONS

Analytical Methods

Mineral phases were analyzed in 26 polished thin sections with a CAMECA BMX electron microprobe operated at 15 kV and a sample current of 15 nA. The microprobe is fitted with a Tracor Northern energy dispersive spectrometer (EDS) and 4 wavelength dispersive spectrometers (WDS), and the optical system of the microprobe is attached to a television camera. Analyzed minerals used for standards in this study include orthoclase, augite, hornblende, pyrope, and apatite. Background-corrected counts were corrected using a Bence-Albee correction scheme (Chambers, 1991) incorporated into a microprobe automation package called TASK8 (Chambers and Doyle, 1990). All iron was assumed to be Fe2+ and tetrahedral sites were filled by Si and Al with the remaining Al allocated to octahedral sites.

Sericite

Microprobe analyses of vein and wall rock sericites from Sulphur Springs have been

grouped into 3 groups: those from the QSP alteration, from the SER-CHL alteration, and those from PROP alteration assemblages (Table A.1). Compositional ranges for sericite from the QSP alteration assemblage differ from compositions of the deeper chlorite-sericite ± pyrite and propylitic assemblages in that they are higher in Si and lower in interlayer cations. Total octahedral site occupancy is greater than 2 and as high as 3.6, and no correlation of Mg with Si or Mg with octahedral site occupancy is apparent. Octahedral Fe and Mg and interlayer Na and K show no systematic variation with depth.

Sulphur Springs sericite are higher in Si and Fe and lower in Al and K than sericites from the Ohaaki-Broadlands system (Lonker at al., 1990). Sericites for the copper deposits tend to be somewhat lower in Si but higher in K and Fe and Na than the Ohaaki-Broadlands and Sulphur Springs (Fig. A.2) (J. Ballantyne, 1981), whereas the sericites from Roosevelt Hot Springs (J. Ballantyne, 1981) have similar amounts of Si to the Sulphur Springs sericites and more variability in the amount of K, which is like Sulphur Springs. The sericites from the Henderson deposit have a similar Si content to the copper deposits, but exhibit higher K contents than the Cu deposits and Sulphur Springs and Roosevelt Hot Springs.

Minor elements Na, Ti, and F show significant compositional variability. Most sericites contain between 0.003 to 0.03 Na ions per formula unit, but two sample depths (370 m CHL-SER and 1694 m PROP) have as high as 0.46 and 0.25 Na ions per formula unit, respectively. Ti ranges from 0.00 to 0.04 ions per formula unit; however, most sericites contain less than 0.01 ions per formula unit. No particular alteration assemblage is higher in Ti than another. Fluorine in most of the samples is below the detection limit (0.5 wt.%). The number of ions per formula unit ranged between 0.017 to 0.19 for sericites with detectable fluorine.

Sericite Inhomogeneity

X-ray diffraction studies of the clay-sized fraction of alteration minerals in geothermal systems indicate a transition from smectite through increasingly illitic mixed-layer illite/smectite to illite to finally high silica muscovite as depth and temperature increase. These phase transition have

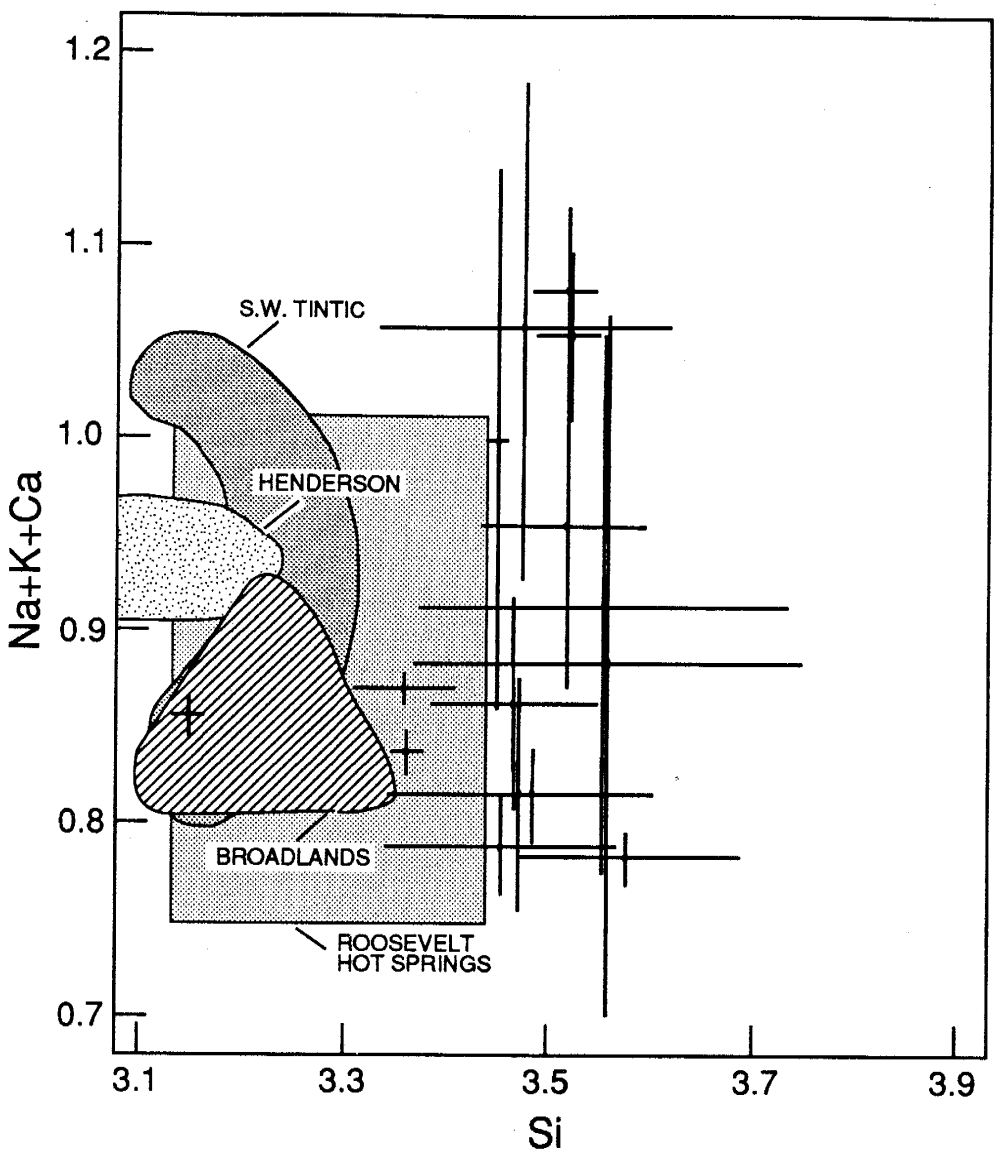

Figure A.2. Compositional heterogeneity in Sulphur Springs sericite compared to other hydrothermal systems, active and fossil. Each point represents the mean for a particular depth of which the analysis represents the mean of 5-10 spots on a single grain or aggregate and the bar represents 1σ. Field for southwest Tintic and Roosevelt Hot Springs from the data of Parry et al. (1984), field for Broadlands from the data of Lonker et al. (1990), and the Henderson field from unpublished data (Musgrave, 1991).

Table A.1. Microprobe Analyses and Structural Formulas for Hydrothermal Sericite, Sulphur Springs, Valles Caldera, New Mexico

	VC2A 96	VC2A 305	VC2A 646	VC2A 1212	VC2A 1485	VC2B 602	VC2B 783	VC2B 849	VC2B 882
SiO_2	50.59	53.05	50.89	47.59	50.14	54.12	53.79	51.60	51.99
TiO_2	0.30	0.00	0.00	0.17	0.00	0.33	0.00	0.19	0.13
Al_2O_3	29.90	33.03	29.58	28.75	31.40	25.60	29.11	28.09	28.99
FeO	1.60	0.85	4.31	0.87	1.69	2.68	0.60	1.38	0.54
MnO	0.03	0.30	0.00	0.04	0.06	0.03	0.02	0.01	0.05
MgO	1.43	1.60	2.14	1.90	1.72	2.03	1.45	2.06	1.78
CaO	0.23	0.00	0.00	0.24	0.11	0.09	0.08	0.04	0.04
Na_2O	0.02	0.00	0.09	3.59	0.17	0.22	0.14	0.16	0.01
K_2O	8.82	8.70	9.33	7.49	8.62	8.50	10.00	9.62	9.35
F	0.30	0.00	0.00	0.00	0.00	0.00	0.21	0.08	0.32
Cl	0.01	0.00	0.00	0.00	0.00	0.02	0.01	0.01	0.03
H_2O^*	6.79	2.48	3.65	9.38	6.10	6.37	4.59	6.77	6.77
Total	93.21	97.52	96.35	90.62	93.90	93.63	95.41	93.23	93.23
Structural Formula (Number of Ions									
Si	3.455	3.514	3.472	3.491	3.449	3.578	3.553	3.465	3.472
Ti	0.014	0.002	0.002	0.009	0.003	0.02	0.03	0.009	0.003
Al	2.409	2.556	2.379	2.494	2.545	2.038	2.23	2.224	2.288
Fe	0.091	0.041	0.247	0.05	0.098	0.149	0.033	0.073	0.03
Mn	0.003	0.006	0.003	0.001	0.003	0	0.002	0	0.003
Mg	0.145	0.154	3.757	0.208	0.176	0.206	0.142	0.206	0.177
Ca	0.016	0.01	0.006	0.018	0.008	0.006	0.006	0.003	0.002
Na	0.003	0.006	0.019	0.464	0.023	0.028	0.018	0.02	0.002
K	0.768	0.729	0.813	0.642	0.758	0.735	0.839	0.825	0.798
F	0.062	n.a.	n.a.	n.a.	n.a.	n.d.	0.053	0.017	0.066
Cl	0.001	n.a.	n.a.	n.a.	n.a	0.001	0.001	0.001	0.001
H	3.015	n.a.	n.a.	n.a.	n.a.	2.708	1.8	2.936	2.907

* Water determined by difference
n.a., not analyzed
n.d., not detected

Table .A.1. Microprobe Analyses and Structural Formulas for Hydrothermal Sericite, Sulphur Springs, Valles Caldera, New Mexico (Cont.)

	VC2B 932	VC2B 1149	VC2B 1152	VC2B 1599	VC2B 4755	VC2B 5557	VC2B 5655	VC2B 5661
SiO_2	51.29	48.09	51.76	49.23	45.96	52.96	50.00	48.64
TiO_2	0.01	0.79	0.06	0.00	0.00	0.05	0.00	0.00
Al_2O_3	30.37	27.58	27.19	29.37	35.13	26.28	29.24	28.60
FeO	1.29	2.97	3.05	2.84	0.12	2.05	2.56	2.14
MnO	0.00	0.00	0.10	0.00	0.00	0.03	0.00	0.03
MgO	1.56	1.71	1.47	1.47	0.13	0.15	1.83	1.56
CaO	0.09	0.08	0.09	0.10	0.05	0.50	0.01	0.00
Na_2O	0.05	0.13	0.03	0.13	0.20	1.93	0.02	0.00
K2O	9.29	9.42	9.97	9.17	9.24	8.32	9.33	9.50
F	0.00	0.00	0.00	0.00	0.00	0.00	0.00	0.83
Cl	0.00	0.00	0.00	0.03	0.01	0.00	0.00	0.00
H_2O*	6.11	9.25	6.29	7.69	9.15	6.44	7.00	8.69
Total	93.89	90.75	93.71	92.31	90.85	93.56	93.00	91.31
Structural Formula (Number of Ions)								
Si	3.484	3.358	3.555	3.361	3.147	3.726	3.513	3.519
Ti	0.001	0.041	0.003	0	0.002	0.005	0	0.002
Al	2.432	2.27	2.141	2.364	2.827	2.175	2.054	2.439
Fe	0.076	0.174	0.101	0.162	0.007	0.12	0.15	0.129
Mn	0	0	0.003	0	0.001	0.004	0	0.002
Mg	0.157	0.178	0.103	0.149	0.013	0.129	0.192	0.168
Ca	0.006	0.006	0.006	0.007	0.005	0.169	0.003	0.001
Na	0.001	0.017	0.005	0.016	0.027	0.255	0.012	0.01
K	0.803	0.839	0.897	0.798	0.808	0.614	0.834	0.877
F	n.d.	n.d.	n.d.	n.d.	n.d.	n.a.	n.a.	0.189
Cl	n.d.	n.d.	n.d.	0.003	0.001	n.a.	n.a.	n.d.
H	2.581	4.156	2.5	3.481	4.123	n.a.	n.a.	n.a.

* Water determined by difference
n.a., not analyzed
n.d., not detected

been observed at Salton Sea (Muffler and White, 1969; McDowell, 1978), Wairakei (Steiner, 1968), Broadlands (Brown and Ellis, 1970; Eslinger and Savin, 1973) and Valles caldera (Hulen et al., 1987; Hulen and Nielson, 1988; Hulen et al., 1989; WoldeGabriel, 1989; WoldeGabriel and Goff, 1989; WoldeGabriel, 1990). Sericite will be used in this report to include fine-grained, white-mica including muscovite, phengite, illite, and other solid solution end members. Detailed X-ray diffraction studies of the clay fraction from VC-2A indicates the sericite is dominated by interstratified illite/smectite (92-98% illite layers) with minor chlorite (WoldeGabriel, 1989; WoldeGabriel and Goff, 1989).

Sericite inhomogeneity has been demonstrated at Butte, Montana (Page and Wenk ,1979) and Roosevelt Hot Springs, Southwest Tintic Utah, and Santa Rita, New Mexico (Ballantyne, 1981; Parry et al., 1984). Greater variability in sericite composition was noted in the active hydrothermal system at Roosevelt Hot Springs than in sericites from Southwest Tintic (Ballantyne, 1981; Parry et al., 1984). Sericites from the Southwest Tintic porphyry Cu mine and the Henderson Mo mine are, generally, more homogeneous than those from the active systems; indicated by the generally tighter clustering of the data from the ore deposits and the bars showing the range of each data point (Fig. A.2). Sericites from Sulphur Springs and Roosevelt Hot Springs have similar numbers of Si atoms per formula unit clustering around 3.5, and those from the ore deposits have similar numbers of Si atom per formula unit clustering at 3.1. Sericites from all the hydrothermal systems have a similar range in the number of interlayer cations with values generally between 0.75 and 0.9.

Chlorite

Chlorite throughout the Sulphur Springs hydrothermal system is green and occurs as a replacement of the albitic component of the perthitic feldspars of the volcanic section, biotite, hornblende and K-feldspar of the Precambrian quartz monzonite and as a vein and fracture filling. Chlorites replacing hornblende and feldspar and in vein fillings are typically aggregates of radiating to randomly oriented crystals. Chlorite chemistry in hydrothermal systems varies mainly in the amount of Mg-Fe substitution in octahedral sites.

Table.A.2 Microprobe Analyses and Structural Formulas for Hydrothermal Chlorite, Sulphur Springs, Valles Caldera, New Mexico

	VC2A 523	VC2A 646	VC2A 651.4	VC2A 652	VC2A 1095	VC2A 1135	VC2B 1149	VC2B 1599	VC2B 1799	VC2B 5237	VC2B 5557	VC2B 5655	VC2B 5661	VC2B 5757
SiO_2	26.35	25.52	28.00	27.23	25.80	26.87	27.77	28.35	27.58	31.47	27.19	27.13	28.47	25.20
TiO_2	0.05	0.09	n.d.	0.03	0.07	0.01	n.d.	n.d.	n.d.	0.17	0.11	0.36	0.10	0.18
Al_2O_3	18.16	19.46	19.12	19.15	18.94	19.83	18.83	20.11	19.50	23.58	19.62	20.70	21.19	20.94
FeO	23.48	31.86	25.14	25.49	29.97	26.02	25.50	23.31	25.40	19.72	23.56	26.40	24.30	28.33
MnO	2.07	2.37	0.83	0.69	2.19	2.13	0.81	1.42	0.92	0.41	0.75	0.70	0.69	0.71
MgO	12.88	6.94	15.51	14.38	10.52	12.57	13.45	12.33	13.48	8.57	15.84	12.29	11.35	13.46
CaO	0.06	0.08	0.50	0.10	0.19	0.08	0.07	0.09	0.23	0.02	0.21	0.02	0.04	0.19
K_2O	n.a.	n.a.	n.a.	n.a.	n.a.	n.a.	n.a.	0.82	0.20	3.07	n.d.	n.d.	n.d.	0.01
F	0.38	n.d.	n.d.	0.05	n.d.	n.d.	0.10	n.d.	n.d.	n.d.	0.33	n.d.	0.26	0.26
Cl	n.d.	0.02	n.d.	n.d.	0.01	n.d.	n.d.	0.03	0.01	n.d.	n.d.	n.d.	n.d.	0.02
H_2O^*	16.65	13.68	10.89	12.89	12.32	12.49	12.41	13.53	12.67	12.99	12.39	12.40	13.61	10.69
Total	83.35	86.32	89.11	87.11	87.68	87.51	86.53	86.47	87.33	87.01	87.61	87.60	86.39	89.31
Structural Formula (Number of ions)														
Si		2.85	2.90	2.89	2.82	2.81	2.77	2.99	2.92	2.46	2.85	2.87	3.00	2.10
Ti		0.01	0.00	0.00	0.00	0.00	0.00	0.00	0.00	0.01	0.01	0.03	0.01	0.01
Al IV		1.10	1.08	1.09	1.17	1.04	1.26	0.93	1.04	n/a	1.19	1.08	1.02	n/a
Al VI		1.52	1.26	1.31	1.28	1.41	1.19	1.63	1.42	n/a	1.18	1.54	1.60	n/a
Fe^{2+}		3.05	2.18	2.22	2.76	2.27	2.39	2.07	2.25	1.30	2.07	2.34	2.17	1.98
Mn		0.22	0.07	0.08	0.21	0.19	0.08	0.13	0.08	0.03	0.07	0.06	0.06	0.05
Mg		1.16	2.39	2.33	1.69	1.96	2.24	1.95	2.13	1.00	2.48	1.94	1.79	1.67
Ca		0.01	0.06	0.01	0.03	0.01	0.01	0.01	0.03	0.00	0.02	0.00	0.00	0.02
K		n.a.	n.a.	n.a.	n.a.	n.a.	0.01	0.11	0.03	0.30	n.a	n.a.	n.a.	n.a.
F		n.a.	n.a.	n.a.	n.a.	n.a.	n.a.	n.a.	n.a.	n.d.	0.06	n.d.	0.09	0.07
H		n.a.	n.a.	n.a.	n.a.	n.a.	11.93	9.53	8.94	6.65	0.00	0.00	0.00	5.89

* Water determined by difference
n.a., not analyzed
n.d., not detected

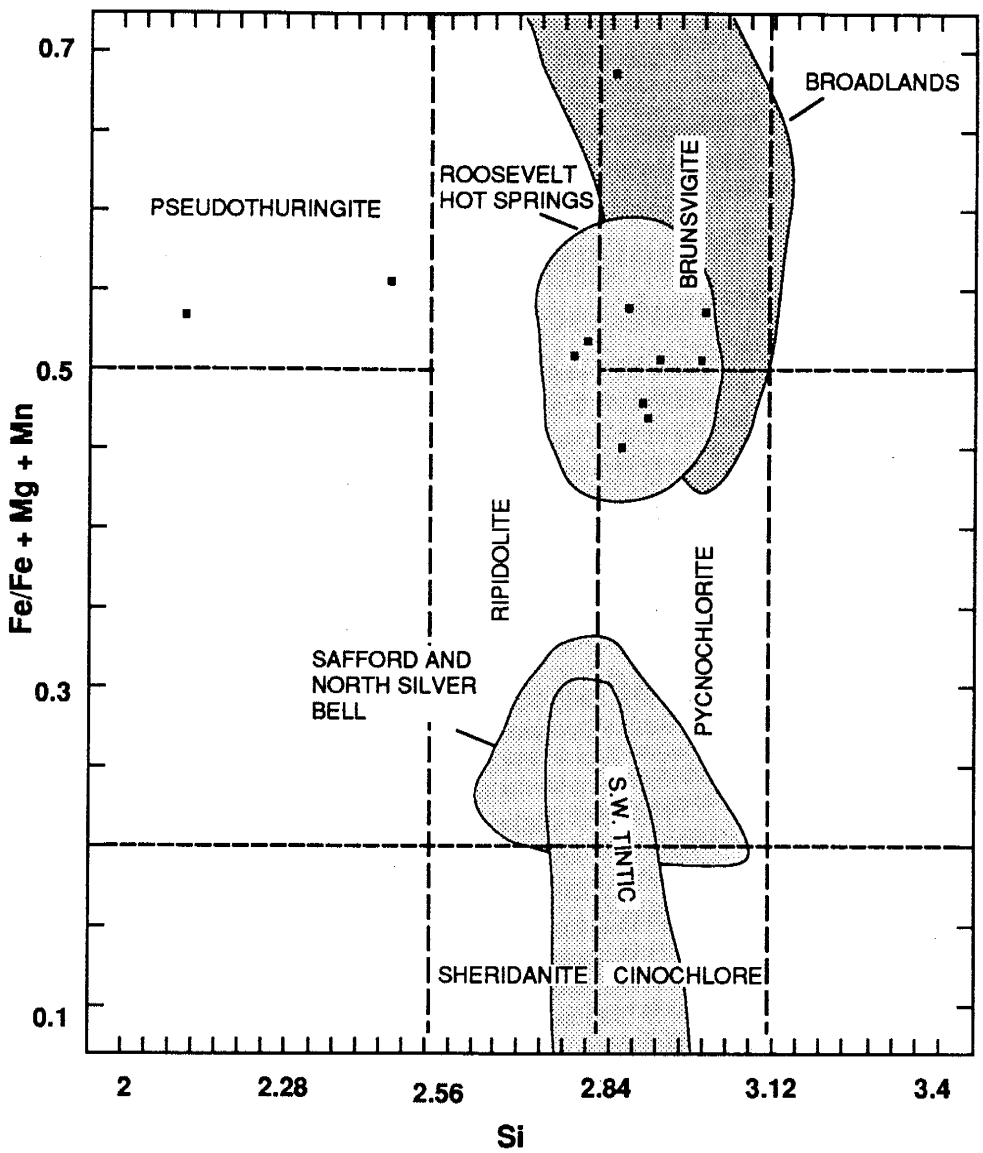

Figure A.3. Octahedral cation ratios and tetrahedral silicon site occupancy in Sulphur Springs chlorite. Data points are from this study. Field of Roosevelt Hot Springs chlorite from J. Ballantyne (1981), field of Safford and North Silver Bell from G. Ballantyne (1981), and Broadlands field from Lonker et al. (1990).

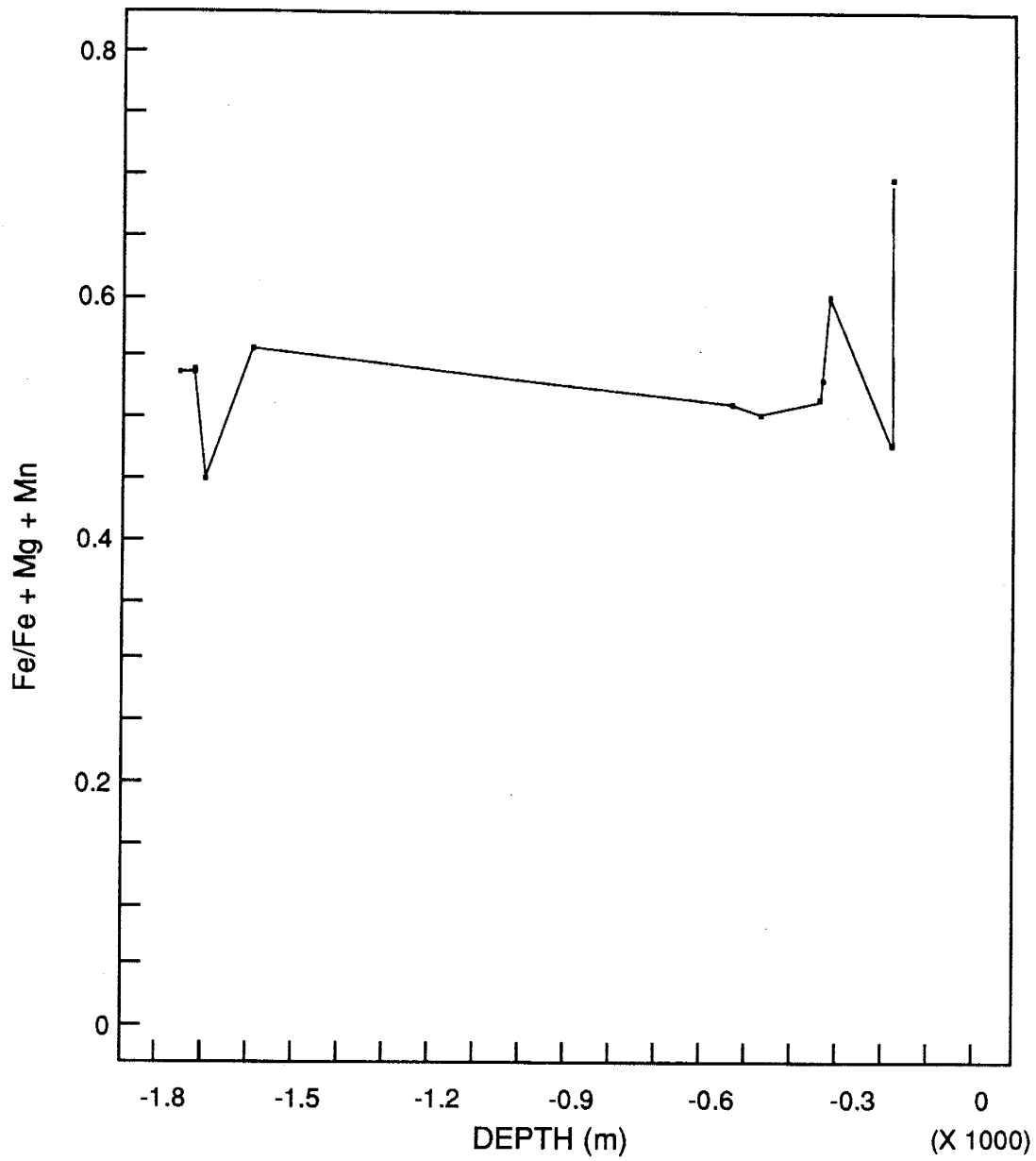

Figure A.4. Fe/Fe+Mg+Mn versus depth for chlorite, Sulphur Springs.

Sulphur Springs chlorites fall in the pycnochlorite, brunsvigite, pseudothuringite, and ripidolite fields, having Fe/Fe+Mg+Mn between 0.4 and 0.7 and Si between 2 and 3.1 (Fig. A.3 and Table A.2). Similar chlorite compositions were noted for Roosevelt Hot Springs and the propylitic zones of the Safford and North Silver Bell porphyry Cu deposits (J. Ballantyne, 1981; G. Ballantyne, 1981). Chlorites from Sulphur Springs are similar to the Ohaaki-Broadlands system and Roosevelt Hot Springs in terms of the Si content, but chlorites from Ohaaki-Broadlands are higher in Fe and lower Mg than either Sulphur Springs or Roosevelt Hot Springs (J. Ballantyne, 1981; Lonker et al., 1990).

Compositional variation is greater for the chlorite from the QSP assemblage than the CHL-SER and PROP assemblages (Fig. A.4). For example, Fe/Fe+Mg+Mn ranges from 0.5 to 0.7 at 197 m in the QSP zone versus 0.45 to 0.55 at 1597 m in the PROP zone (Table A.2). The same generalization is true for Mn and Mg in the QSP versus the CHL-SER and PROP zones. Chlorites from the QSP horizon are the most Fe rich, and there is a general decrease in Fe with depth into the CHL-SER zone and a slight increase again in Fe in the PROP horizon (Fig. A.5). There is a sympathetic relationship between Fe and Mn and an antipathetic relation with Mg. Potassium is as high as 0.3 ions per formula unit. Fluorine is only in detectable concentrations in chlorites from the propylitic assemblage, ranging from 0.0 to 0.09 ions per formula unit.

Chlorite from the QSP zone are highest in Fe content which also corresponds to the horizon where the majority of base metal and MoS_2 mineralization occurs and the fracturing is most intense in this horizon, and chlorites from Archean massive sulfide deposits are higher in Fe within the feeder zone and become progressively more Mg-rich outward into the country rock (Franklin et al., 1981).

Epidote

Epidote is uncommon in the Sulphur Springs system because of the high CO_2 concentration (Henley et al., 1984; Lonker et al., 1990). It occurs as clumps in primary plagioclase and as fans in vein and vugs linings often associated with sericite. Epidote is first noted at depths around 1469

m, which corresponds to a paleo-temperature of about 280-285°C and present day temperature of 275°C. In general, there is not great compositional variability in the epidotes analyzed (Table A.3).

Carbonates

Calcite is common in the Sulphur Springs system. In fact, by volume it is the most abundant vein-filling phase. Rhodochrosite is the second most abundant carbonate phase, but by volume it is typically ≤1%. Trace amounts of Fe-bearing dolomite have also been identified, but only calcite and rhodochrosite have been analyzed chemically (Table A.4). Calcite occurs as coarse blades and rhombohedra filling veins and vugs and as replacements of primary plagioclase. Rhodochrosite occurs as a vein-filling phase in both VC-2A and VC-2B.

Calcites from VC-2A differ from those of VC-2B by containing greater amounts of Mn and less Fe. Rhodochrosite contains nearly the same amounts of Feand Mg regardless of stratigraphic position. Within a given thin section, there is little variability in the concentration of Ca, Mn, Mg and Fe for both calcite and rhodochrosite.

FLUID PROPERTIES

Temperature and Pressure of Fluids

For the present day fluids the current P-T conditions are 210°C, 19 bars at 490 m in VC-2A and 295°C, 86 bars at 1755 m in VC-2B under hydrostatic conditions; however, the gas data from VC-2B indicate the pressure at 1755 m is about 160 bars. Primary fluid inclusions from early formed quartz indicate temperatures for Sulphur Springs ranged from 210 to 310°C depending on stratigraphic position in the system, and fluid pressures ranged between hydrostatic and lithostatic (16 to 450 bars, pure water) (See Parts II and III).

Temperatures calculated from chemical geothermometers show agreement and discrepancies from the measured values depending on the geothermometer used. The quartz conductive geothermometer for fluid produced at 1755 m indicates a temperature which exceeds the formation temperature suggesting wellbore fluids were supersaturated in silica with respect to

Table A.3. Microprobe Analyses and Structural Formulas for Hydrothermal Epidote Sulphur Springs, New Mexico

	VC2B 5557	VC2B 5655	VC2B 5661	VC2B 5757
SiO_2	35.52	38.45	38.04	38.16
TiO_2	0.00	0.00	0.00	0.08
Al_2O_3	21.85	22.28	22.95	23.32
FeO	9.99	13.20	12.96	12.58
MnO	0.48	0.34	0.15	0.25
MgO	0.10	0.13	3.45	0.08
CaO	26.31	22.94	19.97	22.13
K_2O	0.00	0.00	0.00	0.30
F	0.00	0.00	0.00	0.00
Cl	0.00	0.00	0.00	0.02
Total	94.25	97.34	97.52	96.92
Structural Formula (Number of ions)				
Si	6.63	6.30	6.22	5.86
Ti	0.01	0.00	0.00	0.01
Al IV				
Al VI	4.29	4.30	4.41	4.22
Fe_{2+}	1.44	1.81	1.78	1.62
Mn	0.07	0.05	0.03	0.03
Mg	0.04	0.03	0.02	0.02
Ca	3.73	4.06	4.10	3.64
K	0.00	0.00	0.00	0.00
F	0.00	0.00	0.00	0.00

n.a., not analyzed
n.d., not detected

Table.A.4 Microprobe Analyses and Structural Formulas for Vein Carbonates, Sulphur Springs, Valles Caldera, New Mexico

	VC2A 532RHD	VC2A 532CC	VC2A 651.4	VC2A 1095	VC2A 1206RHD	VC2A 1206CC	VC2A 1212	VC2B 5557	VC2B 5655
FeO	0.76	0.46	0.67	1.23	0.74	0.64	0.29	1.13	1.56
MnO	47.25	2.89	2.68	3.75	55.56	3.96	3.34	0.88	0.24
MgO	2.09	0.27	0.19	0.17	2.08	0.47	0.13	0.34	0.19
CaO	1.86	52.89	51.79	53.97	1.98	55.45	56.90	53.60	54.65
SrO	0.06	0.07	0.15	0.10	0.07	0.09	0.01	0.24	0.06
BaO	n.d.	n.d.	0.08	n.d.	0.04	0.01	0.01	n.d.	0.07
CO_2*	47.50	41.88	44.42	40.77	38.53	39.48	39.28	43.77	43.19
Total	99.52	98.46	99.98	99.99	99.00	100.10	99.96	99.96	99.96
Structural Formula									
Fe	0.01	0.01	0.01	0.02	0.01	0.01	0.00	0.02	0.02
Mn	0.67	0.04	0.04	0.05	0.78	0.06	0.05	0.01	0.00
Mg	0.05	0.01	0.00	0.00	0.05	0.01	0.00	0.01	0.00
Ca	0.03	0.94	0.92	0.96	0.04	0.99	1.01	0.96	0.97
Sr	0.00	0.00	0.00	0.00	0.00	0.00	0.00	0.00	0.00
Ba	0.00	0.00	0.00	0.00	0.00	0.00	0.00	0.00	0.00
Fe/(Fe+Mg)	0.21	0.41	0.80	0.86	0.18	—	0.52	0.66	0.86
Mn/(Fe+Mn)	0.98	0.74	0.81	0.83	0.99	—	0.92	0.45	0.16
Mn/(Ca+Mn)	0.95	0.04	0.04	0.05	0.96	0.05	0.04	0.01	0.00

* CO_2 determined by difference

quartz (Goff et al., 1990). Cation geothermometer temperatures for fluid from this horizon are in good agreement with the formation temperature. Calculated temperatures for VC-2A (490 m) based on quartz is close to the formation temperature, whereas the cation temperature is suggestive of equilibration at higher temperatures than the temperature of fluid entry (Goff et al., 1990).

Fluid Composition

Fluids have been collected for chemical analysis from 490 m in VC-2A and 1755 m in VC-2B (Table A.5). The fluids produced are typical of those from other volcanic-hosted geothermal systems from around the world and are similar in the ratios of conservative ions to fluids produced from other wells in the Valles hydrothermal system but are more concentrated (Goff et al., 1989; Shevenell and Goff, 1987). Fluids from VC-2B were collected by downhole sampler, and reaction of the fluid with the steel casing of the well bore is suggested by the elevated concentrations of Fe and Mn. Comparison of the fluid produced from VC-2A, which was collected by surface flow tests, where the water was not in static contact with casing has lower Fe and Mn. VC-2A fluid samples were flash corrected, and because VC-2B fluids were collected by downhole sampler, no correction for flashing were required.

THERMOCHEMICAL CALCULATIONS

Ionic Strength and Activity Coefficients

The stoichiometric ionic strength of the present day fluids produced in VC-2A and VC-2B was calculated according to the equation

$$I = 1/2\Sigma m_i z^2 \quad (A.1)$$

Activity coefficients for the present day fluids were calculated using the extended Debye-Huckel equation (Helgeson et al., 1981). The ionic strength, log molality, log gamma, and log activity are presented in Table A.6 for VC-2A at 210°C and VC-2B at 295°C. Thermodynamic data for mineral dissolution constants and gas fugacity relations are calculated using SUPCRT and supporting data

from Helgeson et al. (1978), Helgeson and Kirkham, (1974a,b), Helgeson et al. (1981) and Helgeson (personal communication of updates and corrections to the data to D.R. Janecky).

Calculation of pH

The pH of hydrothermal fluids at reservoir temperatures cannot be measured directly for active systems, and the crush-leach extraction of inclusion fluids may lead to erroneous estimates of pH for fossil systems. However, fluid-mineral equilibria allow estimation of pH at high temperatures.

The pH of Sulphur Springs fluids was calculated by the reactions

$$3\text{K-spar} + H^+ = \text{K-mica} + 6SiO_2 + K^+ \qquad (A.2)$$

and

$$2\text{K-mica} + 3H_2O + 2H^+ = 3\text{Kaolinite} + 2K^+ \qquad (A.3)$$

because sericite is common among the alteration minerals that includes minor amounts of adularia and kaolinite.

It is possible to calculate the activity of sericite using the composition of sericite determined for the alteration assemblages identified in the Sulphur Springs system. The program GENMIX (Le Maitre, 1979) was used to calculate the solid-solution composition by least-squares methods from the electron microprobe analyses of sericite. End-member compositions of muscovite, paragonite, margarite, annite, phlogopite, and pyrophyllite are used in the calculation of the sericite solid-solution. The data generated by GENMIX are then used as input for ILLITE (R.W. Charles, unpublished) to calculate the sericite activity and the solid-solution mixing term.

Based on the above estimates of mineral activity and solution activity, pH can be estimated. At 230°C the calculated pH for VC-2A QSP horizon is 6.56 based on K-spar/K-mica equilibria and 4.66 for the K-mica/Kaolinite equilibria using present day activity of K^+. For VC-2B SER-CHL alteration zone (230°C), the calculated pH ranges from 4.87 to 5.86 for the above equilibria, and for

the VC-2B PROP assemblage (300°C), the pH ranges form 4.03 to 5.82 for the K-spar/K-Mica and K-mica/Kaolinite equilibria and the present day activity of K^+.

The pH of the fluid was also estimated from the expression

$$\log K = \log aK^+/aH^+ \qquad (A.4)$$

following the approach of Henley et al. (1984) by using the Na/K geothermometer in reverse to determine molality of K^+ and then inserting this value into the K-spar/K-mica equilibria expression to obtain pH. Use of the above expression allows calculation of pH when only an estimate of the salinity of the hydrothermal fluid is available, e.g. fluid inclusion microthermometry. Fluid inclusion data for Sulphur Springs indicates a fluid with salinities as high as 5.0 equiv. wt.% NaCl was once present. pH calculated from equation A.4 is 5.74 for 1.0 equiv. wt.% NaCl at 230°C and 4.66 for 5.0 equiv. wt.% NaCl at 300°C.

Calcite dissolution allows calculation of pH from the expression

$$CaCO_3 + 2H^+ = Ca^{2+} + CO_2 + H_2O \qquad (A.5)$$

where the mole fraction of CO_2 is 0.005 and the log molality and log gamma for Ca^{2+} are from Table A.6. The calculated pH for the present day VC-2B fluid at 300°C is 5.4 and for a 5.0 wt.% NaCl solution the pH is 5.2, which is 0.5 pH higher than the pH based solely on the salinity (Eq. A.4). The pH calculated for the present day VC-2A fluid at 210°C is 5.9.

The pH calculated from the various methods set limits on the pH of the hydrothermal fluids (Table A.7). The estimated pH values suggest fluids at 230°C ranged from mildly acidic to mildly alkaline and the pH estimated for fluids at 300°C is slightly acidic for present day fluid and paleo-fluids. Where pH is required in calculations a pH of 5.5 is chosen as an average value.

Table A.5 . Analyses of Hydrothermal Fluid Produced from VC-2A and VC-2B.

	VC-2A*	VC-2B#	
		Analyzed	Corrected
Major Elements			
SiO_2	315	882	651
As	1.92	0.1	2.7
Ca	5.9	78.5	
Mg	0.14	0.76	
Sr	0.76	1.22	
Na	1842	2350	
K	308	700	
Li	26.5	32.8	
HCO_3	273	105	
CO_3	0	0	
SO_4	54.8	7.8	
F	5.68	5.67	
Cl	2943	4150	
Br	5.9	13.6	
B	25.6	29.6	
Trace Elements			
Ba	0.11	0.32	
Fe	0.33	15.1	0.47
Mn	0.01	3.74	0.014
Mo	0.004	0.002	
Cu	0.002	0.002	
Pb	0.003	0.004	
Zn	0.02	0.02	

*, Average of 5 analyses, VA-295 to 298 and VA-300, taken on 8/27 to 8/2.
#, Sample VC2B-90, Goff et al., 1990.
Analyses by P.E. Trujillo and D. Counce. Values in mg/kg. 8/28/87.

Table A.6. Ionic Strength, log molality, log gamma, and log activitiy for Present Day Fluids from VC-2A and VC-2B.

VC-2A
Temperature = 210
Ionic Strength = 0.09

Ion	Log Molality	Log Gamma	Log Activity
Na^+	-1.094	-0.179	-1.272
K^+	-2.101	-0.193	-2.294
Li^+	-2.415	-0.155	-2.571
Mg^{++}	-5.236	-0.541	-5.777
Ca^{++}	-3.829	-0.613	-4.442
Mn^{++}	-6.736	-0.656	-7.393
Fe^{++}	5.225	-0.656	-5.882
Cl^-	-1.078	-0.186	-1.264
F^-	-3.521	-0.186	-3.707
Br^-	-4.129	-0.193	-4.322
HCO_3^-	-2.346	-0.172	-2.519
SO_4^-	-3.241	0.707	-3.948

VC-2B
Temperature = 295
Ionic Strength = 0.13

Ion	Log Molality	Log Gamma	Log Activity
Na^+	-0.987	-0.282	-1.269
K^+	-1.743	-0.309	-2.053
Li^+	-2.322	-0.239	-2.561
Mg^{++}	-4.501	-0.821	-5.322
Ca^{++}	-2.704	-0.946	-3.650
Mn^{++}	-4.163	-1.024	-7.613
Fe^{++}	-3.564	-1.024	-6.094
Cl^-	-0.928	-0.295	-1.223
F^-	-3.521	-0.295	-3.816
Br^-	-3.765	-0.309	-4.078
HCO_3^-	-2.760	-0.270	-3.030
SO_4^-	-4.086	-1.116	-5.202

Table 4.7. pH of the hydrothermal fluids estimated by various methods.

Method	230°C	300°
K-spar/K-mica	6.56 (QSP), 5.86 (SER-CHL)	5.82
K-mica/Kaolinite	4.66 (QSP), 4.87 (SER-CHL)	4.03
K^+/H^+	5.74	4.66
Calcite	5.9	5.4
$pH_{neutral}$	5.61	5.65

Calculation of fO_2 and fS_2

The major reservoir for hydrogen in hydrothermal systems is water, which reacts to form buffered fugacities of oxygen and hydrogen. The oxygen fugacity of the present day fluid and the paleo-fluids were calculated from the gas data and range from 10^{-33} to $10^{-42.3}$, which corresponds to fugacities at 300°C and 210°C, respectively (Tables 3.1 and A.8). Intermediate temperature fluids have intermediate fO_2 values.

Since the composition of chlorite is known for the different alteration assemblages identified in the Sulphur Springs system, it is possible to calculate the activity of chlorite. The program GENMIX (Le Maitre, 1979) calculates the solid-solution composition by least-squares methods from the electron microprobe analyses of chlorite. End-member compositions used for the calculation of chlorite solid-solution are those of Walshe (1986). The data generated by GENMIX are then used as input for the program CHLORITE (R.W. Charles, unpublished) to calculate the chlorite activity and solid-solution mixing term. It is then possible to calculate the oxygen fugacities from the chlorite analyses using the equation

$$\log fO_2 = 4\log aC_6 - 4\log aC_3 - 4\log K \quad (A.6)$$

where C_3 and C_6 are chlorite components 3 and 6 (Walshe, 1986) and log K is the equilibrium constant for the reaction

$$C_3 + 1/4O_2 = C_6 + 1/2H_2O \quad (A.7)$$

fO_2 was also calculated from the C-CH_4 equilibria (Eq. 3.4), which gave, not surprisingly, for the shallow portion (<700 m) of the system values that are typically 2 log units lower, but the fO_2 calculated from this equilibria for depths > 700 m are in good agreement with the CH_4-CO_2 (Eq. 3.1) and chlorite methods of calculating fO_2.

Table A.8. Oxygen and Sulfur Fugacities Calculated from Analyses of Chlorite from Various Alteration Horizons and Inclusion Gas Analyses

Alteration	% Total Fe as Fe^{3+} in Chlorite	Temperature#	Chlorite Analyses log fO_2	Chlorite Analyses log fS_2	Inclusion Analyses* log fO_2	Inclusion Analyses* log fS_2
VC-2A QSP	45	210	-39.2	-13.6	-41.5	-8.7
VC-2A CHL-SER	30	230	-36.3	-12	-37.5	-10.7
VC-2B CHL-SER	45	230	-38.0	-13.1		
VC-2B PROP	30	300	-34.3	-11.3	-34.3	-12.4

* Average of inclusion analyses from samples of that alteration horizon.
\# Temperature based on fluid inclusion homogenization temperatures.

The best agreement between the fO_2 obtained from the chlorite data and that obtained from the inclusion data is for chlorites which contain between 30% and 45% of the total Fe as Fe^{3+} (about 8 to 16 wt.% Fe^{3+}). The analyzed chlorites of Sulphur Springs are high Fe with $Fe^{2+} + Fe^{3+} \geq 5$ (Musgrave et al., 1991); therefore, the fO_2 from the chlorite analyses are best represented by those with 30 to 45% Fe^{3+}.

Sulfur fugacities calculated from the inclusion analyses were obtained from the equation

$$2H_2O + S_2 = O_2 + 2H_2S \qquad (A.8)$$

using the fO_2 calculated from the CH_4-CO_2 equilibria (Eq. 3.1) and the H_2S concentration obtained from the gas analyses. Sulfur fugacities were also calculated from the chlorite analyses using the equation

$$\log fS_2 = 4/7 \log fO_2 - 1/7 \log aC_4 - 1/7 \log K \qquad (A.9)$$

where C_4 is the chlorite component 4 (Walshe, 1986) and log K is the equilibrium constant for the reaction

$$C_4 + 7S_2 = 7FeS_2 + 4H_2O + 3SiO_2 + 4O_2 \qquad (A.10)$$

In general, the sulfur fugacities calculated from the chlorite data agree with those obtained from the fluid inclusion gas data.

Calculation of Metal Solubilities and Metal Speciation.

The recognition that some present day hydrothermal systems are modern analogs to fossil systems has prompted a great deal of interest in metal transport and deposition in active systems (White, 1955, 1981; Henley and Ellis, 1983, Hulen and Nielson, 1986). Relatively few high

temperature thermodynamic data exist from which to calculate solubilities for metals and metals sulfides. Concentration of Cu, Pb, Zn, Au, and Ag in the hydrothermal fluids were calculated by the program GEOMOD (Norman, unpubl). GEOMOD uses the gas data to calculate fO_2 and fS_2 and salinity to obtain pH for calculation of concentrations of these metals in solution. Concentrations of metals in present day fluids and paleo-fluids were modeled under nonboiling conditions using the data from Table 3.1 for the gas concentrations, the downhole temperatures for the present day fluids, Table A.5 for the present day fluid composition, and the fluid inclusion microthermometry for the paleo-fluids. Examination of the data in Tables A.5 and A.9 shows there is generally fair agreement between the calculated amounts of some metals (Cu and Zn for VC-2A) in solution and the amounts actually in the fluids and other metals are in disagreement up to several of orders of magnitude. For example, the analyzed concentrations of Cu and Pb in VC-2A fluid are 0.002 and 0.003 ppm, respectively, and the calculated concentrations are 0.003 and 0.0006 ppm, respectively. An order of magnitude difference for the Pb. The discrepancies are greater for the VC-2B data; the difference in the Cu and Pb concentrations are about 4 orders of magnitude. These discrepancies may be due to deposition of sulfides (particularly Fe-sulfides) in the wellbore of VC-2B and the incorporation of these metals into the Fe-sulfides as trace metals thereby lowering their concentration.

Calculated solubilities at 300°C and 5.0 wt.% NaCl indicate that in excess of 1000 ppm Zn could be transported in Sulphur Springs hydrothermal fluids, about 35 ppm Pb, about 70 ppm Cu, and more than 20 ppm Ag (Table A.9). However, only about 1.4 ppb Au can be transported in these saline fluids.

Transport of Cu, Pb and Zn in the 5.0 wt.% paleo-fluid was by chloride complexes (Wood et al., 1987), but in low chloride solutions such as the present day fluids and the low salinity shallow paleo-hydrothermal fluid (1.0 equiv. wt. % NaCl, as indicated by the fluid inclusion data), hydroxide and carbonate complexes may be important (Wood et al., 1987). Gold is transported as the bisulfide complex (as $Au(HS)_2^-$) in all fluids.

Table A.9 Calculated Concentration of Ore Metals in Sulphur Springs Hydrothermal Fluids.

Present Day Fluids

Calculation Method: Non-boiling
Modeling option: Solubility
VC-2A fluid produced at 490 m.
Salinity = 0.7 wt% (0.12 molal)
Temperature: 210

Temperature C	Total Cu ppm	Total Pb ppm	Total Zn ppm	Total Au ppm	Total Ag ppm
210	0.004	0.0006	0.09	0.005	0.001

Calculation Method: Non-boiling
Modeling option: Solubility
VC-2B fluid produced at 1755 m.
Salinity = 1.1 wt% (0.19 molal)
Temperature: 295

Temperature C	Total Cu	Total Pb ppm	Total Zn ppm	Total Au ppm	Total Ag ppm
295	0.75	0.1	0.78	0.029	0.13

Paleo-Fluids

Calculation Method: Non-boiling
Modeling option: Solubility
Salinity = 5.0 wt% (0.86 molal)
Temperature: 300

Temperature C	Total Cu ppm	Total Pb ppm	Total Zn ppm	Total Au ppm	Total Ag ppm
300	70	35	2884	0.0014	23

STABLE ISOTOPE DATA

More than 75 samples were collected for light stable isotope measurements (H, C, O) on whole rocks and vein minerals from VC-2A and VC-2B core. The H, C, and O isotopic composition of samples is reported in per mil deviation from a standard. Standards are SMOW for hydrogen and oxygen and PDB for carbon.

Water

The δD values of present day meteoric water and produced hydrothermal fluid fall in the range from -93 to -82 and -97 to -85, respectively (Goff et al., 1981; Vautaz and Goff, 1986; Shevenell et al., 1987; Musgrave et al., 1989). The $\delta^{18}O$ values of present day water and produced hydrothermal fluid range from -12 to -9 and -11 to -7, respectively (Shevenell et al., 1987; Musgrave et al., 1989) (Fig. A.5). δD values of primary magmatic water ranges from -40 to -80 per mil and $\delta^{18}O$ ranges from 5 to 10 per mil (Taylor, 1974).

The oxygen isotopic composition of fluids responsible for the deposition of vein-filling phases was calculated from the $\delta^{18}O$ values of quartz, calcite, and rhodochrosite; the fluid inclusion temperatures; the quartz-water fractionation factors of Matsuhisa et al. (1979), and the calcite-water fractionation factor of Friedman and O'Neil (1977) (Table A.10). The calculated $\delta^{18}O_{H2O}$ values range from -8.22 to -3.39 per mil based on quartz, and the calculated $\delta^{18}O_{H2O}$ based on calcite range from -13.45 to 6.6 per mil. One rhodochrosite sample gave a $\delta^{18}O_{H2O}$ value of -3.85 per mil. All of the calculated $\delta^{18}O_{H2O}$ values are consistent with derivation from waters of meteoric origin, except for the water calculated from the veins in the limestone.

Oxygen isotopic data for the paleo-hydrothermal fluid calculated from the quartz $\delta^{18}O$ values are consistent with the deposition of the quartz from a fluid of meteoric origin. The values of the $\delta^{18}O_{H2O}$ calculated from the vein calcites also are consistent for derivation from a fluid of meteoric origin, but also suggest the dominance of the isotopic control of the marine limestones on the isotopic composition of the fluid which deposited the calcites.

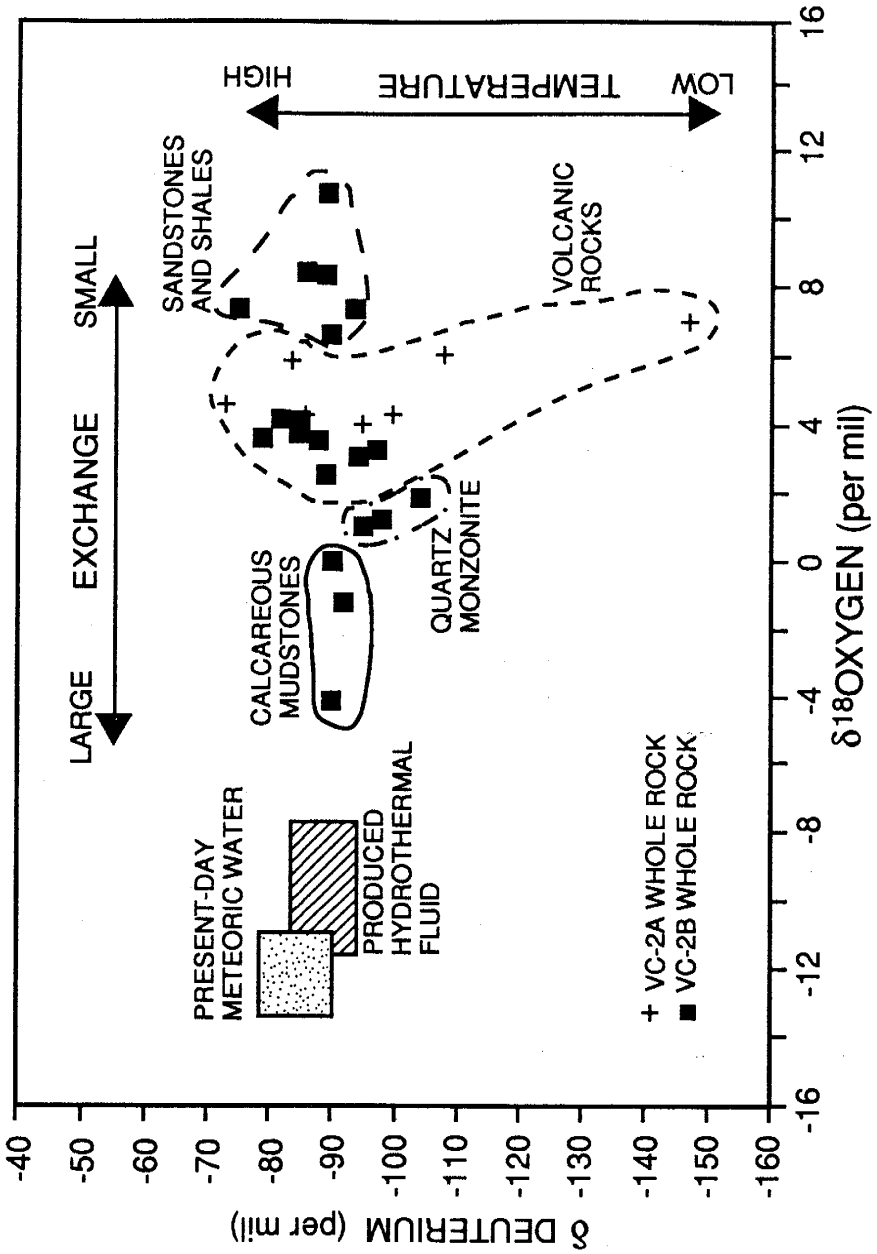

Figure A.5. δD-$\delta^{18}O$ composition of whole rocks, Sulphur Springs. Cross, VC-2A whole rocks; filled-square, VC-2B whole rocks. Included on this figure are possible processes responsible for the isotopic composition of the rocks. VC-2A data are from Musgrave et al. (1989).

Table A.10. $\delta^{18}O$ and Calculated $\delta^{18}O_{H_2O}$ for Vein-filling Phases.

Sample Number	Mineral	$\delta^{18}O$	$\delta^{18}O_{H_2O}$ calculated
VC2A56-6-Q193	Quartz	4	-6.72
VC2A89-8-Q383	Quartz	3.1	-7.22
VC2A241-6A-Q1126	Quartz	6.5	-3.39
VC2B 760	Quartz	2.1	-8.22
VC2B 882	Quartz	3.1	-7.22
VC2B 895	Quartz	2.8	-7.52
VC2B 933	Quartz	2.1	-8.22
VC2B 4755	Quartz	0.8	-6.62
VC2B 5533	Quartz	-0.6	-7.46
VC2A75-3D-C315	Calcite	-5	-13.45
VC2A113-R494	Rhodochrosite	4.6	-3.85
VC2A216-1-C1000	Calcite	0	-8.45
VC2A241-6A-C1126	Calcite	2.7	-5.75
VC2A252-4A1-C1171	Calcite	-1	-9.45
VC2A362-3-C1712	Calcite	-0.3	-8.75
VC2B 1350	Calcite	-0.2	-8.65
VC2B 1507	Calcite	0.1	-8.35
VC2B 1924	Calcite	-0.5	-8.59
VC2B 2183	Calcite	-1.4	-9.49
VC2B 3017	Calcite	-1.1	-8.57
VC2B 4565	Calcite	9.7	3.5
VC2B 4689	Calcite	12.8	6.6

Table A.11. Deuterium and Oxygen Isotopic Composition of Whole Rocks, Sulphur Springs

Sample Number	Rock Type	Oxygen 18	Deuterium
VC2A27-7B 95.8	Tuff	7	-148
VC2A54-4 212.5	Tuff	6.1	-109
VC2A71-2A 292.8	Tuff	4.4	-100
VC2A115-1 500.5	Tuff	4.7	-73
VC2A146-7 653.3	Tuff	4	-84
VC2A187-1 857	Tuff	4.1	-95
VC2A279-1A3 1302	Tuff	4.4	-86
VC2A331-K2 1553	Tuff	3.9	-86
VC2A341-B 1601.6	Tuff	6	-84
VC2A360-4 1701	Tuff	4.1	-85
VC2B 701	Tuff	4.3	-82
VC2B 899	Tuff	3.8	-79
VC2B 1249	Tuff	4.3	-85
VC2B 1447	Tuff	3.4	-97
VC2B 1752	Tuff	3.7	-88
VC2B 2001	Tuff	3.9	-85
VC2B 2199	Tuff	2.7	-89
VC2B 2402	Tuff	3.2	-94
VC2B 2499	Sandstone	8.6	-86
VC2B 2548	Sandstone	7.5	-75
VC2B 2703	Sandstone	6.8	-90
VC2B 3000	Sandstone	7.5	-94
VC2B 3800	Sandstone and Shale	10.85	-89
VC2B 4050	Sandstone and Shale	8.5	-89
VC2B 5000	Limestone	0.1	-90
VC2B 5051	Limestone	-4	-90
VC2B 5100	Limestone	-1.1	-92
VC2B 5302	Quartz Monzonite	1	-94
VC2B 5350	Quartz Monzonite	1.4	-95
VC2B 5530	Quartz Monzonite	2.9	-108

Whole Rocks

Oxygen isotope studies of whole rocks from Sulphur Springs show distinct fields depending on the rock type (Fig. A.5; Table A.11). The $\delta^{18}O$ whole rock values for the volcanic rocks fall into a fairly narrow range from 2.7 to 7 per mil. The altered volcanic rocks are depleted in $\delta^{18}O$ relative to fresh volcanic rocks (Taylor, 1968). Sandstones of Sulphur Springs being composed of quartz are least susceptible to oxygen isotopic exchange, and, therefore, retain whole rock values typical of clastic sedimentary rocks (Hoefs, 1987). The calcareous mudstone and siltstone region of Figure A.6 has been shifted by about 90 per mil in δD and 25 per mil in $\delta^{18}O$ from typical values for marine limestones (0 for δD and 20 to 30 per mil for $\delta^{18}O$; Hoefs, 1987). Quartz monzonite sampled at Sulphur Springs is depleted in $\delta^{18}O$ by 5 to 7 per mil over what is considered an average $\delta^{18}O$ of 8 per mil for quartz monzonite (Taylor, 1968).

The δD and $\delta^{18}O$ data for whole rocks illustrate the effects of isotopic exchange and temperature on the isotopic composition of the rocks at Sulphur Springs (Fig. A.5). δD values for VC-2A volcanic rocks show the greatest influence of temperature effects of the isotopic composition of these rocks because these they represent the shallowest samples where fluctuations in the temperature gradient will be greatest and the effects of cold groundwater are greatest. Isotopic composition of the remainder of the rocks was largely an exchange process by fluids under a fairly homogeneous temperature regime. Siliciclastic rocks composed of mostly quartz are least resistant to exchange and largely preserve their original isotopic composition. The marine limestone being a highly exchangeable rock has undergone the most extensive isotopic exchange with values approaching those of the hydrothermal fluid.

Carbon Isotopic Composition

Samples of host rock limestone and vein calcite and rhodochrosite were analyzed for carbon and oxygen isotopes (Table A.12). Calcite from the Paleozoic carbonate rocks have a wide range in $\delta^{13}C$ values of -7.2 to 0.4 per mil, while the vein carbonates have a narrower range from -6.0 to -3.3 per mil. The oxygen isotopic composition of calcites from the limestones have the

Table A.12. Carbon and Oxygen Isotopic Compostion of Whole Rocks (Limestones) and Vein Carbonates, Sulphur Springs

Sample Number	Carbon 13	Oxygen 18
VC2B 3000	0.4	7.8
VC2B 3015	-2.8	2.6
VC2B 3103	-2.3	2.3
VC2B 3211	-2.1	6
VC2B 3500	-6.2	5.1
VC2B 3552	-5.1	12
VC2B 3600	-4.9	4.8
VC2B 3700	-4.5	6.6
VC2B 3751	-6.3	7.5
VC2B 3950	-4.7	6.6
VC2B 4101	-5.8	5.2
VC2B 4152	-7.2	6.7
VC2B 4254	-4.6	10.3
VC2B 4294	-6.7	12.3
VC2B 4350	-4	7.4
VC2B 4398	-3.8	16.4
VC2B 4463	-5	8.6
VC2B 4501	-2.8	13.1
VC2B 4545	-4.3	10.4
VC2B 4603	-4.7	7.6
VC2B 4655	-6.4	5.3
VC2B 4701	-4.5	12.7
VC2B 4762	-5.1	10.1
VC2B 4799	-3.8	-0.8
VC2B 4851	-3.5	21.5
VC2B 4900	-0.5	21.8
VC2B 4958	-1.9	18
VC2B 5000	-2.7	-1.9
VC2B 5051	-1	9.2
VC2B 5100	-4.4	9.7

Vein Material	Mineral	Carbon 13	Oxygen 18
VC2A75-3D-C315	Calcite	-4.1	-5
VC2A-113-R494	Rhodochrosite	-4.4	4.6
VC2A216-1-C1000	Calcite	-4.8	0
VC2A241-6A-C1126	Calcite	-4.6	2.7
VC2A252-4A1-C1171	Calcite	-6	-1
VC2A362-3-C1712	Calcite	-5.5	-0.3
VC2B 1350	Calcite	-3.6	-0.2
VC2B 1507	Calcite	-4.1	0.1
VC2B 1924	Calcite	-5	-0.5
VC2B 2183	Calcite	-4.6	-1.4
VC2B 3017	Calcite	-3.5	-1.1
VC2B 4565	Calcite	-3.3	9.7
VC2B 4689	Calcite	-4.6	12.8

heaviest isotopic values of rocks analyzed in this study, ranging from -1.9 to 21.8 per mil. By contrast, vein samples are somehwat more restricted in their range, varying between -5.0 to 12.8 per mil, clustering around zero per mil.

Under the fO_2-pH conditions of Sulphur Springs hydrothermal fluids, CO_2 is the dominant carbon species in the fluid. Thus we can assume the $\delta^{13}C_{fluid} = \delta^{13}C_{CO2}$. Using the fractionation factors of Friedman and O'Niel (1977) for Calcite-CO_2, the calculated $\delta^{13}C_{fluid}$ ranges from -5.2 to -1.7 per mil. Such a range in $\delta^{13}C_{fluid}$ is consistent with the range of the $\delta^{13}C$ values for the unaltered Madera Limestone (Fig. A.6); therefore, the carbon isotopic data are indicative of a marine limestone source for the carbon. This is consistent with the source of CO_2 suggested in Part III.

Water-Rock Ratios

In this section the systematics of hydrogen- and oxygen-isotopic exchange between the hydrothermal fluid and rock at Sulphur Springs is examined. Final isotopic composition of water (δ^f_w) after equilibration with rock is a function of (1) the initial (unexchanged) composition of the water (δ^i_w) and rock (δ^i_r), (2) the temperature of equilibration, which determines the fractionation factor between rock and water $\Delta_{r\text{-}w}$, (3) the ratio of exchanged hydrogen and oxygen atoms in the water to those in the rock (w/r) (Field and Fifarek, 1985). This relationship is expressed as

$$(\delta^f_w) = \frac{(\delta^i_r) - \Delta_{r\text{-}w} + [(w/r)\,(\delta^i_w)]}{1 + (w/r)} \qquad (A.11)$$

Sulphur Springs hydrothermal system is hosted in felsic and intermediate igneous rocks and clastic and chemically precipitated sedimentary rocks. Igneous rocks of this compositional range contain as much as 0.11 wt.% hydrogen and approximately 50 wt.% oxygen. Thus the hydrogen and oxygen isotopic composition of a fluid that has equilibrated with igneous rock of these characteristics can be determined from

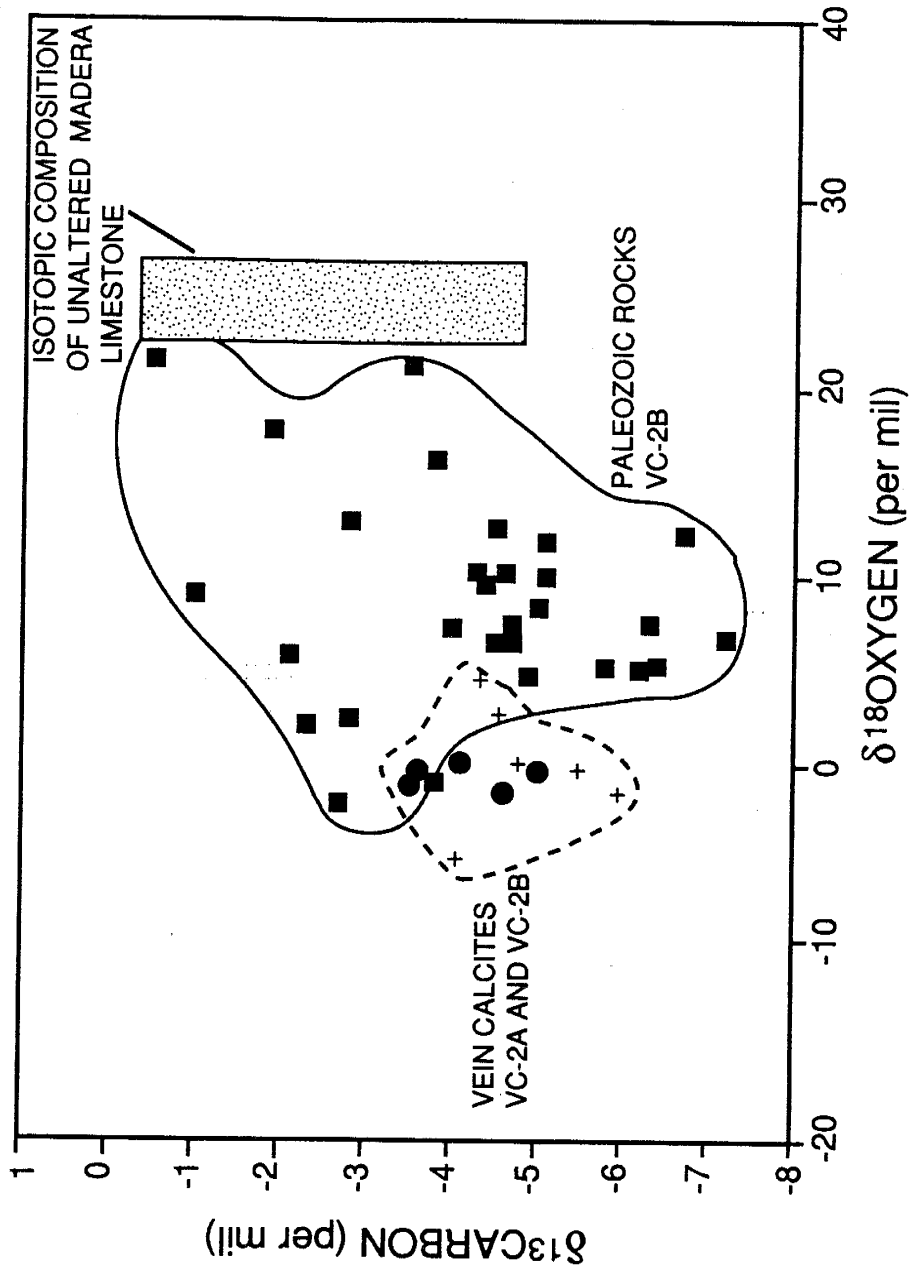

Figure A.6. $\delta^{13}C$-$\delta^{18}O$ composition of whole rock carbonates and vein carbonates. Cross, VC-2A vein carbonates; filled circle, VC-2B vein carbonates. VC-2A data are from Musgrave et al. (1989).

$$(\delta D^{f}_{w}) = \frac{-70 - \Delta_{r\text{-}w} + [(100R)\ (\delta D^{i}_{w})]}{1 + (100R)} \qquad (A.12)$$

and

$$(\delta^{18}O^{f}_{w}) = \frac{8 - \Delta_{r\text{-}w} + [(1.8R)\ (\delta^{18}O^{i}_{w})]}{1 + (1.8R)} \qquad (A.13)$$

where the coefficients 100 and 1.8 represent ratios of the weight-percent hydrogen in H_2O (11.2%) to that in rock (0.112%) and the weight-percent oxygen in H_2O (88.8%) to that in rock (50%), respectively, and R is the water:rock mass ratio. Because values of R represent proportions of water and rock that have isotopically equilibrated, they are easier to relate to natural systems than are values of atomic ratio (w/r) (Field and Fifarek, 1985).

Isotopic compositions of sedimentary rocks are more variable that those of igneous rocks. The sedimentary stratigraphic section of the Sulphur Springs area consists of subequal amounts of siliciclastic and carbonate components, which would average -45 per mil δD and 18 per mil $\delta^{18}O$ and contain about 0.28 wt.% hydrogen (2.5 wt.% H_2O) and 50 wt.% oxygen. The final isotopic composition of a fluid that has equilibrated with a sedimentary rock of this composition can be calculated from

$$(\delta D^{f}_{w}) = \frac{-45 - \Delta_{r\text{-}w} + [(40R)\ (\delta D^{i}_{w})]}{1 + (40R)} \qquad (A.14)$$

and

$$(\delta^{18}O^{f}_{w}) = \frac{18 - \Delta_{r\text{-}w} + [(1.8R)\ (\delta^{18}O^{i}_{w})]}{1 + (1.8R)} \qquad (A.15)$$

Fractionation of hydrogen isotopes between fluid and rocks is assumed to be equivalent to that for chlorite-H_2O (Taylor, 1974). Computations were based on chlorite-H_2O fractionation factors from Taylor (1979, Fig. 6.2). The assumption that oxygen isotope fractionation between plagioclase feldspar (An_{30})-H_2O is similar to that between fluids and rock has been used to calculate the fluid-rock fractionation, $\Delta_{r\text{-}w}$. The fractionation factor for plagioclase feldspar (An_{30}-H_2O) was calculated from the equation of O'Niel and Taylor (1967)

$$1000 \ln\alpha = 2.68 (10^6)/T^2) - 3.29 \quad (A.16)$$

The isotopic composition of a convected hydrothermal fluid will generally differ from a static fluid because the fluid has equilibrated over a range of temperatures and water:rock mass ratios. To model the isotopic composition of Sulphur Springs meteoric water during convection, the isotopic composition was calculated at 50°C intervals from 100°C to 300°C and at 400°C and 500°C. The finial composition of the water (δ^f_w) computed at each temperature became the initial water composition (δ^i_w) for the calculations at the next higher temperature. These calculations were performed at R values of 0.01, 0.1, 1, and 10 because the water:rock mass ratio varies according to the convection path (Field and Fifarek, 1985).

Important points to be made from these calculations are (1) that convecting meteoric water is progressively enriched in D and ^{18}O during heating and exchange with unaltered wall rock (Fig. A.7). Sulphur Springs meteoric water will be isotopically heavier than nonconvecting meteoric water (e.g. pore water) under identical conditions of equilibration because of its pathway of exchange (Field and Fifarek, 1985). (2) Meteoric water may attain compositions similar to those of magmatic or metamorphic waters through exchange at low water:rock mass ratios (0.01-0.1)(Campbell et al., 1984; Field and Fifarek, 1985). Therefore, caution must be used when making the distinction between a magmatic/metamorphic or meteoric source of fluids and the demonstration of mixing between magmatic/metamorphic and meteoric waters.

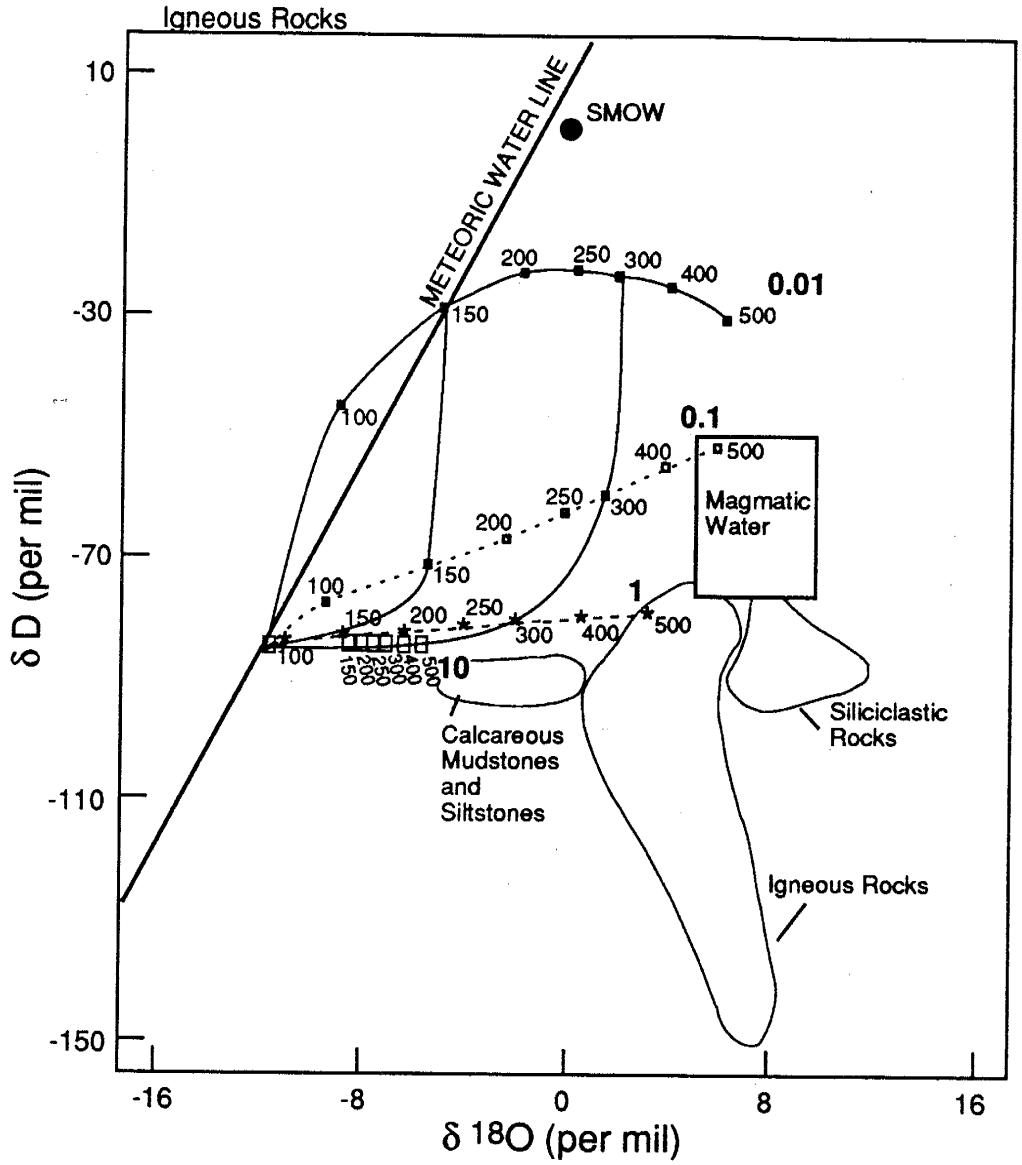

Figure A.7 Variations of δD and $\delta^{18}O$ in Sulphur Springs hydrothermal fluids during convection through igneous as a function of temperature and water:rock mass ratio. Near vertical lines at 150 and 300°C represent the region for Sulphur Springs data based on fluid inclusion data and measured down hole temperatures. Solid line with solid squares is model for water:rock mass ratio = 0.01, dashed line with open squares is model for water:rock mass ratio = 0.1, dashed line with asterisks is model for water:rock mass ratio = 1, and large open boxes model water:rock mass ratio = 10. Modelled for the following initial isotopic compositions: meteoric water, δD = -85 and $\delta^{18}O$ = -12 per mil and igneous rock, δD = -70 and $\delta^{18}O$ = 8 per mil. The region bewteen solid lines at 150°C and 300°C is the temperature range for water-rock equilibration based on fluid inclusion T_h and measured downhole temperatures.

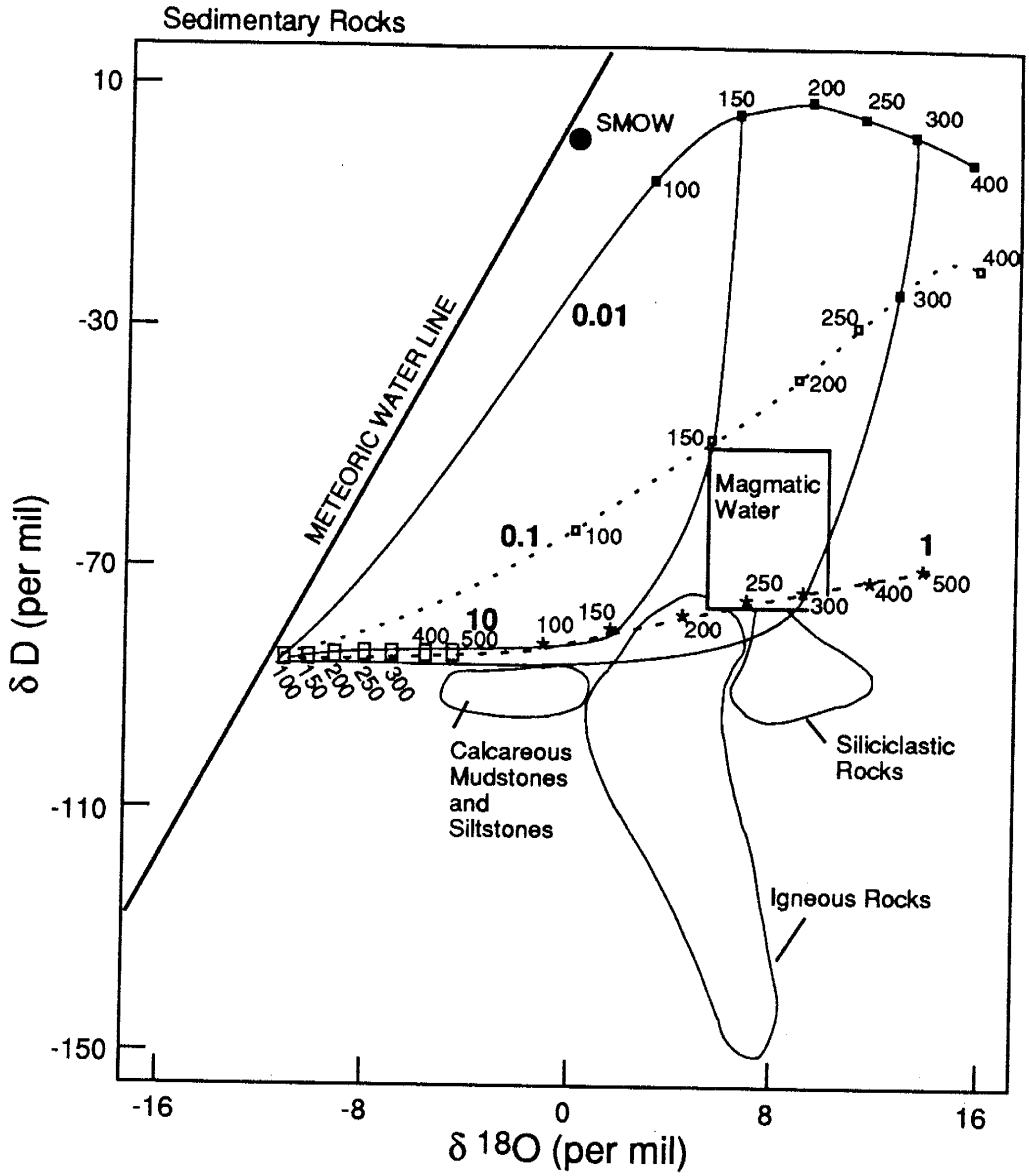

Figure A.7 b. Variations of δD and $\delta^{18}O$ in Sulphur Springs hydrothermal fluids during convection through sedimentary rock as a function of temperature and water:rock mass ratio. Near vertical lines at 150 and 300°C represent the region for Sulphur Springs data based on fluid inclusion data and measured down hole temperatures. Solid line with solid squares is model for water:rock mass ratio = 0.01, dashed line with open squares is model for water:rock mass ratio = 0.1, dashed line with asterisks is model for water:rock mass ratio = 1, and large open boxes model water:rock mass ratio = 10. Modelled for the following initial isotopic compositions: meteoric water, δD = -85 and $\delta^{18}O$ = -12 per mil and sedimentary rock δD = -45 and $\delta^{18}O$ = 18 per mil. The region between solid lines at 150°C and 300°C is the temperature range for water-rock equilibration based on fluid inclusion T_h and measured downhole temperatures.

Isotopic composition of convecting hydrothermal fluids at Sulphur Springs can be interpreted in terms of the calculated curves in Figure A.7. The range in temperatures of water-rock equilibration are taken from the fluid inclusion T_h and measured downhole temperatures (Fig. A.7). The model indicates that Sulphur Springs fluids evolved at high temperatures (≥300°C) from a fluid of similar isotopic composition to present day meteoric water, but it suggests that fluids responsible for hydrothermal alteration and presumably vein formation were slightly lighter in δD (closer -95 per mil) than present day waters. If the calculated curves are shifted 10 per mil in δD to -95, the model accounts for almost all the data, but it cannot account for the large decrease in the δD composition of volcanic rocks from VC-2A. These data are more suggestive of isotopic fractionation at lower temperatures. The calculated δD composition of volcanic rock (assuming present day meteoric water has δD = -85 per mil and fractionation is represented by chlorite-H_2O at 100°C) is -149 per mil. Current temperatures within 50 m of the present land surface are close to 100°C. Therefore, δD values of VC-2A rocks within 100 m of the present land surface are largely due to isotopic fractionation under the current temperature regime defined by the geothermal gradient. This brings up an important point that these water:rock mass ratios should be regarded as tentative because processes (e.g. boiling or mixing of cold groundwater) other than water-rock exchange may have influenced the isotopic composition of the fluids and rocks.

The $\delta^{13}C$-$\delta^{18}O$ data in Figure A.6 suggest extensive exchange between the Paleozoic carbonates and the fluid. Average unaltered Madera Limestone outside the caldera has an isotopic composition of $\delta^{13}C$ = -4.4 per mil and $\delta^{18}O$ = 24 per mil (Goff et al., 1985). This indicates the calcite matrix underwent extensive isotopic exchange, which is most effectively accomplished during recrystallization of the limestone.

DISCUSSION

Chemical Environment

The data indicate that parameters such as pH, fO_2, and fCO_2 remained more or less constant for a given paragenetic stage or depth. Fugacity of CO_2 was lower during early quartz

deposition at depths >700 m and retains a similar value today, but during calcite deposition, the fCO_2 apparently increased. Carbon dioxide fugacity is constant and at a higher value throughout the entire paragenesis for depths <700 m. This may be due to the analysis of numerous gas-filled inclusions in early quartz and intermediate to late stage calcite resulting from boiling. Fluorite may also have been deposited under boiling conditions because one sample of fluorite was intergrown with and paragenetically later than bladed calcite. Early fluids associated with molybdenite and base metal deposition had the highest concentrations of H_2S and highest fS_2 values. In contrast, high sulfur content of the calcite from >700 m may be due to thermal decomposition of organic residues in the Madera Limestone. The data indicate the concentration of reduced sulfur in the hydrothermal fluid controlled deposition of sulfides, and solutions remained in equilibrium with PbS and ZnS (Fig. A.8), and by lack of corrosion of the sulfides. The observed sulfide and sulfosalt minerals combined with the measured fluid inclusion temperatures of 230-310°C and the fluid inclusion gas data from early quartz indicate the values of fS_2 during ore mineral deposition (Fig A.9). The shaded region in Figure A.9 coincides well with the stability of observed sulfide minerals. Pyrargyrite is the silver mineral identified, the pyrite of Sulphur Springs is typically high in As (Musgrave et al., 1990), although no arsenopyrite was positively identified, and chalcopyrite is the copper sulfide (no bornite was identified) present at Sulphur Springs.

Agreement of Mineralogy with Indicated Chemical Environment

Given that, the measurements reported here represent those in the mineralizing fluids, the chemical environment inferred from the analyses should agree with observed mineral assemblages and paragenesis. Temperatures of the proposed chemical environment for depths <700 m based on mineralogic data (Hulen and Nielson, 1988) are consistent with the temperatures indicated by the fluid inclusion data. Temperatures based on the appearance of illitic sericite (<5% expandable layers) are in excess of 200°C, and Hulen and Nielson (1988) found sericites from the QSP zone of VC-2A to contain between 5-14% smectite interlayers. Chlorite appearance usually coincides with temperatures of >220°C in active hydrothermal systems (Browne, 1978), which is consistent with

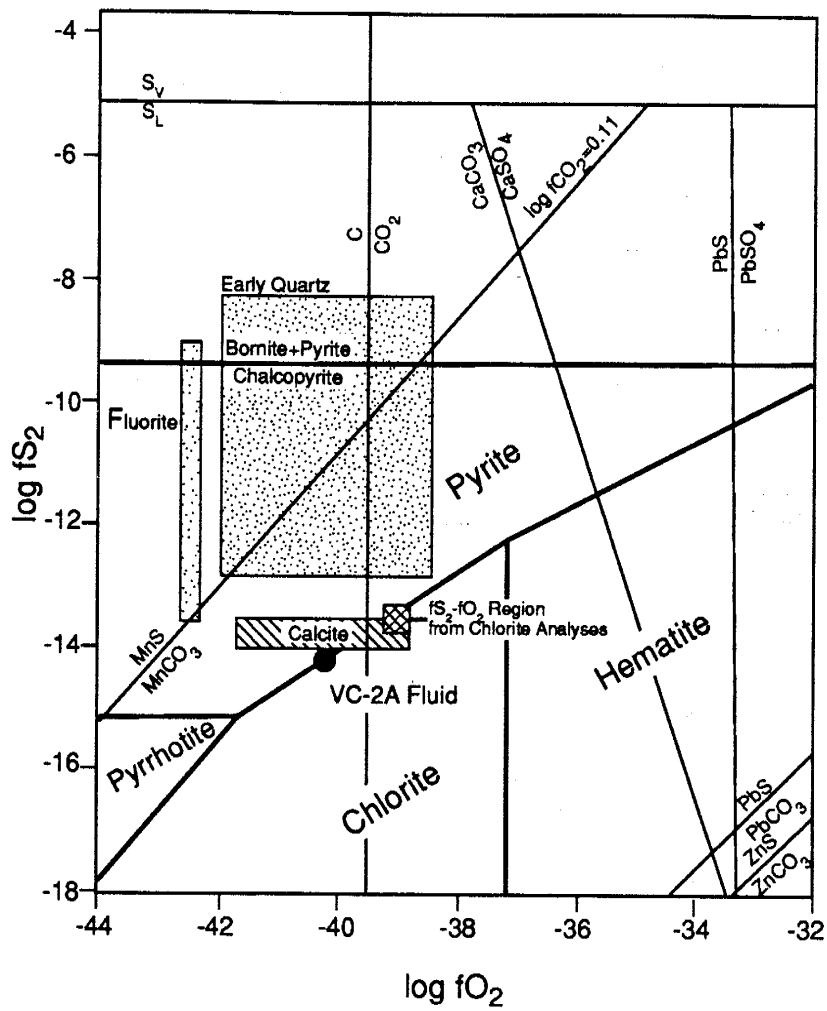

Figure A.8. a. Log fS_2-log fO_2 constructed for 230°C, 0.003 m total sulfur and log fCO_2 = 0.11 and depths <700 m. Chlorite preempted the magnetite field and a portion of the pyrrhotite field. Plotted on the figure are the various log fS_2-log fO_2 fields for quartz, calcite, fluorite, and the present day VC-2A fluid based on the inclusion gas data and from the chlorite analysis.

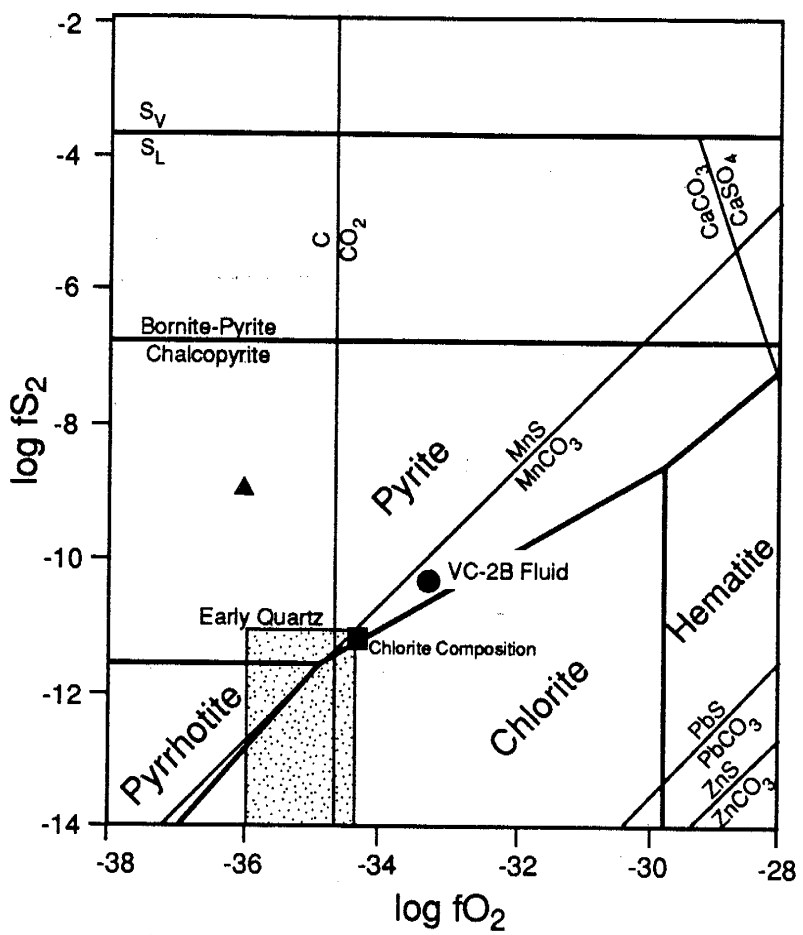

Figure A.8 b. Log fS_2-log fO_2 constructed for 300°C, 0.003 m total sulfur and log fCO_2 = 0.11 and depths >700 m. Chlorite preempted the magnetite field. Plotted on the figure are the various log fS_2-log fO_2 fields for quartz, calcite, and the present day VC-2B fluid based on the inclusion gas data and from the chlorite analysis.

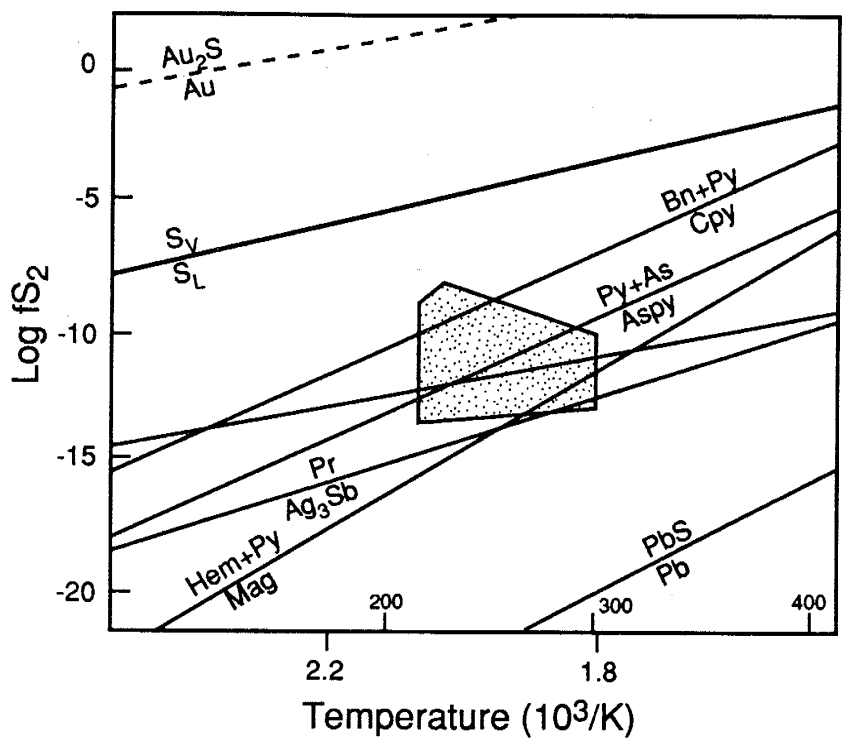

Figure A.9. Univariant temperature versus log fS_2 diagram for sulfide and sulfosalt mineral assemblages at Sulphur Springs. Shaded region represents the conditions of deposition for the ore minerals based on fluid inclusion T_h and gas data for early quartz. Bn, bornite; py, pyrite; cpy, chalcopyrite; aspy, arsenopyrite; pr, pyrargyrite; hem, hematite; mag, magnetite. Diagram modified from Gemmell et al. (1988) and Henley et al. (1984).

the observation that chlorite is first noted at depths below about 160 m in VC-2A. Fluid inclusion temperatures from early quartz for this depth are around 230°C.

Agreement between the calculated stability fields of mineral phases based on the phases calculated to be stable and those observed is good (Fig. A.9). Chlorite is not observed in the early vein filling of VC-2A and VC-2B of the QSP alteration horizon, but it is associated with the intermediate to late stage calcite. Chlorite stability for the PROP horizon of VC-2B is indicated from the analyses, and indeed it is present (Fig. A.9). Early fluids from depths <700 m deposited molybdenite, sphalerite, galena, pyrite, chlorite, sericite, and rhodochrosite from fluids at approximately 230°C and 1.0 equiv. wt.% NaCl. Late fluids deposited pyrargarite, pyrite, sphalerite, calcite, fluorite, sericite, chlorite, and rhodochrosite at about 200°C and 0.7 to 1.0 equiv. wt.% NaCl. Deep fluids (depths >700 m) responsible for early vein filling deposited chlorite, calcite, epidote, pyrite, and hematite from fluids 258 to 334°C and 0.5 to 5 equiv. wt. % NaCl fluids. Late fluids deposited fluorite at about 232-319°C and 0.9-1.7 equiv. wt.% NaCl. The calculated pH and fO_2 values suggest the predominant sulfur species was H_2S for depths <700 m, which agrees with the deposition of sulfides in both the early and late stage mineralization, and the observation that no sulfate minerals are present. The deep fluids may have been closer to the H_2S-SO_4 boundary because of trace amounts of anhydrite and hematite in veins from these depths and SO_2 measured in the fluid inclusions.

MODEL OF EPITHERMAL MINERALIZATION

Hydrothermal fluids in the upper most portions of the earth's crust (<2 km) are generally under hydrostatic pressure conditions (Hedenquist and Henley, 1985a; Hedenquist, 1991). As a result boiling is a common phenomena in the upflow portions of hydrothermal systems, and numerous studies have shown the profound affects of boiling on the physicochemical conditions of the fluid (e.g. Drummond and Ohmoto, 1985; Sypcher and Reed, 1989). Boiling often continues all the way to the surface, where the fluid discharges as boiling springs. Fluid inclusion data indicate the Sulphur Springs area was a region of upflow and boiling (See Part II and Fig. 2.9), and

it continues to be a region of upwelling because of the presence of boiling springs (Goff et al., 1985).

In addition to boiling, mixing can modify the physicochemical nature of the hydrothermal fluids (Spycher and Reed, 1989; Henley et al., 1984; Plumlee, 1989). In almost all geothermal systems, there will be a marginal nonboiling fluid (Hedenquist, 1991). Therefore, boiling of the deep upflow and mixing with a shallow diluent, which can be cold groundwater, steam-heated groundwater, and/or conductively cooled equivalent of the upflow, as it approaches the margin and surface of the system are the two most important processes to consider in the deposition of metals in the epithermal environment of most hydrothermal systems, whether they are active or extinct (Hedenquist, 1991).

Deposition of Sulfide Minerals

Alteration, field, and fluid inclusion studies indicate that sulfide mineral deposition was controlled by the migration of fluids along the faults and fractures in the Sulphur Springs area, which in turn led to mixing and boiling of the ascending fluids with cooler and more dilute waters.

A multistep, isoenthalpic boiling process in which complete removal of the gas phase is accomplished at each step followed by further boiling of the residual liquid is chosen here instead of single-step, closed-system boiling or Rayleigh-type distillation because it represents more realistically what actually takes place in real hydrothermal systems (Seward, 1989). In a boiling model examined by Seward (1989), pyrite and silicates precipitate as a result of a temperature drop. This result is primarily caused by decreased stability of iron chloride complexes and aluminum hydroxides and solubility of silicates with decreasing temperature (Spycher and Reed, 1989). Precipitation of other sulfides results from an increase in pH caused by degassing of CO_2, and to a lesser extent H_2S. Using Zn as a model for base metal precipitation, the following reaction illustrates controls on the precipitation of these base metal sulfide minerals:

$$ZnCl^+ + HS^- = ZnS + H^+ + Cl^- \quad (A.17)$$

Whole rock geochemical analyses of core samples indicates anomalous concentrations of Au with attending Hg and As (Fig. A.10). Under the pH conditions calculated for Sulphur Springs, Au is transported as $Au(HS)_2^-$, and the following reaction can be written:

$$8Au(HS)_2^- + 6H^+ + 4H_2O = 8Au + SO_4^{2-} + 15H_2S \quad (A.18)$$

Gold is easily precipitated from oxidizing or boiling fluids (Spycher and Reed, 1989). Furthermore, in addition to boiling the precipitation of base metal sulfides may affect the stability of $Au(HS)_2^-$ by further diminishing the concentration of reduced sulfur (Seward, 1989). Boiling may lead to depth zonation of the metals, with base metals such as sphalerite and galena precipitated at the onset of boiling and Au left in solution until the ascending two-phase fluid encounters an environment of increased permeability which induces more extensive boiling (Seward, 1989). The highest concentration of Au occurs in the upper 200 m of Sulphur Springs; this also corresponds to the region of most intensely fractured rock. Mixing of the deep hydrothermal fluid with the shallow hydrothermal fluid and/or groundwater can also led to the precipitation of Au by a decrease in temperature and the effects of dilution decreasing the activity of H_2S.

No molybdenite was positively identified below a depth of about 350 m in VC-2A and no molybdenite was identified in VC-2B. It would appear reasonable that if the Mo mineralization was the result of ascending hydrothermal fluids, then other horizons or enhanced concentrations of molybdenite mineralization should have been encountered. Figure A.11 shows the proposed fO_2-pH region inrelation to various Mo species for Sulphur Springs fluids at 230°C and 300°C. It can be seen that at these conditions Mo would have been deposited as MoS_2, and molybdenite should have been observed throughout the core recovered from Sulphur Springs. Whole rock geochemical analysis of core and rocks at Sulphur Springs indicate these rocks contain up to several tens of ppm Mo (Musgrave et al., 1989, and unpublished data). Thus, these rocks are a potentially leachable source of Mo. Local groundwater has a pH of about 8.5, and Mo is more soluble in alkaline solutions, which would then be capable of transporting Mo as MoO_4^{2-}. This Mo-bearing

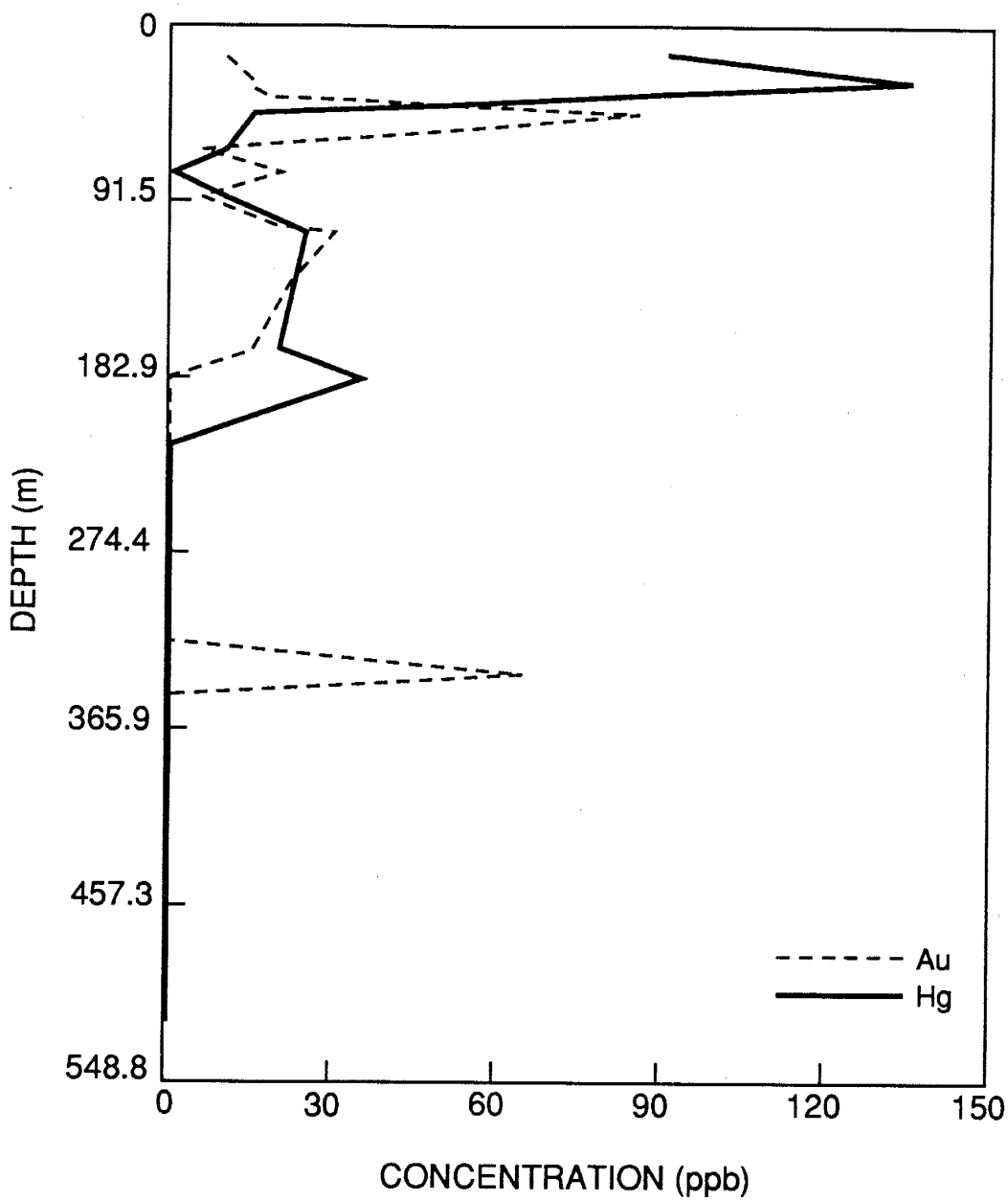

Figure A.10. a. Whole rock trace element geochemistry for Au and Hg versus depth in VC-2A. (Data from Musgrave et al., 1989).

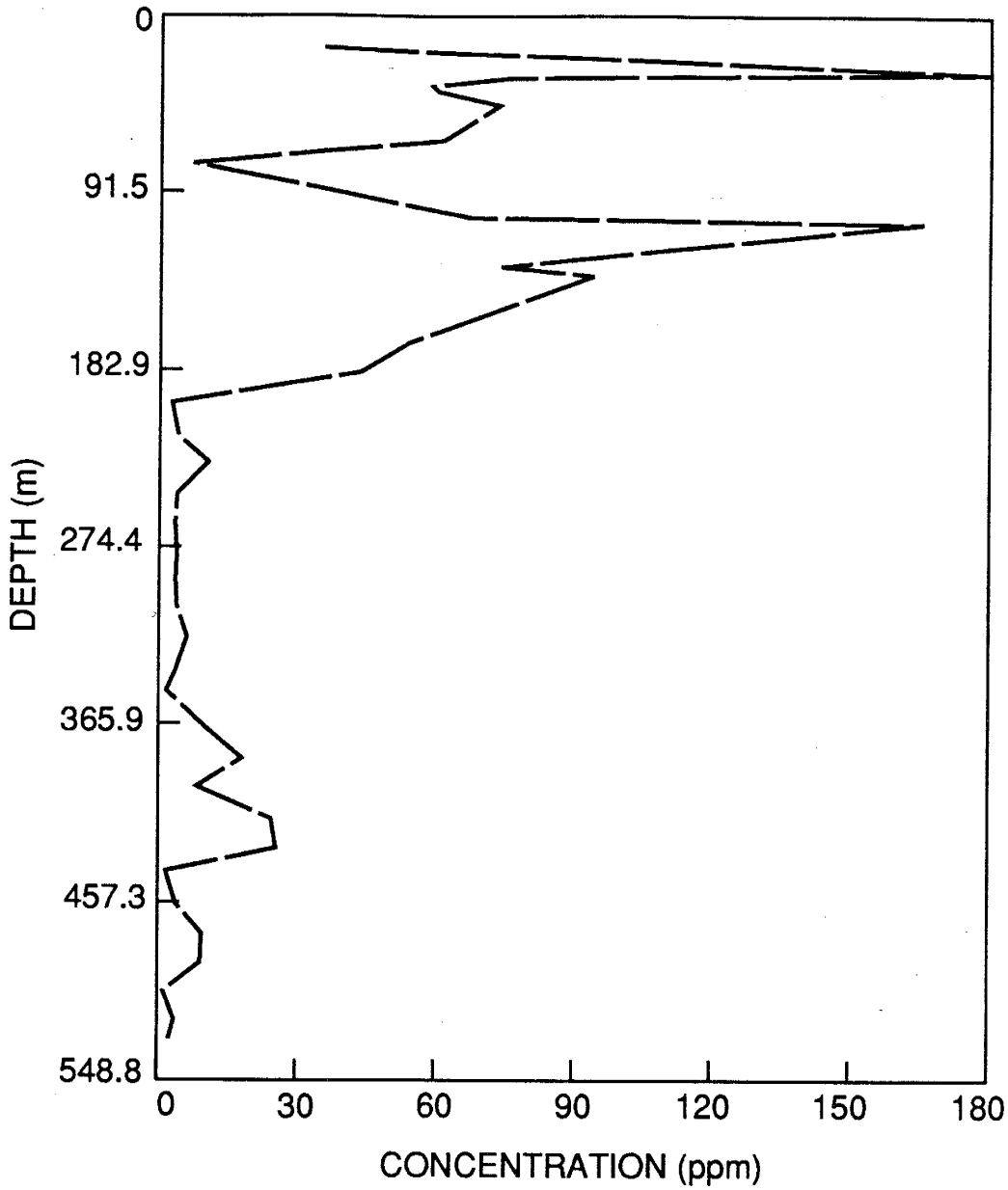

Figure A.10. b. Whole rock trace element geochemistry for As versus depth in VC-2A. (Data from Musgrave et al., 1989).

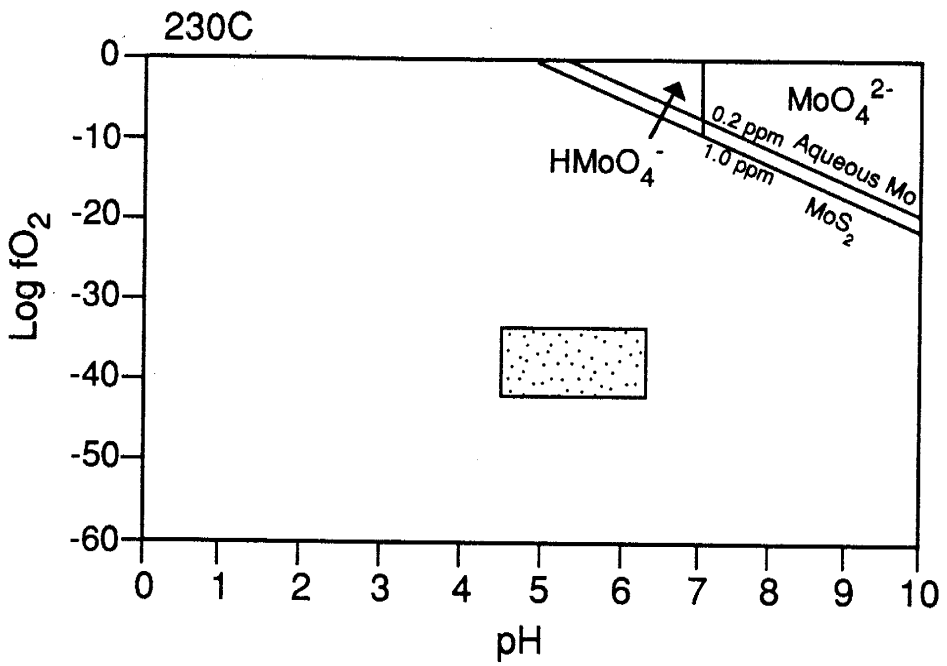

Figure A.11. a. Log fO_2-pH for various molybdenum species at 230°C and 0.003 m total sulfur. The box represent of log fO_2-pH conditions for Sulphur Springs fluids at depths <700 m. Plotted is the line representing the stability of aqueous species and of MoS_2 at 0.2 ppm and 1.0 ppm Mo.

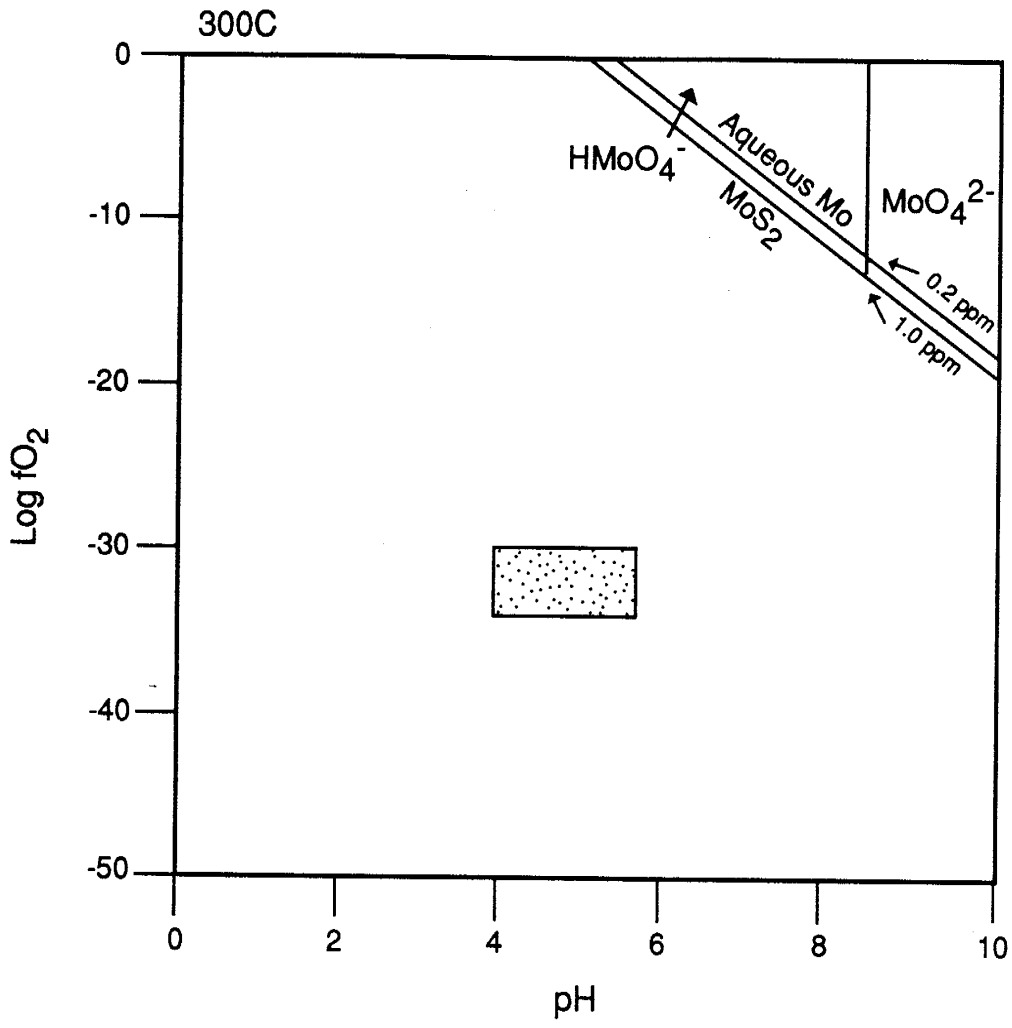

Figure A.11. b. Log fO_2-pH for various molybdenum species at 300°C and 0.003 m total sulfur. The box represent of log fO_2-pH conditions for Sulphur Springs fluids at depths >700 m. Plotted is the line representing the stability of aqueous species and of MoS_2 at 0.2 ppm and 1.0 ppm Mo.

groundwater mixed with the H_2S-bearing hydrothermal fluid in the more permeable shallow portion of the hydrothermal system and was deposited at this shallow level by these low temperature, dilute waters (230°C, 1.0 equiv. wt.% NaCl). This model of molybdenite deposition explains the restriction of this mineralization to depths < 350 m (Fig. A.12). The majority of the Mo mineralization occurs at depth <160 m, which corresponds to the upper most highly fractured zone in VC-2A.

Despite the substantial metal carrying capacity calculated for the present and past Sulphur Springs fluids, no economic mineralization has been intercepted in the numerous holes drilled in the Valles caldera. Some possible reasons could include the source rocks from which the metals would have been derived do not contain sufficient quantities of these metals or drilling to date simply has not been targeted towards finding a "bonanza" ore body. The tectonic setting and the stratigraphy of the Creede, Colorado base- and precious-metal deposit are very similar to Valles caldera (Hulen and Nielson, 1986; and from the data presented in this study), and the fluids may have been of similar composition, up to 5 equiv. wt. NaCl. However, Creede fluids do appear to have higher H_2S concentrations (Landis and Rye, 1989). Whole rock geochemical analysis of core samples suggests these rocks are not "unusual" in that they are not significantly deleted in Cu, Pb, or Zn (Musgrave, et al., 1989, and unpublished data); therefore, the surrounding country rocks appear to be good sources of leachable quantities metals. Hence, all indications are that economic mineralization could be present at Valles. The latter reason may be a more applicable. To date, all drilling in the Valles has largely been directed toward exploration of geothermal energy and not mineral eploration; therefore, geochemical and alteration studies aimed at mineral potential have not been conducted in Valles. Furthermore, Valles caldera is 1.1 Ma as opposed to the 26 Ma Creede deposit, and the level of erosion at Valles has not exposed or brought into reach with current drilling technology exploitable ore deposits.

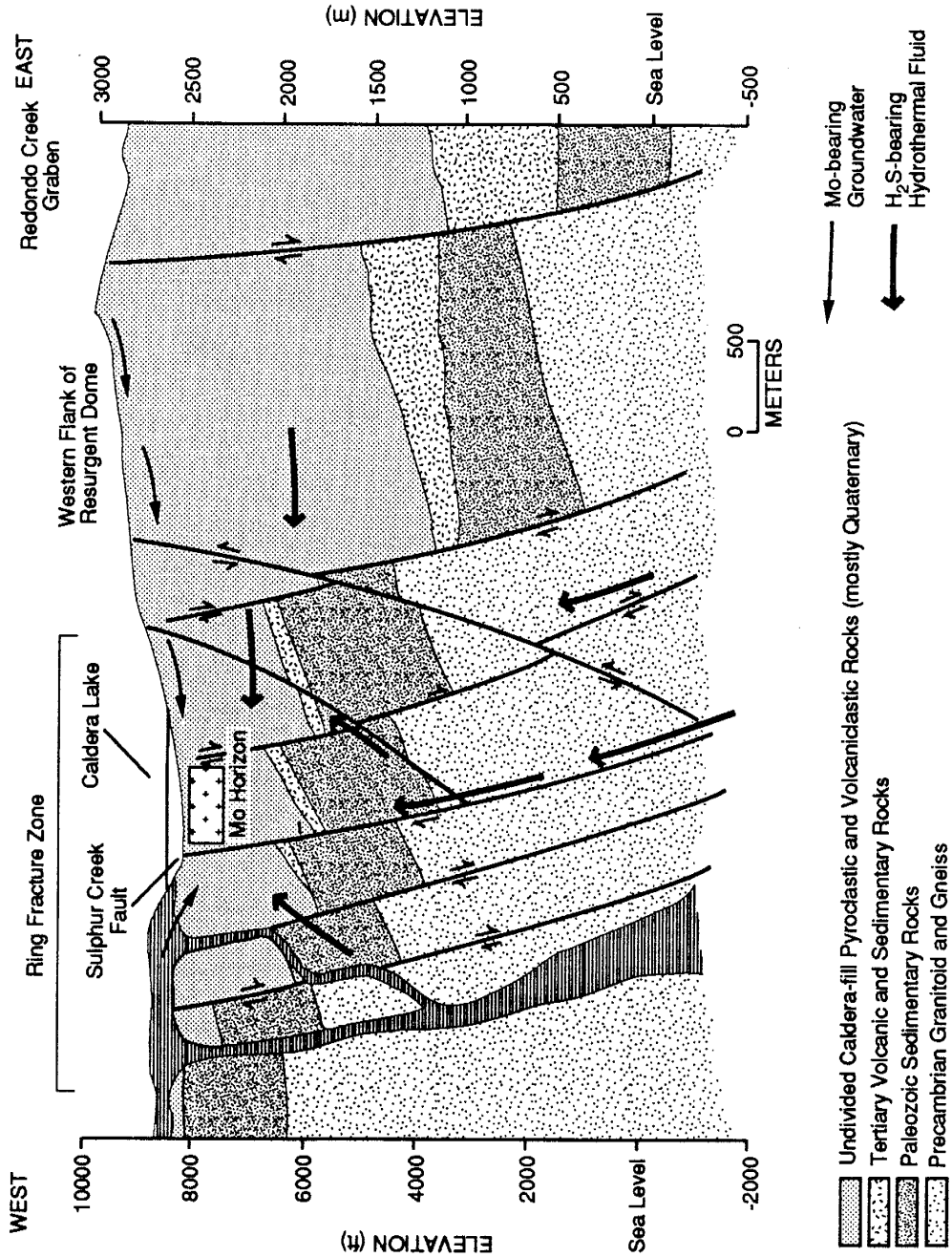

Figure A.12. Model of molybdenite mineralization at Sulphur Springs. Local groundwaters leach Mo from surrounding Mo-rich country rocks and transport it as MoO_4^{2-}. These waters then encounter the H_2S-bearing hydrothermal fluids in the upper, highly permeable portion of the system, where Mo is precipitated as sub-ore grade molybdenite occurrence.

CONCLUSIONS

On the basis of the analyses of vein-filling and wall rock alteration phases; the calculation of mineral stabilities from the chemical analyses of present day fluids, minerals and data from fluid inclusion microthermometry and microanalysis, and stable isotopic data, the following conclusions have been reached:

1) Alteration zones similar to those identified in epithermal ore deposits are recognized at Sulphur Springs and alteration zones at other active hydrothermal systems such as Roosevelt Hot Springs are similar to those at Sulphur Springs. Sericites from Sulphur Springs are compositional more heterogeneous, similar to sericites from other active hydrothermal systems.

3) The pH of the present day fluid is 5.4 at 300°C and that estimated for the paleo-hydrothermal fluid ranged between 4.0 and 6.6 for the temperature range 230-300°C.

4) Data from the analysis of mineral phases and fluid inclusion gas analysis permit reasonable estimation of the chemical conditions during hydrothermal alteration and ore mineral deposition.

5) Calculation of the solubilities of ore metals indicates that both the present day fluids and the paleo-fluids had substantial metal transporting capacity.

6) Stable isotopic data indicate vein-filling phase were deposited from fluids of meteoric origin, but were also modified depending on whether the host rock was igneous, siliciclastic or marine limestone. Carbon isotopic data are consistent with derivation of carbon from marine limestones.

7) Deposition of ore minerals was in response to mixing and boiling of the deep fluid with the shallow fluid and groundwater.

Appendix B

Sample	Mineral	Type	Th °C	Tm_{ICE}	Salinity equiv. wt% NaCl
VC2A 96	FLR	P	188.8	-1.50	2.70
VC2A 96	FLR	P	196.7	-1.50	2.70
VC2A 96	FLR	P	195.7	-1.60	2.90
VC2A 96	FLR	P	154.2	-2.40	4.00
VC2A 96	FLR	P	150.3	-2.40	4.00
VC2A 96	FLR	P		-1.60	2.90
VC2A 96	FLR	P	189.9	-1.60	2.90
VC2A 96	FLR	P	191.5	-1.60	2.90
VC2A 96	FLR	P	171.7	-1.30	2.20
VC2A 96	FLR	P	187.5	-1.80	3.00
VC2A 96	FLR	P	180.9	-1.80	3.00
VC2A 96	FLR	P	167.8	-1.80	3.00
VC2A 96	FLR	P	170.8	-1.40	2.40
VC2A 96	FLR	P	155.5	-0.70	1.20
VC2A 96	FLR	P		-0.15	0.20
VC2A 96	FLR	P	163.1	-0.85	1.50
VC2A 96	FLR	P	168.8	-0.90	1.50
VC2A 96	FLR	P	180.2	-1.60	2.70
VC2A 96	FLR	P	185.3	-1.50	2.50
VC2A 96	FLR	P	190.4	-1.50	2.60
VC2A 96	FLR	P	180.3	-1.30	2.20
VC2A 96	FLR	P	179.6	-1.30	2.20
VC2A 96	FLR	P	154.9	-0.20	0.35
VC2A 96	FLR	P	156.4	-0.20	0.35
VC2A 96	FLR	P	192.3	-1.35	2.30
VC2A 96	FLR	P	196.8	-1.30	2.20
VC2A 96	FLR	P	166.4	-0.15	0.26
VC2A 96	FLR	P	169.6	-0.75	1.30
VC2A 96	FLR	P	182.9	-0.40	0.70
VC2A 96	FLR	P	183.0	-0.40	0.70
VC2A 96	FLR	P	156.5	-0.30	0.50
VC2A 96	FLR	P	183.0		
VC2A 96	FLR	P	174.9		
VC2A 96	FLR	P	169.1		
VC2A 96	FLR	P	171.8		
VC2A 96	FLR	P	176.1		
VC2A 96	FLR	P	165.3		
VC2A 96	FLR	PS	177.4		

Appendix B (Cont)

Sample	Mineral	Type	Th °C	Tm_{ICE}	Salinity equiv. wt% NaCl
VC2A 96	FLR	PS	166.3		
VC2A 96	FLR	PS	180.1		
VC2A107	QTZ	P	211.2	-3.00	4.90
VC2A107	QTZ	P	233.7	-3.00	4.90
VC2A107	QTZ	P	278.0		
VC2A107	QTZ	P	199.7	-2.90	4.70
VC2A107	QTZ	P	212.3	-2.60	4.30
VC2A107	QTZ	P	294.5	-3.00	4.90
VC2A107	QTZ	P	224.1		
VC2A107	QTZ	P	253.3		
VC2A107	QTZ	P	231.2	-3.00	4.90
VC2A107	QTZ	P	260.3	-3.40	5.50
VC2A107	QTZ	P	262.6		
VC2A107	QTZ	P	269.1		
VC2A107	QTZ	P	232.2	-3.20	5.20
VC2A107	QTZ	P	239.5	-2.60	4.30
VC2A107	QTZ	P	268.1		
VC2A107	QTZ	P	232.2		
VC2A107	QTZ	P	229.5		
VC2A107	QTZ	P	223.4		
VC2A107	QTZ	P	218.6		
VC2A107	QTZ	P	206.3		
VC2A107	QTZ	P	223.7		
VC2A107	QTZ	P	246.2		
VC2A107	QTZ	P	271.8		
VC2A107	QTZ	P	259.7		
VC2A107	QTZ	P	266.7		
VC2A107	QTZ	P	239.6		
VC2A107	QTZ	P	236.4		
VC2A107	QTZ	P	291.6		
VC2A107	QTZ	P	275.4		
VC2A107	QTZ	P	248.6		
VC2A107	QTZ	P	211.4	-1.70	2.80
VC2A107	QTZ	P	198.4	-1.30	2.30
VC2A107	QTZ	P	211.0	-1.60	2.70
VC2A107	QTZ	P	200.7		
VC2A107	QTZ	P	206.1		
VC2A107	QTZ	P	206.4		

Appendix B (Cont)

Sample	Mineral	Type	Th °C	Tm_{ICE}	Salinity equiv. wt% NaCl
VC2A107	QTZ	P	274.1		
VC2A107	QTZ	P	267.6		
VC2A173	QTZ	P	248.5		
VC2A173	QTZ	P	203.3		
VC2A173	QTZ	P	197.1		
VC2A173	QTZ	P	280.0		
VC2A173	QTZ	P	286.4		
VC2A173	QTZ	P	242.3		
VC2A173	QTZ	P	252.9		
VC2A173	QTZ	P	211.6		
VC2A173	QTZ	P	234.2		
VC2A173	QTZ	P	237.6		
VC2A173	QTZ	P	224.5		
VC2A173	QTZ	P	224.2		
VC2A173	QTZ	P	256.2		
VC2A173	QTZ	P		-2.20	3.70
VC2A173	QTZ	P		-2.20	3.70
VC2A173	QTZ	P	255.8		
VC2A173	QTZ	P	225.8	-1.10	1.90
VC2A173	QTZ	P	219.6	-1.20	2.00
VC2A173	QTZ	P	228.3	-1.30	2.20
VC2A173	QTZ	P	209.8	-0.90	1.50
VC2A173	QTZ	P	207.5	-0.90	1.50
VC2A173	QTZ	P	209.7	-1.30	2.20
VC2A173	QTZ	P	222.4	-1.20	2.00
VC2A173	QTZ	P	223.7	-1.10	1.90
VC2A173	QTZ	P	213.9	-1.30	2.20
VC2A173	QTZ	P	220.3	-1.40	2.40
VC2A173	QTZ	P	216.8	-1.10	1.90
VC2A173	QTZ	P	225.1	-2.00	3.40
VC2A173	QTZ	P	223.4	-1.20	2.00
VC2A192	QTZ	P	243.2		
VC2A192	QTZ	P	218.4		
VC2A192	QTZ	P	227.6		
VC2A192	QTZ	P	236.3		
VC2A192	QTZ	P	226.7		
VC2A192	QTZ	P	205.7		
VC2A192	QTZ	P	210.3		

Appendix B (Cont)

Sample	Mineral	Type	Th °C	Tm_{ICE}	Salinity equiv. wt% NaCl
VC2A192	QTZ	P	226.4		
VC2A192	QTZ	P	230.8		
VC2A192	QTZ	P	231.5	-1.30	2.20
VC2A192	QTZ	P	218.9	-2.00	3.30
VC2A192	QTZ	P	225.6	-2.00	3.30
VC2A192	QTZ	P	258.9	-2.00	3.30
VC2A192	QTZ	P	238.9	-1.70	2.80
VC2A192	QTZ	P	209.7	-1.60	2.70
VC2A192	QTZ	P		-1.60	2.70
VC2A192	QTZ	P		-1.30	2.20
VC2A192	QTZ	P		-1.10	1.90
VC2A192	QTZ	P	220.3	-1.70	2.80
VC2A192	QTZ	P	220.8	-1.70	2.80
VC2A192	QTZ	P	217.2	-1.70	2.80
VC2A192	QTZ	P	223.6	-1.80	3.00
VC2A192	QTZ	P	217.3	-1.50	2.50
VC2A192	QTZ	P	216.7	-1.40	2.40
VC2A192	QTZ	P	219.1	-1.30	2.20
VC2A192	QTZ	P	220.4	-1.70	2.80
VC2A192	QTZ	P	219.3	-1.80	3.00
VC2A192	QTZ	P	215.5	-1.90	3.20
VC2A192	QTZ	P	222.5	-2.20	3.70
VC2A192	QTZ	P	282.5	-2.20	3.70
VC2A192	QTZ	P	219.8	-1.60	2.70
VC2A192	QTZ	P	211.4	-1.70	2.80
VC2A192	QTZ	P	201.2	-1.90	3.20
VC2A 277	QTZ	P	261.2	-0.08	0.13
VC2A 277	QTZ	P	291.6	-0.20	0.35
VC2A 277	QTZ	P	189.9	-0.05	0.08
VC2A 277	QTZ	P	184.6	-0.02	0.35
VC2A 277	QTZ	P	201.2	-0.10	0.17
VC2A 277	QTZ	P	194.5	-0.10	0.17
VC2A 277	QTZ	P	264.5		
VC2A 277	QTZ	P	277.0		
VC2A 277	QTZ	P	219.5		
VC2A 277	QTZ	P	216.3		
VC2A 277	QTZ	P	226.0		
VC2A 277	QTZ	P	196.1		

Appendix B (Cont)

Sample	Mineral	Type	Th °C	Tm_{ICE}	Salinity equiv. wt% NaCl
VC2A 277	QTZ	P	218.9		
VC2A 277	QTZ	P	221.9		
VC2A 277	QTZ	P	213.9		
VC2A 277	QTZ	P	202.5		
VC2A 277	QTZ	P	213.6		
VC2A 277	QTZ	P	213.7		
VC2A 277	QTZ	P	203.5		
VC2A 277	QTZ	P	203.0		
VC2A 277	QTZ	P		196.1	
VC2A 277	QTZ	P	203.8		
VC2A 277	QTZ	P	217.0		
VC2A 277	QTZ	P	202.2		
VC2A 277	QTZ	P	183.9		
VC2A 277	QTZ	P	189.0		
VC2A 277	QTZ	P	191.8		
VC2A313	QTZ	P	294.6		
VC2A313	QTZ	P	211.2		
VC2A313	QTZ	P	218.3	0.00	0.00
VC2A313	QTZ	P	221.1	0.00	0.00
VC2A313	QTZ	P	198.4	-0.10	0.20
VC2A313	QTZ	P	205.1		
VC2A313	QTZ	P	218.8		
VC2A313	QTZ	P	220.7		
VC2A313	QTZ	P	202.2		
VC2A313	QTZ	P	207.8		
VC2A313	QTZ	P	222.4		
VC2A313	QTZ	P	200.4		
VC2A313	QTZ	P	205.4		
VC2A313	QTZ	P	226.6	-0.20	0.40
VC2A313	QTZ	P	202.5	0.00	0.00
VC2A313	QTZ	P	208.4	0.00	0.00
VC2A313	QTZ	P	271.3		
VC2A313	QTZ	P	222.8		
VC2A313	QTZ	P		-0.10	0.20
VC2A313	QTZ	P	212.6	-0.10	0.20
VC2A313	QTZ	P	211.2	-0.20	0.40
VC2A 425	SL	P	217.8		
VC2A 425	QTZ	P	201.9	-0.55	0.96

Appendix B (Cont)

Sample	Mineral	Type	Th °C	Tm_{ICE}	Salinity equiv. wt% NaCl
VC2A 425	QTZ	P	200.0	-0.60	1.00
VC2A 425	QTZ	P	252.7	-0.40	0.70
VC2A 425	QTZ	P	202.1	-0.70	1.20
VC2A 425	QTZ	P	175.7	-0.75	1.30
VC2A 425	QTZ	P	212.3	-0.75	1.30
VC2A 425	QTZ	P	178.4	-0.25	0.44
VC2A 425	QTZ	P	199.6	-0.15	0.26
VC2A 425	QTZ	P	229.5	-1.85	3.10
VC2A 425	QTZ	P	226.7	-1.95	3.30
VC2A 425	QTZ	P	220.4	-2.35	3.90
VC2A 425	QTZ	P	219.6	-1.85	3.10
VC2A 425	QTZ	P	200.1	-1.95	3.30
VC2A 425	QTZ	P	192.7	-2.00	3.40
VC2A 425	QTZ	P		-0.15	0.26
VC2A 425	QTZ	P	212.1	-0.40	0.70
VC2A 425	QTZ	P	246.8	-0.80	1.40
VC2A 425	QTZ	P	232.7	-0.20	0.35
VC2A 425	QTZ	P	239.8	-0.20	0.35
VC2A 425	QTZ	P	216.1		
VC2A 425	QTZ	P	232.4		
VC2A 425	QTZ	P	232.9		
VC2A 425	QTZ	P	205.3		
VC2A 425	QTZ	P	197.8		
VC2A 425	QTZ	P	241.4		
VC2A 425	QTZ	P	232.5		
VC2A 425	QTZ	P	276.5		
VC2A 425	QTZ	P	222.1		
VC2A 425	QTZ	P	221.4		
VC2A 425	QTZ	P	246.5		
VC2A 425	QTZ	P	224.9		
VC2A 425	QTZ	P	231.0		
VC2A 425	QTZ	P	195.5		
VC2A 425	QTZ	P	217.8		
VC2A 425	QTZ	P	235.3		
VC2A 425	QTZ	P	224.6		
VC2A 425	QTZ	P	219.8		
VC2A 425	QTZ	P	228.2		

Appendix B (Cont)

Sample	Mineral	Type	Th °C	Tm_{ICE}	Salinity equiv. wt% NaCl
VC2A 425	QTZ	P	224.8		
VC2A 555	FLR	P	187.0	-0.03	0.05
VC2A 555	FLR	P	184.7	-0.05	0.05
VC2A 555	FLR	P	184.5	-0.05	0.08
VC2A 555	FLR	P	191.1	0.00	0.00
VC2A 555	FLR	P	155.9		
VC2A 555	FLR	P	193.5		
VC2A 555	FLR	P	188.1		
VC2A 555	FLR	P	175.4		
VC2A 555	FLR	P	182.1		
VC2A 555	FLR	P	192.6		
VC2A 555	FLR	P	202.3		
VC2A 555	FLR	P	200.6		
VC2A 645	FLR	P	194.4	-0.55	0.98
VC2A 645	FLR	P	196.3	-0.50	0.87
VC2A 645	FLR	P		-0.50	0.87
VC2A 645	FLR	P		-0.50	0.87
VC2A 645	FLR	P	196.5		
VC2A 645	FLR	P	197.5		
VC2A 1108	FLR	P		-0.05	0.08
VC2A 1108	FLR	P		-0.05	0.08
VC2A 1108	FLR	P	200.7	0.00	0.00
VC2A 1108	FLR	P	192.4	-0.10	0.17
VC2A 1108	FLR	P	192.9	-0.10	0.17
VC2A 1108	FLR	P	181.3	-0.05	0.08
VC2A 1108	FLR	P	180.5	0.00	0.00
VC2A 1108	FLR	P	195.2	-0.05	0.08
VC2A 1108	FLR	P	195.5	-0.20	0.35
VC2A 1108	FLR	P	195.8	-0.25	0.44
VC2A 1108	FLR	P	199.7	-0.20	0.35
VC2A 1108	FLR	P	198.7	-0.20	0.35
VC2A 1108	FLR	P		-0.12	0.21
VC2A 1108	FLR	P	201.2	-0.30	0.53
VC2A 1108	FLR	P	200.0	-0.32	0.56
VC2A 1108	FLR	P	200.0	-0.40	0.70
VC2A 1108	FLR	P	210.1	-0.45	0.78
VC2A 1108	FLR	P	201.5	-0.40	0.70
VC2A 1108	FLR	P	208.0	-0.40	0.70

Appendix B (Cont)

Sample	Mineral	Type	Th °C	Tm_{ICE}	Salinity equiv. wt% NaCl
VC2A 1108	FLR	P	200.0	-0.43	0.75
VC2A 1108	FLR	P	203.9	-0.25	0.44
VC2A 1108	FLR	P	191.2	-0.25	0.44
VC2A 1108	FLR	P	194.9		
VC2A 1108	FLR	P	210.6		
VC2A 1108	FLR	P	206.0		
VC2A 1108	FLR	P	203.8		
VC2A 1108	FLR	P	207.7		
VC2A 1108	FLR	P	208.4		
VC2A 1137	CC	P	314.8		
VC2A 1137	CC	P	284.4		
VC2A 1137	CC	P	288.5		
VC2A 1137	CC	P	249.0		
VC2A 1137	CC	P	291.6		
VC2A 1137	CC	P	335.9		
VC2A 1137	CC	P	265.7	-0.10	0.17
VC2A 1137	CC	P	217.4	-0.60	1.05
VC2A 1137	CC	P	213.9	-0.25	0.44
VC2A 1137	CC	P		-0.25	0.44
VC2A 1137	CC	P		-0.40	0.70
VC2A 1137	CC	P	253.9	-0.10	0.17
VC2A 1137	CC	P		-0.35	0.60
VC2A 1137	CC	P		-0.60	1.05
VC2A 1137	CC	P	295.4	0.00	0.00
VC2A 1137	CC	P	292.3		
VC2A 1137	CC	P	303.9		
VC2A 1485	CC	PS	203.1	-0.35	0.61
VC2A 1485	CC	PS		-0.35	0.61
VC2A 1485	CC	PS	200.0	-0.35	0.61
VC2A 1485	CC	PS	210.5	-0.35	0.61
VC2A 1485	CC	PS	214.5	-0.35	0.61
VC2A 1485	CC	PS	199.2	-0.40	0.70
VC2A 1485	CC	PS	203.4	-0.45	0.78
VC2A 1485	CC	PS	200.3	-0.30	0.52
VC2A 1485	CC	PS		-0.30	0.52
VC2A 1485	QTZ	P	209.0	-0.70	1.22
VC2A 1485	QTZ	P	212.3	-0.50	0.87
VC2A 1485	QTZ	P	219.9	-0.60	1.00

Appendix B (Cont)

Sample	Mineral	Type	Th °C	Tm_{ICE}	Salinity equiv. wt% NaCl
VC2A 1485	CC	PS	228.3	-0.40	0.70
VC2A 1485	CC	PS	201.7	-0.40	0.70
VC2A 1485	CC	PS	209.2	-0.30	0.53
VC2A 1485	CC	PS	199.3		
VC2A 1485	CC	PS	203.3		
VC2A 1485	CC	PS	199.2		
VC2A 1485	CC	PS	205.4		
VC2A 1485	CC	PS	219.6		
VC2A 1485	SL	P	224.6	-0.40	0.70
VC2A 1485	SL	P	224.9	-0.50	0.87
VC2A 1485	SL	P	225.9	-0.50	0.87
VC2A 1485	SL	P	240.5	-0.70	1.22
VC2A 1485	SL	P	237.6	-0.30	0.53
VC2A 1485	SL	P	236.7	-0.65	1.13
VC2A 1485	SL	P	233.7	-0.30	0.53
VC2A 1485	SL	P		-0.20	0.35
VC2A 1485	SL	P	241.8	-0.65	1.13
VC2A 1485	SL	P		-0.55	0.96
VC2A 1485	QTZ	P		-0.50	0.87
VC2A 1485	QTZ	P		-0.50	0.87
VC2A 1485	QTZ	P		-0.50	0.87
VC2A 1485	QTZ	P	236.5		
VC2A 1485	QTZ	P	240.1		
VC2A 1485	SL	P	239.8		
VC2A 1485	SL	P	243.6		
VC2A 1485	SL	P	255.3	-0.90	1.56
VC2A 1485	SL	P	319.4	-0.80	1.39
VC2A 1485	QTZ	P	294.7	-1.00	1.73
VC2A 1485	QTZ	P	226.5		
VC2A 1485	QTZ	P	247.5	-0.20	0.35
VC2A 1485	QTZ	P	212.9	-0.20	0.35
VC2A 1485	QTZ	P	229.4	-0.25	0.44
VC2A 1485	QTZ	P	260.3		
VC2A 1485	QTZ	P	241.8	-0.20	0.35
VC2A 1485	QTZ	P	248.6		
VC2A 1485	QTZ	P	228.0	-0.30	0.53
VC2A 1485	QTZ	P	250.6		
VC2A 1485	QTZ	P	251.4	-0.40	0.70

Appendix B (Cont)

Sample	Mineral	Type	Th °C	Tm_{ICE}	Salinity equiv. wt% NaCl
VC2A 1485	QTZ	P	253.4	-0.20	0.35
VC2A 1485	QTZ	P	-0.90	1.56	
VC2A 96	FLR	S	143.7		
VC2A 96	FLR	S	138.9		
VC2A 96	FLR	S	133.5		
VC2A 277	QTZ	S	157.6	-0.15	0.26
VC2A 277	QTZ	S	165.4	-0.10	0.17
VC2A 555	FLR	S	157.1		
VC2A 555	FLR	S	165.5	-0.23	0.38
VC2A 555	FLR	S	174.6	-0.05	0.08
VC2A 555	FLR	S		0.00	0.00
VC2A 555	FLR	S			
VC2A 555	FLR	S			
VC2A 555	FLR	S	170.8		
VC2A 555	FLR	S	174.2	-1.08	1.70
VC2A 555	FLR	S	170.4		
VC2A 555	FLR	S	158.8		
VC2A 555	FLR	S	171.7		
VC2A 555	FLR	S	173.2		
VC2A 555	FLR	S	164.2		
VC2A 555	FLR	S	180.6		
VC2A 555	FLR	S	182.4		
VC2A 555	FLR	S	174.9		
VC2A 555	FLR	S	166.5		
VC2A 555	FLR	S	172.1		
VC2A 555	FLR	S	173.1		
VC2A 555	FLR	S	174.3		
VC2A 555	FLR	S	174.5		
VC2A 645	FLR	S	160.2	-0.50	0.87
VC2A 645	FLR	S	163.1	-0.20	0.35
VC2A 645	FLR	S	180.2	-0.45	0.78
VC2A 645	FLR	S	161.9	-0.40	0.70
VC2A 645	FLR	S	161.3	-0.50	0.87
VC2A 1108	FLR	S	174.1	0.00	0.00
VC2A 1108	FLR	S	178.9		
VC2A 1108	FLR	S	182.9		
VC2A 1108	FLR	S	180.8		
VC2A 1108	FLR	S	169.9		

Appendix B (Cont)

Sample	Mineral	Type	Th °C	Tm_{ICE}	Salinity equiv. wt% NaCl
VC2A 1108	FLR	S	168.8		
VC2A 1108	FLR	S	180.7		
VC2A 1108	FLR	S	169.0		
VC2A 1108	FLR	S	169.5		
VC2A 1108	FLR	S	169.2		
VC2A 1108	FLR	S	168.0		
VC2A 1108	FLR	S	172.8		
VC2A 1108	FLR	S	173.5		
VC2A 1108	FLR	S	158.6		
VC2A 1108	FLR	S	150.6		
VC2A 1108	FLR	S	151.6		
VC2A 1108	FLR	S	156.7		
VC2A 1108	FLR	S	156.5		
VC2A 1108	FLR	S	153.3		
VC2A 1108	FLR	S	158.4		
VC2B 656	CC	P	217.1	-0.20	0.35
VC2B 656	CC	P	218.7	-0.20	0.35
VC2B 656	CC	P	214.5	-0.20	0.35
VC2B 656	CC	P	214.7	-0.10	0.17
VC2B 656	CC	P	215.8	-0.10	0.17
VC2B 656	CC	P	214.2	-0.10	0.17
VC2B 656	CC	P	214.5		
VC2B 656	CC	P	213.9		
VC2B 656	CC	P	215.8		
VC2B 757	QTZ	P	213.7	0.00	0.00
VC2B 757	QTZ	P	211.3	0.00	0.00
VC2B 757	QTZ	P	211.4	-0.20	0.35
VC2B 757	QTZ	P	228.4	-0.20	0.35
VC2B 757	QTZ	P	210.3	-0.20	0.35
VC2B 757	QTZ	P	223.8	-0.20	0.35
VC2B 757	QTZ	P	210.9	0.00	0.00
VC2B 757	QTZ	P	217.5	0.00	0.00
VC2B 757	QTZ	P	211.9	0.00	0.00
VC2B 757	QTZ	P	209.8	0.00	0.00
VC2B 757	QTZ	P	229.4		
VC2B 757	QTZ	P	218.2		
VC2B 757	QTZ	P	211.1		
VC2B 757	QTZ	P	220.3		

Appendix B (Cont)

Sample	Mineral	Type	Th °C	Tm_{ICE}	Salinity equiv. wt% NaCl
VC2B 757	QTZ	P	219.1		
VC2B 757	QTZ	PS	250.0		
VC2B 757	QTZ	PS	250.4		
VC2B 757	QTZ	PS	210.4	-0.20	0.35
VC2B 757	QTZ	P	198.0	-0.20	0.35
VC2B 757	QTZ	P	269.6	-0.20	0.35
VC2B 757	QTZ	P	214.6	-0.15	0.26
VC2B 757	QTZ	P	205.7	-0.15	0.26
VC2B 757	QTZ	P	206.1	-0.25	0.44
VC2B 757	QTZ	P	209.1	-0.15	0.26
VC2B 757	QTZ	P	214.4		
VC2B 757	QTZ	P	211.5		
VC2B 757	QTZ	P	221.9		
VC2B 757	QTZ	P	238.0		
VC2B 757	QTZ	P	209.1		
VC2B 757	QTZ	P	213.0		
VC2B 757	QTZ	P	229.6		
VC2B 757	QTZ	P	213.6		
VC2B 757	QTZ	P	217.1		
VC2B 757	QTZ	P	215.1		
VC2B 757	QTZ	P	211.1		
VC2B 757	QTZ	P	210.8		
VC2B 757	QTZ	P	220.8		
VC2B 757	QTZ	P	260.1		
VC2B 757	QTZ	P	258.9		
VC2B 932	QTZ	P	208.9	0.00	0.00
VC2B 932	QTZ	P	223.9	0.00	0.00
VC2B 932	QTZ	P	213.5	-0.05	0.04
VC2B 932	QTZ	P	217.1	-0.05	0.04
VC2B 932	QTZ	P	216.5	-0.05	0.04
VC2B 932	QTZ	P	217.9	0.00	0.00
VC2B 932	QTZ	P	216.1	0.00	0.00
VC2B 932	QTZ	P	211.6	0.00	0.00
VC2B 932	QTZ	P	218.5	0.00	0.00
VC2B 932	QTZ	P	220.5	0.00	0.00
VC2B 932	QTZ	P	216.7	0.00	0.00
VC2B 932	QTZ	P	219.1	0.00	0.00
VC2B 932	QTZ	P	259.0	0.00	0.00

Appendix B (Cont)

Sample	Mineral	Type	Th °C	Tm_{ICE}	Salinity equiv. wt% NaCl
VC2B 932	QTZ	P	216.5	0.00	0.00
VC2B 932	QTZ	P	210.9	0.00	0.00
VC2B 932	QTZ	P	216.4	0.00	0.00
VC2B 932	QTZ	P	221.5	0.00	0.00
VC2B 932	QTZ	P	213.4	0.00	0.00
VC2B 932	QTZ	P	216.8	0.00	0.00
VC2B 932	QTZ	P	209.9	0.00	0.00
VC2B 932	QTZ	P	251.2		
VC2B 932	QTZ	P	221.5		
VC2B 932	QTZ	P	217.2		
VC2B 932	QTZ	P	217.5		
VC2B 932	QTZ	P	217.8		
VC2B 932	QTZ	P	215.8		
VC2B 932	QTZ	P	216.9		
VC2B 932	QTZ	P	219.7		
VC2B 932	QTZ	P	217.9		
VC2B 932	QTZ	P	219.6		
VC2B 932	QTZ	P	262.8		
VC2B 932	QTZ	P	220.6		
VC2B 932	QTZ	P	221.8		
VC2B 932	QTZ	P	221.1		
VC2B 2183	CC	P	229.9	-0.25	0.44
VC2B 2183	CC	P	227.7	-0.25	0.44
VC2B 2183	CC	P	231.6	-0.25	0.44
VC2B 2183	CC	P	228.7	-0.20	0.35
VC2B 2183	CC	P	224.6	-0.20	0.35
VC2B 2183	CC	P	229.6	-0.20	0.35
VC2B 2183	CC	P	237.5	-0.30	0.53
VC2B 2183	CC	P	227.0	-0.30	0.53
VC2B 2183	CC	P	224.2	-0.30	0.53
VC2B 2183	CC	P		-0.25	0.44
VC2B 2183	CC	P	227.2	-0.25	0.44
VC2B 2183	CC	P	226.8	-0.25	0.44
VC2B 2183	CC	P	246.3		
VC2B 2183	CC	P	246.4		
VC2B 2183	CC	P	246.3		
VC2B 2183	CC	P	246.1		
VC2B 2183	CC	P	215.5		

Appendix B (Cont)

Sample	Mineral	Type	Th °C	Tm_{ICE}	Salinity equiv. wt% NaCl
VC2B 2183	CC	P	230.0		
VC2B 2183	CC	P	236.2		
VC2B 2183	CC	P	226.5		
VC2B 2183	CC	P	234.0		
VC2B 2183	CC	P	233.1		
VC2B 3017	CC	P	226.4	-0.25	0.44
VC2B 3017	CC	P	222.5	-0.25	0.44
VC2B 3017	CC	P		-0.20	0.35
VC2B 3017	CC	P		-0.20	0.35
VC2B 3017	CC	P	207.9	-0.20	0.35
VC2B 3017	CC	P	221.7	-0.25	0.44
VC2B 3017	CC	P	219.0	-0.25	0.44
VC2B 3017	CC	P	221.0	-0.10	0.17
VC2B 3017	CC	P	220.0	-0.20	0.35
VC2B 3017	CC	P		-0.10	0.17
VC2B 3017	CC	P		-0.10	0.17
VC2B 3017	CC	P	221.0	0.00	0.00
VC2B 3017	CC	P	220.1	0.00	0.00
VC2B 3017	CC	P	221.9	-0.15	0.26
VC2B 3017	CC	P	217.8	-0.10	0.17
VC2B 3017	CC	P	224.4		
VC2B 3017	CC	P	223.8		
VC2B 3017	CC	P	223.9		
VC2B 3017	CC	P	216.8		
VC2B 3017	CC	P	225.1		
VC2B 3017	CC	P	220.5		
VC2B 3017	CC	P	223.6		
VC2B 3017	CC	P	220.0		
VC2B 3017	CC	P	224.2		
VC2B 3017	CC	P	221.6		
VC2B 3017	CC	P	223.9		
VC2B 3017	CC	P	220.8		
VC2B 3017	CC	P	220.7		
VC2B 3017	CC	P	220.4		
VC2B 3017	CC	P	220.3		
VC2B 3017	CC	P	221.8		
VC2B 3017	CC	P	221.7		
VC2B 4565	CC	P	290.2	-1.90	3.21

Appendix B (Cont)

Sample	Mineral	Type	Th °C	Tm_{ICE}	Salinity equiv. wt% NaCl
VC2B 4565	CC	P	269.3	-2.20	3.69
VC2B 4565	CC	P	270.2	-2.10	3.50
VC2B 4565	CC	P	255.9	-3.10	5.10
VC2B 4565	CC	P	269.5	-2.50	4.16
VC2B 4565	CC	P	287.8	-2.40	4.00
VC2B 4565	CC	P	288.5	-2.40	4.00
VC2B 4565	CC	P	280.1	-2.20	3.70
VC2B 4565	CC	P	280.4	-2.20	3.70
VC2B 4565	CC	P	293.3	-1.70	2.88
VC2B 4565	CC	P	275.3	-2.50	4.16
VC2B 4565	CC	P	282.3	-2.20	3.69
VC2B 4565	CC	P	260.0		
VC2B 4565	CC	P	268.1		
VC2B 4565	CC	P	263.3		
VC2B 4565	CC	P	271.8		
VC2B 4565	CC	P	273.2		
VC2B 4565	CC	P	277.9		
VC2B 4565	CC	P	278.8		
VC2B 4565	CC	P	274.4		
VC2B 4565	CC	P	274.0		
VC2B 4565	CC	P	273.7		
VC2B 4565	CC	P	274.4		
VC2B 4565	CC	P	278.2		
VC2B 4565	CC	P	265.6		
VC2B 4565	CC	P	263.3		
VC2B 4565	CC	P	274.6		
VC2B 4565	CC	P	266.4		
VC2B 4565	CC	P	286.3		
VC2B 4565	CC	P	268.8		
VC2B 4565	CC	P	272.3		
VC2B 4565	CC	P	268.7		
VC2B 4565	CC	P	293.1		
VC2B 4565	CC	P	313.0		
VC2B 4565	CC	P	301.5		
VC2B 4565	CC	P	258.6		
VC2B 4565	CC	P	259.8		
VC2B 4755	QTZ	P	304.5	-1.50	2.56
VC2B 4755	QTZ	P	300.2	-1.50	2.56

Appendix B (Cont)

Sample	Mineral	Type	Th °C	Tm_{ICE}	Salinity equiv. wt% NaCl
VC2B 4755	QTZ	P	301.7	-1.50	2.56
VC2B 4755	QTZ	P	275.8	-1.50	2.56
VC2B 4755	QTZ	P	291.6	-1.50	2.56
VC2B 4755	QTZ	P	279.6	-1.50	2.56
VC2B 4755	QTZ	PS	274.8	-1.20	2.06
VC2B 4755	QTZ	PS	270.3	-1.20	2.06
VC2B 4755	QTZ	P	310.3	-2.00	3.37
VC2B 4755	QTZ	P	289.0	-2.00	3.37
VC2B 4755	QTZ	P	266.7	-1.40	2.39
VC2B 4755	QTZ	P	274.4	-1.50	2.56
VC2B 4755	QTZ	P	273.6	-1.00	1.89
VC2B 4755	QTZ	P	280.4	-1.80	3.05
VC2B 4755	QTZ	P	292.9		
VC2B 4755	QTZ	P	291.8	-1.30	2.23
VC2B 4755	QTZ	P	291.8	-1.35	2.39
VC2B 4755	QTZ	P	285.2	-1.50	2.56
VC2B 4755	QTZ	P	307.6	-1.40	2.39
VC2B 4755	QTZ	P	315.3		
VC2B 4755	QTZ	P	317.3		
VC2B 4755	QTZ	P	315.6		
VC2B 4755	QTZ	P	281.8		
VC2B 4755	QTZ	P	277.6		
VC2B 4755	QTZ	P	293.3		
VC2B 4755	QTZ	P	309.2		
VC2B 4755	QTZ	P	307.8		
VC2B 4755	QTZ	P	314.3		
VC2B 4755	QTZ	P	297.0		
VC2B 4755	QTZ	P	294.6		
VC2B 4755	QTZ	P	295.0		
VC2B 4755	QTZ	P	270.6		
VC2B 4755	QTZ	P	273.4		
VC2B 4755	QTZ	P	273.8		
VC2B 4755	QTZ	P	275.4		
VC2B 4755	QTZ	P	274.9		
VC2B 4755	QTZ	P	321.8		
VC2B 4755	QTZ	P	329.6		
VC2B 5237	QTZ	PS	299.6	-1.00	1.65
VC2B 5237	QTZ	PS	301.6	-1.10	1.82

Appendix B (Cont)

Sample	Mineral	Type	Th °C	Tm_{ICE}	Salinity equiv. wt% NaCl
VC2B 5237	QTZ	PS	301.0	-1.10	1.82
VC2B 5237	QTZ	PS	282.4	-1.05	1.73
VC2B 5237	QTZ	PS	269.5	-1.05	1.73
VC2B 5237	QTZ	PS	298.7	-1.80	2.96
VC2B 5237	QTZ	PS	309.6	-1.80	2.96
VC2B 5237	QTZ	PS	295.4	-2.50	4.07
VC2B 5237	QTZ	PS	304.6	-2.40	3.92
VC2B 5237	QTZ	P	325.7	-1.40	2.30
VC2B 5237	QTZ	P	311.0	-1.55	2.55
VC2B 5237	QTZ	P	288.3	-1.95	3.20
VC2B 5237	QTZ	P	321.9	-1.95	3.20
VC2B 5237	QTZ	P	305.5	-1.50	2.47
VC2B 5237	QTZ	P	295.6	-1.30	2.14
VC2B 5237	QTZ	P	295.7	-1.45	2.39
VC2B 5237	QTZ	P	299.8	-1.25	2.06
VC2B 5237	QTZ	P	334.4		
VC2B 5237	QTZ	P	301.7		
VC2B 5237	QTZ	P	300.5		
VC2B 5237	QTZ	P	306.4		
VC2B 5237	QTZ	P	326.6		
VC2B 5237	QTZ	P	313.5		
VC2B 5237	QTZ	P	314.2		
VC2B 5237	QTZ	P	324.9		
VC2B 5533	QTZ	P	286.2	-0.90	1.55
VC2B 5533	QTZ	P	276.9	-0.75	1.30
VC2B 5533	QTZ	P	289.7	-1.20	2.06
VC2B 5533	QTZ	P	291.4	-1.10	1.89
VC2B 5533	QTZ	P	293.8	-1.50	2.56
VC2B 5533	QTZ	P	288.3		
VC2B 5533	QTZ	P	288.3		
VC2B 5533	QTZ	P	288.9		
VC2B 5533	QTZ	P	290.1		
VC2B 5533	QTZ	P	289.2		
VC2B 5533	QTZ	P	285.0		
VC2B 5533	QTZ	P	280.9		
VC2B 5533	QTZ	P	282.4		
VC2B 5533	QTZ	P	285.7		
VC2B 5533	QTZ	P	254.1	-0.35	0.58

Appendix B (Cont)

Sample	Mineral	Type	Th °C	Tm_{ICE}	Salinity equiv. wt% NaCl
VC2B 5533	QTZ	P	254.3	-0.40	0.66
VC2B 5533	QTZ	P	250.5	-0.45	0.75
VC2B 5533	QTZ	P	243.9	-0.45	0.75
VC2B 5533	QTZ	P	250.1	-0.70	1.16
VC2B 5533	QTZ	P	246.5	-0.60	0.99
VC2B 5533	QTZ	P	247.0	-0.50	0.83
VC2B 5533	QTZ	P	251.4	-0.50	0.83
VC2B 5533	QTZ	P	252.3	-0.50	0.83
VC2B 5533	QTZ	P	238.1	-0.50	0.83
VC2B 5533	QTZ	P	245.4	-0.50	0.83
VC2B 5533	QTZ	P	243.1	-0.50	0.83
VC2B 5533	QTZ	P	247.6		
VC2B 5533	QTZ	P	237.9		
VC2B 5533	QTZ	P	243.8		
VC2B 5533	QTZ	P	262.7		
VC2B 5533	QTZ	P	298.8		
VC2B 5533	QTZ	P	302.0		
VC2B 5533	QTZ	P	299.2		
VC2B 5533	QTZ	P	290.1		
VC2B 5533	QTZ	P	298.7		
VC2B 5533	QTZ	P	300.2		
VC2B 5533	QTZ	P	272.8		
VC2B 5533	QTZ	P	274.3		
VC2B 5533	QTZ	P	281.5		
VC2B 5533	QTZ	P	291.4		
VC2B 5533	QTZ	P	280.0		
VC2B 5661	FLR	P	251.8		
VC2B 5661	FLR	P		-0.70	1.20
VC2B 5661	FLR	P	258.5	-0.60	1.00
VC2B 5661	FLR	P	302.2	-0.70	1.20
VC2B 5661	FLR	P	300.9	-0.65	1.10
VC2B 5661	FLR	P	302.7	-0.60	1.00
VC2B 5661	FLR	P	303.0	-1.03	1.11
VC2B 5661	FLR	P	288.7	-0.55	0.96
VC2B 5661	FLR	P	304.7		
VC2B 5661	FLR	P	306.5		
VC2B 5661	FLR	P	310.4		
VC2B 5661	FLR	P	232.4		

Appendix B (Cont)

Sample	Mineral	Type	Th °C	Tm_{ICE}	Salinity equiv. wt% NaCl
VC2B 5661	FLR	P	301.4		
VC2B 5661	FLR	P	299.6		
VC2B 5661	FLR	PS	317.6		
VC2B 5661	FLR	PS	318.3		
VC2B 5661	FLR	PS	319.0		
VC2B 1246	FLR	P	189.2		
VC2B 1246	FLR	P	191.4	-0.40	0.70
VC2B 1246	FLR	P	188.2		
VC2B 1246	FLR	P	191.4		
VC2B 1246	FLR	P	187.2		
VC2B 1246	FLR	P	192.3	-0.20	0.35
VC2B 1246	FLR	P	195.4		
VC2B 1246	FLR	P	198.1		
VC2B 1246	FLR	P	188.8		
VC2B 1246	FLR	P	212.0		
VC2B 1246	FLR	P	210.3		
VC2B 1246	FLR	P	200.0		
VC2B 1322	FLR	P	219.0		
VC2B 2183	FLR	PS	187.8	-0.40	0.70
VC2B 2183	FLR	PS	184.4	-0.40	0.70
VC2B 2183	FLR	PS	183.9	-0.40	0.70
VC2B 2183	FLR	P	192.4		
VC2B 2183	FLR	P	193.0		
VC2B 2183	FLR	P	192.4		
VC2B 2183	FLR	P	191.5		
VC2B 2183	FLR	P	193.5		
VC2B 2183	FLR	P	192.7		
VC2B 1246	FLR	S	152.9		
VC2B 1246	FLR	S	153.4		
VC2B 1246	FLR	S	176.7	-0.10	0.17
VC2B 1246	FLR	S	148.6		
VC2B 1246	FLR	S	149.4		
VC2B 1246	FLR	S	161.0	-0.10	0.17
VC2B 1246	FLR	S	166.8	-0.10	0.17
VC2B 1246	FLR	S	175.9	-0.10	0.17
VC2B 1246	FLR	S	174.5		
VC2B 1246	FLR	S	174.5		
VC2B 1246	FLR	S	174.5		

Appendix B (Cont)

Sample	Mineral	Type	Th °C	Tm_{ICE}	Salinity equiv. wt% NaCl
VC2B 1246	FLR	S	174.5		
VC2B 1246	FLR	S	174.5		
VC2B 1246	FLR	S	175.3		
VC2B 1246	FLR	S	175.3		
VC2B 1246	FLR	S	175.3		
VC2B 1246	FLR	S	175.3		
VC2B 1246	FLR	S	175.3		
VC2B 1246	FLR	S	175.3		
VC2B 1246	FLR	S	175.3		
VC2B 1246	FLR	S	175.9		
VC2B 1246	FLR	S	175.9		
VC2B 1246	FLR	S	175.9		
VC2B 1246	FLR	S	171.8		
VC2B 1246	FLR	S	171.8		
VC2B 1246	FLR	S	171.8		
VC2B 1246	FLR	S	171.8		
VC2B 1246	FLR	S	171.8		
VC2B 1246	FLR	S	171.8		
VC2B 1246	FLR	S	171.8		
VC2B 1246	FLR	S	171.8		
VC2B 1246	FLR	S	175.3		
VC2B 1246	FLR	S	175.3		
VC2B 1246	FLR	S	175.3		
VC2B 1246	FLR	S	175.3		
VC2B 1246	FLR	S	175.3		
VC2B 1246	FLR	S	175.3		
VC2B 1246	FLR	S	176.6		
VC2B 1246	FLR	S	176.6		
VC2B 1246	FLR	S	176.6		
VC2B 1246	FLR	S	178.3	-0.20	0.35
VC2B 1246	FLR	S	176.0	-0.20	0.35
VC2B 1246	FLR	S	177.0	-0.20	0.35
VC2B 1246	FLR	S	169.9		
VC2B 1246	FLR	S	170.4		
VC2B 1246	FLR	S	174.3		
VC2B 1246	FLR	S		-0.20	0.35
VC2B 1246	FLR	S	176.4	-0.20	0.35
VC2B 1246	FLR	S	162.0		

Appendix B (Cont)

Sample	Mineral	Type	Th °C	Tm_{ICE}	Salinity equiv. wt% NaCl
VC2B 1246	FLR	S	160.7		
VC2B 1246	FLR	S	161.7		
VC2B 1246	FLR	S	180.5		
VC2B 1246	FLR	S	181.4		
VC2B 1246	FLR	S	181.3		
VC2B 1246	FLR	S	171.5		
VC2B 1246	FLR	S	179.0		
VC2B 1246	FLR	S	180.1		
VC2B 1246	FLR	S	177.0		
VC2B 1246	FLR	S	176.8		
VC2B 1246	FLR	S	176.4		
VC2B 1322	FLR	S	166.5	-0.10	0.17
VC2B 1322	FLR	S	171.9	-0.20	0.35
VC2B 1322	FLR	S	183.0	-0.20	0.35
VC2B 1322	FLR	S	183.5	-0.20	0.35
VC2B 1322	FLR	S	182.0	-0.20	0.35
VC2B 1322	FLR	S	177.6	-0.20	0.35
VC2B 1322	FLR	S	165.5	-0.20	0.35
VC2B 1322	FLR	S	175.3	-0.20	0.35
VC2B 1322	FLR	S	173.6		
VC2B 1322	FLR	S	178.0	-0.20	0.35
VC2B 1322	FLR	S	159.8	-0.10	0.17
VC2B 1322	FLR	S	155.9		
VC2B 1322	FLR	S	159.5		
VC2B 1322	FLR	S	160.8		
VC2B 1322	FLR	S	164.8		
VC2B 1322	FLR	S	164.8		
VC2B 1322	FLR	S	182.8		
VC2B 1322	FLR	S	178.5		
VC2B 1322	FLR	S	187.1		
VC2B 1322	FLR	S	181.8		
VC2B 1322	FLR	S	158.6		
VC2B 1322	FLR	S	162.7		
VC2B 2183	FLR	S	177.0	-0.50	0.87
VC2B 2183	FLR	S	177.2	-0.50	0.87
VC2B 2183	FLR	S	178.7	-0.50	0.87
VC2B 2183	FLR	S	175.7	-0.40	0.70
VC2B 2183	FLR	S	175.5	-0.40	0.70

Appendix B (Cont)

Sample	Mineral	Type	Th °C	Tm_{ICE}	Salinity equiv. wt% NaCl
VC2B 2183	FLR	S	175.6	-0.40	0.70
VC2B 2183	FLR	S	175.6		
VC2B 2183	FLR	S	174.2		
VC2B 2183	FLR	S	175.3		
VC2B 2183	FLR	S	175.4		
VC2B 2183	FLR	S	174.7		
VC2B 2183	FLR	S	175.0		
VC2B 2183	FLR	S	179.7		
VC2B 2183	FLR	S	179.0		
VC2B 2183	FLR	S	179.4		

APPENDIX C

THERMODYNAMIC DATA

	Log K 230°C	300°C
$3Kspar + 2H^+ = Muscovite + 6SiO_2 + 2K^+$	8.04	7.72
$2Muscovite + 3H_2O + 2H^+ = 3Kaolinite + 2K^+$	4.19	3.57
$Calcite + 2H^+ = Ca^{++} + CO_2 + H_2O$	8.71	8.40
$H_2S(g) + 0.5\ O_2(g) = H_2O + 0.5\ S_2(g)$	16.79	12.80
$4FeS_2 + Cu_5FeS_4 = 5CuFeS_2 + S_2(g)$	-9.45	-6.76
$2Fe_2O_3 + Cu_5FeS_4 + 3S_2 = 5CuFeS_2 + 3O_2(g)$	70.34	-61.94
$FeS_2 = FeS + 0.5S_2(g)$	-7.57	-5.78
$2FeS_2 + 1.5O_2(g) = Fe_2O_3 + 2S_2(g)$	30.45	27.59
$2Fe_3O_4 + 0.5O_2 = 3Fe_2O_3$	18.63	15.51
$3FeS_2 + 2O_2(g) = Fe_3O_4 + 3S_2$	36.36	33.63
$CHL4 + 7S_2 = 7FeS_2 + 3SiO_2 + 4H_2O + 4O_2$	-60.22	-56.62
$CHL4 + 3.5S_2 = 7FeS + 4H_2O + 3SiO_2 + 4O_2$	-113.24	-97.08
$3FeS + 2O_2 = Fe_3O_4 + 1.5S_2$	59.08	50.97
$3CHL4 + 2O_2 = 7Fe_3O_4 + 12H_2O + 9SiO_2$	73.85	65.56
$MoO_4^{2-} + 2H^+ + 2H_2S(g) = MoS_2 + 3H_2O + 0.5O_2$	5.74	5.18
$MnS + CO_2 + 0.5O_2 = MnCO_3 + 0.5S_2$	13.11	10.36
$ZnS + CO_2 + 0.5O_2 = ZnCO_3 + 0.5S_2$	6.28	4.41
$PbS + CO_2 + 0.5O_2 = PbCO_3 + 0.5S_2$	6.79	4.96
$PbS + 2O_2 = PbSO_4$	66.85	56.42
$CaSO_4 + CO_2 = CaCO_3 + 0.5S_2 + 1.5O_2$	-60.79	-52.10
$S_{2(g)} = 2S_{(l)}$*	-5.19	-3.72

For the construction of Figure 3.10

	150°C	200°C	250°C	Log K 300°C
$Ni + 0.5O_2 = NiO$	24.68	21.56	19.05	16.98
$C + O_2 = CO_2$	48.74	43.59	39.44	36.00
$3FeS_2 + 2O_2g) = Fe_3O_4 + 3S_2$		37.78	35.50	33.63
$FeS + H_2S + 0.5O2 = FeS2 + H_2O$#		24.40	20.88	17.98
$H_2S + 2O_2 = SO_4^{2-} + 2H^+$#	79.05	66.65	56.30	47.33

*, From Barton and Skinner, 1979
#, From Henley et al., 1984

REFERENCES

Aldrich, M.J., and Laughlin, A.W., 1984, A model for the development of the southeastern Colorado Plateau boundary: Journal of Geophysical Research, **89**, 10,207-10,218.

Apodaca, L.E., 1989, Geochemical study of the Cochiti mining district, Sandoval County, New Mexico: Unpublished M.S. thesis, New Mexico Institute of Mining and Technology, 99 p.

Bailey, R.A., Smith, R.L., and Ross, C.S., 1969, Stratigraphic nomenclature of volcanic rocks in the Jemez Mountains, New Mexico: U.S. Geological Survey Bulletin, 1274-P, 19p.

Bailey, R.A., Darymple, G.B., and Lanphere, M.A., 1976, Volcanism, structure, and geochronology of Long Valley caldera, Mono county, California,: Jornal of Geophysical Research, **81**, 725-744.

Ballantyne, G.H., 1981, Chemical and mineralogical variations in propylitic zones surrounding porphyry copper deposits: Unpublished Ph.D. thesis, University of Utah, 208 p.

Ballantyne, J.M., 1981, Geochemistry of hydrothermal sericite and chlorite: Unpublished Ph.D. thesis, University of Utah, 134 p.

Bargar, K.E., and Fournier, R.O., 1988, Effects of glacial ice on subsurface temperatures of hydrothermal systems in Yellowstone National Park, Wyoming: Geology, **16**, 1077-1080.

Barton, P.B. Jr., Bethke, P.M., and Roedder, E., 1977, Environment of ore deposition in the Creede mining district, San Juan Mountains, Colorado: Part III. Progress toward interpretation of the chemistry of the ore-forming fluid for the OH vein: Economic Geology, **72**, p. 1-24.

Barton, P.B. Jr., and Skinner, 1979, Sulfide mineral stabilities, in Barnes, H.L., (ed.), Geochemistry of Hydrothermal Ore Deposits: New York, Wiley-Interscience, 278-403.

Beane, R.E., and Titely, S.R., 1981, Porphyry Copper Deposits: Part II. Hydrothermal alteration and mineralization: Economic Geology 75th Anniversary Volume, 235-269.

Berger, B.R., and Silberman, M.L., 1985, Relationships of trace-element patterns to geology in hot-spring-type precious-metal deposits: Reviews in Economic Geology, 2, p. 233-247.

Berger, B.R, and Henley R.W., 1989, Advances in the understanding of epithermal gold-silver deposits, with special reference to the western United States. The Geology of Gold Deposits: The Perspective in 1988, Economic Geology Monograph 6, 405-423.

Bethke, P.M., Lysne, P., Sweetkind, D.S., and Landis, G.P., 1990, In-situ fluid sampling by synthetic fluid inclusions, VC-2B, Valles caldera, New Mexico (abstr): EOS, **71**, 1683.

Bird, D.K., and Norton, D.L., 1981, Theoretical prediction of phase relations among aqueous solutions and minerals: Salton Sea geothermal system: Geochimica et Cosmochimica Acta, **45**, p. 1479-1493.

Bodnar, R.J., T.J., Reynolds, and Kuehn, C.A., 1985, Fluid inclusion systematics in epithermal systems: Geology and Geochemistry of Epithermal systems, Reviews in Economic Geology, 2, 73-96.

Brimhall, G.H., and Ghiorso M.S., 1983, Origin and ore-forming consequences of the advanced argillic alteration process in hypogene environments by magmatic gas contamination of meteoric

fluids: Economic Geology, **78**, 73-90.

Brown, P.E., and Lamb, W.M., 1989, P-V-T properties of fluids in the system H_2O-CO_2-NaCl: New graphical presentations and implications for fluid inclusion studies: Geochimica et Cosmochimica Acta, **53**, 1209-1221.

Browne, P.R.L., 1978, Hydrothermal alteration in active geothermal fields: Annual Reviews in Earth and Planetary Sciences, 6, 229-250.

Browne, P.R.L., and Ellis, A.J., 1970, The Ohaki-Broadlands geothermal area, New Zealand: Mineralogy and related geochemistry: American Journal of Science, **269**, 97-131.

Campbell, A., Rye, D., and Petersen, U., 1984, A hydrogen and oxygen isotope study of the San Cristobal Mine, Peru: Implications of the role of water to rock ratio for the genesis of wolframite deposits: Economic Geology, **79**, 1818-1832.

Capuano, R.M., and Cole, D.R., 1982, Fluid-mineral equilibria in a hydrothermal system, Roosevelt Hot Springs, Utah: Geochimica et Cosmochimica Acta, **46**, p. 1353-1364.

Chambers, W.F., 1991, BA85: A Bence-Albee oxide analysis routine with mineral code capabilities: Sandia National Laboratories Report SAND90-1702.

Chambers, W.F., and Doyle, J.H., 1990, SANDIA TASK8, Version C, A subrountined electron microprobe automation system: Sandia National Laboratories Report SAND90-1703.

Charles, R.W., Buden, R.J.V., and Goff, F., 1986, An interpretation of the alteration assemblages at Sulphur Springs, Valles caldera, New Mexico: Journal of Geophysical Research, **91**, 1887-1898.

Charles, R.W., Musgrave, J., Goff, F., and Janecky, D., 1990, The state of equilibrium in CSDP corehole VC-2B, Valles caldera, New Mexico (abstr): EOS, **71**, 1684.

Cooper, J.E., and Abedin K.Z., 1981, The relationship between fixed ammonium-nitrogen and potassium in clays from a deep well on the Texas Gulf Coast: Texas Journal of Science, **33**, 103-111.

D' Amore, F., and Gianelli, G, 1984, Mineral assemblages and oxygen and sulfur fugacities in natural rock-water interaction processes, Geochimica et Cosmochimica Acta, **48**, 847-857.

Doell, R.R., Dalrymple, G.B., Smith, R.L., and Bailey, R.A., 1968, Paleomagnetism, potassium-argon ages, and geology of rhyolites and associated rocks of the Valles caldera, New Mexico. *in* Coates, R.R., Hay, R.L., and Anderson, C.A., eds., Studies in volcanology: Geological Society of America, Memoir 116, 211-248.

Drummond, S.E., and Ohmoto, H., 1985, Chemical evolution and mineral deposition in boiling hydrothermal systems: Economic Geology, **80**, 126-147.

Eslinger, E.V., and Savin, S.M., 1973, Mineralogy and oxygen isotope geochemistry of the hydrothermally altered rocks of the Okaahi-Broadlands, New Zealand geothermal area: America Journal of Science, **273**, p. 260-267.

Evans, C.R., and Staplin F.L., 1971, Regional facies of organic metamorphism. *in* Geochemical Exploration (eds. R.W. Boyle and J.I. McGerrigle): CIMM Special Paper 11, 517-520.

Evans, C.R., Rogers M.A., and Bailey N.J.L., 1971, Evolution and alteration of petroleum in western Canada: Chemical Geology, 8, 147-170.

Ferry, J.M. and Baumgartner, L., 1986, Thermodynamic models of molecular fluids at the elevated pressures and temperatures of crustal metamorphism: Thermodynamic modeling of Geological Materials: Minerals, Fluids and Melts, Reviews in Mineralogy, **17**, 207-262.

Field, C.W., and Fifarek, R.H., 1985, Light stable-isotope systematics in the epithermal environment: Geology and Geochemistry of Epithermal systems, Reviews in Economic Geology, 2, 99-128.

Fournier, R.O., 1979, Geochemical and hydrologic considerations and the use of enthalpy-chloride diagrams in the prediction of underground conditions in hot-springs systems: Journal of Volcanology and Geothermal Research, 5, 1-16.

Franklin, J.M., Lydon, J.W., and Sangster, D.F., 1981, Volcanic-associated massive sulfide deposits: Economic Geology 75th Anniversary Volume, 485-627.

Frantz, J.D., Zhang, Y-G., Hickmott, D.D., and Hoering, T.C., 1989, Hydrothermal reaction involving equilibrium between minerals and mixed volatiles. I. Techniques for experimentally loading and analyzing gases and their application to synthetic fluid inclusions: Chemical Geology, **76**, 57-70.

Friedman, I., and O'Niel, J.R., 1977, Compilation of stable isotope fractionation factors of geochemical interest: *in* Fleischer, M. (ed.), Data of Geochemistry, Sixth Edition: U.S. Geological Survey Professional Paper 440-KK, p KK1-KK12.

Gardner, J.N., Goff, F., Garcia, S., and Hagan., R.C., 1986 Stratigraphic relations and lithologic variations in the Jemez volcanic field, New Mexico: Journal of Geophysical Research, **91**, 1763-1778.

Gardner, J.N., Hulen, J.B, Lysne, P., Jacobson, R., Goff, F., Nielson, D.L., Pisto, L., Criswell, C.W., Gribble, R., Meeker, K., Musgrave, J.A., Smith, T., and Wilson, D., 1989, Scientific core hole Valles Caldera #2B (VC-2B), New Mexico: drilling and some initial results: Transactions, Geothermal Resources Council, **13**, 133-139.

Gemmell, J.B., Simmons, S.F., and Zantop, H., 1988, The Santo Nino silver-lead-zinc vein, Fresnillo district, Zacatecas, Mexico: Part I. Structure, vein stratigraphy, and mineralogy: Economic Geology, **83**, 1597-1618.

Giggenbach, W.F., 1980, Geothermal gas equilibria: Geochimica et Cosmochimica Acta, **44**, 2021-2032.

Giggenbach, W.F., 1981, Geothermal mineral equilibria: Geochmicia et Cosmochimica Acta, **45**, 393-410.

Giggenbach, W.F., 1986, The use of gas chemistry in delineating the origin of fluids discharged over the Taupo Volcanic Zone: Proceedings of the International Volcanological Congress, Session V, Auckland, 47-50.

Goff, F., and Gardner, J.N., 1980, Geologic map of the Sulphur Springs area, Valles caldera geothermal system, New Mexico: Los Alamos National Laboratory Report LA-8634-MAP, Los Alamos National Laboratory, Los Alamos, N.M.

Goff, F., and Grigsby, C.O., 1982, Valles caldera geothermal systems, New Mexico, USA: Journal of Hydrology, **56**, 119-136.

Goff, F., and Nielson, D.L., 1986, Caldera processes and magma-hydrothermal systems, Continental Scientific Drilling Program - Thermal Regimes, Valles caldera research, scientific and management plan: Los Alamos National Laboratory Report LA-10737-OBES, 163 p.

Goff, F., and Shevenell, L., 1987, Travertine deposits of Soda Dam, New Mexico and their implication for the age and evolution of the Valles caldera hydrothermal system: Geological Society of America Bulletin, **99**, 292-302.

Goff, F., Gardner, J.N., Vidale, R., and Charles, R., 1985, Geochemistry and isotopes of fluids from Sulphur Springs, Valles caldera, New Mexico: Journal of Volcanology and Geothermal Research, **23**, 273-297.

Goff, F., Nielson, D.L., Gardner, J.N., Hulen, J.B., Lysne, P., Shevenell, L., and Rowley, J.C., 1987, Scientific Drilling at Sulphur Springs, Valles caldera, New Mexico: Corehole VC-2A: EOS, **68**, 661-662.

Goff, F., Shevenell, L., Gardner, J.N., Vuataz , F.-D., and Grigsby, C.O., 1988, The hydrothermal outflow plume of Valles caldera, New Mexico, and a comparison with other outflow plumes: Journal of Geophysical Research, **93**, 6041-6058.

Goff, F., Gardner, J.N., Baldridge, W.S., Hulen, J.B., Nielson, D.L., Vaniman, D., Heiken, G., Dungan, M.A., and Broxton, D., 1989, Volcanic and hydrothermal evolution of Valles caldera and Jemez volcanic field: New Mexico Bureau of Mines and Mineral Resources Memoir 46, 381-434.

Goff, F., Gardner, J.N., Solbau, R.D., Adams, A., Lippert, D.R., Jacobson, R., Bayhurst, G., Evans, W., Trujillo, P.E. Jr., Counce, D., and Dixon, P., 1990, The "art" of in situ fluid sampling and the remarkable compositional variations in the wellbore fluid of VC-2B, Valles caldera, New Mexico: Transactions, Geothermal Resources Council, **14(1)**, 403-410.

Gonzalez, C.M., 1988, Fluid inclusion study of the vein mineralization in the VC-2A Core hole, Valles caldera, New Mexico: Unpublished M.S. thesis, University of California, Riverside, 59 p.

Hayba, D.O., Bethke P.M., Heald P., and Foley N.K., 1985, Geologic, mineralogic, and geochemical characteristics of volcanic-hosted epithermal precious-metal deposits: Reviews in Economic Geology, 2, 129-167.

Heaton, T.H.E., and Vogel J.C., 1981, "Excess air" in groundwater: Journal of Hydrology, **50**, 201-216.

Hedenquist, J.W., 1991, Boiling and dilution in the shallow portion of the Waiotapu geothermal system, New Zealand: Geochimica et Cosmochimica Acta, **55**, 2753-2765.

Hedenquist, J.W., and Henley, R.W., 1985a, The importance of CO_2 on freezing point measurements of fluid inclusions. Evidence from active geothermal systems and implications for epithermal ore deposition: Economic Geology, **80**, 1379- 1406.

Hedenquist, J.W., and Henley, R.W., 1985b, Hydrothermal eruptions in the Waiotapu geothermal system, New Zealand: Their origin, associated breccias and relation to precious metal mineralization: Economic Geology, **80**, 1640-1668.

Hedenquist, J.W., and Browne, P.R.L., 1989, The evolution of the Waiotapu geothermal system, based on chemical and isotopic composition of its fluids, minerals and rocks: Geochimica et Cosmochimica Acta, **53**, 2235-2257.

Helgeson, H.C., and Kirkham, D.H., 1974a, Theoretical prediction of the behavior of aqueous electrolytes at high pressures and temperatures. I. Summary of the thermodynamic/electrostatic properties of the solvent: American Journal of Science, **274** , 1089-1198.

Helgeson, H.C., and Kirkham, D.H., 1974b, Theoretical prediction of the behavior of aqueous electrolytes at high pressures and temperatures. III. Equation of state for aqueous species at infinite dilution: American Journal of Science, **276** , 97-240.

Helgeson, H.C., Delany, J.M., Nesbitt, H.W., and Bird, D.K., 1978, Summary and critique of the thermodynamic properties of rock-forming minerals: American Journal of Science, **278-A** , 1-229.

Helgeson, H.C., Kirkham, D.H., and Flowers, G.C., 1981, Theoretical prediction of the behavior of aqueous electrolytes at high pressures and temperatures: Calculation of activity coefficients, osmotic coefficients, and apparent molal and standard and relative partial molal properties to 600°C and 5kb: American Journal of Science, **281** , 1249-1516.

Henley, R.W., 1984, Gaseous components in geothermal processes: Fluid-mineral equilibria in hydrothermal systems, Reviews in Economic Geology, 1, 45-56.

Henley, R.W., 1985, The geothermal framework for epithermal deposits:, Geology and Geochemistry of Epithermal systems, Reviews in Economic Geology, 2, 1-24.

Henley, R.W., and Ellis, A.J., 1983, Geothermal systems, ancient and modern: Earth Science Reviews, **19** , 1-50.

Hofstra, A.H., Landis, G.P., and Rowe, W.A., 1987, Sediment-hosted disseminated gold mineralization at Jerrit canyon, Nevada. IV -- Fluid Geochemistry: (abstr), Geological Society of America, Abstracts with Programs, **19** , 704.

Hulen, J.B., and Nielson, D.L., 1986, Hydrothermal alteration in the Baca geothermal system, Redondo dome, Valles caldera, New Mexico: Journal of Geophysical Research, **91** , 1867-1886.

Hulen, J.B., and Nielson, D.L., 1988, Hydrothermal brecciation in the Jemez fault zone, Valles caldera, New Mexico: Results from Continental Scientific Drilling Program core hole VC-1: Journal of Geophysical Research, **93** , 6077-6089.

Hulen, J.B., Nielson, D.L., Goff, F., Gardner, J.N., and Charles, R.W., 1987, Molybdenum mineralization in an active geothermal system, Valles caldera, New Mexico: Geology, **15** , 748-752.

Hulen, J.B., and Gardner, J.N., 1989, Field geologic log for Continental Scientific Drilling Program core hole VC-2B, Valles caldera, New Mexico: University of Utah Research Institute, Earth Science Laboratory Report ESL-89025-TR, 92 p.

Hulen, J.B., Gardner, J.N., Goff, F., Nielson, D.L., Moore, J.N., Musgrave, J.A., Lemieux, M.M., Meeker, K., and Snow, M.G., 1989, The Sulphur Springs hydrothermal system, past and present: Initial results from Continental Scientific Drilling Program corehole VC-2B, Valles caldera, New Mexico: Transactions, Geothermal Resources Council, **13** , 149-156.

Kieth, T.E.C., White, D.E., and Beeson, M.H., 1978, Hydrothermal alteration and self-sealing in Y-7 and Y-8 drillholes in northern part of Upper Geyser Basin, Yellowstone National Park, Wyoming: USGS Professional Paper 1054A,

Kinghorn, R.R.F., 1983, An Introduction to the Physics and Chemistry of Petroleum: J. Wiley & Sons.

Landis, G.P. and Rye, R.O., 1989, Reconnaissance gas chemistry of the Creede, Colorado hydrothermal system: USGS Open File Report 89-84, 51p.

Lonker, S.W., Fitzgerald, J.D., Hedenquist, J.W., and Walshe, J.L., 1990, Mineral-fluid interaction in the Broadlands-Ohaaki geothermal system, New Zealand: American Journal of Science, **290** , p. 995-1068.

Matsuhisa, Y., Goldsmith, J.R., and Clayton, R.N., 1979, Oxygen isotopic fractionation in the system quartz-albite-anorthite-water: Geochimica et Cosmochimica Acta, **43** , p. 1131-1140.

Mazor, E., 1976, Atmospheric and radiogenic gases in thermal waters: Their potential application to prospecting and steam production steam studies. *in* Proceedings of the 2nd U.N. Symposium on Geothermal Energy, San Francisco, 1975, U.S. Government Printing Office, 793-802.

McDowell, S.D. 1978, Layer silicate minerals in borehole Elmore No. 1, Salton Sea geothermal field, California, U.S.A.: University of California, Institute of Geophysics and Planetary Physics Report UCR/IGPP-78/15.

McKibben, M.A., and Elders, 1985, Fe-Zn-Cu-Pb mineralization in the Salton Sea geothermal system, Imperial Valley, California: Economic Geology, **80** , p. 539-559.

McKibben, M.A.,and Williams, A.E., 1989, Metal speciation and solubility in saline hydrothermal fluids: An empirical approach based on geothermal brine data: Economic Geology, **84** , p. 1996-2007.

McKibben, M.A., and Eldridge, C.S., 1990, Radical sulfur isotopic zonation of pyrite accompanying boiling and epithermal gold deposition: a SHRIMP study of the Valles caldera: Economic Geology, **85** , 1917-1925.

McKibben, M.A., Williams, A.E., Elders, W.A.,and Eldridge, C.S., 1987, Saline brines and metallogenesis in a sediment filled rift: The Salton Sea geothermal system, California: Applied Geochemistry, 2, 563-578.

McKibben, M.A., Andes, J.P., Jr., and Williams, A.E., 1988, Active ore-fromation at a brine interface in metamorphosed deltaic-lacustrine sediments: The Salton Sea geothermal system, California: Economic Geology, **83** , 511-523.

Muffler, L.P., and White, D.E., 1969, Active metamorphism of Upper Cenozoic sediments in the Salton Sea geothermal field and the Salton trough, southeastern California: Geological Society of America Bulletin, **80** , p. 157-182.

Muffler, L.J.P., White, D.E., and Truesdell, A.H., 1971, Hydrothermal explosion craters in Yellowstone National Park: Geological Society of America Bulletin, **82** , 723-740.

Musgrave, J. A., and Norman, D.I., 1988, Analysis of fluid inclusion gases from Continental Scientific Drilling Program corehole VC-2A, Valles caldera, New Mexico (abstr): EOS, **69** , 1508.

Musgrave, J.A., and Norman, D.I., 1989, Initial results of fluid inclusion studies from Continental Scientific Drilling Program corehole VC-2A, Valles caldera, New Mexico (abstr): PACROFI II, Program with Abstracts, 2, Blacksburg, VA, January 4-7, 1989, 47.

Musgrave, J.A. and Hulen, J.B., 1989, Vein, vug, and fracture mineralization and paragenesis of Continental Scientific Drilling Program coreholes VC-2A and VC-2B, Valles Caldera, New Mexico (abstr): EOS, **70**, 1414.

Musgrave, J.A., Goff, F., Shevenell, L., Trujillo, P.E., Jr., Counce, D., Luedemann, G., Garcia, S., Dennis, B., Hulen, J.B., Janik, C., and Tomei, F.A., 1989, Selected data from Continental Scientific Drilling Program core holes VC-1 and VC-2A, Valles caldera, New Mexico: Los Alamos National Laboratory Report LA-11496-OBES, 70p.

Musgrave, J.A., and Norman, D.I., 1990a, State of the Sulphur Springs hydrothermal system, Valles caldera, New Mexico: Fluid inclusion evidence (abstr): PACROFI III, Program with abstracts, 3, Toronto, May 20-22, 1990, 62.

Musgrave, J.A., and Norman, D.I., 1990b, Precious- and base-metal deposition in an active hydrothermal system, Sulphur Springs area, Valles caldera, New Mexico: (abstr). Great Basin Symposium: Geology and Ore Deposits of the Great Basin, Program with abstracts, Reno, NV, April 1-5, 1990, 105.

Musgrave, J.A., Dixon, P.R., Janecky, D.R., and Goff, F., 1990, Sulphur Springs, Valles caldera, New Mexico, USA: Fluid chemistry - Past and present (abstr): EOS, **71**, 1684.

Musgrave, J.A., Poths, J., and Norman, D.I., 1991, Noble gases in fluid inclusions from Valles caldera and St. Cloud mine, Chloride mining district, New Mexico: (abstr.) Alfred O. Nier Symposium on Inorganic Mass Spectrometry, Durango, CO, May 7-9, 1991, 40.

Nakamura, H., Sumi K., Katageri K., and Iwate T., 1970, The geological environment of Matsukawa geothermal area, Japan: Geothermics Special Issue 2, 221-231.

Nielson, D.L., and Hulen, J.B., 1984, Internal geology and evolution of the Redondo dome, Valles caldera, New Mexico: Journal of Geophysical Research, **89**, 8695-8711.

Norman, D.I., Harrison, R.W., and Anders-Behr, C., 1991a, Geology and geochemical analysis of mineralizing fluids at St. Cloud and U.S. Treasury mines, Chloride mining district, New Mexico: Journal of Geochemical Exploration (in press).

Norman, D.I., Benton, L.D., and Albinson, T.F., 1991b, Calculation of fO_2 and fS_2 of ore fluids and depth and pressure of mineralization from fluid inclusion gas analyses for the Fresnillo, Colorado, and Sombrete Pb-Zn-Ag deposits, Mexico: Proceedings: SGA Anniversary Meeting: Source, Transport, and Deposition of Metals, Nancy, France, August 30 - September 3, 1991, 209-212.

Norman, D.I., and Sawkins, F.J., 1987, Analysis of volatiles in fluid inclusions by mass spectrometry: Chemical Geology, **61**, 1-10.

Ohmoto, H., 1972: Systematics of sulfur and carbon isotopes in hydrothermal ore deposits: Economic Geology, **67**, 551-578.

O'Neil, J.R., and Taylor, H.P., 1967, The oxygen isotope and cation exchange chemistry of feldspars: American Mineralogist, **52**, 1414-1437.

Olsen, K.H., Braile, L.W., Stewart, J.N., Daudt, C.R., Keller, G.R., Ankeny, L.A., and Wolff, J.J., 1986, Jemez Mountains volcanic field, New Mexico: Time tem interpretation of the CARDEX seismic experiment and comparison with Bouguer gravity: Journal of Geophysical Research, **91**, 6175-6187.

Page and Wenk, 1979, Phyllosilicate alteration of plagioclase studied by transmission electron microscopy: Geology, 7, p. 393-397.

Palin, J.M., Gas analysis of phyllosilicate-bearing rock and its application to mineral exploration: Unpublished M.S. thesis, New Mexico Institute of Mining and Technology, Socorro.

Parry, W.T., Ballantyne, J.m., and Jacobs, D.C., 1984, Geochemistry of hydrothermal sericite from Roosevelt Hot Springs and the Tintic and Santa Rita porphyry copper systems: Economic Geology, **79**, p. 72-86.

Piperov, N.B., and Penchev, N.P., 1973, A study on gas inclusions in minerals. Analysis of the gases from micro-inclusions in allanite: Geochimica et Cosmochimica Acta, **37**, 2075-2097.

Plumlee, G.S., 1989, Processes controlling epithermal mineral distribution in the Creede Mining District, Colorado: Unpublished Ph.D thesis, Harvard University.

Reyes, A.G., 1990, Petrology of active Philippine geothermal areas: Applications of alteration mineralogy in geothermal exploration and development: Journal of Volcanology and Geothermal Rsearch, **43**, 207-309.

Robie, R.A., Hemingway, B.S., and Fisher, J.R., 1979, Thermodynamic properties of minerals and related substances at 298.15K and 1 bar pressure and at higher temperatures: U.S. Geological Survey Bulletin 1492, 456p.

Roedder E., 1984, Fluid inclusions: Reviews in Mineralogy, **12**, 644 p.

Rogers, P.S.Z., Musgrave, J.A., Charles, R.W., and Hulen, J.B., 1990, Nuclear microprobe determination of trace element distribution in the Continental Scientific Drilling Program core hole VC-2A, Valles caldera, New Mexico: (abstr.), EOS, **71**, 1692.

Sasada, M., 1987, Fluid inclusions from VC-2A core hole in Valles cladera, New Mexico, U.S.A. - Evidence for a transition from hot water-dominated to vaopr-dominated system: (abstr.), Geothermal Research Society of Japan, Annual Meeting.

Sasada, M., 1988, Microthermometry of fluid inclusions from the VC-1 core hole in Valles caldera, New Mexico: Journal of Geophysical Research, **93**, 6091-6096.

Sasada, M., 1989, Fluid inclusion evidence for recent temperature increases at Fenton Hill Hot dry Rock test site west of the Valles caldera, New Mexico, USA: Journal of Volcanology and Geothermal Research, **36**, 257-266.

Sasada, M., and Goff, F., 1989, Fluid inclusions in minerals from the VC-2A core hole of CSDP at the Valles caldera, New Mexico: PACROFI II, Program with Abstracts, 2, January 4-7, 1989, Blacksburg, VA, 57.

Seward, T.M., 1989, The hydrothermal chemistry of gold and its implications for ore formation: Boiling and conductive cooling as examples: Economic Geology Monograph 6, p. 398-404.

Shevenell, L., Goff, F., Vuataz, F., Trujillo, P., Counce, D., Janik, C., Evans, B., 1987, Hydrogeochemical data for thermal and nonthermal waters and gases of the Valles caldera, southern Jemez Mountains region, New Mexico: Los Alamos National Laboratory Report, LA-10923-_OBES, 100 p.

Silberman, M.L., and Berger, B.R., 1985, Trace element patterns to alteration and morphology in epithermal precious-metal deposits: Reviews in Economic Geology, 2, p. 203-232

Sillitoe, R.H., 1985, Ore-related breccias in volcanoplutonic arcs: Economic Geology, **80**, 1476-1514.

Simmons, S.F., 1991, Hydrologic implications of alteration and fluid inclusion studies in the Fresnillo district, Mexico: Evidence for a brine reservoir and a descending water table during formation of hydrothermal Ag-Pb-Zn orebodies: Economic Geology, **86**, 1579-1601.

Slack, J.F., 1980, Multistage vein ores of the Lake City district, western San Juan Mountains, Colorado. Economic Geology, **75**, 963-991.

Sloan, R.C., Williams, A.E., and McKibben, M.A., 1991, Do fluid inclusions preserve representative ratios of gases in mineralizing fluids? Implications of a RATFINC study of veins and fluids in active geothermal systems: (abstr), Geological Society of America, Abstracts with Programs,

Smith, R.L., and Bailey, R.A., 1968, Resurgent cauldrons: Studies in Volcanology, Coates, R.R., Hay, R.L., and Anderson, C.A., eds., Geological Society of America Memoir 116, 613-632.

Smith R.L., Bailey, R.A. and Ross, C.S., 1970, Geologic map of the Jemez Mountains, New Mexico: USGS Miscellaneous Field Investigation Map I-571.

Smith, R.W., 1983, Aqueous chemistry of molybdenum at elevated temperatures and pressures with applications to porphyry molybdenum deposits: Unpublished Ph.D. thesis, New Mexico Institute of Mining and Technology, 311 p.

Smith, S.P., and Kennedy, B.M., 1985, Noble gas evidence for two fluids in the Baca (Valles caldera) geothermal reservoir: Geochimica et Cosmochimica Acta, **49**, 893-902

Spell, T.L., and Kyle, P, R., 1989, Petrogenesis of the Valle Grande Member Rhyolites, Valles caldera, New Mexico: Implications for evolution of the Jemez Mountains magmatic system: Journal of Geophysical Research, **94**, 10379-10396.

Spell, T.L., Harrison, T.M., and Wolff, J.A., 1989, $^{40}Ar/^{39}Ar$ dating of the Bandelier Tuff and associated ignimbrites: Constraints on evolution of the Bandelier magma system (abstr): EOS, **70**, 1413.

Spycher, N.F., and Reed, M.H., 1989, Evolution of a Broadlands-type Epithermal ore fluid along alternative P-T paths: Implications for transport and deposition of base, precious and volatile metals: Economic Geology, **84**, 328-358.

Srodon, J., and Eberl, D.D., 1984, Illite: Reviews in Mineralogy, **13**, 495-544.

Steiner, 1968, Clay minerals in hydrothermally altered rocks at Wairakei, New Zealand: Clays and Clay Minerals, **16**, p. 193-213.

Sterne, E.J., Reynold, R.C., and Zantop, H., 1982, Natural ammonium illites from blacks shales hosting a stratiform base metal deposit, Delong Mountains, northern Alaska: Clay and Clay Minerals, **30**, 161-166.

Stoffregen, R., 1987, Genesis of acid-sulfate alteration and Au-Cu-Ag mineralization at Summitville, Colorado: Economic Geology, **82**, 1575-1591.

Taguchi, S., and Hayashi, M., 1983, Past and present subsurface thermal structures of the Kirishima

geothermal area, Japan: Geothermal Resources Council Transaction, 7, 199-203.

Taylor, H.P., 1968, The oxygen isotope geochemistry of igneous rocks: Contributions to Mineralogy and Petrology, **19**, p. 1-71.

Taylor, H.P. 1974, The application of oxygen and hydrogen isotopes studies to problems of hydrothermal alteration and ore deposition: Economic Geology, **69**, p. 843-883.

Taylor, H.P., 1979, Oxygen and hydrogen isotope relationships in hydrothermal mineral deposits: *in* Barnes, H.L. (ed.), Geochemistry of Hydrothermal Ore Deposits, Second Edition: John Wiley and Sons, New York, 236-277.

Trainer, F.W., 1974, Groundwater in the southwestern part of the Jemez Mountains volcanic regions, New Mexico: New Mexico Geological Society, Field Conference Guidebook 25, 337-345.

Trainer, F.W., 1984, Thermal springs in Canon de San Diego as a window into Valles caldera, New Mexico: New Mexico Geological Society, Field Conference Guidebook 35, 249-255.

Truesdell, A.H., and Janik, C.J., 1986 Reservoir processes and fluid origins in the Baca Geothermal system, Valles caldera, New Mexico: Journal of Geophysical Research, **91**, 1817-1833.

Tulloch, A.J., 1982 Mineralogical observations on carbonate scaling in geothermal wells at Kawerau and Broadlands: Proceedings, Pacific Geothermal Conference, 1, 131-134.

Vuataz, F.-D., and Goff, F., 1986, Isotope geochemistry of thermal and nonthermal waters in the Valles caldera, Jemez Mountains, northern New Mexico: Journal of Geophysical Research, **91**, 1835-1853.

Walshe, J.L., 1986, A six component solid solution model and the conditions of chlorite formation in hydrothermal and geothermal systems: Economic Geology, 81, 681-703.

Wen, C.S., Chilingarian G.V., and Yen T.F., 1978, Properties and structures of bitumens. In Bitumens, Asphalts and Tar Sands (eds. G.V. Chilingarian and T.F. Yen): Developments in petroleum science 7, 155-190. Elsevier.

White, D.E., 1955, Thermal Springs and epithermal ore deposits: Economic Geology, Fiftieth Anniversary Volume, 99-154.

WoldeGabriel, G., 1989, Hydrothermal systems in two areas of the Jemez volcanic field: Sulphur Springs and the Cochiti mining district: Los Alamos National Laboratory Report, LA-11509-OBES, 66 p.

WoldeGabriel, G., and Goff, F., 1989, Temporal relations of volcanism and hydrothermal systems in two areas of the Jemez volcanic field, New Mexico: Geology, **17**, 968-989.

WoldeGabriel, G., 1990, Hydrothermal alteration in the Valles caldera ring fracture zone and core hole VC-1: evidence for multiple hydrothermal systems: Journal of Volcanology and Geothermal Research, **40**, 105-122.

WoldeGabriel, G., and Goff, F., 1991, Alteration processes and K/Ar dates of hydrothermal clays from core hole VC-2B, Valles caldera, New Mexico and their realtion to subsurface geology of a large hydrothermal system: Journal of Volcanology and Geothermal Research (in press).

Wronkiewicz, D., Norman, D., Parkinson, G., and Emanuel, K., 1984, Geology of the Cochiti mining district, Sandoval County, New Mexico: *in* Baldridge, W.S., Dickerson, P.W., Riecker, R.E., and Zidek, J., eds., Rio Grande rift: Northern Mew Mexico. New Mexico Geological Society, Guidebook 35, 219-222.

Wood, S.A. Crerar, D.A., Borcsik, M.P., 1987, Solubility of the assemblage pyrite-pyrrhotite-magnetite-sphalerite-galena-gold-stibnite-bismuthinite-argentite-molybdenite in H_2O-NaCl-CO_2 solutions from 200°-350°C: Economic Geology, **82**, p. 1864-1887.

This dissertation is accepted on behalf of the faculty of the Institute by the following committee:

David L. Nornon
Adviser

David P. Landau

Andrew Campbell

Fred M. Phillips

20 Nov 1991
Date